Universidade do Minho
Escola de Engenharia

Norma Yolanda Gaibor Vaca

Alkali activation of ceramic solid wastes to incorporate in non-structural panels

Universidade do Minho
Escola de Engenharia

Norma Yolanda Gaibor Vaca

Alkali activation of ceramic solid wastes to incorporate in non-structural panels

Doctoral Thesis
Doctoral Program in Solid Waste Management and Treatment

Work performed under the supervision of
Professor Doctor Dinis Leitão
Professor Doctor Nuno Cristelo

July 2022

DIREITOS DE AUTOR E CONDIÇÕES DE UTILIZAÇÃO DO TRABALHO POR TERCEIROS

Este é um trabalho académico que pode ser utilizado por terceiros desde que respeitadas as regras e boas práticas internacionalmente aceites, no que concerne aos direitos de autor e direitos conexos.

Assim, o presente trabalho pode ser utilizado nos termos previstos na licença abaixo indicada.

Caso o utilizador necessite de permissão para poder fazer um uso do trabalho em condições não previstas no licenciamento indicado, deverá contactar o autor, através do RepositóriUM da Universidade do Minho.

Licença concedida aos utilizadores deste trabalho

ACKNOWLEDGEMENTS

I must assume that at this point in my life it is normal to have mixed feelings. After a period of almost five years invested in the research of this Doctoral Thesis, I am pleased to present this project to the scientific community. However, the completion of a Doctoral Thesis involves much more than the work reflected in this final document, since it represents a whole set of knowledge and experiences acquired of which I take with me the memorable ones, and after having overcome the undesirable ones (the covid-19 pandemic included), I also value them because they made me the woman I am today, more determined and at the same time humbler. Behind personal achievements, besides a considerable self-effort, a large number of contributions, support, suggestions, comments, or criticisms coming from many people usually are hidden. Their importance, in this case, is so valuable that, without them, it would certainly have been very difficult to get any noteworthy result. So that, it is a delight to express my deepest gratitude to all people who made this research work possible, to wit:

A special mention goes to Professor Cândida Vilarinho, who at the time I started my studies was the director of the Ph.D. program ''Solid Waste Management and Treatment''. It is undeniable her total support from the first moment I arrived in Portugal, and it is through Prof. Candida that I came in contact with the wonderful task force that has accompanied me during this time, my supervisors.

My heartfelt acknowledge to my direct advisors, Prof. Dinis Leitão and Prof. Nuno Cristelo, as well as to Prof. Vítor Cunha, Prof. Eduardo Pereira, Prof. Tiago Miranda, and Prof. Ana Briga-Sá. I would like to highlight their excellent professionalism and the highest human qualities. Thanks for your ethics, advice, guidance, patience, support, and great ability to listen in those not-so-good moments. Thank you for trusting in me and the opportunity to be part of the research group. I feel myself the luckiest person since I met you professors. It has been a great honor to learn from this outstanding work team.

I will always be indebted to my parents, Rosaura Vaca and Carlos Gaibor for giving me the education, opportunities, and experiences that took me where I am now. Also, to my siblings, Edith, Juan Carlos, and Katty. They selflessly motivated me to look into new directions in life and seek my best way. My gratitude for their unfailing emotional support. It was their love that raised up to me again and again when I got weary. This journey would not have been possible if not for them. Thank you for showing how proud you have always been of me.

Last but not least, I thank with loving my husband, Eduardo, for his special care and attention to me during this roller-coaster period of my life, especially in the most difficult moments. You were the one who helped me endure the frequent frustrations. Thank you for your unconditional trust, timely encouragement, and endless patience. I dedicate this achievement to my family and my husband.
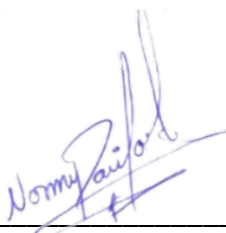
STATEMENT OF INTEGRITY

I hereby declare having conducted this academic work with integrity. I confirm that I have not used plagiarism or any form of undue use of information or falsification of results along the process leading to its elaboration.

I further declare that I have fully acknowledged the Code of Ethical Conduct of the University of Minho.

University of Minho, July 2022

Full name: Norma Yolanda Gaibor Vaca

_____

Signature

RESUMO

Este estudo foi motivado principalmente pela necessidade cada vez mais urgente de desenvolver ligantes alternativos ao conhecido Cimento Portland Ordinário (OPC). Assim, o desenvolvimento de novos cimentos alcalinos, utilizando diferentes resíduos industriais, muitos dos quais ainda em grande parte inexplorados, é uma solução promissora para a construção civil. Em todo o mundo, os materiais cerâmicos são amplamente utilizados na construção, no entanto, 30% da produção total de cerâmica é transformada em resíduo e 45% dos resíduos de construção e demolição resultam de materiais cerâmicos. Neste contexto, o principal objetivo deste trabalho foi investigar o potencial de dois resíduos industriais abundantes e menos comuns em cimentos alcalinos: resíduos cerâmicos (RC) − principal precursor − e escória de forno panela (LFS) − para correção de composição. Silicato de sódio (SS) foi utilizado como o principal ativador em cimentos alcalinos para incorporação em painéis não estruturais. Para atingir este objetivo foi inicialmente realizada uma ampla campanha experimental para determinar a melhor formulação. A mistura selecionada (75% CW + 25% LFS) foi reforçada com diferentes teores (0%, 0,5 % e 1% em volume) de fibras de poliacrilonitrila (PAN). Foram testadas duas condições de cura: temperatura de 70°C e 20°C com 60% HR. Estas misturas foram avaliadas quanto às suas propriedades físicas, mecânicas, mineralógicas e microestruturais, aos 14, 28 e 90 dias de cura. Os resultados mostraram que a solução mais adequada para a finalidade específica, ou seja, a execução de painéis não estruturais, foi o cimento alcalino ativado (AAc) curado à temperatura ambiente, contendo 1% de fibra de PAN. Posteriormente, foram desenvolvidas duas soluções de painéis sanduíche, onde cada uma era composta por uma fina camada de AAc e uma camada isolante mais espessa de espuma de poliestireno extrudido ou aglomerado de cortiça expandida. Os resultados do comportamento mecânico indicaram a viabilidade do fabrico destes painéis, embora existam diferenças claras entre as duas soluções propostas foram observadas. Os resultados também demonstram que a tecnologia de ativação alcalina aumenta a condutibilidade térmica do AAc. A caracterização térmica dos painéis evidência desempenhos promissores após comparação com os materiais e soluções de construção correntes. Finalmente, a avaliação de sustentabilidade revelou que os dois painéis sanduíche propostos eram as alternativas mais sustentáveis em comparação com as três tecnologias convencionais selecionadas, uma vez que melhor combina os fatores ambientais, funcionais e económicos.

Palavras-chave: ativação alcalina, economia circular, painéis não estruturais, resíduos industriais, sustentabilidade.

ABSTRACT

This study was mostly motivated by the increasingly urgent need to develop alternative binders to the well-known Ordinary Portland Cement (OPC). In this way, the development of new alkali-activated materials, using different industrial by-products or wastes, many of which are still largely unexplored, is a promising solution for the construction industry. Worldwide, ceramic materials are extensively used in different types of construction, with a significant percentage ending up as a waste. Two significant numbers support this paradigm – approximately 30% of the total ceramic production is transformed in waste, and 45% of the construction and demolition waste result from ceramic materials. Thus, this study aimed to investigate the potential of two abundant and, at the same time, less common industrial wastes in alkaline cements: ceramic wastes (CW) – as a main precursor, and ladle furnace slag (LFS) – for composition correction. Sodium silicate (SS) was used as the main activator for the alkali activated cements that were incorporated in non-structural panels. To accomplish this objective, a comprehensive experimental campaign to determine the best blend composition was carried out, first. The selected mixture (75% CW + 25% LFS / SS-based) was reinforced using polyacrylonitrile (PAN) fibers with different content (0%, 0.5%, and 1% in volume). Moreover, two curing conditions were experimented, i.e., thermal curing under 70°C and 60% HR $\pm$ 5% and curing at ambient temperature (20°C and 60% HR $\pm$ 5%). Up to this point, all the mixtures were evaluated with respect to their physical, mechanical, mineralogical, and microstructure properties at 14, 28, and 90 curing days. Results showed that the most suitable solution for the specific purpose of its application, i.e., the manufacture of non-structural panels, was the alkali-activated cement (AAc) cured at ambient temperature containing 1% PAN fiber. Afterwards, two sandwich panel solutions were developed, each was composed of a thin layer of AAc and a thicker insulating layer of extruded polystyrene foam or expanded cork agglomerate. The results of the mechanical behavior indicated the feasibility of manufacturing these panels, although clear differences between the two proposed solutions were observed. Findings also suggested that the alkali-activation technology improves the thermal conductivity of the developed AAc. Thermal characterization of the two panels showed a promising performance when compared to currently available building materials. Furthermore, a Sustainability Assessment revealed that the two proposed half-sandwich panels were the most sustainable alternatives compared to the three selected conventional technologies since they combined the best the environmental, functional, and economic factors.

Keywords: alkali activation, circular economy, industrial wastes, non-structural panels, sustainability

TABLE OF CONTENTS

LIST OF FIGURES

LIST OF TABLES

LIST OF ACRONYMS

AAc	alkali-activated cement
AAm	alkali-activated mortars
AAMs	alkali activated materials
ACP	panel of alkali-activated cement based on ceramic wastes and slag only
AP	acidification Potential
AP_{ICB}	Panel with insulation corkboard
AP_{XPS}	Panel with extruded polystyrene foam
$AP_{XPS}^{\parallel}$	Parallel direction of the grooves of the XPS insulation material
$AP_{XPS}^{\perp}$	Perpendicular direction of the grooves of the XPS insulation material
C	water absorption
C-A-S-H	calcium aluminum silicate hydrate
CBW	Ceramic bricks waste
CC	Construction Cost
CDW	construction and demolition wastes
CE	circular economy
Cf	fiber content
CoV	coefficient of variation
CR	ceramic residue
C–S–H	calcium-silicate hydrate
CW	ceramic waste
e.g.	for example
E_{cm}	elasticity modulus
EDX	X-ray Energy Dispersive Analyzer
EE_T	total embodied energy
EE_NR	non-renewable Embodied energy
EP	eutrophication potential
EU	European Union
f_{ct}^{f}	flexural strength
$f_{R0.3mm}$	flexural strength mouth opening displacements of 0.3 mm
$f_{R0.5mm}$	flexural strength mouth opening displacements of 0.5 mm

FA   fly ash

FTIR   Fourier Transform Infrared Spectroscopy

GBFS   ground blast furnace slag

GHG   greenhouse gas

GP   geopolymer

GPa   Gigapascals

GWP   Global Warming Potential

HF_n HFP01SC plate sensors

HWR   heavyweight reference masonry partition wall

ICB   insulation corkboard

λ   thermal conductivity

LAC   Latin America and the Caribbean

LCA   Life Cycle Assessment

LCC   Life Cycle Costing

LC-CBA   Life-Cycle Cost-Benefit Analysis

LCI   Life Cycle Inventory

LCIR   Life Cycle Interpretation of results

LFS   ladle furnace slag

LVDTs   linear variable differential transformers

LWR   lightweight reference plasterboard partition wall

LWS   lightweight sandwich solution

MARS-SC   multicriteria decision-making support method

MDF   medium-density fiberboard

MMC   Modern Methods of Construction

MPa   Megapascals

MSW   municipal solid waste

N-A-S-H   sodium aluminum silicate hydrate

ND_A environmental sustainability dimension

ND_E economic sustainability dimension

ND_F functional sustainability dimension

ND_j performance at the level of the dimension j

NS   sustainability score

ODP	ozone layer depletion
OPC	Ordinary Portland Cement
P	open porosity
PAN	polyacrylonitrile
PE	person Equivalent
PERH	Plano Estratégico de Resíduos Hospitalares; (Strategic Plan for Hospital Waste)
PERSU	Plano Estratégico para os Resíduos Sólidos 2020; (Strategic Plan for Solid Waste)
PESGRI	Plano Estratégico de Gestão dos Resíduos Industriais; (Strategic Plan for the Industrial Waste Management)
PEWPS	Prefabricated Enclosure Wall Panel Systems
$\overline{P}_i$	normalized indicator
PNAPRI	Plano Nacional de Prevenção de Resíduos Indústrias; (National Plan for the Industrial Waste Prevention)
PNGR	National Waste Management Plan (Portuguese acronym)
POCP	Photochemical oxidation
PSD	particle size distribution
PU	polyurethane foam
PVA	Polyvinyl alcohol
PVC	polyvinyl chloride
q_n	heat flux
R	thermal resistance
Rse	external superficial thermal resistances
Rsi	internal superficial thermal resistances
SA	sensitivity analysis
SAB	US Environmental Protection Agency's Science Advisory Board
SDGs	Sustainable Development Goals
SEM	Scanning electron microscope
SH	sodium hydroxide
SI	sustainability indicator
SIPs	structurally insulated panels
SP	superplasticizer
SS	sodium silicate

Te	exterior temperature
Ti	interior temperature
τ_s	shear bond
Tsi_n	inner surface temperature sensors
U	thermal transmission coefficient
UCS	uniaxial compressive strength
UN	United Nations
UTAD	University of Trás-os-Montes and Alto Douro
WBP	waste red clay brick powder
WCP	waste ceramic powder
w_i	weight of the ith indicators
XPS	extruded polystyrene
XRD	X-ray diffraction

Introduction

1.1. MOTIVATION

Environmental concerns are becoming increasingly more significant worldwide. The shortage of natural resources, in addition to high energy consumption and growing levels of greenhouse gas emissions to the atmosphere, creates a scenario that points to developing new sustainable alternatives in the industrial sector. The use of different kinds of industrial waste and by-products as alternative materials in the architecture, engineering, and construction industry has proved to be a very effective way of contributing to such sustainability. These alternative materials may be incorporated during non-structural materials production for urban applications (panels) by partially replacing conventional raw materials into the raw mix or by including active additions to it.

The ceramic industry is plentifully located in different parts of the world. China and Europe are the world leaders in ceramic production. It is also exported to other regions due to its durability and variety in design. In the European Union (EU), the ceramic industry represents an annual production value of around €30 billion, which represent approximately 25% of the global production. The major producing countries in the EU are Italy, Germany, Spain, France, the United Kingdom, Portugal, and Austria. The EU ceramics industry has an export approach with 30% of its production sold outside the EU market [1]. Except for the ceramic industry's vast economic benefits, it causes adverse environmental impacts. The ceramic industries produce a huge amount of waste that is disposed of without any further treatment. This solid waste leads to severe environmental pollution and significant land location. Waste materials produced are about one-third of the total ceramic production [2]. The search for sustainable solutions that take advantage to waste materials from the ceramic industry is currently a crucial challenge for this sector.

With the prompt industrialization in the last few decades of developed and particularly developing countries and some of the reasons explained above, there must be openness on the part of the various actors in our society (legislators, manufacturers, the academic community, owners, among others) for more widespread use of recycled aggregates and new alternative materials based on waste. It is known

that the linear model of economic growth based on the "extract-make-consume - throw away" principle must be dropped out and replaced by a circular model, in which the waste valorization itself becomes relevant. This is a key step toward restoring a healthier environment, and it can simultaneously be a lever to accelerate some of the economic sectors whose activity may have slowed down [3].

The technical-scientific community has devoted, in recent years, special attention to the study of aggregates usage of waste in the manufacture of mortars and concrete with different applications. In the present work, the raw materials used will be exclusively from industrial waste, whose essential condition will be the abundant existence not only in Portugal, but also, if possible, in Ecuador to take advantage of endogenous resources and, at the same time, to alleviate the environmental burden inevitably associated with the treatment and subsequent landfilling of these materials. The conjugation and transformation of the wastes into binder materials will be achieved through the alkaline activation technique, which has been known as a strong development in the last 15 years, and this technique is increasingly recognized as a strong alternative to Portland cement [4]. Based on the activation (alkaline solution) of one or more precursors (moderately amorphous residues), it is possible to obtain a binder matrix of high mechanical quality and durability, with the incorporation of residues having significant economic and environmental advantages.

1.2. AIM

Faced with the vast possible applications for recycled materials in the construction sector, the main aim of this doctoral project is to develop cementitious materials through the alkaline activation of industrial wastes, specifically ceramic residues, and study the feasibility of incorporating them into non-structural panels. It would strongly contribute to the sustainability of the ceramic industry and, at the same time, alleviate the ineludible environmental burden if these materials are landfilling without any treatment.

The present research was carried out in several consecutive stages. Therefore, the following specific objectives were considered:

✓ Defining and establishing the relevance of the treatment of ceramic solid waste and the subsequent use as a precursor for alkali activation in non-structural materials in the construction sector.
This objective corresponds to Chapter 2 of this Doctoral Thesis.

✓ Knowing the fundamental properties of the ceramic residue and the starting materials to determine the optimum mixtures from the mechanical and physical point of view, complemented by a mineralogical and microstructural characterization.
This objective corresponds to Chapters 3, 4, and 5 of this Doctoral Thesis.

✓ Studying the feasibility of the optimum defined mixture to be used in the construction of non-structural panel elements, performing conformance and functional tests related to mechanical and thermal behavior.
This objective corresponds to Chapter 6 of this Doctoral Thesis

✓ Assessing the sustainability of the proposed non-structural panels based on industrial wastes compared with other traditional solutions offered by the construction sector.
This objective corresponds to Chapter 7 of this Doctoral Thesis

1.3. THESIS STRUCTURE

The present document is structured in a total of eight chapters which are organized as follows:

Chapter 1 is the introductory chapter and provides a framework for the work developed, while also presenting the motivation and aim of the research, as well as a detailed description of the contents.

Chapter 2 introduces the literature review focused on the theoretical background of the central topics discussed in the thesis, guaranteeing that the most recent main scientific advances related to the study area are covered. Furthermore, an assessment of the relevance of the topic, at both national and international levels, was also included. This literature review is organized into four sections: waste management and sustainability, to have an overview of the current environmental policies; basic definitions of circular economy and life cycle assessment; a general review of alkaline activation and its important factors; and finally, an introduction about construction systems for prefabricated panels.

Chapter 3. In this first stage of the experimental work, the alkali activation of ceramic residue (CR) resulting from construction and demolition waste, in combination with fly ash (FA) or ladle furnace slag (LFS), was achieved with sodium silicate (SS) or sodium hydroxide (SH) solutions. Four types of pastes were fabricated and tested, each contemplating five different formulations. From a total of 20 pastes, the combination of 75% CR + 25% LFS, activated with SS, was selected as the single most performing, in terms of mechanical strength, since it reached the highest compressive strength values. The composition of this paste was thus considered the starting point for the next stages of this doctoral project. The work produced in this chapter has resulted in the following JCR journal paper and conference presentation:

- Gaibor, N., Coelho, J., Leitão, D., Miranda, T., Tavares, P., & Cristelo, N. (2020). **Alkali activation of recycled ceramic aggregates from construction and demolition wastes**. Materiales de Construcción, 70(339), 222. https://doi.org/10.3989/mc.2020.13619

- Gaibor, N., Leitão, D., Miranda, T., & Cristelo, N. (2019). **Development of alkali-activated ceramic residue and fly ash blends**. In Wastes: Solutions, Treatments, and Opportunities III (pp. 591–599). CRC Press. https://doi.org/10.1201/9780429289798-94

Chapters 4. Since the origin and type of ceramic waste (CW) used in this part of the study are different (i.e., from the ceramic industry), this stage of the work started with the characterization of this new precursor. Afterward, an experimental study followed aiming to define the most adequate formulation, considering the final workability of the paste needed to allow the incorporation and dispersion of polyacrylonitrile (PAN) fibers. These fibers were tested to improve the final tensile strength of the panels. Two different fiber contents were analyzed (apart from the control paste with 0%): 0.5% and 1%, in volume. This work was presented in the following JCR journal paper:

▪ Gaibor, Norma, Leitão, D., Miranda, T., Cristelo, N., Pereira, E. N. B., & Cunha, V. M. C. F. (2021). **Effect of polyacrylonitrile fiber on the properties of alkali-activated ceramic/slag-based mortar**. *Journal of Building Engineering, 44*, 103367. https://doi.org/10.1016/J.JOBE.2021.103367

Chapters 5. The experimental work developed during this stage aimed to optimize the results obtained and presented in the previous chapter, either in terms of mechanical or environmental performance. The strategy was based on increasing the water content while maintaining the fiber content (i.e., 0%; 0.5%, and 1% in volume), which allowed for improved workability of the paste and more efficient fiber dispersion. A second step consisted of curing the pastes under ambient conditions of temperature and relative humidity (20°C and 60% HR ± 5%). Finally, and based on the physical and mechanical performance, the ambient-cured alkali-activated mortar containing 1% of PAN fibers was selected to be used in the next stage of the study (i.e., the manufacture of the non-structural panels). The work developed across this chapter was presented in the following scientific papers:

▪ Gaibor, Norma, Leitão, D., Miranda, T., Cristelo, N., Fernandes L., Pereira, E. N. B., & Cunha, V. M. C. F. (2022). **Fiber Reinforced Alkali Activated Cements from Ceramic Waste and Ladle Furnace Slag cured at ambient temperature** (under review since 04-23-2022). *Journal of Materials in Civil Engineering*. Manuscript number: MTENG-14776, 2022.

▪ Gaibor, N., Leitão, D., Miranda, T., Cunha, V., & Cristelo, N. (2021). **Effect of curing conditions on compressive strength behavior on alkali-activated ceramic wastes** Efecto de las condiciones de curado en el comportamiento de resistencia a la compresión en residuos cerámicos activados

alcalinamente Efeito das condições de c. *Polo Del Conocimiento*, *6*(3), 977–990. http://repositorium.sdum.uminho.pt/handle/1822/70790

Chapter 6. This chapter presents the design and construction of the non-structural panels with the optimum defined mixture, i.e., 75% CR + 25% LFS /SS-based, reinforced with 1% in volume of PAN fibers, and ambient cured (20°C and 60% HR ± 5%). It was manufactured two semi-sandwich panels, the alkali-activated ceramic developed material (AAc) + extruded polystyrene (XPS) and the AAc + Insulation corkboard (ICB). Functional tests related to mechanical and thermal behavior were performed for each solution. The results of this part of the work have also been structured as a full article that will be submitted to an important journal shortly. It is entitled as follows:

- "Development of half-sandwich panels with alkali-activated ceramic and slag wastes: Mechanical and thermal characterization"

Chapter 7. The work carried out at this phase aimed to assess the sustainability of the two proposed half-sandwich panels based on alkali-activated ceramic/slag wastes composed of different conventional thermo-insulating materials, either the rigid extruded polystyrene foam or expanded cork agglomerate. Within this scope, the environmental, functional, and economic performances of the proposed alternatives were evaluated and compared with three reference technologies for partition walls, i) a conventional heavyweight partition wall, ii) a lightweight gypsum wall panel, and iii) a conceptual lightweight sandwich membrane building technology. The analysis of these novelty solutions intended to contribute to the Circular Economy in the construction sector, as well as to the development of the state-of-art since no similar ones have been found. Therefore, the results are also presented as a full paper to be submitted to a journal forthcoming. The title is as follows:

- "Sustainability assessment of half-sandwich panels based on alkali-activated ceramic/slag wastes cement versus conventional technologies"

Chapter 8 presents the general conclusions with the major results achieved throughout our research work, and it also addresses some suggestions for future research lines.

2.1. WASTE MANAGEMENT AND SUSTAINABILITY

2.1.1. Sustainable development: a global objective

For stimulating sustainable development, the United Nations has elaborated "the 2030 Agenda'', a plan of action for people, the planet, and prosperity. It includes 17 Sustainable Development Goals (SDGs) (Figure 2-1) and 169 targets. Heads of State and Government at a special UN conference implemented it on 25 September 2015. The 2030 Agenda is a commitment to eradicate poverty and achieve sustainable development by 2030 worldwide, ensuring that no one is left behind. The adoption of the 2030 Agenda was a landmark achievement, providing for a shared global vision toward sustainable development for all [5]. In the case of Portugal, it has founded a council for the sustainable development of companies (BCSD) that provides resources to its organization. BCSD's activity is supported by the global network of the WBCSD, the largest international business organization dedicated to sustainable development [6].

Figure 2-1. Sustainable Development Goals [7]

Solid waste management and treatment are in some way linked with some of the goals in the 2030 Agenda, as is exhibited in Figure 2-2. Besides, it is strongly bonded with "Goal 12. Ensure sustainable consumption and production patterns". Monitoring SDG 12 responsible consumption and production in an EU context focuses on the sub-themes of decoupling environmental impacts from economic growth, energy consumption, and waste generation and management. Goal 12 has 11 targets which are listed below:

1. Implement the 10-year framework of programs on sustainable consumption and production, all countries taking action, with developed countries taking the lead, considering the development and capabilities of developing countries;
2. By 2030, achieve the sustainable management and efficient use of the natural resource;
3. By 2030, halve per capita global food waste at the retail and consumer levels and reduce food losses along production and supply chains, including post-harvest losses;
4. By 2030, achieve the environmentally sound management of chemicals and all wastes throughout their life cycle, in accordance with agreed international frameworks, and significantly reduce their release to air, water, and soil in order to minimize their adverse impacts on human health and the environment;
5. By 2030, substantially reduce waste generation through prevention, reduction, recycling, and reuse;
6. Encourage companies, especially large and transnational companies, to adopt sustainable practices and to integrate sustainability information into their reporting cycle;
7. Promote public procurement practices that are sustainable, and in accordance with national policies and priorities;
8. By 2030, ensure that people everywhere have the relevant information and awareness for sustainable development and lifestyles in harmony with nature;
9. Support developing countries to strengthen their scientific and technological capacity to move towards more sustainable patterns of consumption and production;
10. Develop and implement tools to monitor sustainable development impacts for sustainable tourism that creates jobs and promotes local culture and products;
11. Rationalize inefficient fossil-fuel subsidies that encourage wasteful consumption by removing market distortions, in accordance with national circumstances, including by restructuring taxation and phasing out those harmful subsidies, where they exist, to reflect their environmental impacts,

taking fully into account the specific needs and conditions of developing countries and minimizing the possible adverse impacts on their development in a manner that protects the poor and the affected communities." [5]

Figure 2-2. Goals for sustainable development related to waste management.

Being sustainable development, specifically, the management of solid waste a concern for different areas, government, producers, academics, etc., in terms of sustainable construction some studies had been done from different perspectives. It was established that concrete waste could be used to substitute up to 50% of the clay whereas ceramic wastes could only substitute a maximum of 30% of the clay [8]. Another study showed that in Europe policies are needed to stimulate high-quality recycling of construction and demolition waste (CDW). Life cycle assessment (LCA) shows that landfilling is the scenario having the highest environmental impacts in terms of person equivalent (PE), followed by downcycling and recycling (-36%) and recycling after selective demolition (-59%). The decrease in environmental impacts is mostly due to the avoided landfilling of CDW and the recovery of materials from selective demolition. Life cycle costing (LCC) results indicate that landfilling is the scenario bearing the highest total economic costs [9]. In the United States, in the way of incorporating

construction sectors within the concept of sustainable building, which also concerns waste management, it was developed a study that sets a statistical paradigm with field-based values for typical construction projects to be followed as a guide, indicating how much cost can be saved, and how much landfill volume can be relieved when material waste is recycled [10]. In Singapore, there is a research report which undertook to review perceptions and awareness of sustainable construction methods and policies within the Singaporean construction industry. The main conclusion of the work is that government regulatory and incentive programs may be able to drive positive change effectively and efficiently, but this needs to happen alongside initiatives to support client awareness and adoption of sustainable practice [11].

2.1.2. Solid waste management, the legal framework in EU and Portugal

The waste management approach was the last environmental affair that was tackled in all the countries that have framed and implemented environmental policies. Water quality, sewage collection, reduction and control of gas emissions issues were addressed first. Even in the context of the European Union (EU), waste concerns were the object of particular legislation only in the 1970s. Moreover, in Portugal, waste management has deemed a priority until the 1990s [12]. So that, to manage and protect natural resources, environmental protection policies emerged to raise awareness of the importance of caring for the environment. In this scene, the EU consolidated its management policy in the documents Directive 2006/12/EC [13] and Directive 2008/98/EC [14], as amended Directive (EU) 2018/851 [15], which provides the "framework for the handling of waste in the Community". It defines key concepts such as waste, recovery, and disposal and puts in place the essential requirements for the management of waste, notably an obligation, especially the responsibility for the waste management operators to have a permit/license or be registered, and an obligation for the Member States to draw up waste management plans. It also establishes major principles, such as an obligation to handle waste in a way that does not have a negative impact on the environment or human health [16].

Sustainable waste management has two main objectives, which are (i) the decrease in waste generation and (ii) the reduction of resource exploitation. These objectives are built-in the waste hierarchy (Figure 2-3), which has become a fully accepted guideline for waste management operations by the Directive 2008/98/EC [17]. It is in agreement with the polluter pays principle, which requires

10

that the cost associated with the waste disposal must be borne by the current holder of the waste, by the previous holders, or by the producers of the waste.

| Preventin and reduction | Preparation for reuse | Reclycle | Valorization | Disposal |
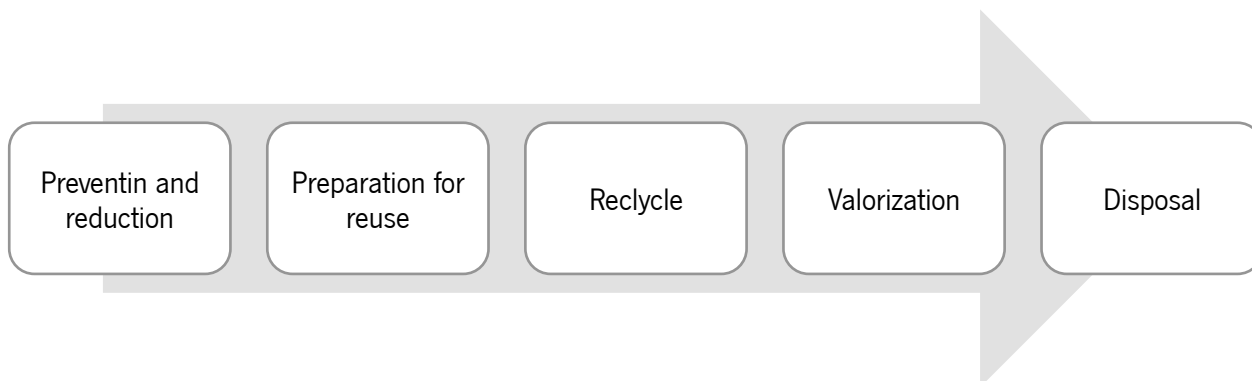
Figure 2-3. Waste hierarchy (Adapted from Decree-Law n. ° 73/ June 17th, 2011)

The European Union's (EU) environmental policies are transposed to its member states. Therefore, Portugal, one of them, must fulfill these objectives and create laws from a pre-conceived EU standard. Thus, with the document already generated by the EU, Portugal modified and created the Decree-Law (DL 73/2011), of June 17th, under which "the Government considers it a priority to reinforce the prevention of waste production and encourage its reuse and recycling with a view to prolonging their use in the economy before returning them in conditions suitable for the natural environment (...), considers it important to promote the full use of the new organized waste market as a way to consolidate the recovery of waste, with advantages for economic agents, as well as to promote the use of specific waste with high recovery potential", in transposition of Directive No. 2008/98/EC, of the European Parliament and of the Council, of 19 November, about waste" [18]. More specifically, in Decree-Law No. 73/2011 - Article 7, the recycling and re-use of waste are identified in the scope of the 2030 targets. Regarding waste recycling, the aim is to achieve a recycling rate of at least 50% of the value of the waste produced. Another target for 2030 is related to the reuse of these wastes so that such waste can be incorporated as a substitute for natural materials. Thus, Decree-Law No. 18/2008 of January 29, established the obligation to use at least 5% of the recycled material in public works construction, to prevent the extraction of natural materials and use other than the disposal of waste in landfills. Some other important solid waste management policies [19] are described below:

— Statement of Rectification No. 14/2021, rectifies the Law n. ° 20/2021, of April 16, regards to the General Regime for waste management approved by Decree-Law No. 178/2006, of 5 September;

11

— Decree-Law No. 102-D/2020: Approves the general regime for waste management, the legal regime for the disposal of waste in landfills and amends the regime for the management of specific waste flows, transposing Directives (EU) 2018/ 849, 2018/850, 2018/851 and 2018/852.

— Decree-Law No. 92/2020: Changes the general regime for waste management.

— Decree-Law No. 152-D/2017: Unifies the regime for the management of specific waste streams subject to the principle of extended producer responsibility, transposing Directives No. 2015/720/EU, 2016/774/EU, and 2017 /2096/EU.

— Ordinance No. 335/97 (Portaria n° 335/97): Establishes the rules to which waste transportation within the national territory is subject

— Decree-Law No. 210/2009: Establishes the constitution, management, and operation of the organized waste market.

— Decree-Law No. 152/2002: Establishes the legal regime to which the procedure for issuing a license, installation, operation, closure, and post-closure maintenance of landfills for waste disposal is subject and proceeds with the transposition to order national legal framework of Directive 1999/31/EC, of the Council, on the disposal of waste in landfills.

— Decree-Law No. 46/2008: Validates the construction and demolition waste management regime.

— Ordinance No. 28/2019: Amends Ordinance No. 145/2017, of April 26, which defines the applicable rules to road, rail, river, sea, and air transport of waste in national territory and creates electronic guides for monitoring of waste (e-GAR).

It is noteworthy that in Portugal the strategies that guide waste planning and management are reflected in specific plans, as of Decree-Law No. 73/2011, to integrate the waste issue in the country, the National Waste Management Plan (PNGR – Portuguese acronym) was created by the National Waste Authority (NRA) to establish national strategic guidelines for waste prevention and management policy and the rules that ensure the consistency of the specific waste management instruments. The diagnostic elements of this plan were made available in public consultation at the end of 2020 to be updated and be called PNGR-2030, to allow interested parties to present technical contributions for its preparation. The elaboration of the PNGR 2030 was determined by Dispatch No. 4242/2020, of 7 April, of the Offices of the Minister of State, Economy and Digital Transition, the Ministers of Planning and Environment and Climate Action, the Minister of Agriculture, and the Minister of the Sea [20]. The PNGR 2030 is based on two objectives: to promote the efficiency of the natural resources used in the

economy and prevent or reduce adverse impacts arising from the production and management of waste [21]. APA is the entity responsible for preparing, reviewing, and implementing the National Waste Management Plan, namely, Strategic Plan for Hospital Waste (PERH[1]), Strategic Plan for the Industrial Waste Management (PESGRI[1]), National Plan for the Industrial Waste Prevention (PNAPRI[1]) and the Strategic Plan for Urban Solid Waste (PERSU[1] 2020+) approved by Portaria n.° 241-B/2019. PERSU[1] 2020+ helps to manage municipal waste and is a tool that provides strategies and targets, which are described in DL 73/2011.

2.1.3. Solid waste generation in the EU and Portugal

Worldwide, increasing population density along with population migration from rural to urban areas and industrial expansion lead to great amounts of waste generation resulting in socio-economic and environmental issues. A report from The World Bank estimates that currently 1.3 billion tons of waste is generated per year all over the world, and by 2025 this amount will increase to 2.2 billion tons per year. These data show an urgent need for strategies to treat the increasing rate of generation around the planet [22]. Waste generation varies as a function of affluence, however, regional and country variations can be significant, as can generation rates within the same city. The global impacts of solid waste are growing fast. Solid waste is a large source of methane, a powerful greenhouse gas (GHG) that is particularly impactful in the short term. The recycling industry, with more than two million informal waste pickers, is now a global business with international markets and extensive supply and transportation networks. Table 2-1 presents the waste generation projections for 2025 by region in the world. According to World Bank Group, in 2018, most of the waste generated is from East Asia & the Pacific region, representing 23% of the total, followed by Europe & Central Asia with 20%, North America with 17%, Latin America with 14%, the Caribbean 11%, and the Middle East & North Africa region are the lowest generation rates with 9% [23], Figure 2-4. Moreover, Figure 2-5 shows the correlation between income levels and waste generation. High-income countries constitute 16% of the global population, however, they are in charge of over one-third of the world's waste.

---

[1] Portuguese Acronym

Table 2-1. Waste generation projections for 2025 by region, [24]

| Region | Current Available Data | | | Projections for 2025 | | | |
| | Total Urban population (millions) | Urban Waste Generation | | Projected population | | Projected Urban Waste | |
		Per Capita (kg/capita/day)	Total (Tons/day)	Total population (millions)	Urban population (millions)	Per Capita (kg/capita/day)	Total (Tons/day)
AFR	260	0.65	169,119	1,152	518	0.85	441,840
EAP	777	0.95	738,958	2,124	1,229	1.5	1,865,379
ECA	227	1.1	254,389	339	239	1.5	354,810
LCR	399	1.1	437,545	681	466	1.6	728,392
MENA	162	1.1	173,545	379	257	1.43	396,320
OECD	729	2.2	1,566,286	1,031	842	2.1	1,742,417
SAR	426	0.45	192,410	1,938	734	0.77	567,545
Total	2980	1.2	3,532,252	7,644	4,285	1.4	6,069,703

AFR: Africa; EAP: East Asia & Pacific; ECA: Eastern & Central Asia; LAC: Latin America & the Caribbean; MENA: the Middle East & North Africa; OECD: Organization for Economic Co-operation and Development; SAR: South Asia
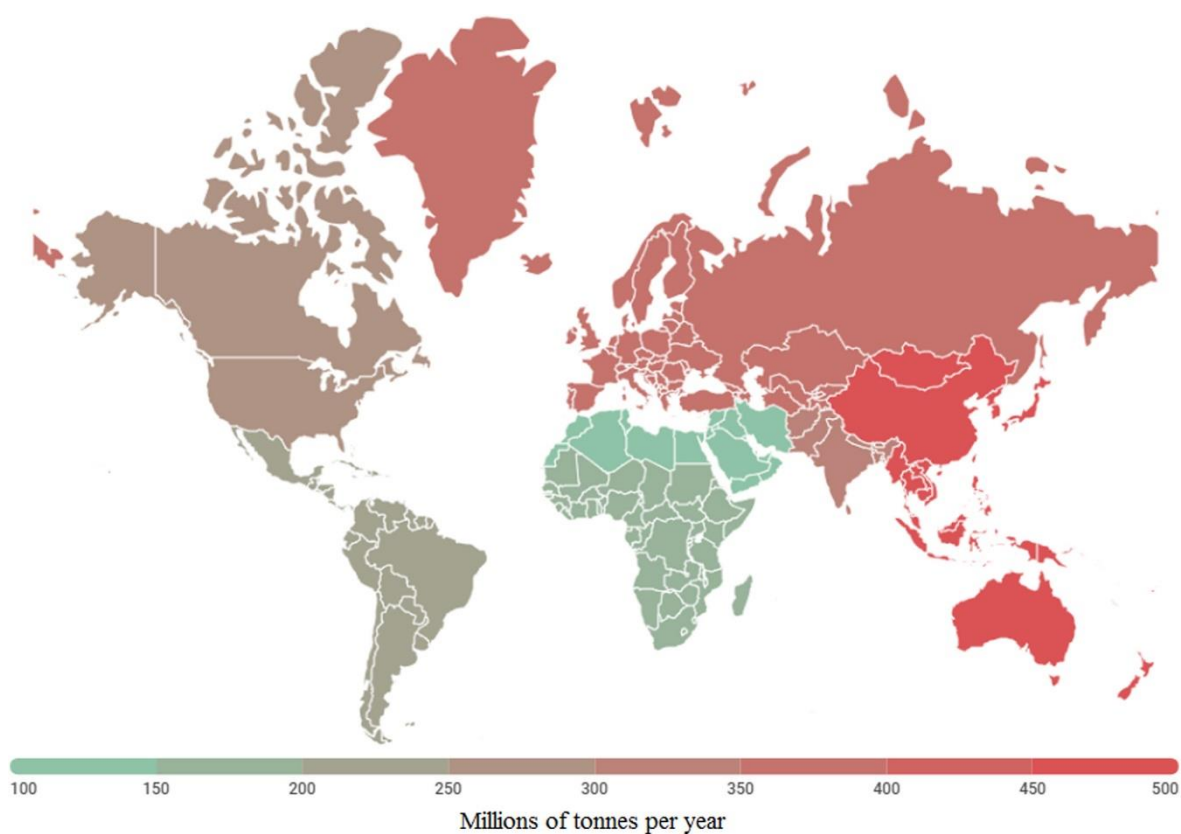
Figure 2-4. Waste generation by region of the world, [23]
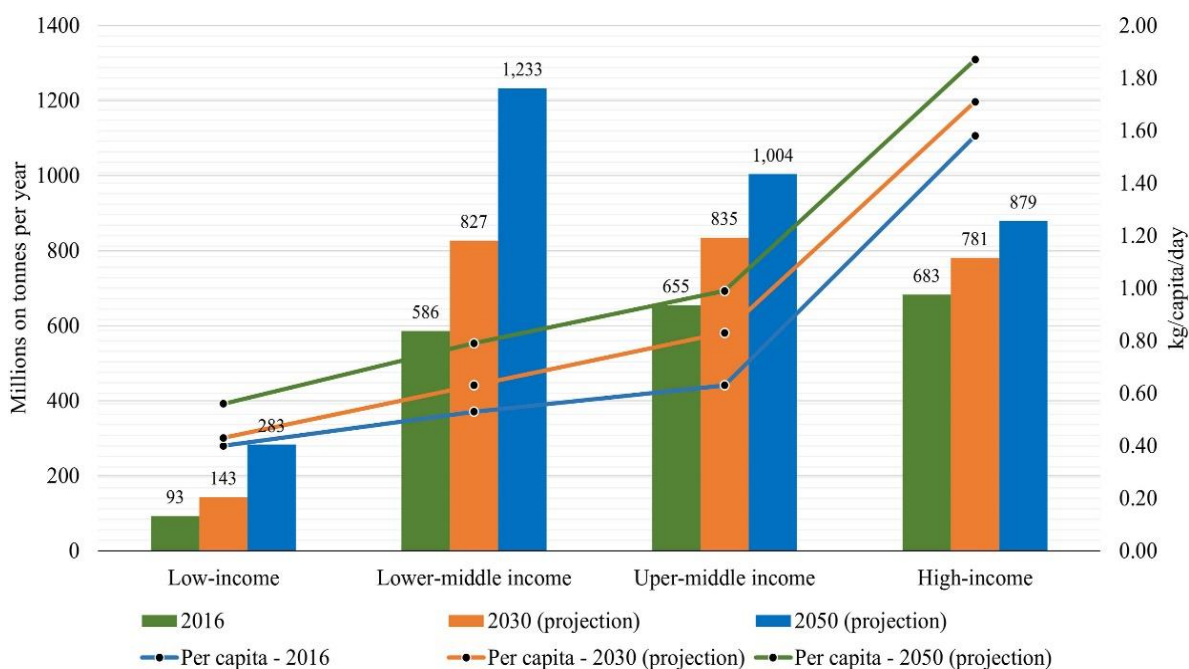
Figure 2-5. Waste generated by income level, [23]

According to the last data available, in 2018, the total waste generated by all activities and households for the twenty-eight members of the European Union (EU-28) reached 2337 million tons (being the highest amount during the last 10 years reported) which translates into an average of 4931 kg per inhabitant of the EU. On the other hand, data from the same year shows that the EU-28 generated 812 million tons of waste excluding major mineral wastes, equivalent to 35 % of the total waste generated, Table 2-2. It means, on average, 1.8 tons per inhabitant of waste excluding major mineral wastes were produced [25].

Figure 2-6 shows the production of waste by economic activities and households in the EU. According to these data, it can be observed that the construction sector accounted for 34.7% of the total waste generated, and manufacturing represented 10.2%.
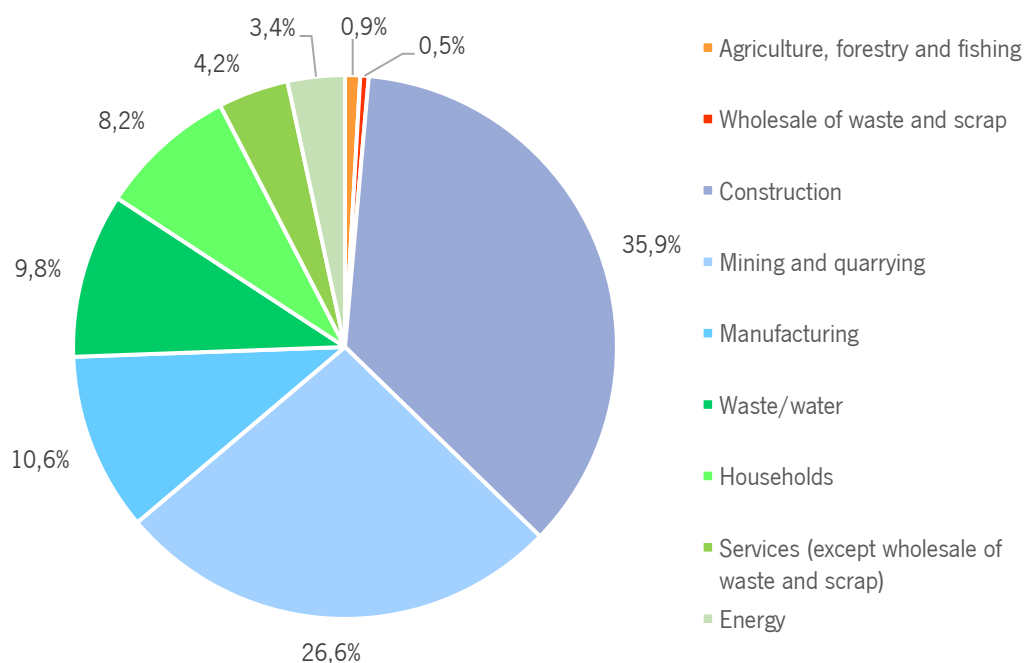
Figure 2-6. Waste generation by economic activities and households, EU-28, 2018 (%), [26]

Waste generation, excluding major mineral wastes, increased, on average, by 4.2% between 2004 and 2018, and when expressed about population size, the EU generated, on average, 1.8 tons per capita in 2018. Regarding each waste component (Table 2-2), it should be noticed that the construction waste increased by 20.1% during the 2004- 2018 period, thus showing an opposite behavior compared with other sectors. In contrast, in the same period the manufacturing waste generation, decreased quite considerably, by 24.9%. However, there is no doubt that there is still a lot to do. Ceramic production and its corresponding waste generation are strongly related to both sectors. The numbers confirm the relevance of waste valorization to proposing new management and treatment alternatives.

Regarding waste treatment, in 2018, around 2200 million tons of waste were treated in the EU. It excludes the exported waste but includes the treatment of waste imported into the EU. Thus, the registered data cannot be directly compared with those on waste generation. The recycled waste used for backfilling, i.e., the waste used in excavated areas for slope reclamation, safety, landscape engineering purposes, or incinerated with energy recovery rose by 33.9 % from 2004 to 2018. As a result, the share of such recovery in total waste treatment grew from 45.9% in 2004 to 54.6% in 2018, consequently, the waste final disposal diminished by 4.2%. The share of disposal in total waste treatment reduced from 54.1% in 2004 to 45.4% in 2018.

Table 2-2. Waste generation rate of change, excluding major mineral wastes, EU-28, 2004-2018, [26]

	2004	2006	2008	2010	2012	2014	2016	2018	Rate of change 2018-2004 (%)
Total	779.5	789.9	760.5	758.7	758.0	769.0	784.7	812.0	4.2
Agriculture, forestry, and fishing	62.3	56.7	45.5	20.2	20.4	17.7	19.7	19.5	-68.8
Mining and quarrying	10.4	7.1	10.0	7.9	7.5	7.7	6.9	8.1	-22.6
Manufacturing	239.9	225.8	216.8	190.5	176.4	175.9	178.9	180.1	-24.9
Energy	85.4	93.3	84.1	78.6	88.8	87.4	74.7	75.7	-11.4
Waste/Water	75.2	83.3	98.9	129.9	155.0	180.7	196.9	207.6	175.9
Construction	34.4	33.4	34.8	42.5	39.8	38.6	37.8	41.3	20.1
Other sectors	97.7	112.2	88.8	102.3	88.9	85.1	88.8	94.0	-3.7
Households	174.1	179.2	181.6	186.0	180.7	175.9	181.4	185.7	6.7

Portugal is a country with a population of around 10 million people. It has two territories, the islands, and the continental region which is composed of 5 regions. In the past two decades, Portugal has increased by 13% the generation of municipal solid waste (MSW) and Figure 2-7 represents it by region. According to PORDATA (2002 to 2018), Portugal collects 100% of the generated MSW, of which around 60% corresponds to landfill disposal, 16% accounted for energy valorization of MSW treatment while recycling 13% and composting 8.4%. However, in 2018, the selective collection represented 20.4% and the other 79.6% of Portugal's waste had an undifferentiated collection [23]. Moreover, in the physical composition of wastes, the organic fraction (36%) is the predominant, plastic and textiles wastes correspond to 12%, each, followed by paper (10%), glass (7%), and others (23%).
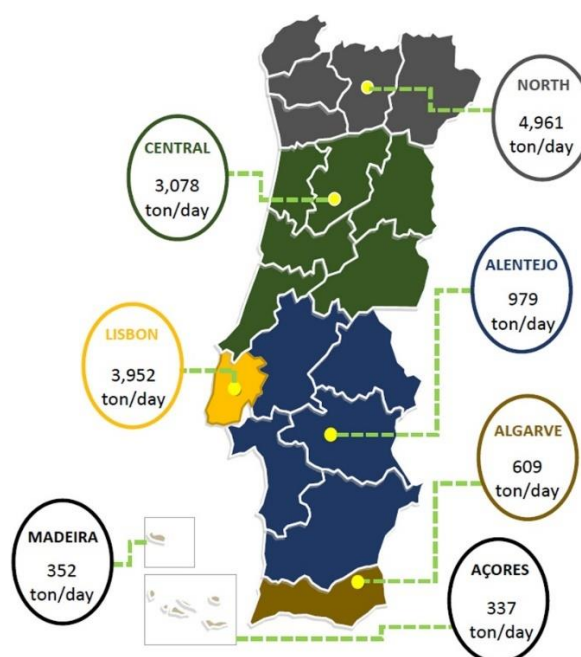
Figure 2-7. Total collected MSW by region in Portugal, [23]

17

On the other hand, according to the World Bank, in Latin America, 160 million tons of solid waste are produced per year, with an average per capita value of 1.1 kg/day. Even more, by 2030, with a predicted population increase of 17%, totaling 705 million, waste generation per capita will increase above 45%, reaching 1.6 kg/day, [27]. Besides, in the Latin America and the Caribbean (LAC) region, over 35,000 tons of waste is left uncollected every day, affecting over 40 million people, approximately 7% of the population, especially people in marginal areas, such as slums and informal settlements, and some rural areas. In LAC only around 1–20% is reused or recycled, while up 60% of the waste ends up in improperly controlled landfills. It is known that solid waste composition in Latin America is mostly organic, although it is expected it will change, becoming mostly non-biodegradable [28].

In general, it can be concluded that the waste collection management and final disposal change depending on several factors, such as the country's area, population and city densities, government policies, and the income level that affect waste generation.

2.1.4. Industrial ceramic waste

Ceramic materials are manufactured abundantly in different parts of the world, it is also exported to other regions due to their durability and variety in design. Except for the ceramic industry's vast economic benefits, it causes adverse environmental impacts through high large pollutant releases and energy consumption [29].

In general, the term ''ceramic'' (ceramic products) is used to designate inorganic materials (with some possible organic content), consisting of metallic and non-metallic elements; and of permanent manufacture by a firing process becomes a solid object that has a partially crystalline and partly vitreous structure. Among the general properties of ceramic products is high mechanical resistance, wear resistance, long service life, chemical inertness, safety, resistance to heat and fire, and sometimes also specific porosity.

The industrial activities that belong to the ceramic industry description are varied and the largest manufacturing sectors for ceramic products are the following: floor and wall tiles, bricks and roof tiles, ornamentalware (household ceramics), refractory products, sanitaryware, technical ceramics, vitrified clay pipes, expanded clay aggregates, inorganic bonded abrasives, [30].

In the process of different ceramic materials production, several types of industrial pollutants are released into the environment, like emissions to air, water, and soil. The quantity, type of emissions,

and waste depend on several parameters such as used raw materials, auxiliary agents used, fuels, and production methods. It is shortly described below [31]:

- *Emissions to the air*: particulate matter / ceramic dust, soot, emissions of combustion gases (carbon oxides CO_x, nitrogen oxides NO_x, sulfur oxides SO_x,) inorganic compounds of fluorine and chlorine, volatile organic compounds that may come from processes such as: grinding, polishing, enameling and firing or baking.

- *Emissions to water:* the wastewater from the process contains mainly mineral components (insoluble particulate material), small amounts of organic material, as well as some heavy metals that come mainly from washing operations.

- *Solid waste:* Ceramic industries produce a large amount of solid waste which is discarded without any further treatment. This solid waste led to severe environmental pollution and significant land occupation. Waste materials produced are about one-third of the total ceramic production. The ability to handle this waste depends on the geographic location of the industry, resource availability, company size, and strategic attitude [2]. An important amount of ceramic waste (e.g., pellets, ash-powder, different types of sludge, broken ceramics) is produced in different phases such as grinding, cutting, dressing, and polishing inside the industrial plant.

The construction industry shows an increasing demand for new, bold, sustainable structural and non-structural materials. Ceramic products represent a significant part of the construction industry and, consequently, the requirements in terms of raw materials are also raising. Natural resources are facing a decrease with time due to uncontrolled uses. It is worth noting that progress in the incorporation of alternative materials might be a useful way to diminish the use of natural resources by recycling the ceramic waste coming out from the industries. Recycling and reuse of waste materials suggest energy saving, cost reduction, possibly superior products, and fewer or no hazards to the surrounding environment [32]. The use of waste materials also reduces the problem of land-filling, environmental, and health concerns. It is the motivation for the development of this project, therefore solid waste as the floor and wall tiles and sanitaryware from the ceramic industry will be used. It is also considered the possibility to use ceramic waste from construction and demolition waste, due to their availability and generation trend. As it will be shortly explained below.

In the ceramic industries mentioned above, solid waste is mainly generated: by the rejection of ceramic products already fired, the plaster molds that have fulfilled their useful life and cannot be reused. The improper handling of raw materials, the generation of sludge by the treatment of liquid waste, mainly from washing processes, and dust from air pollution control equipment. It should also be noted that the rejection of ceramic products is due to a failure depending on the quality required of the final product. In a well-controlled industrial plant, approximately 80% of the parts that come out of the kiln are acceptable. The remaining 20% is divided into 6% percent of rejects and 14% percent of recoverable material; this recoverable percentage is subjected again to: fired and glazed; and you get an acceptable 10% percent and a 4% percent that is rejected again. In this way, 90% of the total number of pieces entering the kiln can be obtained as a salable product. It should be taken into account that it is very likely that not all ceramic industries will obtain these returns [30].

In recent years, China is the largest producer (i.e., 47% of global output) and consumer (i.e., 41% of total consumption) of ceramic tiles in the world. It occupies more than half of all ceramic production around the world [33]. In Europe, Spain for example, the manufacturers' sector of ceramic tiles has reached a production superior to the six hundred million square meters in the last years, situating itself between the four first producers of the world. This may involve the generation of around 50,000 tons of fired waste per year [34]. In Ecuador, there is a study about the use of the ceramic residue, of one sanitaryware ceramic industry called "EDESA", for the manufacture of pavements. Where it is mentioned that 350 to 450 tons per month are generated and disposed into the sanitary landfill of the city of Quito (capital of Ecuador) [30].

2.1.5. Construction systems with waste incorporation

Nowadays, industrial waste generation is a significant concern in terms of the environment, health, and its final disposal. Recycling and using such wastes in innovative construction materials appears to be a viable solution not only to the pollution problem but also an economical option in the construction sector by providing a potentially sustainable source. However, integrating recycled materials in newer construction purposes is not a fresh concept, it has been practiced since the Roman Empire times when people reused stones obtained from former roads in building new ones. Recycled materials have been into study for their incorporation in new construction works for quite some time [35]. Still, the construction industry shows an important possibility to apply, in a direct or indirect strategy, significant percentages of several types of by-products and/or waste. Some of the best

common examples are mentioned: fly ash, construction, and demolition waste, blast furnace slags, which have been used as a cement or aggregate replacement, embankment fill, road, and railway pavement foundation, among others. It is thought that there is room for the further use of increased volumes of these residues and, also, to introduce new types of industrial by-products in the production chain [36].

Table 2-3 shows the usage of different industrial waste *in the* design and development of construction and mortar) as results of the various test conducted on construction material by various researchers during their research work.

Table 2-3. Design and development of construction material using industrial waste, [37].

No.	% of waste material used for the production of mortar or concrete	Size of molds for casting	Curing Days	Conducted Tests
1	Quarry Dust, (0 -40%) Rice Husk Ash (0 -20%)	150x150x150mm 50x50x50 mm	3, 7, 21, 28, 56, 90	Compressive strength, mini-slump cone test, mini v-funnel test,
2	Crumb Rubber (0 – 30%)	50x50x50 mm 25x25x200mm 25x25x28.5mm	28	Compressive strength, flexural strength, length change, the stress-strain curve
3	Sewage Sludge Ash (0 – 20%)	Cylinders of 50 mm dia. and 100 mm ht.	7, 28	Compressive strength
4	Paper Mill Sludge Ash (0.4 – 20%)	40x40x160mm	1, 7, 28, 60	Compressive strength, water to binder ratio
5	Class F-Fly ash (10 – 30%)	70.7x70.7x70.7mm	28	Compressive strength
6	Rice Husk Ash (0 – 20%)	150x150x150mm 50x50x50 mm	28, 90, 180	Compressive strength, setting time, water absorption, tensile and flexural strength
7	Fly Ash (0 – 100%)	50x50x50mm	7, 28	Compressive strength, the effect of thermal exposure
8	Paper Pulp in concrete (5 – 20%)	150x150x150mm 100x100x500 mm	14, 28	Compressive strength, flexural strength, split tensile strength,
9	Pumice Fine Aggregate (0 – 100%)	40x40x160mm	2, 7, 28, 56	Compressive strength
10	Ground Granulated Blast Furnace Slag (0 – 65%)	150x150x150mm 70.7x70.7x70.7mm	3, 7, 28	Compressive strength

New techniques aiming at controlling and reducing the environmental impacts of the construction chain have become important, particularly concerning building materials. Some studies related to waste incorporation in civil construction are showing up next and along with the present document.

Buratti et al. [38], produced panels using rice husk (RH) by gluing and pressing the raw material. The recycled waste panels underwent tests of thermal, acoustic, and environmental. Its acoustic and thermal performance was compared with the ones of six panels composed of other recycled materials (cork scraps, end-life tires, coffee chaff, wastepaper, textile fiber mats, wool fiber scraps), manufactured with similar techniques. The results lead to the conclusion that considering the acoustic and thermal behavior, the wool fiber scraps present a very good performance. Life cycle analysis was made in compliance with ISO 14040. The production of 1 m² of RH and coffee chaff panels presented the best environmental performance.

Wiemes et al. [39], incorporated great amounts of different types of waste as raw material in brick's formulation (automotive industry waste sludge with heavy metals presence; glass waste (GW), from a galvanic plant, and wood ash (WA) from the ceramic burning furnace). It was a case study on a laboratory scale. The work was focused on the waste minimization line, with a change in the process, replacing clay with industrial waste. The obtained results showed that obtaining a red ceramic (brick) is considered technically feasible in firing temperature to 800 °C for 6 h, by incorporating a significant number of wastes from the automobile industry, more addition of GW and WA. However, special attention should be given to initial sample preparation (the mixture of materials), compaction, and free of clumps, which can prejudge the outcome of the final product. There was no detection of heavy metals in the composition, demonstrated by leaching and solubility tests, that confirm the presence of a vitreous phase in the obtained ceramic.

Munir et al. [40], used waste marble sludge (WMS) in the production of energy-efficient burnt clay bricks on an industrial scale. In an industrial brick kiln, burnt clay bricks were prepared using several dosages of WMS (i.e., 5%, 10%, 15%, 20%, and 25% by weight of clay), under actual field conditions. It was observed different physic-mechanical and thermal properties. It was detected that lightweight bricks can be manufactured using WMS (up to 15%), therefore the overall construction costs are lower. Based on this study, for the manufacturing of burnt clay bricks, 15 wt% WMS is considered optimum. It helps to lead with sustainable, economic, environmentally responsible energy-efficient construction.

Coppola et al [41], manufactured Portland-free mortars for conservation, restoration, and retrofitting of existing masonry buildings and concrete structures using a ground granulated blast furnace slag

activated with alkali powder. It is highlighted that the key parameter that regulates most of the properties both in the fresh and hardened state of alkali-activated compounds is the activator/precursor ratio, influencing the mechanical performances, the rheological properties, and the shrinkage: the higher the activator dosage, the higher the consistency class and shrinkage. Furthermore, the elastic modulus of slag-based mortars is lower than that of OPC mortars in the same strength class. Alkali Activated Materials (AAMs) resemble to have promise for a sustainable future in construction since the Global Warming Potential (GWP) and Gross Energy Requirement (GER) are reduced by about 80% compared with traditional Portland cement mortars with the same compressive strength.

Briga-Sá et al. [42], used different percentages (6.25%, 8.16%, and 8.75%) of textiles wastes (TW) to be incorporated into cement-based lightweight blocks (LWB). The study aimed to know the thermal performance of the developed LWB, where results showed their suitability for thermal insulation applications. Thermal resistance values of 0.34 m2°C/W, 0.61 m2°C/W, and 0.67 m2°C/W for the LWB1, LWB2, and LWB3 were estimated, respectively. Concluding that higher thermal stability is achieved when a higher percentage of TW is incorporated in the cementitious mixture composition. The comparison of the LWB with currently available building materials, such as simple masonry walls and insulating concrete forms, revealed promising results for the proposed textile waste-based materials.

Bagarić et al. [43], presented a case study of dynamic hygrothermal performance of a developed building envelope system under real outdoor climate conditions and with real occupants living in the house for one year in 2017/2018, (Croatia). For this purpose, ventilated prefabricated sandwich walls, containing a high amount of construction and demolition waste (50%), were built. The impact of panels' high massiveness on the energy performance of an exemplary building was assessed according to the new EN ISO 52016-1:2017 standard for different climates and different operating modes of technical systems. After experimental monitoring and transient numerical simulations, it was concluded that a heavyweight envelope constructed with ventilated prefabricated wall panels from CDW can perform satisfactorily, from both hygric and thermal aspects. Therefore, the presented envelope system could foster the large-scale deployment of buildings, however, the applicability for other climates and conditions of use should be verified first. Future work is needed especially related to the efficiency of ventilation for different conditions (climate and building use), monitoring of indoor comfort (in terms of temperature, relative humidity, CO_2), and energy consumption in ground floor apartments.

Benallel et al. [44], develop and characterized new thermal insulation materials from cardboard waste and plant fibers. Four different types of agricultural by-products plenty available in the South-East of Morocco (reed, alfa, fig branches, and olive leaves) with different mass fractions of cardboard waste (20%, 30%, 40%, 50%, and 60%) were used. Results showed that the increase in fiber content caused a slight increase in bulk density and thermal conductivity while the maximum rate of water absorption decreased significantly. The lowest thermal conductivity value was 0.072 W/m.K with a density of 176 kg/m^3 and a maximum water absorption rate of 262%, which corresponded to the composite of 40% alfa fibers and 60% cardboard waste. It was concluded that the developed insulation panels exhibited good insulating properties compared to conventional insulation materials and several environmental and economic advantages were identified.

Lazorenko et al. [45], studied the influence of shape and size of plastic waste on the fresh-state and hardened-state properties of geopolymer (GP) mortars. GP was made using fly ash and waste plastic bottle (PET) in form of shredded flakes, strips, and grinded particles of different sizes. Results showed that regardless of the shape of plastic aggregate, adding the waste PET to fresh geopolymer mortars reduced workability. However, the GP including PET particles had near workability and flexural strength to the control sample, the compressive strength and splitting tensile strength were lower due to poor interaction between PET particles and the matrix. Still, the PET grinded particles were the most effective form of aggregate. Future work is needed to enhance the adhesion at the interface of PET particles and GP mortars.

2.2. CIRCULAR ECONOMY

Population in the world is growing and with it the demand for raw materials. However, the supply of pivotal raw materials is restricted. Moreover, extracting and using raw materials has a major impact on the environment. It also increases energy consumption and CO_2 emissions. Nevertheless, smarter use of raw materials can lower CO_2 emissions. The European Commission is convinced that the transition to this circular model, outlined in Figure 2-8, will contribute to the creation of more jobs and will encourage companies to invest in the innovation of their products and processes. At the same time, the protection of human beings and the environment will be safeguarded.
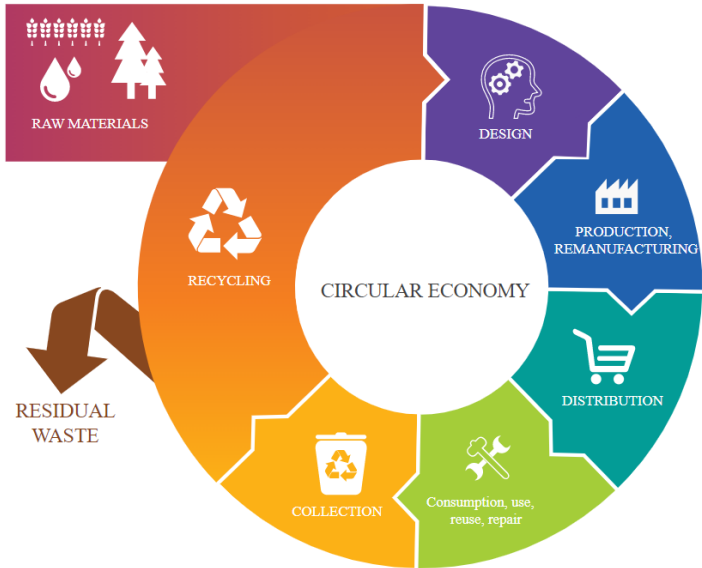
Figure 2-8. Circular economy model,[46]

The concept of the "circular economy" has gained significant traction since its introduction a half-century ago. Scholars, practitioners, governments, and non-governmental organizations have recognized the apparent appeal of closing material loops, reusing and recycling industrial "nutrients" to extract their maximum value with minimum waste. The intense activism by the Ellen Macarthur Foundation since its foundation in 2010 [47], and its international partners, which involves large organizations such as Google, Unilever, Philips, and Renault, shows the concern from the industries side. While from the scientific side the interest has significantly grown, where 75% of all CE publications have taken place in the last 5 years, as exhibited in Figure 2-9.
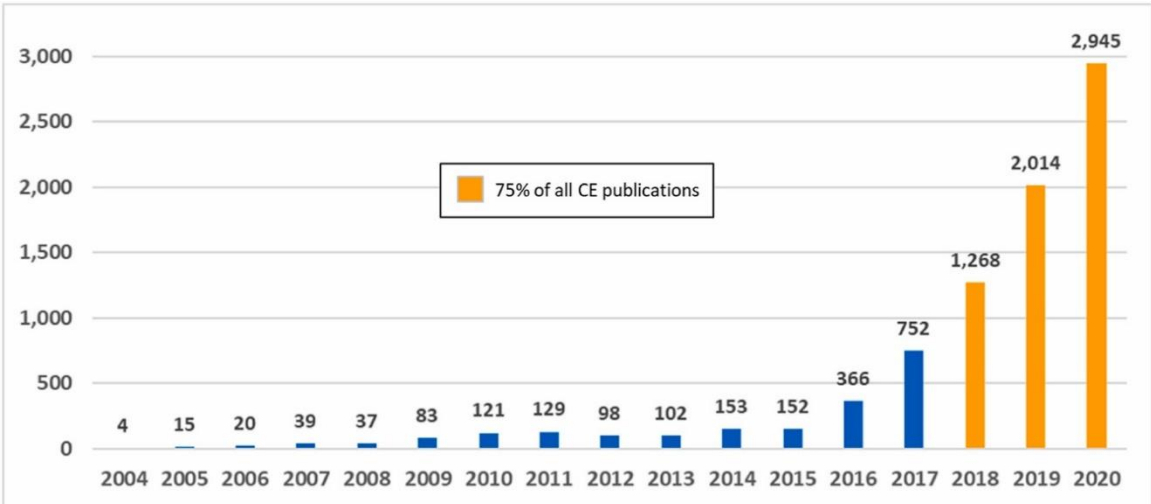
Figure 2-9. Circular Economy publications (source: Scopus®), [48]

Table 2-4 is presented a few CE concept definitions from different authors, while Table 2-5 shows the basic principles related to CE. It can be confirmed once more that waste management is one of the fundamental principles to consolidate a CE.

Table 2-4. Circular Economy sources and definitions, adapted from [48]

ID	Author	Citations	Circular Economy Definition
1	Ghisellini, Patrizia	1495	"Circular economy (CE) as a new model of economic development promotes the maximum reuse/recycling of materials, goods, and components to decrease waste generation to the largest possible extent. It aims to innovate the entire chain of production, consumption, distribution, and recovery of materials and energy according to a cradle to cradle vision", [49]
2	Geissdoerfer, Martin	1364	"A regenerative system in which resource input and waste, emission, and energy leakage are minimized by slowing, closing, and narrowing material and energy loops. This can be achieved through long-lasting design, maintenance, repair, reuse, remanufacturing, refurbishing, and recycling", [50]
3	Bocken, Nancy M. P.	1137	"The circular approach contrasts with the traditional linear business model of production of take-make-use- dispose and an industrial system largely reliant on fossil fuels, because the aim of the business shifts from generating profits from selling artifacts to generating profits from the flow of materials and products over time", [51] "Circular business models thus can enable economically viable ways to continually reuse products and materials, using renewable resources where possible", [51]
4	Korhonen, Jouni	867	"Circular economy is an economy constructed from societal production-consumption systems that maximize the service produced from the linear nature-society-nature material and energy throughput flow. This is done by using cyclical materials flows, renewable energy sources, and cascading1-type energy flows. A successful circular economy contributes to all three dimensions of sustainable development. Circular economy limits the throughput flow to a level that nature tolerates and utilizes ecosystem cycles in economic cycles by respecting their natural reproduction rates", [52]
5	Ellen MacArthur Foundation	N/A	"A circular economy is based on the principles of designing out waste and pollution, keeping products and materials in use, and regenerating natural systems", [47]

Table 2-5. Circular Economy-related basic principles

ID	Principle	Description
1	9R Framework	A set of 9 strategies to be considered for a CE approach, in order of priority: Refuse, Rethink, Reduce, Reuse, Repair, Refurbish, Remanufacture, Repurpose, Recycle, Recover.
2	Waste Hierarchy	A priority operations order in waste management: prevention, preparing for reuse, recycling, another recovery (including energy recovery), and disposal.
3	Clean and Renewable Energies	The use of clean and renewable energy sources instead of fossil and polluting sources.
4	Upcycle	Transforming waste materials, useless, or unwanted products into new materials or products with high perceived value.
5	Resource Efficiency	The use of the planet's limited resources in a sustainable manner and minimizing environmental impacts, delivering greater value with less input.
6	CE Categories	Re-principles, waste, efficiency, value retention, sustainability, resources, design, system perspective, energy, cycles.

The CE is based on three essential principles: "(1) Designing waste and pollution, (2) keeping products and materials in use, and (3) regenerating natural systems". Moreover, the CE is a complex system that links different markets, stakeholders, material, information, and energy flows. CE transition goes further than market changes and indeed impacts sustainability, so it is important to identify the high complexity emerging from the relationships between actors, strategies, energy, material flows, and the circular ecosystem.

Assessing the sustainability impacts of circular systems is another significant challenge. Although the circularity action can be estimated by different methodologies, such as Life Cycle Assessment, Data Envelopment Analysis, Simulation, Material Flow Analysis, and others, a practical measuring method is not an easy task. The circularity complexity has been classified into five levels; the first one is short-time and micro-scale, including single products or services. The complexity grows as the time lengthens and the unit of analysis extends to industries, industrial parks, regions, countries, and the whole planet. These levels of complexity drive to different CE execution levels (policy level, organizational level, and consumer level). There are several barriers to the implementation of CE despite its benefits linked to strategies to achieve sustainability and minimize the environmental impact of economic growth. It has been implemented guided by soft drivers, such as legislative policies, but at the same time, it has challenging barriers, such as lack of technical solutions and low financial investment. Some authors account for six limitations and challenges for a CE that is associated with (1) system boundaries, (2) physical scale of economy, (3) governance, (4) thermodynamic, (5) social, and (6) cultural context. Singularly, the mentioned thermodynamic limit is about the transformation in the system to close the loop. Nevertheless, new flows of resources are constituted with CE, causing more waste and emissions [53].

On the other hand, it is well known that industrial activities worldwide, annually produce massive quantities of waste that induce huge problems for their treatment and disposal, along with a financial loss and energy emission. Hence, creating novel sustainable materials and products, developing green manufacturing processes, and following a reliable life cycle management is the only feasible way to reverse the actual situation, to enhance the Circular Economy. In this way, the so-called geopolymers (GP) are a sustainable typology of hydraulic (alkali-activated) binders that are widely studied globally being a promising and valid substitution of the traditional cementitious materials, such as the OPC. Lately, the use and production of GP products have called the attention of more and more researchers for their superior mechanical properties that make them suited for different applications in

construction. Concerning climate change and greenhouse gas emissions, GP could efficiently mitigate the CO_2 emissions released by the cement plants and the related industries (i.e., aggregate, additive, etc.). Furthermore, GPs' manufacture represents a relatively low energy consumption with low emissions of the pollutant. Also, GP technology offers the indisputable benefit of the great potential of incorporating vast typologies of wastes as raw materials improving the sustainability of processes and products. So far, different by-products and wastes have been studied, so, GP raises high expectations as a new binder material to be widely used in construction as, e.g., a substitute for OPC. Therefore, GPs enable the redirection of the current waste streams from landfills and the substitution of a carbon-intensive product, in the perspective of the circular economy [54].

2.2.1. Life cycle assessment (LCA)

Life Cycle Assessment (LCA) is an efficient and methodical tool for measuring the potential environmental burdens related to a product, process, or activity by determining, quantifying, and evaluating the impact of the used energy, materials, and wastes discharged to the environment. LCA considers the possible environmental impacts along a product's life cycle (i.e., cradle-to-grave) from raw material acquisition through production, use, and disposal [55]. LCA is an iterative process, as illustrated in Figure 2-10, that involves the ISO 14000 series in the development of its main stages:

i)   Goal and Scope Definition, and

ii)   Life Cycle Inventory (LCI); International Standard ISO 14041

iii)   Life Cycle Impact Assessment (LCIA); International Standard ISO 14042

iv)   Life Cycle Interpretation of results (LCIR); International Standard ISO 14043

The goal and scope definition of an LCA describe the product system in terms of the system boundaries and a functional unit. The functional unit is the essential basis that allows alternative goods, or services, to be compared and evaluated. The functional unit is defined as a quantitative description of the service performance (the needs fulfilled) of the investigated product system(s).

LCI stage includes compiling data for each unit process regarding all relevant inputs and outputs of energy and mass flow, air emissions, and soil and water discharges caused by or otherwise attributable to a product's life cycle. This phase also includes calculating both, the material and energy input and output of a building system. The Life Cycle Impact Assessment (LCIA) is an evaluation of a product life cycle, on a functional unit basis, in terms of several impact categories by analyzing all

environmental burdens obtained in the LCI. Finally, Life cycle interpretation ensues at every phase in an LCA. When two product options are compared and one of them shows higher consumption of each material and each resource, an interpretation purely based on the LCI can be irrefutable. However, it is possible to compare across impact categories, especially when there are trade-offs between product alternatives, or if it is worthwhile to prioritize areas of concern within a single life cycle study.
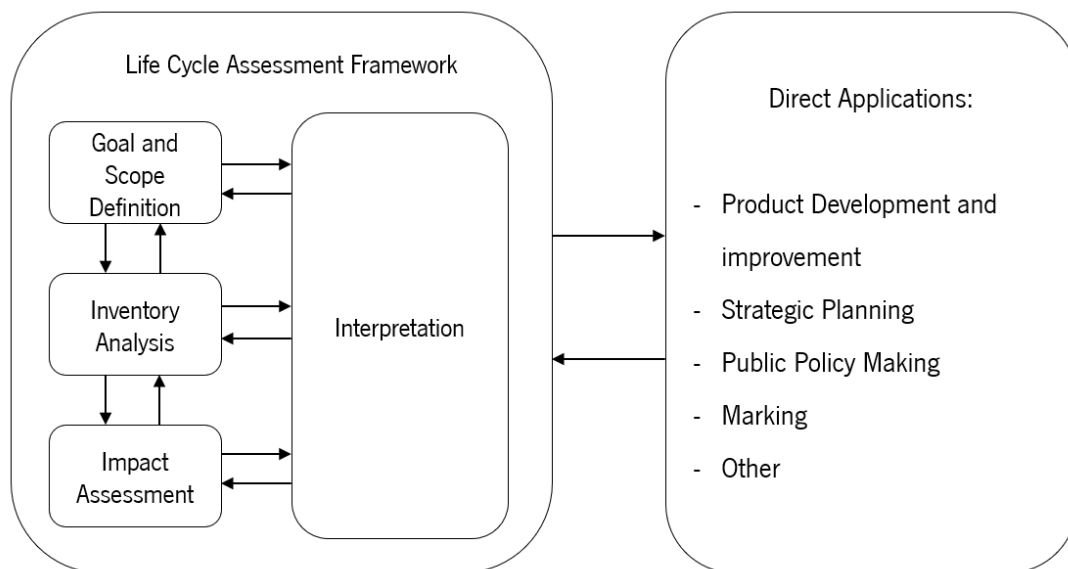
Figure 2-10. Phases and applications of an LCA, (ISO 14040:2006)

For the development of LCA, the use of the software is needed as the main tool, and depending on the potential users, there is dedicated software. In general, it can be classified into three types of software:

• Generic LCA software is commonly designed for use by researchers, consultants, and other LCA specialists.

• Specialized LCA-based software of different types for specific decision-makers, generally intended for use by designers in engineering or construction, the purchasing department, or environmental and waste managers.

• Tailored LCA software systems to be used for clearly determining applications in specific IT environments (as interfaces to business management software). These are usually firm-specific adaptations of generic software or software packages programmed directly for the needs of the firm [56].

Regarding LCA, government, and policy, Governments play a key position in instituting the frameworks and conditions for the production and consumption patterns of goods and services in our societies.

As a tool undertaking the environmental mainstay within the concept of sustainable development, LCA is relevant in developing and supporting linked strategies to help diminish wastes, emissions, and the resources consumption that are ascribed to the supply and consumption of goods and services.

The EU policy seeks for developing a sustainable, climate-neutral, circular, and bio-based economy. Some of these policy initiatives have been conceived under the umbrella of the European Green Deal, which specifies the EC's priorities for the period 2019-24. Summing up, the policies aim to support the unlink of economic growth from resource use; allow the gradual implementation of the net-zero GHG emissions target by 2050, with transitional goals for 2030; and guarantee that people and regions are implicated and not outpace in this transition. In this way, each of the policy documents contributes by sketching specific targets and strategies for their specific field of action and related stakeholders. Figure 2-11 depicts five policy pursuits related to EU building stock development and building construction and operations:

Policy documents

Policy objectives	European Green Deal	Circular Economy Action Plan	Biodiversity Strategy for 2030	European Climate Law	Renovation Wave for Europe	A Clean Planet for All	Bioeconomy Strategy	New Industrial Strategy	EU SDGs	Waste Framework Directive
1. Improvements to energy efficiency	++	.	.	.	+++	++	.	+	++	.
2. Increases in renewable energy	++	.	+	.	++	+	.	+	++	.
3. Low-carbon material uptake	++	++	.	.	+	+	++	++	++	++
4. Climate change adaptation and resilience	++	+	+	+	+	+	.	.	++	++
5. Monitoring of environmental performance	++	++	+++	+++	++	.	++	+	++	.

Figure 2-11. Mapping of the EU policy documents with defined policy objectives, highlighting their focus, [57]

On the other hand, in LCA when a process generates more than one product, the environmental impact of this process needs to be assigned between the product and the by-product. If the by-product is considered waste, all impacts are allocated to the main product, but if this by-product is considered a co-product of the process, then environmental impacts must be shared between the main and co-products. Allocation can be done by mass or any other physical characteristic (e.g., energy). When no physical characteristic is relevant, then allocation can be done by a non-physical one (e.g., economic value) [58].

Partial analyses are useful for civil engineering materials like concrete or alkali-activated materials because they can be included in end-products having different life cycles. As it is known, 1 m³ of concrete can be used in a structure, a wall, a bridge, or a road. Therefore, it is of definite interest to have quantified environmental impacts by providing results for 1 m³ of concrete or any other materials. The use of these data for the construction sector when compared to other materials such as wood or bricks must be made with great attention as the material with the lowest environmental impact per unit of volume (or mass) is not necessarily the one that will have the lowest environmental impact once integrated into a structure over its service life [59].

There are several studies about the life cycle assessment of geopolymers to determine how significant are the environmental impact. Table 2-6 shows the main results of the first LCA articles found about geopolymers, where the conclusions are varied, and they highly depend on the studied product.

Table 2-6. First articles on the life cycle assessment of geopolymers, [58]

References	Weil et al., 2009	Habert et al., 2011	McLellan et al., 2011	Turner and Collins, 2013	Yang et al., 2013
Functional unit	1m of compliant concrete	1m of Concrete with a mix design	1m concrete	1m concrete of 40 MPa	1m concrete of 24,40,70 MPa
System boundaries	Cradle to grate	Cradle to grate	Cradle to grate	Cradle to construction	Cradle to preconstruction
Reference OPC	Freeze-thaw resistant concrete according to DIN EN 206 1 DIN 1045 4	Equivalent mechanical strength	100% OPC (2) OPC and slag (2) OPC and FA (2)	1 OPC	100% OPC (3); OPC+ SCM (3)
Number of geopolymers	1 hybrid slag fly/ash ratio 80:20 cured, room cure	FA (8 refs, 48 mixes) GBFS (4 refs, 12 mixes) MK (4 refs, 17 mixes)	FA (4)	FA (1)	AA GGBS (3), AA FA (3), AA MK (1)
Data source	Ecoinvent, literature, industry	Ecoinvent, literature, industry	Literature, calculation	Industry and the Australian government	Korea LCI Database Information Network, Japanese database
Data quality	Very good to adequate	Good, but lack control for MK No, mass, economic	Good, but lack control for MK	Good	Good

Table 2.6. (*Continued*). First articles on the life cycle assessment of geopolymers, [58]

Impact considered	3 indicators: ADP, GWP, CED	10 indicators	Energy, greenhouse emissions, and cost	Co2 footprint	Co2 footprint
Conclusion	Improvement on GWP, but a similar impact on ADP and CED	Higher impacts in other categories than global warming	Results depend on the transport distance	Small improvement when taking into account the process	Favorable to geopolymers

Note, OPC: Ordinary Portland cement; AA: alkali-activated; SCM: supplementary cementitious materials; FA: fly ash; GBFS: ground blast furnace slag; MK: metakaolin; ADP: abiotic depletion potential; GWP: global warming potential; CED: cumulative energy demand.

More recently, different studies with different LCA approaches have been carried out, to mention, a study conducted in Italy that applied the LCA methodology to evaluate the environmental performance of the current regional management of CDW and to identify critical aspects and possible improving actions [60]. In Hong Kong, it was developed a Life-Cycle Cost-Benefit Analysis (LC-CBA) framework through the integration of the life-cycle assessment (LCA) and cost-benefit analysis (CBA) to guide decision-making in sustainable food waste management. The author suggests the LC-CBA developed in the study is widely applicable to inform decision-making on sustainable food waste management worldwide [61]. More recently studies of LCA related to the incorporation of different wastes, such as in road construction as a tool to quantify the potential impacts derived from the use of traditional and alternative materials [62] have been made.

Salas et al. [63], conducted an LCA of a Geopolymer Concrete (GC) after scaling up the LCI from laboratory scale to industrial scale and concluded that sodium hydroxide production is the most relevant life cycle process regarding the environmental performance of GC, as it is also a main raw material in the production of sodium silicate. Other items such as concrete mixing facilities, curing process, and transport, affect a few impact categories each one.

Bianco et al. [64], studied concrete of strength classes 35, 50, and 70 MPa and developed a silicate activator derived from waste glass (AABR). It was compared with the Ordinary Portland Cement concrete and alkali-activated concrete made with commercially available chemicals (AABC). Results showed that when waste glass-based activator is used, a significant reduction in every environmental category is evidenced in comparison to the use of commercially available chemicals. Besides, usage of alkali-activated concretes rather than of OPC concrete lets a significant decrease in environmental categories, such as global warming (≈64% for AABC and 70% for AABR), acidification potential (≈23% for AABC and 35% for AABR), and terrestrial eutrophication (≈53% for AABC and 60% for AABR).

2.3. GENERAL DESCRIPTION OF ALKALI ACTIVATION

Alkali activation is the generic term that is used to designate the reaction of a solid aluminosilicate (named the 'precursor') with an 'alkali activator, to produce a hardened binder, resulting from the combination of hydrous alkali-aluminosilicate and/or alkali-alkali earth-aluminosilicate phases [65]. Alkali-activated binders (AA) have been associated with a set of possible cement replacement materials able to present similar mechanical performances, but with lower environmental effects [66], [67].

A large terminology is often used regarding these materials, including alkaline cement, geocement, hydroceramic, mineral polymers, inorganic polymers, vitreous inorganic polymers, geopolymer, and alkaline activated materials. All these names refer to similar materials, obtained from similar reactions and procedures [4]. It is common to find the term "Geopolymer" as a synonym for "alkaline activated materials". However, these material systems generally fall within the broader domain of alkali-activation, as explained below.

The word "geopolymer" is often referred to as a subset of alkaline-activated materials Figure 2-12. When the calcium content of the starting materials that react is low, the formation of pseudo-zeolitic structures occurs instead of the characteristic chains of the calcium silicate hydrates, and subsequently, the main gel originates. The activator will normally be an alkali metal hydroxide or silicate. Fly ash with a low calcium content and calcined clays are the most common precursors used in the synthesis of the geopolymer. It should also be noted that the use of the word geopolymer is used by researchers and commercials in a much broader sense, especially in the face of commercialization. The term geopolymer was coined in the 1970s by French scientist and engineer Joseph Davidovits [68], [69].
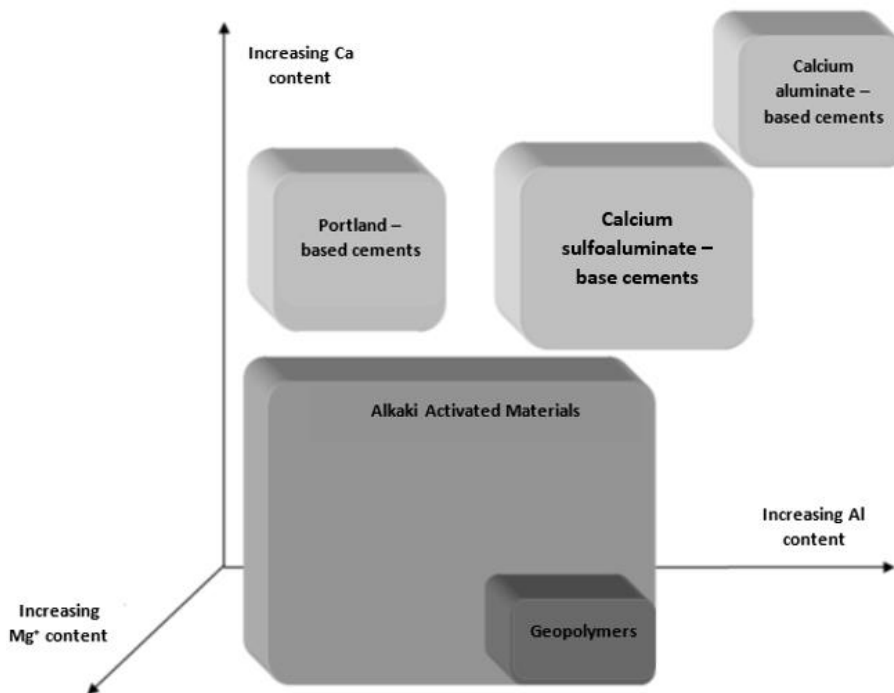
Note: The shading indicates the approximate content of alkali, where the darkest shading corresponds to higher concentrations of Na and/or K.

Figure 2-12. Classification of alkali-activated materials, with comparisons between OPC and calcium sulfoaluminates, [70]

Alkali-activated material is the broadest classification, which essentially embraces any binder obtained by a reaction between a source of alkaline metal (solid or soluble) and a silicate powder [70]. These solids can be calcium-rich or calcium-poor aluminosilicates, such as blast furnace slags or fly ash, respectively. Alkaline sources may include alkali hydroxides, silicates, carbonates, sulfates, aluminates, or oxides, basically any soluble substance that can provide alkali metal cations, increasing the pH of the reaction mixture, and accelerate the solution of the solid precursor.

Two important characteristics attracted attention to alkaline activated materials as host phase for industrial waste: a) these materials are set at low temperature (10–100 °C) to give an amorphous semi-crystalline structure, and b) the product material has some superior properties to Portland cement as chemistry stabilized from acid medium [71]. It can be also stated that the alkali activation process can be divided into three different phases: dissolution of the amorphous phase present in the raw material and nucleation of the resulting species; followed by the precipitation of the nuclei after reaching critical mass; and finally, the crystallization of such nuclei [72].

2.3.1. Factors in the alkaline activation

Alkaline activation is strongly conditioned by some factors as, the starting materials, namely the precursor and activator, as well as the experimental conditions under which the alkaline activation process is carried out (type and concentration, of the alkaline activator, curing time and temperature, pH, among others) [36]. How each of these variables affects the final properties of alkali-activated materials is briefly described below.

2.3.1.1. Potential of hydrogen – pH

The degree of hydrolysis of the aluminosilicates increases with increasing the pH of the solution, although this is true up to a certain point from which an increase in the concentration of OH^- ions do not modify, notably, the amount of solubilized material.

An optimum pH is required to perform the alkaline activation process of aluminosilicates, low basicity leads to a fall in the mechanical strengths of the obtained cement by this process since the ionic strength generated in the "binder-activator solution" system is not high enough to satisfactorily hydrolyze silicon and aluminum present in the starting materials. The amount of hydrolyzed material is directly related to the number of reaction products that are formed in the medium, and therefore, this factor also directly influences the mechanical strengths that will be developed [73].

2.3.1.2. Curing time and temperature

The curing conditions also have a significant effect on the development of the microstructure and the mechanical performance of alkaline cement with silicon aluminium base. In general, the process of alkaline activation of aluminosilicates is carried out at temperatures between [50 - 90] $^{\circ}$C to favor the dissolution of the starting aluminosilicate since, at room temperature, the rate of dissolution of this type of material is considerably slow [74], [75]. The mechanical strengths of alkaline cement increase as the curing temperature increases, especially during the first hours of reaction. This is due to an increase in temperature affecting the kinetics of the reaction, accelerating it, so that, from a very young age, the cement obtained can develop considerable mechanical resistance. However, it can be adopted until a certain point from which, the increasing mechanical resistance as a consequence of increasing the temperature, is no longer significant [76].

The temperature factor is closely related to the time factor, so a longer thermal curing time translates into a significant improvement in mechanical properties. As happened with the temperature factor, from a certain point, the improvement of the mechanical properties over time is not so relevant because the degree of reaction is already high, and the diffusion mechanisms (slow) control the end of the reactions.

In addition to time and temperature, the relative humidity conditions in the initial curing processes affect the course of alkaline activation reactions. In general, it is suggested to work in conditions of relative humidity greater than 90% since, in this way, the possible carbonation of the cement by the action of atmospheric CO_2 is avoided [76]–[78].

2.3.1.3. Granulometry

The susceptibility of the starting aluminosilicates to the alkaline activation process significantly depends on the amount of amorphous/vitreous phase present in them, since these phases, and not the crystalline phases, are hydrolyzed in a basic medium. An inadequate granulometry reduces the initial aptitude of a material to be used as a source of silicon and aluminum in the synthesis of alkaline cement [76]. Therefore, smaller particle size exposes more vitreous mass, hence, providing more raw material for the reaction. Moreover, the particle size distribution of the waste potentially used as a precursor to geopolymers can have several effects, such as the coarser particles being less active in the geopolymerization process, and they also induce higher porosity of resulting activated material. The result of higher porosity is lower thermal conductivity and faster water and water vapor transport in materials containing coarser precursors [79].

2.3.1.4. Precursor

The most studied precursors in the process of alkaline activation have traditionally been blast furnace slag, metakaolin, and fly ash. More recently, construction and demolition waste (CDW) and waste originating from the ceramics industry [80] have also been studied with that application in mind. Generally, these materials can be classified into two differentiated groups: materials with high and low CaO content [76].

The precursor may be, directly mined as a natural resource (e.g., volcanic ash), intentionally arranged by an activation method from a natural resource (e.g., calcined clay), secondary product (e.g., blast furnace slag), or waste (construction and demolition waste; various wastes from metallurgy) [79]. The solid precursor should be mainly rich in silica and alumina, with the highest possible amorphization degree. This process has been demonstrated to be highly practical for transforming industrial waste and by-products with suitable characteristics into useful materials [81]. Several studies have already proved the suitability of alkali-activated materials to substitute OPC, in a wide variety of applications [82], [83], [82]. There is a study of alkali-activated building materials made with recycled construction and demolition wastes, where ceramic waste takes an important part of this research [84]. More specifically, [34] evaluated the use of residues from ceramic floor tile produced with red and white clays for geopolymer cement, where the residue was activated with NaOH and waterglass.

2.3.1.5. Activator

It is necessary to have a "background" that allows understanding the different possibilities of the combination of the precursors with the activators. In general, alkali salts or alkaline hydroxides are those used as alkaline activators of alkali-activated cement and concretes. They are classified into six groups according to their chemical composition, [4]

1. Alkaline hydroxides: MOH
2. Salts of weak acids: M_2CO_3, M_2SO_3, M_3PO_4, MF, etc.
3. Silicates: $M2O \cdot nH_2O$
4. Aluminates: $M2O \cdot nAl_2O_3$
5. Aluminosilicates: $M_2O \cdot Al_2O_3 \cdot (2\text{-}6) \ SiO_2$
6. Salts of strong acids: M_2SO_4

Where M is an alkaline ion Na (sodium) type, K (potassium) type or Li (lithium) type, or alkaline earth as Ca (calcium). The most widely available chemical products (activators) are $NaOH$, Na_2CO_3, $Na_2O \cdot SiO_2$, and Na_2SO_4. Some potassium compounds have been used in laboratory studies. However, its possible applications are limited due to its availability and cost. On the other hand, sodium and potassium compounds' properties are very similar.

2.3.2. Alkali activator solutions

2.3.2.1.Alkali hydroxides

The alkali metal hydroxides (sodium and/or potassium) are the most common chemical product used for the alkaline activation process for several waste materials. Sodium hydroxide or also known as caustic soda is one of the most important compounds in the chemical industry, sharing this position with sodium carbonate and sulfuric acid. There is hardly a single chemical that does not require the presence of one of these basic chemical products for production, additionally, most industrial products depend on caustic soda. The extensive use of NaOH as an activator in geopolymer synthesis, from different precursors, is due to its low cost, abundance, and low viscosity. Furthermore, leaching of Al^{3+} and Si^{4+} ions are generally high with NaOH solution compared to potassium hydroxide (KOH) solution. As an activator, NaOH accelerates the reaction more rapidly. Sodium hydroxide provides both hydroxide anion (OH^-), which acts as a catalyst for the dissolution of the aluminosilicates in the first stage, and sodium cation (Na^+) which acts as a structure-forming element, balancing the negative framework charge carried by tetrahedral aluminum in the last stage [85].

The use of sodium hydroxide activators in geopolymers is well known to lead to the formation of observable zeolitic structures, particularly after prolonged curing periods under humid conditions or even after a brief period at elevated temperatures. Investigations are still ongoing on whether this phenomenon will be linked to any change in the behavior of the materials since a certain correlation has been observed between the formation of zeolites and resistances decreasing. However, it is still unclear if this is specifically a causal effect (i.e., that the formation of zeolite leads to a loss in performance), or if it is a factor or combination of factors that cause such loss of performance. The efflorescence (formation of white sodium carbonate or bicarbonate crystals) is also a known problem in alkaline activated materials with high NaOH solution concentrations, where the excess alkali reacts with atmospheric CO_2. This phenomenon is unsightly but not always detrimental to the structural integrity of the material [4].

2.3.2.2. Sodium hydroxide production

Sodium hydroxide is produced predominantly through the Chlor-alkali process, in parallel with Cl_2. This production process has important environmental implications for its use in alkaline activation, both in

38

terms of greenhouse gas emissions (through electricity consumption) and in terms of emissions of other components, such as mercury which sometimes is used in this process.

The main energy consumption in the sodium hydroxide production process occurs in the electrolytic cell, which has a high electrical power requirement despite being extremely efficient when the membrane cell is used. For example, from different audits related to the amount of energy consumption by Australian manufacturers of sodium hydroxide, its membrane cell produces 2,800 kW/h per ton of chlorine. These data were used to estimate the results of CO_2 emissions per kg of NaOH produced,

Table 2-7. From where a total emission of 1.95 kg of CO_2 per kg of NaOH [66] was estimated.

Table 2-7. Estimated emissions in the NaOH production process, (adapted from [4]) [2]

Activity	Emission	Unit
Electricity consumption in the cell per ton of NaOH	1.285	kW/h
Emissions from the cell	1.581	kg CO_2
Proportion of cell electricity consumption in the process	115.8	%
Overall emissions from electricity	1.830	kg CO_2
Percentage of cell electricity used in fuel	25.3	%
Energy consumption on fuel	0.325	kW/h
Overall emissions from fuel	0.086	Kg CO_2
Total emissions	1.915	Kg CO_2

2.3.2.3. Alkali silicates

Sodium silicate is the generic name for a series of compounds with the formula $Na_2O \cdot nSiO_2$. In theory, the number n can be any number. Sodium silicates with different values in the number n can have different properties with highly diversified industrial applications. Generally, sodium silicates usually have a ratio of 1.6 to 3.85.

---

[2] The references cited in

Table 2-7 are presented as in [4]

The SiO_4^{4-} anion is a key constituent in high-performance alkali-activated materials because it advantages the formation of a denser and stronger structure [70]. Sodium silicate in combination with sodium hydroxide provides an important reactive part of silica that is widely used to produce the activator. However, the main drawbacks of sodium silicate are, that it is the most expensive raw material to produce alkali-activated materials and the highest emitter of greenhouse gases among the basic materials [86]. The cost of sodium silicate can be around 20% to produce an alkali-activated materials concrete, depending on the dosage. Regarding the greenhouse gases, the authors found that emissions from the production of sodium silicate represent 50–70% of the total in an alkali-activated materials concrete design [87].

It was mentioned that, commercially, liquid sodium silicates are usually produced with a mass SiO_2/Na_2O ratio that varies between 1.60 to 3.85, which means that there is no defined composition. This causes the structure and properties of these liquid vitreous silicates to vary. Table 2-8 is presented some physical and thermodynamic properties of anhydrous and hydrated sodium silicates.

Table 2-8. Physical and thermodynamic properties of anhydrous and hydrated sodium silicates, [88]

Formula	Density (g/cm³)	Melting point (°C)	Heat Formation ΔH (Kcal/g·mol)	Free Energy ΔG (Kcal/g·mol)	Entropy (S)
$Na_2O \cdot SiO_2$	2.614	1089	-359.8	-338	29
$Na_2O \cdot 2SiO_2$	2.5	874	-576.1	-541.2	39.4
$Na_2O \cdot nSiO_2$	-	-	$151.8 - 28.3n$	$-142.6 - 195.6n$	$18 + 11n$
$Na_2O \cdot SiO_2 \cdot 5H_2O$	1.75	72.2	-722	-631.5	77
$Na_2O \cdot SiO_2 \cdot 6H_2O$	1.81	62.9	-792.6	-688.2	87
$Na_2O \cdot SiO_2 \cdot 9H_2O$	1.65	47.9	-1005.1	-803.3	107

Two very important factors to consider when using this type of activator are:
   a) The concentration of silica, and
   b) The molar ratio SiO_2/Me_2O

A solution with a low molar concentration (1/1) is composed mainly of monomers (SiO_4^4) and dimers ($Si_2O_5^2$), while a solution with a high molar ratio (3.3/1) has a higher proportion of polymeric species. The pH value of the solution depends on its molar ratio SiO_2/R_2O. At pH values lower than 10, the solution starts to gel. To avoid this phenomenon, what is usually done is to control the SiO_2/Na_2O ratio

and raise the pH value by the addition of alkalis, which is usually in the form of NaOH. The result is known as "waterglass" ($xSiO_3 \cdot YNa_2O \cdot nH_2O$) [4].

2.3.2.4. Sodium silicate production

Sodium silicates, also known as "waterglass", are inorganic chemical compounds produced from the combination, in different proportions, of high purity silica sands (SiO_2) and sodium carbonate (Na_2CO_3). The fusion of these materials at temperatures above 1000 °C results in the sodium silicate in stone ($Na_2O \cdot xSiO_3$) in the form of an amorphous crystal. This solid silicate is dissolved in water to obtain the soluble or liquid silicate, which is used in several industrial applications, such as detergents and soaps, paper and cardboard, civil engineering, water treatment, cement, adhesives, etc.

Sodium silicates are synthesized through two possible production methods: the dry process and the wet process. The raw materials used in the dry process are soda ash and silicon oxide, while caustic soda and silica are the essential materials used in the wet process [4].

Like most industrial processes, sodium silicate production requires an important amount of energy, and it will be translated into CO_2 emissions (Table 2-9).

It is known that silicate solutions are the most used in the alkaline activation of aluminosilicates (slag, fly ash, and metakaolin). The availability of soluble silica is of importance in these systems, since it affects the workability, the adjustment, and the development of mechanical resistances, modifying both the composition of the gels and the microstructure of the material formed [4].

41

Table 2-9. Estimates of emissions arising due to sodium silicate manufacture, [86]

	Emissions arising from the energy expended during manufacturing	
	Energy flow (MJ/1000 kg)	Emissions (kg CO_2-e/kg)
Electricity	3118	1.065
Coal	296	0.027
Oil (heavy)	9	0.001
Average/light	456	0.003
Diesel oil	144	0.01
Gas	1270	0.076
Others	78	0.009
Total	5371	1.222
	Emissions caused by transport	
	Air emissions (kg/1000 kg)	Emissions (kg CO_2-e/kg)
Carbon dioxide (CO2)	288.7	0.289
Methane (CH4)	0.128	0.003
	Total	0.292
	Grand total (kg CO_2-e/kg)	1.514

2.3.3. Applications of Alkali-activated materials

The earliest endeavor to use alkalis in cement date back to 1930, when H. Kühl published research on the setting of slag mixed with dry potash solutions L. Chassevent and R. Feret afterward defined the need to investigate slag as a cement component. In 1940, A.O. Purdon published the outcomes of the first large-scale laboratory study on cement made with slag and live lime in the absence of Portland clinker. Later, in 1957, Victor Glukhovsky was the first to research the probability of formulating low-calcium or even calcium-free cementitious materials, which initially was called "soil cement", using clays and alkaline metal solutions [89]. Table 2-10 presents a chronology summary of the highlights of the research on alkaline cement.

The alkali activation of industrial waste materials has become an important area of research in many laboratories due to the probability to use these materials to synthesize low-cost and environmentally sound cementlike construction materials. During the last five decades, alkaline cement and concretes have aroused great interest among the scientific community and the construction industry. During the years 1999-2000, a group of scientists in Ukraine inspected several concrete structures built with alkali-activated slag cement, among which were different buildings such as silage ditches, railway

embankments built-in 1982, residential buildings of up to fifteen plants built-in 1960, and buildings manufactured during the period 1999-2000, special concrete pavements for heavy-duty trucks (50-60 tons) built-in 1984, etc. [4], [90], Figure 2-13.

Table 2-10. Chronology of alkaline cement (adapted from [89])[3].

Year	Name	Country	Study/Impact
1930	Kühl	Germany	Slag setting in the presence of dry potash
1937	Chassevent	Unknown	Slag reactivity measurement using a dry potash and soda solution
1940	Purdon	Belgium	Clinker-free cement consisting of slag and caustic soda or slag and caustic alkalis synthesized with a base and an alkaline salt
1957	Glukhovsky	USSR	Binder synthesis using hydrous and anhydrous aluminosilicates (vitreous rocks, clays, steel mill slag) and alkalis; proposal for a $Me_2O-MeO-Me_2O_3-SiO_2-H_2O$ cementitious system; coining of the term "soil cement"
1981	Davidovits	France	Alkalis mixed with a blend of burnt kaolinite, limestone, and dolomite, and trademarks such as Geopolymer, Pyrament, Geopolycem, Geopolymite
1986	Krivenko	USSR	Principles governing system $Me_2O-MeO-Me_2O_3-SiO_2-Al_2O_3$ properties; proposal for the generic name "alkaline cement" and the specific name "geocement"
1999	Palomo	Spain	Production of hardened cementitious materials from alkali-activated type F fly ashes
2006	Shi & Krivenko & Roy	Ukraine - USA	First book on alkali-activated cement
2014	Provis J., & van Deventer J.S. J	UK & Australia	Alkali activated Materials State of the art Report. RILEM TC 224-AAM

Table 2-11 presents some examples of the applications that have been studied until 2010. While more updated advances on geopolymers developments in engineering applications have been reported by Nawaz et al. [91], who mentioned that due to the geopolymers' outstanding mechanical properties, better acid and thermal resistance, low carbon emissions, low energy requirements for processing, etc. make them propitious to use in civil engineering in contrast with traditional cementitious materials like cement and lime. More specific studies from different authors regarding the applications of geopolymers in soil stabilization, concrete and mortars, fire resistance, coastal or marine applications, self-cleaning concrete applications to inhibit microbial attack, building insulation, and manufacture of ceramic products were listed in Table 2-11.

---

[3] The references cited in Table 2-10 are presented as in [89]
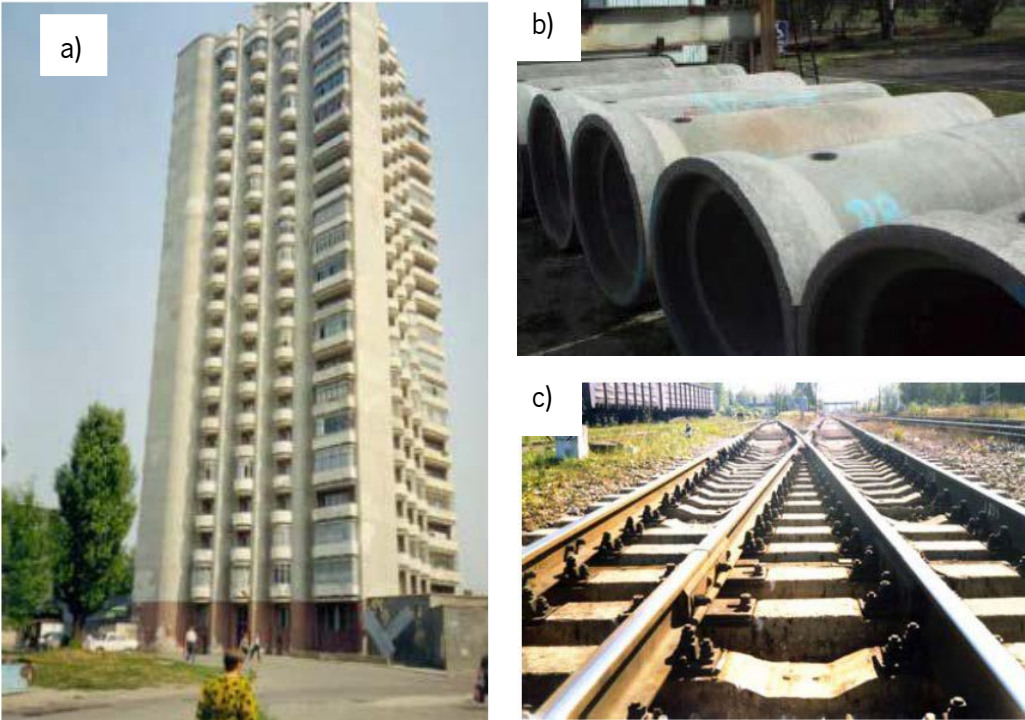
a) Building constructed with alkaline activated slag concrete, Berezina Street 2, Lipetsk, Russia, 1994; b) Pipes for the sewerage system (1500 mm diameter) (Gourly and Johnson, 2005); c) Prestressed concrete sleepers produced by alkaline slag activation. Moscow-Saint Petersburg line (Russia) was built-in 1989.

Figure 2-13. Applications with alkali-activated fly ash concrete (Pictures taken from [4] Doctoral Thesis Document).

Table 2-11. Applications for alkaline cement, [89].

Year	Civil engineering						Non-civil engineering
	Hydraulic	Roads	Agricultural	Industrial	Residential	Mining	
2010	Corrosion-resistant concretes for marine engineering applications. Immobilization of liquid radioactive waste in alkali-activated cement						
2000	Inorganic adhesives and glues, protective coatings for corrosive and high-temperature environments						
1990				Acid-resistant concrete articles and structures	High-rise building with precast and cast-in-situ concrete		Compounds for radioactive waste immobilization Precision tool housing
1985				Cast-in-situ concrete floors and landings	Concrete blocks for buildings, garages, storage houses, etc.		
1980				Heat-resistant concrete articles and structures	Floor slabs, foundation wall blocks, foundation blocks, piles	Oil well mortars and grouts	Linings of MD-pumps for aluminum melts
1975		Strengthened soils for road bases					

44

Table 2-11 (*continued*) Applications for alkaline cement, [89]

| 1970 | Tubing of anti-slide systems | Cast-in-situ concrete pavements and precast reinforced concrete pavers | Cast-in-situ and precast concrete pasture sites, fertilizer storage space, silo pits | Foundation blocks, floor slabs, columns, beams, foundation wall blocs, elements of a cleaning-up system | Rein-forced pit props, sleepers | |
| 1960 | Cast-in-situ and precast prestressed concrete sea break-waters, irrigation systems components | Pavement slabs, kerbs, landing field slabs | | | | |

2.4. CONSTRUCTION SYSTEMS IN PREFABRICATED PANELS

Prefabricated Enclosure Wall Panel Systems (PEWPS) are often used for several reasons, such as allowing the construction process to be streamlined as it can be carried out in parallel with earlier phases of construction, fewer human resources are needed, there is a greater guarantee of the homogeneity and final quality of the construction elements, due to the higher control of the production parameters, optimization of resources and materials and, consequently, reduction of waste generation. This can translate into lower costs when the quantities of panels required for building work are high. In some cases, it may also have a specific aesthetic purpose.

2.4.1. Constructive methods
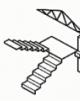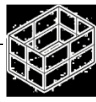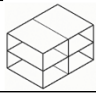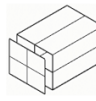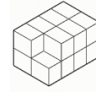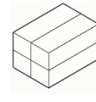
The methods of building construction are the way how units and components are produced and assembled. The way of managing this process varies from region to region and is subjected to the size of the project, the level of technology, and the materials available. Thus, three different contemporary construction methods are distinguished, categorized by ascending technologic level and descending flexibility, as exhibited in Table 2-12. To understand the benefits and limitations of Prefabricated Enclosure Wall Panel Systems (PEWPS), for example, it is helpful to identify and analyze the different so-called Modern Methods of Construction (MMC) (also known as "system building methods") that have fostered recently. Although the post-war boom of prefabricated construction in several countries has led to some partial perception that prefabricated buildings are unsightly or of lower quality, there

is a restored and increasing interest in prefabricated building systems, as they mean savings in time and materials as well as higher standards of quality over more conventional methods of construction. Despite there are several innovative site-based modern methods of construction (such as stick-built timber/metal framing, in situ concrete tunnel-formwork, building blocks, etc.), the off-site MMC (also known as "Off-site manufacturing (OSM) methods"), i.e., prefabrication elements or parts of structures, constructed in the factory, then transported and assembled on-site have called the attention of the construction industry. Table 2-13 explains a unified classification of off-site MMC, where the spotlighted area defines the category of the constructional system focused on the present section.

Table 2-12. Relationship between building construction methods, [92]

	Tradicional methods	Post-traditional methods (on-site manufacturing)	System building (off-site manufacturing)
	Decreasing flexibility and need for on-site skilled labor →		
	Increasing efficiency, accuracy, availability of materials and solutions		
Type of construction	Small up to mid-scale dwellings guided by local style and traditional building trades and practice (e.g., carpentry, plastering, joinery).	Small up to large-scale complex buildings with many individual architectural requirements.	Small up to large-scale systematized buildings, based on principles such as prefabrication, pre-assembly, sub-assembly, etc.
Materials, components, and availability	Limited range of local traditional materials (e.g., traditional brick and stone masonry, wood, adobe, etc.).	Vast range of both traditional and new materials and components (e.g., reinforced concrete, steel, blockwork, etc.)	The increasing availability of new commercial systems, materials, and finishings (e.g., precast concrete frames, wall panels, etc.).
Fabrication site	The fabrication and assembly take place at the site (usually at the position where the completed structure is to be located).	The amount of on-site fabrication has been reduced by the introduction of some prefabricated and standardized factory-produced components.	Most of the building's components are factory-produced and site assembled and are usually related to a specific building type.
Equipment and labor	Typically, only requires rudimentary equipment. Need for skilled craftsmanship, familiar with the operation in their trade	Requires expensive machinery for many different operations. Still needs for labor-intensive operations (e.g., bricklaying and carpentry).	May require lifting machinery. Specialized off-site manufacture and low-skilled labor on-site for fast assembly.
Efficiency and flexibility	Low efficiency and replicability. Maximum flexibility: each task can be tailored for each purpose.	Need to organize the construction process efficiently during the design stage. Medium flexibility	Efficient factory production of many similar building components. Relatively high inflexibility owing to the high level of accuracy required, making mistakes comprises the assembly process.

Table 2-13. The unified classification system of offsite modern methods of construction, [92]

	Level	Category	Subcategory	Definition	Examples	Scheme
Non-volumetric systems (2D)	1	Components and sub assemblies	Factory-made components (simpler elements)	These elements, although predominantly associated with traditional methods, are made in a factory to help improve the construction process on-site. These items are not full housing 'systems' and are usually factory made or, occasionally, site-assembled.	Door and window sets, furniture, etc.	
			Sub-assemblies (major building elements)		Pre-cast concrete assemblies (foundations, stairs, columns, beams, etc.), roof trusses, etc	
	2	Panelised systems	Wall cladding (nonloadbearing)	Two-dimensional units built in a factory and transported to site for assembly into a three-dimensional structure or to fit within an existing structure, creating or separating usable space.	Cladding panels	
			Vertical panels (may be loadbearing)		Enclosure walls and partitions	
			Non-vertical panels (usually loadbearing)		Structural floor and roof panels (cassettes)	
Volumetric systems (3D)	3	Hybrid systems (or semi volumetric)		Combination of volumetric and panelised methods of construction. The hybrid approach can be used to bring flexibility to the development and can also reduce uniformity of design.	Highly serviced areas such as kitchens or bathrooms constructed as volumetric units, with the rest of the dwelling constructed with panelised systems	
	4	Volumetric or modular systems	Volumetric construction ("pods")	Pre-assembled smaller three dimensional units which create usable space and are usually fully factory finished internally and completed with plumbing and wiring, to be installed within, or onto an independent structural frame.	Bathroom and kitchen pods	
			Modular construction (whole building)	Pre-assembled larger three dimensional units produced in a factory, fully fitted out before being transported to site and stacked onto prepared foundations to form the actual structure and fabric of the building.	Outskirt units, hotels, prison blocks, medium rise residential, student accommodation.	

Left margin labels: Increasing degree of prefabrication, size of prefabricated components and complexity of pre-assembly / Decreasing degree of on-site construction labour, customization and flexibility

2.4.2. Classification of panels

Table 2-14 illustrates a wide classification system for PEWPS following the different constructional and functional criteria. Even though there are innumerable commercial solutions available in the market, the following six most common PEWPS have been chosen for comparison purposes, ranked by decreasing order of weightiness: pre-cast concrete wall panels; structurally insulated panels (SIPs); self-supporting composite lightweight panels; curtain wall panels; light-frame wall panels, and rainscreen/cladding panels (ventilated façade).

Table 2-14. Classification of common PEWPS according to functional and constructional criteria, [92]

Correspondence: ● usual (or binding) ○ possible (or optional)		Common PEWPS (organized by decreasing order of weightiness)		Pre-cast concrete wall panels	Structurally insulated panels (SIPs)	Self-supporting composite lightweight panels	Curtain wall panels	Light-frame wall panels	Rainscreen/cladding panels (ventilated façades)
Classification criteria	Classification methods	Classification results							
Constructional	Structural role	Non-loadbearing		●	●	●	●	○	○
		Loadbearing			●			●	●
	Size of the panels (and degree of prefabrication of the system)	Infill walling panels			●			●	●
		Unitized wall panels			○	●	○	●	●
		Spandrel wall panels		●		●	●		
		Stick-built wall panels			●	●			
	Weight	Heavyweight						○	●
		Lightweight		●	●	●	●	●	
	Type of assembly	Panel-to-structure assembly			●			○	●
		Panel-to-panel assembly			●	○	●	●	●
		Panel-to-subframe assembly				●			
		Cladding panels		●					
	Construction in leave	Single leaf			●	●	●	●	
		Multiple leaves		●	○		●		
	Construction in layers	Single layer		●		●			●
		Multiple layers	Layered (or composite)	○		●			
			Sandwich (or trilayer)			●	●	○	
			Cellular-core (or honeycomb-core)	○			○		○
			Stud frame (or skeletal)		●				
Functional	Ventilation	Without air cavity			●	●	●	●	●
		With air cavity	Stationary	○	○	○			
			Vented	○					
			Ventilated	●					
			Pressure-moderated (or equalized)	●		○			
	Weathertightness	Perfect barriers (barrier walls)	Face-sealed	○	○	●	●	○	○
			Concealed barrier						○
		Imperfect barriers	Mass or storage systems						○
			Screened and drained walls	●					
	Insulation layer/core	None		●		○	○		●
		Yes, but not specific to the panel		○			○		
		Yes, specific to the panel			●	○	●	●	○

2.4.2.1. Constructional criteria

• Structural role

Except for the structural role of any eventual pre-existent backing wall, from a constructional point of view, two fundamental types of PEWPS can be determined:

i) *Non-loadbearing wall panels* do not strengthen the structure on which they are placed, nor support vertical loads other than their self-weight but can transfer lateral forces to the building structure. These panels are easier to demolish, dismantle or replace;

ii) *Loadbearing wall panels*, provide stability to the structure on which they are placed and comprise themselves a loadbearing external wall that may support vertical loads beyond their self-weight. The wall panels may also resist lateral loads as well as wind and/or seismic loads.

- **Size of the panels**

The size and complexity of the individual components have a significant effect on the degree of prefabrication of a system, thus conditioning time and cost parameters, as well as other factors governing the assembly of the façade and conceivably, is later dismantling. Bigger prefabricated panels include fewer ties and need less on-site time but are usually heavier, making transporting and handling more complex. Smaller panels are comprised of more and smaller elements, requiring higher on-site construction labor, but offer the most flexibility in planning. According to the terminology in EN 13830, the type of panel façade methods can be classified as follows, listed by reducing panel size:

i) Infill walling panels: these panels are set up on each slab and are limited by the primary structural frame (limited horizontally by columns or transversal walls, and vertically by slabs or spandrel beams), to build a full confined façade;

ii) Unitized wall panels: pre-assembled interlinking storey height or multi-storey height modules;

iii) Spandrel wall panels: pre-assembled interlinking part-storey height modules;

iv) Stick-built wall panels: light carrier framework of site assembled components supporting prefabricated opaque and/or translucent infill panels.

- **Weight**

It is naturally dependent on the size and the material constitution (i.e., density) of the panels, quantified either for each element or by the unit of area. Therefore, prefabricated wall panels can be classified as heavyweight or lightweight, being, yet their distinction not consensual. However, the following values can be used as a reference:

i) *Heavyweight*: when heavier than 100 kg/m², usually requiring special lifting/moving equipment;

ii) *Lightweight:* when lighter than 100 kg/m², and ideally can be handled by one or two workers.

- **Type of assembly**

PEWPS can be grouped into four basic types of panel assemblies

i) *Panel-to-structure assembly*: fixed directly to the primary structural frame, and the requirements set for infill walling panels shall apply;

ii) *Panel-to-panel assembly*: fully prefabricated panels jointed to each other via the joints and fixed directly to the primary structural frame. The so-called "self-supporting panels" are also under this type of assembly, which consist of wall panels able to support their own weight only and of bearing the force of the wind blowing action, but usually without needing a secondary frame. Panel-to-panel assemblies, especially those using tongue and groove joints, usually depend on sequential stacking;

iii) *Cladding panels* (also known as "rain-screen panels"): panels mounted outwardly into a carrier system, or fixed directly to the substrate wall, with an air cavity between the two parts of the construction. These panels offer only a first-stage barrier to the internal layers against driving rain. The substrate wall (which typically contains an external continuous insulation layer covered by a drainage layer) provides the needed hygrothermal performance and can be constructed using one of the forenamed types of assembly. Open drained joints (or small butt joints) between panels are feasible using this method.

- **Construction in terms of leaves**

Leaves are planar elements with a higher degree of structural autonomy than layers. A leaf can include some layers and form the actual wall constitution on its own, or in consolidation with other leaves:

i) *Single leaf*, the structural and performance properties are defined only by a single wall panel, which can be monolithic (single-material layer) or composite (multiple layers);

ii) *Multiple leaves,* in multi-leaf façades, an air cavity amid two leaves can be included, which is either fully enclosed or connected to the outside. The exterior and internal leaves may be in part connected, but do not comprise a single constructional unit.

- Construction in terms of layers

A layer is a single "functional level" of the structural order of a certain constructional system, which has smaller loadbearing importance, as thinner and less resistant the layer is, e.g., structurally irrelevant foils, films, and coatings, air cavities, membranes, insulation, plaster, and render, etc. Hence, a wall panel can be classified according to the number and type of layers:

i) *Single-layer* (monolithic/homogeneous panels), the structural and performance properties are defined essentially by the material and its thickness. The material of the wall must consequently satisfy various functions in this approach. In addition, the sizes of openings in the wall panels are restricted due to these weakening the loadbearing behavior of the wall;

ii) *Multiple layers* (composite/layered panels), the materials and thicknesses of each layer and/or leaves can be optimized to fit their respective functions. Thus, the definition of the series of layers is first controlled by functional and performance factors and secondly by constructional aspects, so that the facade works efficiently and prevents early degradation. The following multi-layered construction methods are possible:

   — Layered (or composite) construction

   — Sandwich (or trilayer) construction

   — Cellular-core (or honeycomb-core) construction

   — Stud frame (or skeletal) construction (open or closed panel systems), [92].

2.4.2.2. Functional criteria

Understanding how much a façade surface can respond to varying conditions is of foremost importance for making decisions, because of its primary influence on the energy balance of a building. In this regard, façades can be classified by the different functional requirements that a certain system is capable to fulfil.

- Ventilation

Depending on the local weather conditions and requirements set on a building, PEWPS can be designed consonant to the preferential construction system and the appropriate method to disperse runoff water condensation and/or heat effectively through thermal flux. Therefore, a proper ventilation

recess behind a facing leaf should prevent mold formation and the decay of the inner layers, and at the same time, reduce temperature fluctuations in the building's interior and improve the overall energy efficiency of the building. Thus, concerning the ventilation basis, PEWPS may be categorized as follows:

i)   *Without air cavity*, i.e., single leaf construction systems (but not necessarily single layer panels);

ii)   *With air cavity*: multi-leaf walls including an external skin (e.g., cladding panels), with or without extra elements concealing or closing the joints, which is fixed to an airtight backing wall (normally insulated and covered with a water-resistant barrier) and separated by an air cavity. Depending on the degree of ventilation permitted in the cavity, which is in its turn defined by the width, number, and type of joins (or even wall vents), as well as on the thickness and constitution of the air gap, they can be categorized as:

— *Stationary* (sealed cavity façade): if there is no ventilation between layers or leaves acting as a thermal insulation layer;

— *Vented*: allow some degree of water vapor diffusion through vents and redistribution inside the cavity by air mixing and vapor diffusion;

— *Ventilated*: allows an important flow of air to facilitate drying by mass vapor movement;

— *Pressure-moderated* (or equalized): it moderates air pressure differences across the screen so that water and humidity are not induced to be driven or sucked through the joints and the wall element can breathe, thus diminishing the risk of condensation. If perfect moderation is achieved (a theoretical condition), it is termed "pressure equalized".

• **Weathertightness**

The degree of permeability defines the quality of the building envelope and the comfort of the indoors by contributing to enhanced protection from the effect of weathering (rain, wind, snow, etc.). It is categorized according to the method by which the wall system controls water penetration, as follows:

i)   *Perfect barriers* (also referred to as "barrier walls") contain all water penetration at a single plane, as much as a perfect air barrier would avoid airflow, e.g., window frames, exterior insulation and finish systems, and metal and glass curtain wall systems. They can be sub-divided into:

— *Face-sealed*: air- and water-impermeable exterior materials and sealed joints (if applicable), which must be continuous with no irregularities or openings to keep air and water to the exterior of the compartment;

— *Concealed barrier*: the primary enclosure material is a porous cladding material, which works only as a secondary water control layer, and the weathertightness requirement depends on a second barrier layer, impermeable to water.

ii)   *Imperfect barriers*: since building and maintaining a perfect barrier wall is very difficult, most walls perform as imperfect barrier wall systems, which means that it is presumed that moisture will penetrate to some point within the system. They can be sub-divided into:

— *Mass or storage systems* control rain penetration by absorbing and storing some rainwater that infiltrates the outer surface, but not entirely through the material (e.g., precast concrete, stone, wood, etc.). In a functional mass wall, moisture is eventually cleared by evaporative drying before it reaches the interior surface of the wall. This system considers the material thickness, storage capacity, and material density to resist air infiltration and water penetration;

— *Screened and drained wall systems* (also referred to as "cavity walls") control rain penetration by removing most of the water that is not shed by the screen by gravity drainage and airflow. This moisture is controlled and diverted back to the exterior using supplementary mechanisms, such as a capillary break (e.g., cavity), multiple drainage planes, flashings, weep holes, etc.

- **Insulation layer/core**

The presence or absence of an insulation layer/core lets to class PEWPS as follows:

i)   *None*, if the system neither includes nor requires an insulation layer/core;

ii)   *Yes*, *but not specific to the panel*, if the system does not include but requires an insulation layer/core;

iii)   *Yes*, specific to the panel if the system comes complete with a preinstalled insulation layer/core, [92].

REFERENCES

[1]   Cerame-Unie, "Ceramic industry | Cerame-Unie - The European Ceramic Industry Association." https://cerameunie.eu/ (accessed Apr. 22, 2022).

[2]   M. S. Khan, M. Sohail, N. S. Khattak, and M. Sayed, "Industrial ceramic waste in Pakistan, valuable material for possible applications," *J. Clean. Prod.*, vol. 139, pp. 1520–1528, Dec. 2016, doi: 10.1016/J.JCLEPRO.2016.08.131.

[3]   E. P. PE, "Circular economy: definition, importance, and benefits | News | European Parliament," *201*, 2015. http://www.europarl.europa.eu/news/en/headlines/economy/20151201STO05603/circular-economy-definition-importance-and-benefits (accessed Apr. 30, 2018).

[4]   C. M. Torres, "Reutilización de residuos vítreos urbanos industriales en la fabricación de cementos alcalinos: Activación, comportamiento y durabilidad," 2015.

[5]   United Nations, "Transforming our world: the 2030 Agenda for Sustainable Development," *Department of Economic and Social Affairs Sustainable Development*, 2021. https://sdgs.un.org/2030agenda (accessed Aug. 30, 2021).

[6]   C. E. para o D. S. BCSD, "Objetivos de Desenvolvimento Sustentável (ODS) - BCSD Portugal," *BCSD Portugal*, 2021. https://www.ods.pt/ (accessed Jul. 30, 2021).

[7]   United Nations, "THE 17 GOALS | Sustainable Development," *United Nations*, 2022. https://sdgs.un.org/goals (accessed Apr. 18, 2022).

[8]   A. Seco, J. Omer, S. Marcelino, S. Espuelas, and E. Prieto, "Sustainable unfired bricks manufacturing from construction and demolition wastes," *Constr. Build. Mater.*, vol. 167, pp. 154–165, Apr. 2018, doi: 10.1016/J.CONBUILDMAT.2018.02.026.

[9]   A. Di Maria, J. Eyckmans, and K. Van Acker, "Downcycling versus recycling of construction and demolition waste: Combining LCA and LCC to support sustainable policy making," *Waste Manag.*, vol. 75, pp. 3–21, May 2018, doi: 10.1016/J.WASMAN.2018.01.028.

[10]   M. I. M. Ibrahim, "Estimating the sustainability returns of recycling construction waste from building projects," *Sustain. Cities Soc.*, vol. 23, pp. 78–93, May 2016, doi: 10.1016/J.SCS.2016.03.005.

[11]   B. C. L. Yin, R. Laing, M. Leon, and L. Mabon, "An evaluation of sustainable construction perceptions and practices in Singapore," *Sustain. Cities Soc.*, vol. 39, pp. 613–620, May 2018, doi: 10.1016/J.SCS.2018.03.024.

[12]   D. A. Pássaro, "Report: waste management in Portugal between 1996 and 2002," *Waste Manag.*, vol. 23, no. 1, pp. 97–99, Jan. 2003, doi: 10.1016/S0956-053X(02)00142-3.

[13]   P. European, "DIRECTIVE 2006/12/EC," *EUR-Lex, Official Journal of the European Union*, 2006. https://eur-lex.europa.eu/legal-content/EN/TXT/?uri=CELEX%3A32006L0012 (accessed Jul. 23, 2021).

[14]   P. European, "Directive 2008/98/EC," *EUR-Lex, Official Journal of the European Union*, 2008. https://eur-lex.europa.eu/legal-content/EN/TXT/?uri=celex%3A32008L0098 (accessed Jul. 23, 2021).

[15]   P. European, "Directive (EU) 2018/851 (EN)," *EUR-Lex, Official Journal of the European Union*, 2018. https://eur-lex.europa.eu/legal-content/EN/TXT/?uri=celex%3A32018L0851 (accessed Jul. 23, 2021).

[16]   U. E. UE, "DIRECTIVE 2008/98/EC OF THE EUROPEAN PARLIAMENT AND OF THE COUNCIL of 19 November 2008," *Off. J. Eur. Union*, 2008, Accessed: Jun. 06, 2018. [Online]. Available: https://eur-lex.europa.eu/legal-content/EN/TXT/PDF/?uri=CELEX:32008L0098&from=PT.

[17]   H. Niska and A. Serkkola, "Data analytics approach to create waste generation profiles for waste management and collection," *Waste Manag.*, May 2018, doi: 10.1016/j.wasman.2018.04.033.

[18]   R. Branco, "E-pública Revista Eletrónica de Direito Público," *Faculdade de Direito da Universidade de Lisboa*, 2021. https://www.e-publica.pt/volumes/v7n2a07.html (accessed Jul. 27, 2021).

[19]   OERN, "Legislação - Resíduos," *Portal oficial da Ordem dos Engenheiros Região Norte - OERN*, 2021. .

[20]   A. P. do A. APA, "Plano Nacional de Gestão de Resíduos (PNGR) | Agência Portuguesa do Ambiente," *APA*, 2021. https://apambiente.pt/residuos/plano-nacional-de-gestao-de-residuos-pngr (accessed Jul. 27, 2021).

[21]   APA, "Plano Nacional de Gestão de Resíduos (PNGR)," 2018. http://www.apambiente.pt/index.php?ref=16&subref=84&sub2ref=108&sub3ref=1095 (accessed Jun. 06, 2018).

[22]   D. Moya, C. Aldás, G. López, and P. Kaparaju, "Municipal solid waste as a valuable renewable energy resource: a worldwide opportunity of energy recovery by using Waste-To-Energy Technologies," *Energy Procedia*, vol. 134, pp. 286–295, Oct. 2017, doi: 10.1016/J.EGYPRO.2017.09.618.

[23]   V. A. Ferraz de Campos, V. B. Silva, J. S. Cardoso, P. S. Brito, C. E. Tuna, and J. L. Silveira, "A review of waste management in Brazil and Portugal: Waste-to-energy as pathway for sustainable development," *Renew. Energy*, vol. 178, pp. 802–820, Nov. 2021, doi: 10.1016/J.RENENE.2021.06.107.

[24]   D. Hoornweg and P. Bhada-Tata, "WHAT A WASTE, A Global Review of Solid Waste Management," 2012. Accessed: May 03, 2018. [Online]. Available: https://siteresources.worldbank.org/INTURBANDEVELOPMENT/Resources/336387-1334852610766/What_a_Waste2012_Final.pdf.

[25]   Eurostat, "Waste statistics - Statistics Explained," 2021. http://ec.europa.eu/eurostat/statistics-explained/index.php/Waste_statistics (accessed May 03, 2018).

[26]   Eurostat, "Waste statistics - Statistics Explained," 2018. https://ec.europa.eu/eurostat/statistics-explained/index.php?title=Waste_statistics#Total_waste_generation (accessed Apr. 18, 2022).

[27]   ECCA, "The position of Latin America in the context of circular economy – ECCA," 2017. http://circularconstruction.eu/2017/06/28/the-position-of-latin-america-in-the-context-of-

circular-economy/ (accessed May 03, 2018).

[28] P. Schröder, M. Albaladejo, A. Ribas, M. Macewen, and J. Tilkanen, "The circular economy in Latin America and the Caribbean Opportunities for building resilience."

[29] H. Wang, Z. Chen, L. Liu, R. Ji, and X. Wang, "Synthesis of a foam ceramic based on ceramic tile polishing waste using SiC as foaming agent," *Ceram. Int.*, vol. 44, no. 9, pp. 10078–10086, Jun. 2018, doi: 10.1016/J.CERAMINT.2018.02.211.

[30] O. A. S. Simons, "Utilización Del Desecho Cerámico De La Fábrica De Sanitarios Edesa, Para La Fabricación De Adoquines," Escuela Politécnica Nacional, 2015.

[31] European Commission, "Best Available Techniques in the Ceramic Manufacturing Industry," 2007. Accessed: May 02, 2018. [Online]. Available: http://eippcb.jrc.ec.europa.eu/reference/BREF/cer_bref_0807.pdf.

[32] H.-J. Chen, T. Yen, and K.-H. Chen, "Use of building rubbles as recycled aggregates," *Cem. Concr. Res.*, vol. 33, no. 1, pp. 125–132, Jan. 2003, doi: 10.1016/S0008-8846(02)00938-9.

[33] X. Ma, T. Zhang, X. Shen, Y. Zhai, and J. Hong, "Environmental footprint assessment of China's ceramic tile production from energy-carbon-water nexus insight," *J. Clean. Prod.*, vol. 337, p. 130606, Feb. 2022, doi: 10.1016/J.JCLEPRO.2022.130606.

[34] F. Puertas, A. Barba, M. F. Gazulla, M. P. Gómez, M. Palacios, and S. Martínez-Ramírez, "CERAMIC WASTES AS RAW MATERIALS IN PORTLAND CEMENT CLINKER FABRICATION.· CHARACTERIZATION AND ALKALINE ACTIVATION," vol. 56, no. 281, pp. 73–84, 2006, Accessed: Apr. 23, 2018. [Online]. Available: http://digital.csic.es/bitstream/10261/26676/1/134.pdf.

[35] A. Jindal and G. D. Ransinchung R.N., "Behavioural study of pavement quality concrete containing construction, industrial and agricultural wastes," *Int. J. Pavement Res. Technol.*, Apr. 2018, doi: 10.1016/J.IJPRT.2018.03.007.

[36] N. Cristelo, A. Fernández-Jiménez, T. Miranda, and Á. Palomo, "Sustainable alkali activated materials: Precursor and activator derived from industrial wastes," *J. Clean. Prod.*, vol. 162, pp. 1200–1209, 2017, doi: 10.1016/j.jclepro.2017.06.151.

[37] D. Agrawal, P. Hinge, U. P. Waghe, and S. P. Raut, "Utilization of industrial waste in construction material – A review," *Int. J. Innov. Res. Sci. Eng. Technol. (An ISO Certif. Organ.*, vol. 3297, no. 1, 2007, Accessed: May 04, 2018. [Online]. Available: www.ijirset.com.

[38] C. Buratti, E. Belloni, E. Lascaro, F. Merli, and P. Ricciardi, "Rice husk panels for building applications: Thermal, acoustic and environmental characterization and comparison with other innovative recycled waste materials," *Constr. Build. Mater.*, vol. 171, pp. 338–349, May 2018, doi: 10.1016/J.CONBUILDMAT.2018.03.089.

[39] L. Wiemes, U. Pawlowsky, and V. Mymrin, "Incorporation of industrial wastes as raw materials in brick's formulation," *J. Clean. Prod.*, vol. 142, pp. 69–77, Jan. 2017, doi: 10.1016/J.JCLEPRO.2016.06.174.

[40] M. J. Munir, S. M. S. Kazmi, Y.-F. Wu, A. Hanif, and M. U. A. Khan, "Thermally efficient fired clay bricks incorporating waste marble sludge: An industrial-scale study," *J. Clean. Prod.*, vol. 174, pp. 1122–1135, Feb. 2018, doi: 10.1016/J.JCLEPRO.2017.11.060.

[41]   L. Coppola, D. Coffetti, and E. Crotti, "Pre-packed alkali activated cement-free mortars for repair of existing masonry buildings and concrete structures," *Constr. Build. Mater.*, vol. 173, pp. 111–117, Jun. 2018, doi: 10.1016/J.CONBUILDMAT.2018.04.034.

[42]   A. Briga-Sá, N. Gaibor, L. Magalhães, T. Pinto, and D. Leitão, "Thermal performance characterization of cement-based lightweight blocks incorporating textile waste," *Constr. Build. Mater.*, vol. 321, no. January, p. 126330, 2022, doi: 10.1016/j.conbuildmat.2022.126330.

[43]   M. Bagarić, I. Banjad Pečur, and B. Milovanović, "Hygrothermal performance of ventilated prefabricated sandwich wall panel from recycled construction and demolition waste – A case study," *Energy Build.*, vol. 206, p. 109573, Jan. 2020, doi: 10.1016/J.ENBUILD.2019.109573.

[44]   A. Benallel, A. Tilioua, M. Ettakni, M. Ouakarrouch, M. Garoum, and M. Ahmed Alaoui Hamdi, "Design and thermophysical characterization of new thermal insulation panels based on cardboard waste and vegetable fibers," *Sustain. Energy Technol. Assessments*, vol. 48, p. 101639, Dec. 2021, doi: 10.1016/J.SETA.2021.101639.

[45]   G. Lazorenko, A. Kasprzhitskii, and E. H. Fini, "Sustainable construction via novel geopolymer composites incorporating waste plastic of different sizes and shapes," *Constr. Build. Mater.*, vol. 324, p. 126697, Mar. 2022, doi: 10.1016/J.CONBUILDMAT.2022.126697.

[46]   European Parliament, "Circular economy: definition, importance and benefits | News | European Parliament," *News Eupopean Parliament*, 2021. https://www.europarl.europa.eu/news/en/headlines/economy/20151201STO05603/circular-economy-definition-importance-and-benefits (accessed Apr. 20, 2022).

[47]   EMF, "How to build a circular economy | Ellen MacArthur Foundation," *Ellen MacArthur Foundation*, 2022. https://ellenmacarthurfoundation.org/ (accessed Apr. 20, 2022).

[48]   G. C. Nobre and E. Tavares, "The quest for a circular economy final definition: A scientific perspective," *J. Clean. Prod.*, vol. 314, p. 127973, Sep. 2021, doi: 10.1016/J.JCLEPRO.2021.127973.

[49]   P. Ghisellini, M. Ripa, and S. Ulgiati, "Exploring environmental and economic costs and benefits of a circular economy approach to the construction and demolition sector. A literature review," *J. Clean. Prod.*, vol. 178, pp. 618–643, Mar. 2018, doi: 10.1016/J.JCLEPRO.2017.11.207.

[50]   M. Geissdoerfer, P. Savaget, N. M. P. Bocken, and E. J. Hultink, "The Circular Economy – A new sustainability paradigm?," *J. Clean. Prod.*, vol. 143, pp. 757–768, Feb. 2017, doi: 10.1016/J.JCLEPRO.2016.12.048.

[51]   N. M. P. Bocken, I. de Pauw, C. Bakker, and B. van der Grinten, "Product design and business model strategies for a circular economy," *https://doi.org/10.1080/21681015.2016.1172124*, vol. 33, no. 5, pp. 308–320, Jul. 2016, doi: 10.1080/21681015.2016.1172124.

[52]   J. Korhonen, A. Honkasalo, and J. Seppälä, "Circular Economy: The Concept and its Limitations," *Ecol. Econ.*, vol. 143, pp. 37–46, Jan. 2018, doi: 10.1016/J.ECOLECON.2017.06.041.

[53]   C. G. Castro, A. H. Trevisan, D. C. A. Pigosso, and J. Mascarenhas, "The rebound effect of circular economy: Definitions, mechanisms and a research agenda," *J. Clean. Prod.*, vol. 345,

p. 131136, Apr. 2022, doi: 10.1016/J.JCLEPRO.2022.131136.

[54] G. La Scalia, M. Saeli, L. Adelfio, and R. Micale, "From lab to industry: Scaling up green geopolymeric mortars manufacturing towards circular economy," *J. Clean. Prod.*, vol. 316, p. 128164, Sep. 2021, doi: 10.1016/J.JCLEPRO.2021.128164.

[55] R. Mateus, S. Neiva, L. Bragança, P. Mendonça, and M. Macieira, "Sustainability assessment of an innovative lightweight building technology for partition walls – Comparison with conventional technologies," *Build. Environ.*, vol. 67, pp. 147–159, Sep. 2013, doi: 10.1016/J.BUILDENV.2013.05.012.

[56] G. Rebitzer *et al.*, "Life cycle assessment: Part 1: Framework, goal and scope definition, inventory analysis, and applications," *Environ. Int.*, vol. 30, no. 5, pp. 701–720, Jul. 2004, doi: 10.1016/J.ENVINT.2003.11.005.

[57] M. Röck, E. Baldereschi, E. Verellen, A. Passer, S. Sala, and K. Allacker, "Environmental modelling of building stocks – An integrated review of life cycle-based assessment models to support EU policy making," *Renew. Sustain. Energy Rev.*, vol. 151, p. 111550, Nov. 2021, doi: 10.1016/J.RSER.2021.111550.

[58] C. Ouellet-Plamondon and G. Habert, "Life cycle assessment (LCA) of alkali-activated cements and concretes," in *Handbook of Alkali-Activated Cements, Mortars and Concretes*, Elsevier, 2015, pp. 663–686.

[59] P. Purnell, "Material Nature versus Structural Nurture: The Embodied Carbon of Fundamental Structural Elements," *Environ. Sci. Technol.*, vol. 46, no. 1, pp. 454–461, Jan. 2012, doi: 10.1021/es202190r.

[60] G. Borghi, S. Pantini, and L. Rigamonti, "Life cycle assessment of non-hazardous Construction and Demolition Waste (CDW) management in Lombardy Region (Italy)," *J. Clean. Prod.*, vol. 184, pp. 815–825, May 2018, doi: 10.1016/J.JCLEPRO.2018.02.287.

[61] S.-C. Hsu, C.-M. Lam, I. K. M. Yu, F. Medel, D. C. W. Tsang, and C. S. Poon, "Life-cycle cost-benefit analysis on sustainable food waste management: The case of Hong Kong International Airport," *J. Clean. Prod.*, vol. 187, pp. 751–762, Jun. 2018, doi: 10.1016/J.JCLEPRO.2018.03.160.

[62] G. I. Carvajal, A. Balaguera, J. Albertí, and P. Fullana-i-Palmer, "Life cycle assessment of road construction alternative materials: A literature review," *Resour. Conserv. Recycl.*, vol. 132, pp. 37–48, May 2018, doi: 10.1016/J.RESCONREC.2018.01.003.

[63] D. A. Salas, A. D. Ramirez, N. Ulloa, H. Baykara, and A. J. Boero, "Life cycle assessment of geopolymer concrete," *Constr. Build. Mater.*, vol. 190, pp. 170–177, Nov. 2018, doi: 10.1016/J.CONBUILDMAT.2018.09.123.

[64] I. Bianco, B. Ap Dafydd Tomos, and R. Vinai, "Analysis of the environmental impacts of alkali-activated concrete produced with waste glass-derived silicate activator – A LCA study," *J. Clean. Prod.*, vol. 316, p. 128383, Sep. 2021, doi: 10.1016/J.JCLEPRO.2021.128383.

[65] J. L. Provis, "Alkali-activated materials," *Cem. Concr. Res.*, Mar. 2017, doi: 10.1016/j.cemconres.2017.02.009.

[66] L. K. Turner and F. G. Collins, "Carbon dioxide equivalent (CO2-e) emissions: A comparison between geopolymer and OPC cement concrete," *Constr. Build. Mater.*, vol. 43, pp. 125–130,

Jun. 2013, doi: 10.1016/J.CONBUILDMAT.2013.01.023.

[67] K.-H. Yang, J.-K. Song, and K.-I. Song, "Assessment of CO2 reduction of alkali-activated concrete," *J. Clean. Prod.*, vol. 39, pp. 265–272, Jan. 2013, doi: 10.1016/J.JCLEPRO.2012.08.001.

[68] M. Izquierdo, X. Querol, J. Davidovits, D. Antenucci, H. Nugteren, and C. Fernández-Pereira, "Coal fly ash-slag-based geopolymers: Microstructure and metal leaching," *J. Hazard. Mater.*, vol. 166, no. 1, pp. 561–566, 2009, doi: 10.1016/j.jhazmat.2008.11.063.

[69] J. Davidovits, "PROPERTIES OF GEOPOLYMER CEMENTS," 1994, Accessed: Apr. 19, 2018. [Online]. Available: https://www.geopolymer.org/fichiers_pdf/KIEV.pdf.

[70] J. L. Provis and J. S. . Van Deventer, "Alkali Activated Materials: State-of-the-Art Report," 2014. doi: 10.1007/978-94-007-7672-2_5.

[71] N. Gaibor, J. Coelho, D. Leitão, T. Miranda, P. Tavares, and N. Cristelo, "Alkali activation of recycled ceramic aggregates from construction and demolition wastes," *Mater. Construcción*, vol. 70, no. 339, p. 222, Jul. 2020, doi: 10.3989/mc.2020.13619.

[72] T. Miranda *et al.*, "Application of alkali-activated industrial wastes for the stabilisation of a full-scale (sub)base layer," *J. Clean. Prod.*, vol. 242, p. 118427, Jan. 2020, doi: 10.1016/J.JCLEPRO.2019.118427.

[73] M. L. Granizo, S. Alonso, M. T. Blanco-Varela, and A. Palomo, "Alkaline Activation of Metakaolin: Effect of Calcium Hydroxide in the Products of Reaction," *J. Am. Ceram. Soc.*, vol. 85, no. 1, pp. 225–231, Dec. 2004, doi: 10.1111/j.1151-2916.2002.tb00070.x.

[74] M. Tuyan, Ö. Andiç-Çakir, and K. Ramyar, "Effect of alkali activator concentration and curing condition on strength and microstructure of waste clay brick powder-based geopolymer," *Compos. Part B Eng.*, vol. 135, pp. 242–252, Feb. 2018, doi: 10.1016/j.compositesb.2017.10.013.

[75] N. Gaibor, D. Leitão, T. Miranda, V. Cunha, and N. Cristelo, "Effect of curing conditions on compressive strength behavior on alkali-activated ceramic wastes Efecto de las condiciones de curado en el comportamiento de resistencia a la compresión en residuos cerámicos activados alcalinamente Efeito das condições de c," *Polo del Conoc.*, vol. 6, no. 3, pp. 977–990, 2021, doi: 10.23857/pc.v6i3.2416.

[76] S. Q. G. C. Ruiz, "Materias primas alternativas para el desarrollo de nuevos cementos: activación alcalina de vidrios silicoaluminosos," 2013.

[77] A. Fernández-Jiménez, G. Kovalchuk, and A. Palomo, "Alkali-activated fly ash: Effect of thermal curing conditions on mechanical and microstructural development – Part II," *Fuel*, vol. 86, no. 3, pp. 315–322, Feb. 2007, doi: 10.1016/J.FUEL.2006.07.010.

[78] A. Fernández-Jiménez, M. Criado, and A. Palomo, "Alkali activation of fly ashes. Part 1: Effect of curing conditions on the carbonation of the reaction products," *Fuel*, vol. 84, no. 16, pp. 2048–2054, Nov. 2005, doi: 10.1016/J.FUEL.2005.03.030.

[79] V. Pommer, E. Vejmelková, R. Černý, and M. Keppert, "Alkali-activated waste ceramics: Importance of precursor particle size distribution," *Ceram. Int.*, Aug. 2021, doi: 10.1016/J.CERAMINT.2021.08.037.

[80] R. A. Robayo-Salazar, J. F. Rivera, and R. Mejía de Gutiérrez, "Alkali-activated building materials made with recycled construction and demolition wastes," *Constr. Build. Mater.*, vol. 149, pp. 130–138, Sep. 2017, doi: 10.1016/j.conbuildmat.2017.05.122.

[81] N. Cristelo *et al.*, "One-part hybrid cements from fly ash and electric arc furnace slag activated by sodium sulphate or sodium chloride," *J. Build. Eng.*, vol. 44, p. 103298, Dec. 2021, doi: 10.1016/J.JOBE.2021.103298.

[82] E. Gomaa, A. Gheni, and M. A. ElGawady, "Repair of ordinary Portland cement concrete using ambient-cured alkali-activated concrete: Interfacial behavior," *Cem. Concr. Res.*, vol. 129, p. 105968, Mar. 2020, doi: 10.1016/J.CEMCONRES.2019.105968.

[83] O. Mahmoodi, H. Siad, M. Lachemi, S. Dadsetan, and M. Sahmaran, "Development of optimized binary ceramic tile and concrete wastes geopolymer binders for in-situ applications," *J. Build. Eng.*, vol. 43, p. 102906, Nov. 2021, doi: 10.1016/J.JOBE.2021.102906.

[84] R. Mejía de Gutiérrez, A. R. Robayo-Salazar, and J. F. Rivera, "Alkali-activated building materials made with recycled construction and demolition wastes," *Constr. Build. Mater.*, vol. 149, pp. 130–138, Sep. 2017, doi: 10.1016/J.CONBUILDMAT.2017.05.122.

[85] N. A. M. Sani, R. M. Shamsuddin, K. A. Azizli, and K. Z. K. Shaari, "Determination of Excess Sodium Hydroxide in Geopolymer by Volumetric Analysis," *Procedia Eng.*, vol. 148, pp. 298–301, Jan. 2016, doi: 10.1016/J.PROENG.2016.06.621.

[86] F. G. Collins and L. K. Turner, "Carbon dioxide equivalent (CO2-e) emissions: A comparison between geopolymer and OPC cement concrete," *Constr. Build. Mater.*, vol. 43, pp. 125–130, Jun. 2013, doi: 10.1016/J.CONBUILDMAT.2013.01.023.

[87] J. Payá *et al.*, "New use of sugar cane straw ash in alkali-activated materials: A silica source for the preparation of the alkaline activator," *Constr. Build. Mater.*, vol. 171, pp. 611–621, May 2018, doi: 10.1016/j.conbuildmat.2018.03.230.

[88] C. Shi, D. Roy, and P. Krivenko, *Alkali-Activated Cements and Concretes*. London and New York: Taylor and Francis, 2006.

[89] A. Palomo *et al.*, "A review on alkaline activation: new analytical perspectives," *Mater. Construcción*, vol. 64, no. 315, p. e022, Sep. 2014, doi: 10.3989/mc.2014.00314.

[90] J. S. J. Van Deventer, J. L. Provis, P. Duxson, and D. G. Brice, "Chemical Research and Climate Change as Drivers in the Commercial Adoption of Alkali Activated Materials," *Waste and Biomass Valorization*, vol. 1, no. 1, pp. 145–155, Mar. 2010, doi: 10.1007/s12649-010-9015-9.

[91] M. Nawaz, A. Heitor, and M. Sivakumar, "Geopolymers in construction - recent developments," *Constr. Build. Mater.*, vol. 260, p. 120472, Nov. 2020, doi: 10.1016/J.CONBUILDMAT.2020.120472.

[92] G. C. Lopes, V. Romeu, and T. M. Ferreira, "A systematic review of prefabricated enclosure wall panel systems: focus on technology driven for functional requirements," 2017, Accessed: Apr. 28, 2022. [Online]. Available: https://www.researchgate.net/publication/320197604_A_systematic_review_of_prefabricated_enclosure_wall_panel_systems_focus_on_technology_driven_for_functional_requirements#fullTextFileContent.

Alkali Activation of Recycled Ceramic Aggregates

Alkali-activation of different types of industrial wastes has been extensively explored. However, scarce studies about ceramic wastes were found. Therefore, this part of the research focused on reusing the ceramic fraction from the CDW due to their availability and generation trend. The fundamental properties and the behavior in alkaline activated systems of this ceramic residue alone or in combination with other industrial wastes (fly ash or ladle furnace slag) were investigated.

Alkali activation of recycled ceramic aggregates from construction and demolition wastes

N. Gaibor [a] ✉, J. Coelho [b], D. Leitão [a], T. Miranda [c], P. Tavares [d], N. Cristelo [e]

a. CTAC, Department of Civil Engineering, Azurém Campus, University of Minho, (Guimarães, Portugal)

b. School of Engineering of the University of Minho, Azurém Campus, (Guimarães, Portugal)

c. ISISE, Institute for Science and Innovation for Bio-Sustainability (IB-S), Department of Civil Engineering, University of Minho, (Guimarães, Portugal)

d. CQ-VR, Centro de Química - Vila Real, Department of Chemistry, University of Trás-os-Montes e Alto Douro, (Vila Real, Portugal)

e. CQ-VR, Centro de Química - Vila Real, Department of Engineering, University of Trás-os-Montes e Alto Douro, (Vila Real, Portugal)

✉ normygaibor@gmail.com

Abstract

Environmental concerns are becoming increasingly more significant worldwide, thus creating the urgent need for new sustainable alternatives in the industrial sector. The present study assesses the fundamental properties of ceramic residue (CR) originated by demolition operations, specifically, the floor and wall tiles and sanitaryware furniture, for further incorporation in the construction sector, namely in alkali-activated binders, mixed with other better-known precursors - fly ash (FA) and ladle furnace slag (LFS). Different CR/FA and CR/LFS weight ratios were considered and analyzed by mechanical behavior and microstructural analysis, which included uniaxial compression strength (UCS) tests, Scanning Electron Microscopy (SEM), X-ray Energy Dispersive Analyser (EDX), X-ray diffraction (XRD) and Fourier Transform Infrared Spectroscopy (FTIR). Results obtained showed that the combination of CR and FA or LFS activated with sodium silicate, produced UCS values higher than 20 MPa and 59 MPa, respectively, after 90 days of curing.

Keywords: Alkali activation; Ceramic; Physical properties; Mechanical properties; Waste treatment.

Resumen

Globalmente, las preocupaciones ambientales son cada vez más significativas, creando así la necesidad urgente de nuevas alternativas sostenibles en el sector industrial. El presente estudio evalúa las propiedades fundamentales de los residuos cerámicos (CR) provenientes de demolición, para ser reincorporados en el sector de la construcción, estos son, ligantes activados alcalinamente, mezclados con otros precursores más conocidos: cenizas volantes (FA) y escorias de horno de cuchara (LFS). Se consideraron diferentes relaciones de peso CR/FA y CR/LFS, se analizó el comportamiento mecánico y análisis microestructural, que incluye pruebas de resistencia a la compresión uniaxial (UCS), microscopía electrónica de barrido (SEM), análisis por energías dispersivas de rayos X (EDX), Rayos-X (XRD) y espectroscopía infrarroja por transformada de Fourier (FTIR). Los resultados obtenidos mostraron que, a 90 días de curado, la combinación de CR y FA o LFS activada con silicato de sodio produjo valores de UCS superiores a 20 MPa y 59 MPa, respectivamente.

Palabras Clave: Cerámica; Cemento activado alcalinamente; Tratamiento de residuos; Propiedades mecánicas; Propiedades físicas.

3.1. INTRODUCTION

Worldwide environmental concerns are becoming increasingly more significant. The shortage of natural resources and the increasing levels of greenhouse gas emissions to the atmosphere frames a scenario that inevitably, forces mankind to create new sustainable alternatives for the industrial sector. The use of different kinds of industrial waste and residues as alternative materials in the construction industry can contribute in a very effective way to such sustainability.

On the other hand, the generation of construction and demolition wastes (CDW) and, specifically, the generation of brick and ceramic waste fractions, is accelerating globally due to the increasing renovation and reconstruction of old buildings, which constitute about 45% of the total CDW [1]. In 2014, the total waste generated by all activities for the twenty-eight members of the European Union (EU-28), reached 2503 million tons (being the highest amount during the last 10 years reported). The generation of CDW increased by 57.2 % during the 2004-2014 period, thus showing an inversed trend, when compared with other sectors. For instance, the generation of manufacturing waste, in the same period, decreased by 32.2 %. The numbers confirm the relevance of reinforcing waste valorization in order to propose new management and treatment alternatives [2].

The ceramic industry is plentifully located in different parts of the world. China and Europe are the world leaders in ceramic production. It is also exported to other regions due to its durability and variety in design. In the European Union (EU), the ceramic industry represents approximately 25% of global production. The major producing countries in the EU are Italy, Germany, Spain, France, the United Kingdom, Portugal, and Austria [3]. Except for the ceramic industry's vast economic benefits, it causes adverse environmental impacts. Ceramic industries produce around one-third of the total ceramic production which is disposed of without any further treatment. This solid waste leads to severe environmental pollution and significant land location [4]. The search for sustainable solutions that take advantage to waste materials from the ceramic industry is currently a crucial challenge for this sector.

The construction industry shows an increasing demand for new, bold, sustainable structural and non-structural materials. Ceramic products represent a significant part of the construction industry and, therefore, the requirements in terms of raw materials are also raising. Natural resources are facing a decrease with time due to uncontrolled uses. It is worth noting that progress in the incorporation of

alternative materials might be a useful way to diminish the use of natural resources by recycling the ceramic residue coming out from CDW [5]. However, recycling and using such wastes for newer construction purposes is not a fresh concept; it has been practiced since the Roman Empire when people reused stones obtained from former roads in the construction of new ones [6]. Still, the construction industry represents a very significant possibility to apply, using direct or indirect strategies, significant percentages of several types of by-products and/or wastes. Some common examples are fly ash, CDW, or blast furnace slags, which have been used as a cement or aggregate replacement, embankment fill, and road and railway pavement foundation, among others. It is thought that there is room for the further use of increased volumes of these residues and, also, to introduce of new types of industrial by-products in the production chain [7]. Some studies related to waste incorporation in civil construction are showing up next and along with the present document.

Ceramic residues are hard, durable, extremely resistant to chemical, physical, and biological degradations, and highly thermally stable [4]. Ceramic producers and the construction sector are looking for valuable waste disposal ways due to an increase in the pile-up of them. There is important research work in the development of sustainable alkali-activated building materials using ceramic wastes, such as bricks manufacturing [8], [9], hybrid binder based on ceramic tile wastes [10], ceramic materials from ecofriendly geopolymer precursors [11], ceramic roof tiles [12], among others. As it can be evidenced, for the synthesis of geo-polymers, ceramics waste as an efficient alternative has been employed [13], Huseien et al. [14] stated the geopolymer industries can use the ceramic wastes safely without requiring any remarkable change in the production and application process. The author studied the performance of waste ceramic powder (WCP), at different content of 50%,60%, and 70%, as a binder on the mechanical and microstructure properties of alkali-activated mortars (AAms), mixed with ground blast furnace slag (GBFS) and fly ash (FA). The specimens were left for 24 hours at ambient temperature (27 ±1.5) °C and relative humidity of 75%, then tested at ages of 1, 3, 7, 28, 56, 90, 180, and 360 days. Results showed a compressive strength higher than 70 MPa at age of 28 days. While Hwang et al. [1] used waste red clay brick powder (WBP) and waste ceramic powder (WCP) as source materials to develop an alkali-activated paste. The ceramic waste was 60% of the total weight of the precursors, and the remaining 40% contained fly ash (FA) and ground granulated blast furnace slag (GGBFS). The alkali-activator solutions were Na_2SiO_3 and NaOH. Samples were cured at ambient temperature for 3, 7, 28, and 56 days. The alkali-activated paste with WBP presented higher compressive strength (36–70 MPa). It was due to the finer particle size and higher CaO content

of the WBP as compared to the WCP. Reig et al. [15], reported the use of tile ceramic waste as both a recycled aggregate (TCWA) and a precursor (TCWP). Samples were cured at 65 °C for 3 days. The mechanical properties of the mortars prepared with TCWA reached 53 MPa at 65 °C for 28 days. According to Rakhimova et al. [16] who have studied the potential of introducing WBP in alkali-activated slag cement attested the combination of both improves the compressive and flexural strength. However, it highly depends on the sodium concentration (percentage of Na_2O), silica modulus (SiO_2/Na_2O), and curing methods. The sustainability of mortars fabricated from alkali-activated waste ceramic tile powder and fly ash (FA) exposed to various hostile environments was investigated by Huseien et al. [17]. The assessment in terms of durability suggested that freezing-thawing resistance improved by increasing the FA content in the mortar. It also improved the performance in terms of sulfate and acid environments, as well as decreased energy consumption, financial cost, and CO2 emission. The same authors also studied the performance of this material when exposed to elevated temperatures, concluding that the mechanical strength was enhanced with the increase in ceramic powder content, from 50 to 70% [18].

This work focuses on the reusability of the CDW ceramic residue fraction, such as floor and wall tiles and sanitaryware. It is due to their availability and generation trend. This paper aims to know the ceramic residue's fundamental properties for further incorporation. In this way, the behavior of ceramic residue exhibited in alkaline activated systems mixed with other industrial wastes (fly ash or ladle furnace slag) was analyzed. In addition, the mechanical behavior test was also conducted. The research was complemented by a microstructural analysis, including Scanning Electron Microscopy (SEM), X-ray Energy Dispersive Analysis (EDX), X-ray diffraction (XRD), and Fourier Transform Infrared Spectroscopy (FTIR).

3.2. MATERIALS AND METHODS

3.2.1. Materials

The pastes studied within the scope of the present research are composed of different wastes – ceramic residue (CR), fly ash (FA), and ladle furnace slag (LFS); and alkaline activators in solution form – sodium hydroxide (NaOH) and sodium silicate (Na_2SiO_3). The CR (Figure 3-1a) was provided by a Portuguese licensed waste management operator. Based on the technical sheet, it is part of a batch from demolition operations and, specifically, from the selected floor and wall tiles and sanitaryware

furniture. After dried, it was mechanically milled (MCR, Figure 3-1b), for 32 hours, in a purposely built ball mill, with an increased capacity of 5 kg. The FA (Figure 3-1c) was obtained from a Portuguese thermo-electric power plant, owned by the company *PEGOP*, and the LFS (Figure 3-1d) was supplied by the Portuguese ironwork company *Megasa*, located in Maia, in the north of Portugal.

Figure 3-1. Precursors used in the laboratory experiments: a) original ceramic residue (CR); b) ceramic residue (MCR) milled for 32 hours, c) fly ash (FA), d) ladle furnace slag (LFS)

The particle size distribution (PSD) of all precursors (CR, MCR, FA, and LFS), presented in Figure 3-2, were determined by laser granulometry, on a Sympatec Helos BF analyzer, able to measure particles from 0.9 to 175 μm and using Fraunhofer diffraction theory. The analyses were conducted after a 5-min ultrasonic bath, on a water-ethanol solution, for increased particle dispersion. The PSD of the original CR revealed a poorly graded material, with all particles above 0.075 mm (fine/course reference line). This scenario was significantly modified after the milling process, which produced a more well-graded material, with a fine fraction of approximately 35%.
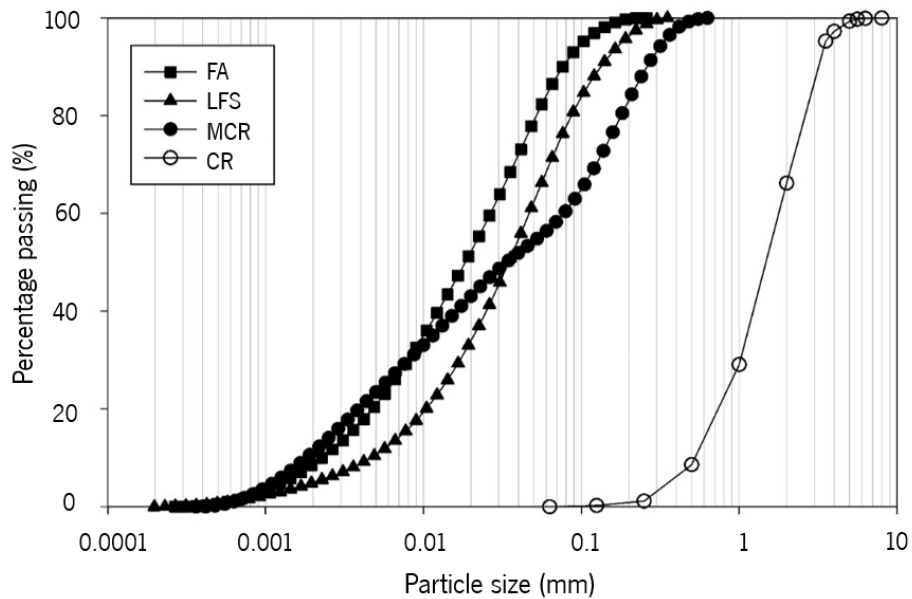
Figure 3-2. Particle size distribution (PSD)

The chemical composition of the original wastes was determined by X-ray fluorescence (Table 3-1). The main constituents of the CR are silica (70.98%) and alumina (17.87%), with a calcium content of 3.72%. The FA showed a similar composition, with significant silica (56.11%) and alumina (21.44%) contents, although with a lower calcium content of 1.30%. The composition of the LFS contains an important calcium content (49.48%), while its significant silica content (18.79%) is, nonetheless, the lowest of the three wastes.

Table 3-1. Chemical composition of the CR, FA, and LFS (% wt)

Material	Al_2O_3	CaO	Cr_2O_3	Fe_2O_3	K_2O	MgO	MnO	Na_2O	P_2O_5	SiO_2	SO_3	TiO_2	ZnO	Otros
CR	17.87	3.72	-	1.20	3.18	1.31	-	1.27	-	70.98	-	0.47	-	-
FA	21.44	1.30	0.06	8.20	2.81	1.46	0.07	1.12	0.25	56.11	0.66	1.15	0.03	5.34
LFS	7.39	49.48	0.68	10.07	0.03	5.41	1.43	0.13	0.07	18.79	3.42	0.40	1.25	1.45

The mineralogy of the original materials precursors and the subsequent pastes was assessed on a PANalytical X'Pert Pro diffractometer, fitted with an X'Celerator detector and secondary monochromator, using CuKα radiation at 40kV and 30mA. The scans were acquired with Bragg-Brentano geometry, covering a 2θ range between 7 and 85°, with a nominal step size of 0.017° and 100 s/step. In the case of the CR, LFS, and resulting pastes, phase quantification was performed on diffraction patterns applying Rietveld [19], with the code Highscore Plus 4.8. The values are presented in weight percentage, in Table 3-2. For the FA refinement, the code PowderCell 2.4 [20] was applied

instead. The amorphous phase was simulated through the Le Bail model [21]. Volume percentages were converted into weight percentages using the respective density. Figure 3-3 presents the X-ray diffractograms, showing that the CR is essentially quartz, although several other minor phases were also detected, such as sillimanite, oligoclase, mullite, and anorthite. The main crystalline phases identified in the FA were quartz, mullite, hematite, and graphite. The last one shares the main peak in the same location as quartz, a halo between 25 and 27°(2θ). While the LFS presents several crystalline phases, namely calcio, olivine, andradite, calcite, cuspidine, titanite, and larnite, it presented mostly crystalline structures. The slag presents a slight halo, between 27 and 40°(2θ), characteristic of vitreous/amorphous materials [22], while the fly ash and ceramic residue showed a similar halo, although between 2θ ≈ [25 - 30]°.
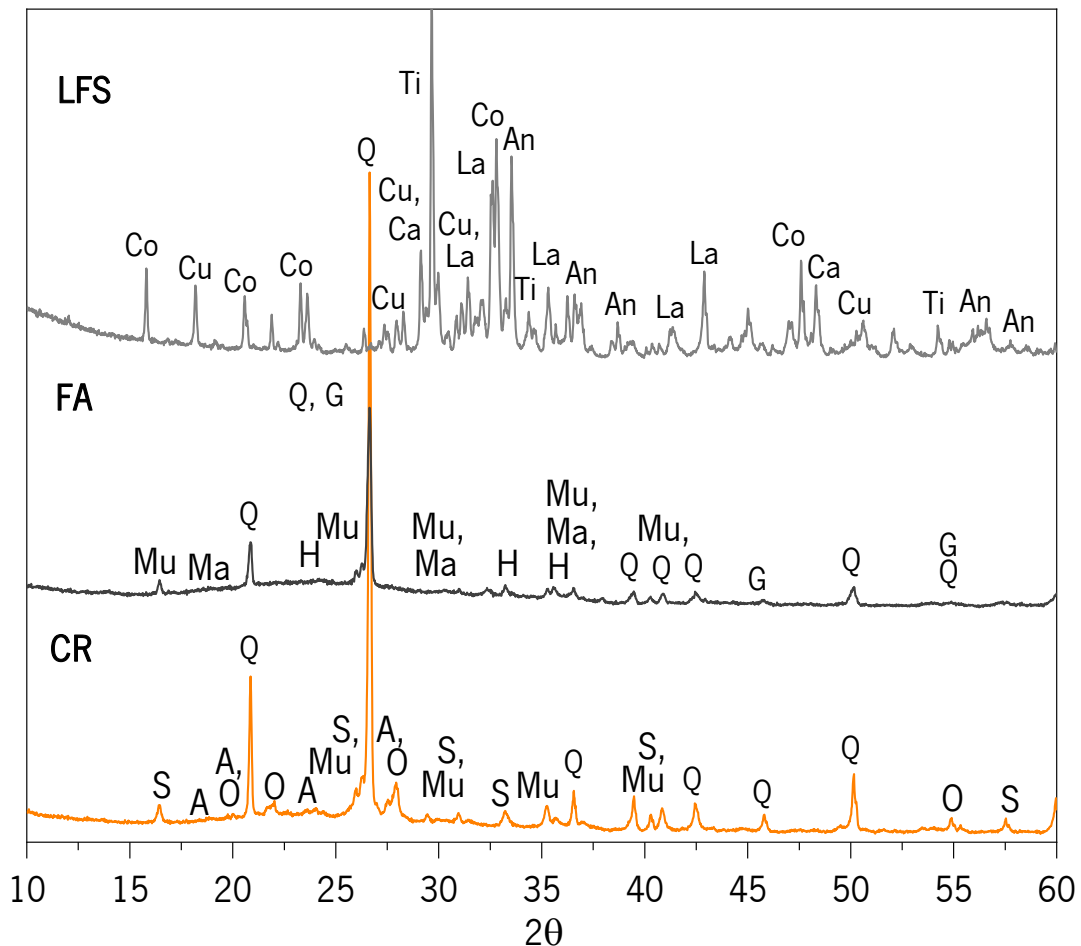
Figure 3-3. XRD spectra of the ceramic residue (CR) – milled for 32 hours; Fly Ash (FA); ladle furnace slag (LFS) (S: Sillimanite; O: Oligoclase; Q: Quartz; Mu: Mullite; A: Anorthite; Ma: Magnetite; H: Hematite; G: Graphite; Co: Calcio Olivina; Cu: Cuspidine; Ca: Calcite; Ti: Titanite; La: Larnite; An: Andradite).

Table 3-2. Minerals quantification in starting materials, ceramic residue (CR) – milled for 32 hours; Fly Ash (FA); ladle furnace slag (LFS), (% wt)

Material	S	O	Q	Mu	A	Ma	H	G	Co	Cu	Ca	Ti	La	An	Amorphous	R_{wp} (%)
CR	2.3 ±0.8	8.2 ±0.9	62.3 ±2.0	19.8 ±1.5	7.4 ±1.5	-	-	-	-	-	-	-	-	-	-	9.3
FA	-	-	9.7 ±0.9	10.2 ±0.9		1.0 ±0.1	0.7 ±0.1	1.3 ±0.2	-	-	-	-	-	-	77.1±4	7.7
LFS	-	-	-	-		-	-	-	49.2 ±2	13.4 ±0.9	2.8 ±0.2	1.3 ±0.2	22.5 ±1	10.7 ±0.9	-	8.1

S: Sillimanite; O: Oligoclase; Q: Quartz; Mu: Mullite; A: Anorthite; Ma: Magnetite; H: Hematite; G: Graphite; Co: Calcio Olivina; Cu: Cuspidine; Ca: Calcite; Ti: Titanite; La: Larnite; An: Andradite

Sodium hydroxide (SH) and sodium silicate (SS), in solution form, were used as activators throughout this study. The SH was prepared 4 to 6 h before the fabrication of the pastes, with a concentration of 8 molal, using deionized water. The sodium silicate had a unit weight of 1.464 g/cm^3 at 20°C, a SiO_2/Na_2O weight ratio of 2.0 (molar oxide ratio of 2.063), and a Na_2O concentration in the solution of 13.0%.

3.2.2. Preparation and development of the experimental work

The composition of the mixtures was defined based on the results of a preliminary test where the variation of the solid/liquid ratio between the precursor and the activator determined the appropriate ratio to obtain better workability of the mixtures. The performance of sodium hydroxide (SH) or sodium silicate (SS) was studied in separate experiments. Each experimental setup included a parallel treatment of both precursors and covered the same alkali activator concentrations (SH or SS). Table 3-3 presents the studied pastes, including their respective activator/precursor ratio. CR was tested without the addition of an additional precursor (FA or LFS), to assess the possibility of direct activation, which would translate into more economical and less logistical demanding pastes.

Table 3-3. Identification and characterization of the tested pastes

Paste ID	Precursor			Activ	Precursors/ Activator. (wt. ratio)	CaO / SiO_2	Na_2O / Al_2O_3	SiO_2 / Al_2O_3	SiO_2 / Na_2O
	CR	FA	LFS						
M1	100	0	-	SH 8m	0.32	0.05	0.41	3.97	9.74
	75	25	-		0.34	0.05	0.41	3.58	8.82
	50	50	-		0.36	0.04	0.41	3.23	7.98
	25	75	-		0.38	0.03	0.40	2.91	7.21
	0	100	-		0.40	0.02	0.40	2.62	6.49
M2	100	0	-	SS	0.40	0.05	0.36	4.55	12.58
	75	25	-		0.43	0.04	0.36	4.18	11.50
	50	50	-		0.46	0.03	0.37	3.84	10.52
	25	75	-		0.49	0.03	0.37	3.53	9.64
	0	100	-		0.52	0.02	0.37	3.25	8.84
M3	100	-	0	SH 8m	0.32	0.05	0.41	3.97	9.74
	75	-	25		0.34	0.26	0.48	3.80	7.85
	50	-	50		0.36	0.59	0.59	3.55	6.01
	25	-	75		0.38	1.19	0.76	3.18	4.21
	0	-	100		0.40	2.63	1.04	2.54	2.46
M4	100	-	0	SS	0.40	0.05	0.36	4.55	12.58
	75	-	25		0.43	0.22	0.43	4.53	10.51
	50	-	50		0.46	0.47	0.53	4.50	8.51
	25	-	75		0.49	0.85	0.68	4.45	6.57
	0	-	100		0.52	1.53	0.93	4.37	4.69

The sodium hydroxide was prepared 4 to 6 hours before use because it generates an exothermic reaction that needs to cool down. The activator temperature at the time of the mixing was 20°C ± 1°C. A mechanical mixing process followed, for a period of 3 minutes, complemented by manual homogenization, with the help of a spatula (whenever required, the mechanical homogenization period was extended for 2 minutes).

The homogenized paste was then poured into cubic stainless-steel molds and mechanically compacted for 2 minutes. Three cubic specimens of 40 x 40 x 40 mm_3 (nominal dimensions) were fabricated for each paste, and each curing period. The initial curing period lasted 1 day at 70°C, with the pastes still inside the molds. It was followed by 14, 28, and 90 days of curing at ambient temperature and humidity 20-23 °C and around 60% RH, respectively. After being measured and weighed, each specimen was then subjected to a uniaxial compression strength test (UCS), on a servo-hydraulic testing machine, using three different actuators, with load capacities of 40, 100, and 120 kN. These tests were carried out under monotonic displacement control, at a rate of 0.6 mm/min, and stress-strain curves were plotted for all tests performed.

The present research was complemented by microstructural analysis, which included Scanning Electron Microscopy (SEM), X-ray Energy Dispersive Spectroscopy (EDX), X-ray diffraction (XRD), and

Fourier Transform Infrared Spectroscopy (FTIR). SEM analyses were developed on an *FEI Quanta 400* scanning electron microscope, at 30 kV, in low vacuum mode, with partial pressure inside the chamber (1.3 mbar), avoiding the deposition of a conductive layer. An EDS analyzer, from EDAX, allowed a chemical analysis of the elements present in each sample, using the same spectrum acquisition time and a ZAF correction model.

The FTIR spectra were acquired using a Thermo Scientific Nicolet iS50 FTIR spectrometer, resorting to an ATR (Attenuated Total Reflectance) accessory with a diamond crystal. The instrument was controlled by the Omnic software package, version 9.2.28, from Thermo Fisher Scientific Inc. A spectrum range of 4000 to 400 cm^{-1} was defined, with a resolution of 4 cm^{-1} and 64 scans by 90 seconds for each sample.

3.3. RESULTS AND DISCUSSION

3.3.1. Compressive strength

The uniaxial compressive strength (UCS) results are presented in Figure 3-4, showing the data for the pastes prepared with CR and FA, and Figure 3-5, showing the data for the pastes with CR and LFS. the effectiveness of the CR, pastes with an increasing amount of FA and LFS (up to, and including, a 100% content for each case) are also presented, so that a threshold could be established, and direct comparison could easily be made. Curing periods of 1, 14, 28, and 90 days are presented, yet it is important to remember, at this stage, that the 1-day curing specimens were exclusively cured at 70°C, while the remaining specimens were cured for 1 day, at 70°C, while the remaining curing was developed at ambient temperature (20 - 23°C).

In general, curing time increased the UCS, regardless of the type of precursor (CR+FA or CR+LFS) or activator (SH or SS). Also evident are the higher strength values obtained with the SS-based pastes, comparatively to the SH-based specimens, irrespective of whether the precursor combination. Finally, the third and most relevant observation is the higher UCS achieved by the CR+LFS precursor combination, when compared with the CR+FA blend.

For the CR+FA combination, activated with SH, the most effective solution was the 50% CR and 50% FA. When SS was used, the proportion of 75% CR and 25% FA achieved the highest UCS value after 90 days. However, it is significant, considering that the purpose of the present study is the disposal of the ceramic residue, that the 100% CR paste (which represents the highest possible volume of CR

incorporated) showed the highest UCS for the CR+FA combination after 1, 14 and 28 days, and showed only a marginally lower UCS after 90 days. This suggests that the use of FA is not absolutely required, which would represent a significant gain in terms of economic and logistical efforts.

Regarding the CR+LFS combination, the scenario was slightly different for the SH-based pastes, with the 75% CR + 25% LFS representing the higher UCS. Another significant difference was the extent of such strength increase, at the 90-day mark: the addition of 50% FA produced a UCS improvement of 1.9x, relatively to the 100% CR, while the addition of 25% LFS produced a UCS improvement of 4.6x, relatively to the same 100% CR paste. For the SS-based pastes, the CR+LFS scenario was similar to the one described for the CR+FA pastes, i.e., the addition of 25% of the alternative precursor repre-sented the most performing combination for both cases. However, the 75%CR + 25%LFS paste now showed higher UCS values for all curing periods, and not just for 90 days. Not only that, but the difference, at the 90-day mark, between the 100%CR and the 75%CR + 25%LFS was clearly more significant (3.15x) than the difference between the 100%CR and the 75%CR + 25%FA (1.1x).
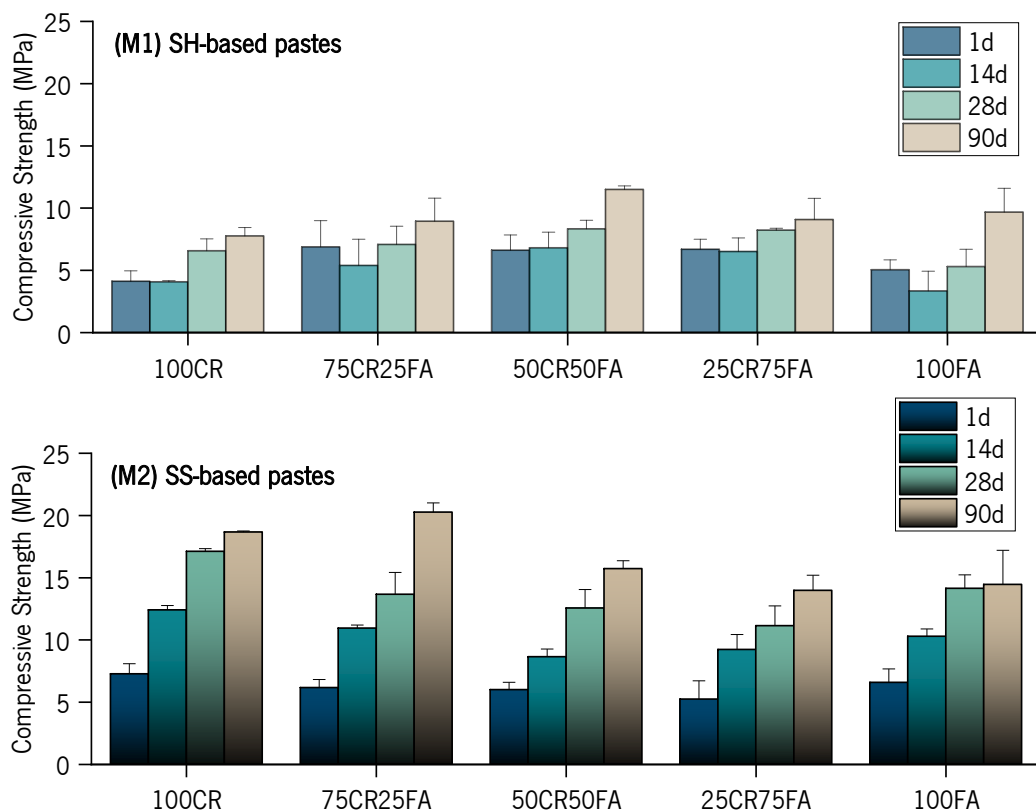
Figure 3-4. UCS of the CR+FA pastes, prepared with SH (M1) or SS (M2), after 1, 14, 28, and 90 days of curing
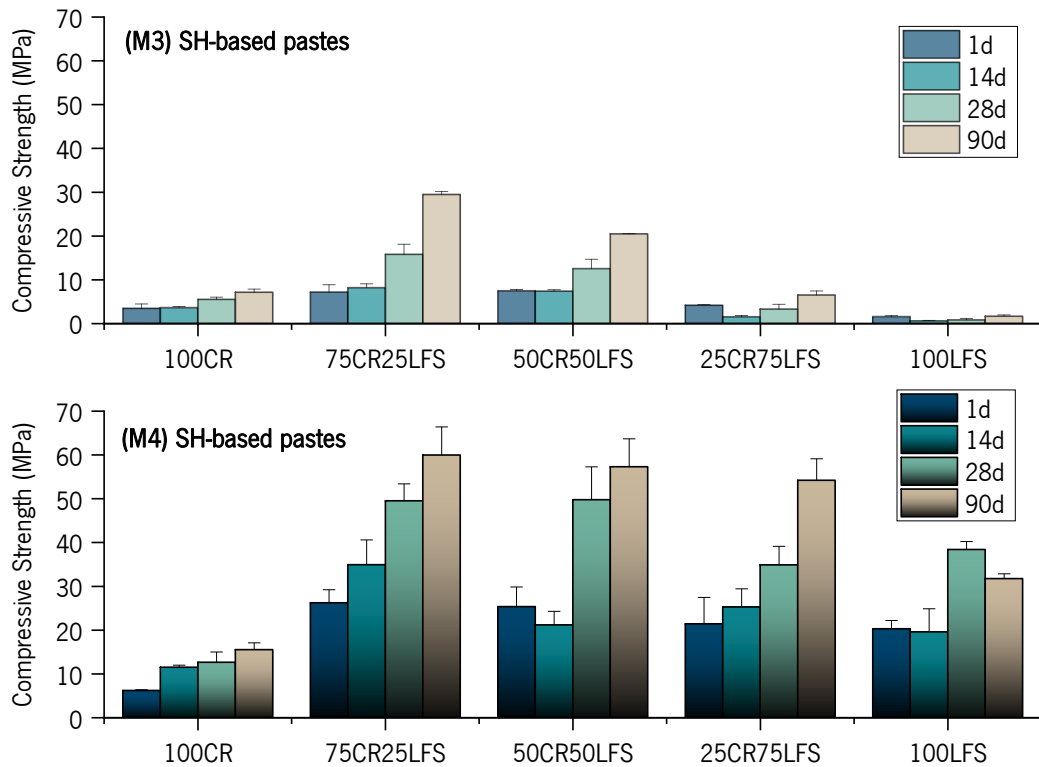
Figure 3-5. UCS of the CR+LFS pastes, prepared with SH (M3) or SS (M4), after 1, 14, 28, and 90 days of curing

3.3.2. Mineralogical and microstructural characterization

The pastes with the highest strength values from each set (M1, M2, M3, and M4), corresponding in most cases to the composition 75% CR + 25% (FA or LFS), were selected for microstructural analyses, using XRD, SEM/EDS, and FTIR to characterize the cementitious materials developed during their respective reactions throughout the initial 90 days of curing.

Figure 3-6 shows the XRD diffractograms of the different pastes, 75CR+25FA (SH or SS) (M1 and M2) and 75CR+25LFS (SH or SS) (M3 and M4). The products resulting from the activation reaction present similar peaks which were also found in the initial materials, suggesting that the equivalent phases are essentially inert to the alkaline activation process. In cases where a slight reduction of their intensity is detected, it is due to the material dilution (induced by the blend with the activator). The presence of mullite in M1 (25.1 ± 1.5) and M2 (23.2 ± 1.5) is somewhat higher in comparison to the other two mixtures (see Table 3-4), fundamentally influenced by the outset constituents, CR and FA with significant Si content (Table 3-1). Crystalline phases of Mu in the pastes were also displaced in range, from 28 – 30°(2θ) to 30 to 35°(2θ) in contrast to CR and FA XDR diffractograms (Figure 3-3). These

variations are a consequence of the formation of amorphous phases in the aluminosilicate gel, which will partially crystalize, in time (zeolitic precursor) [22]–[24]. The anorthite (A) was identified in the four mixtures since the CR is the major component. However, higher A content was evidenced in M3 (16.5 ± 1.1) and M4 (15.0 ± 1.1) (Table 3-4) as a result of having a precursor (LFS) with high Ca content. In all blends, the main peak was registered at approximately 26° (2q), corresponding to quartz, which makes it the most relevant crystalline phase. It is also worth mentioning that for neither case the $Na_2CO_3.H_2O$ (thermonatrite) phase was found, denoting that the Na was retained in the gel, thus not migrating to the surface.
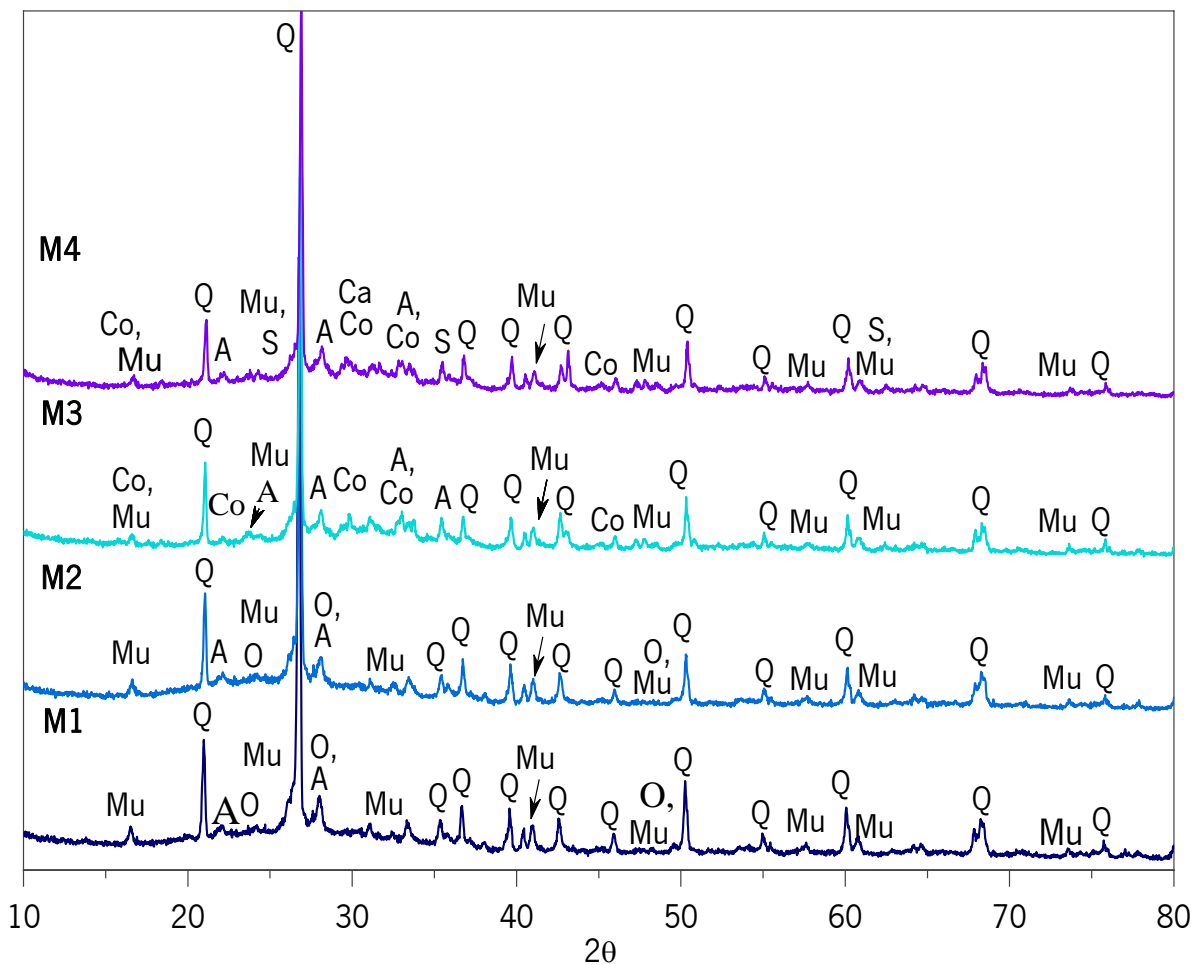
Figure 3-6. XRD patterns of the 75CR-25FA/SH or SS mixtures (M1 and M2) and 75CR-25LFS/SH or SS mixtures (M3 and M4), after 90 days of curing time (O: Oligoclase; Q: Quartz; Mu: Mullite; A: Anorthite; Co: Calcio Olivina; Ca: Calcite; S: Sillimanite).

Table 3-4. Minerals quantification of the 75CR-25FA/SH or SS mixtures (M1 and M2) and 75CR-25LFS/SH or SS mixtures (M3 and M4), after 90 days of curing time (% wt)

Material	O	Q	Mu	A	Co	Ca	S	R_{wp} (%)
M1	9.1 ± 0.9	55.9 ± 2.0	25.1 ± 1.5	9.9 ± 0.9	-	-	-	8.4
M2	13.8 ± 1.1	53.4 ± 2.0	23.2 ± 1.5	9.7 ± 0.9	-	-	-	8.4
M3	-	46.9 ±2.0	21.6 ± 1.5	16.5 ± 1.1	13.8 ± 1.1	1.2 ± 0.1		10.0
M4	-	48.6 ± 2.0	19.2 ± 1.5	15.0 ± 1.1	10.8 ± 1.0	2.3 ± 0.2	4.1 ± 0.4	9.9

O: Oligoclase; Q: Quartz; Mu: Mullite; A: Anorthite; Co: Calcio Olivina; Ca: Calcite; S: Sillimanite

The same four pastes, cured at ambient temperature for 90 days, were analyzed with SEM. The chemical composition was also obtained, with 10 points per image.

Figure 3-7 shows SEM images of selected samples, enabling an understanding of the morphology and general distribution of the different constituents in the mixtures. Based on all the images exhibited, it can be said that the resulting paste is generally compacted, homogeneous, and with low porosity. In M1(75CR-25FA/SH) is possible to observe several FA (points A) or CR (points C) unreacted particles covered with reaction products. However, in M2 (75CR-25FA/SS), even after 90 days, an unreacted particle without any signs of Na 'attack', can still be detected (points A). It was also observed a slightly higher Ca content in the M2 paste, compared with the M1, which might result from a higher dissolution degree. Regarding the type of gel developed, an N-A-S-H type was detected (point *) when using FA as a complementary precursor, regardless of the activator solution used (SH or SS).

A similar situation can be seen for the 75CR-25FA/SH (M3) and 75CR-25LFS/SH (M4) pastes. Some small LFS (points B) and CR (points C) unreacted particles are distinguished. The most significant aspect of M4 was the Ca content varies throughout the sample, which can be due to the incidence of particles with an important presence of Ca. Concerning the type of gel developed, and when LFS in combination with CR was used, its calcium content naturally affected the composition of the gel, which can be classified as an N, C-A-S-H, if SH acted as an activator (M3), or C-A-S-H (points *) [25], [26], when the precursors were instead activated with SS (M4),

Figure 3-7. The general chemical composition of the four studied mixtures is summarized in Table 3-5, where is presented the average value of the analyzed points and their standard deviation (SD).
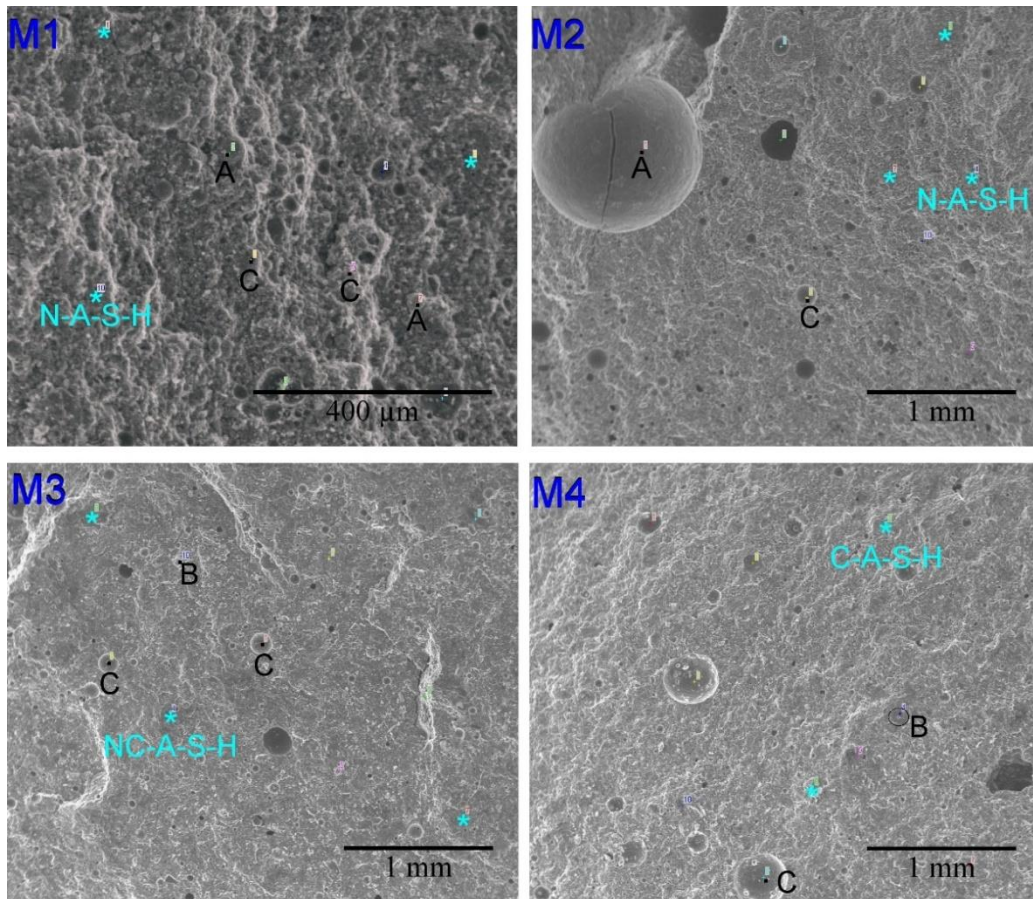
Figure 3-7. SEM images of 75CR-25FA/SH or SS mixtures (M1 and M2) and 75CR-25LFS/SH or SS mixtures (M3 and M4) mixtures, after 90 days of curing time.

Table 3-5. Chemical composition of mixtures at 90 days curing time, %Wt, (SD in parentheses)

	M1 75CR-25FA/SH	M2 75CR-25FA/SS	M3 75CR-25LFS/SH	M4 75CR-25LFS/SS
Na_2O	6.66 (1.93)	15.06 (3.47)	10.49 (1.04)	5.24 (1.77)
MgO	0.84 (0.26)	1.47 (0.82)	1.79 (0.91)	1.80 (1.61)
Al_2O_3	19.53 (5.44)	14.58 (1.33)	16.65 (4.43)	12.26 (4.86)
SiO_2	63.35 (3.59)	57.92 (5.34)	52.12 (3.12)	59.09 (11.30)
SO_3	-	-	2.22 (1.47)	2.55 (3.32)
K_2O	5.81(1.24)	2.61 (0.61)	2.44 (0.26)	2.03 (1.03)
CaO	1.84 (1.03)	2.70 (0.59)	11.44 (3.07)	15.52 (11.73)
TiO_2	0.52 (0.32)	0.84 (0.33)	0.66 (0.23)	0.57 (0.29)
MnO	-	-	-	0.11 (0.26)
Fe_2O_3	1.46 (0.50)	4.82 (4.67)	2.21 (2.15)	0.83 (0.42)
CaO/SiO_2	0.01 (0.00)	0.02 (0.01)	0.22 (0.06)	0.27 (0.36)
NaO/Al_2O_3	0.36 (0.14)	1.05 (0.28)	0.67 (0.18)	0.48 (0.27)
SiO_2/Al_2O_3	3.44 (0.84)	3.97 (0.18)	3.31 (0.82)	5.41 (2.03)
SiO_2/Na_2O	10.24 (2.86)	4.06 (1.18)	5.01 (0.59)	12.62 (4.74)

Figure 3-8, shows the FTIR spectra for the starting materials (LFS, CR, and FA) as well as the M1 (75CR25FA), M2 (75CR25FA), M3 (75CR25FA), and M4 (75CR25FA) pastes activated with SH or SS, after 90 days of curing, which present a set of bands centered in the frequency range between [400 - 2000] cm^{-1}. Different behavior in the spectra of each of the materials is observed, for LFS two main bands are detected at 840 cm^{-1} and 1040 cm^{-1}, which are generally associated with deformation vibration of carbonates (CO_3^{2-}), C-O, while the 560 cm^{-1} band is linked with the Al-O-Al bond and 490 cm^{-1} and 440 cm^{-1} are associated with O-Si-O connections. The fly ash (FA) evidences a wide main band at 1015 cm^{-1}, this is associated with Si-O-Si or Si-O-Al bonds, while the 790 cm^{-1} and 420 cm^{-1} bands are related to Si-O bonds (quartz). In addition, the presence of another band that records at 550 cm^{-1} is associated with the octahedral aluminum (Al-O-Al bonds) of the mullite [27], previously distinguished in this material by XRD, (see Figure 3-3). The CR sample shows a deep and wide main band that appears around 1040 cm^{-1}. This is typical of asymmetric tension vibration, related to Si-O-Si or Si-O-Al, confirming some crystallinity of the material. The bands at 795 cm^{-1}, 775 cm^{-1}, and 420 cm^{-1} correspond to O-Si-O bonds (quartz).

The FTIR spectra of the four different mixtures are also presented in Figure 3-8, where basically the characteristic vibration bands of the main components of the starting materials are shown. At the end of the 90 days of curing, the most significant change was the displacement of the main CR band (1040 cm^{-1}), for shorter wavelengths, which is attributed to a structural reorganization caused by the formation of reaction products [28]. But, in mixtures of the studied proportions of M1 and M2, the displacement was between 995 cm^{-1} and 1010 cm^{-1}, which is related to the formation of the typical N-A-S-H gel, while M3 and M4 shifted around 960 cm^{-1}, this translation is connected to the presence of LFS in the composition, promoting the formation of N, C-A-S-H type gel.
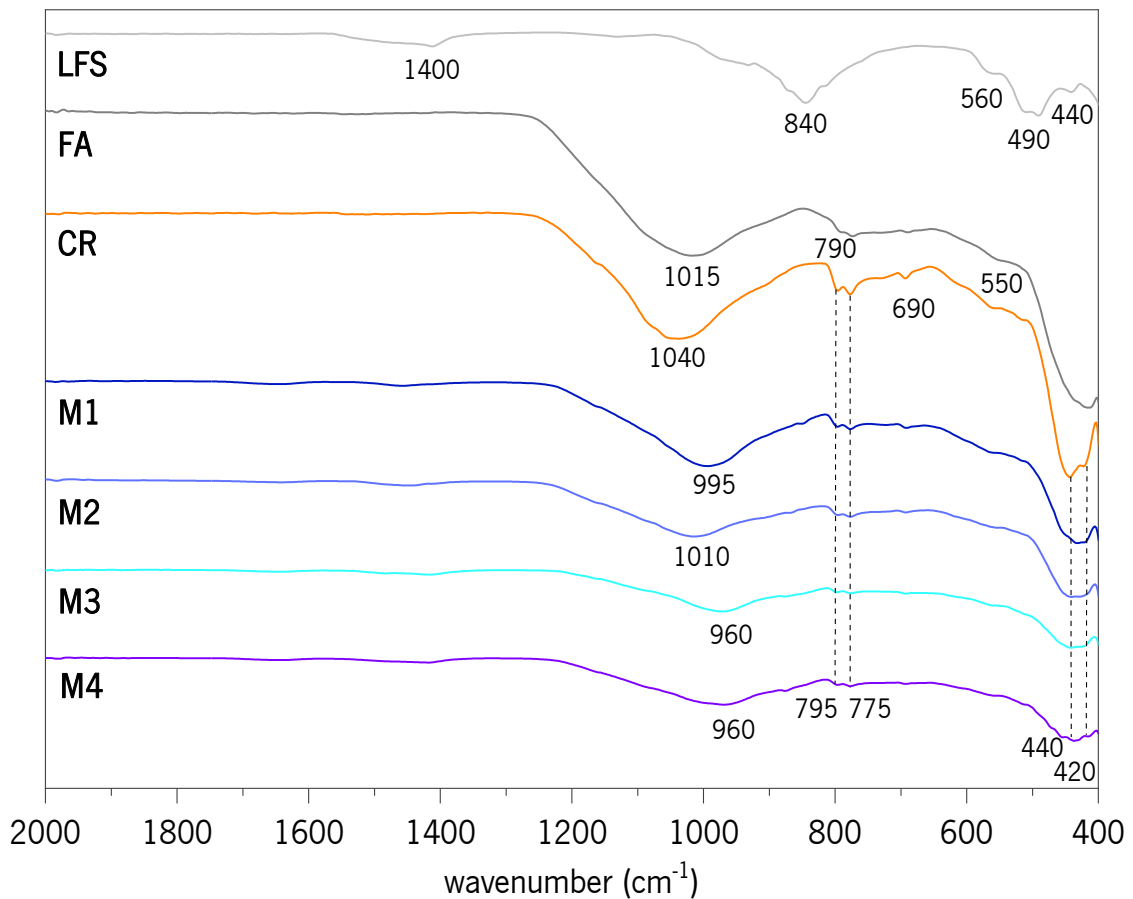
Figure 3-8. FTIR spectra of starting materials, the ladle furnace slag (LFS); ceramic residue (MCR) – milled for 32 hours; fly ash (FA), and 75CR-25FA/SH or SS mixtures (M1 and M2) and 75CR-25LFS/SH or SS mixtures (M3 and M4), after 90 days curing time.

3.4. CONCLUSIONS

The fundamental properties of the ceramic residue from an operator with a Portuguese license and their performance in combination with fly ash (FA) or ladle furnace slag (LFS) as precursors of alkali activation were studied and tested four different mixture compositions, in accordance with the main aim of this study. The following are the main conclusions obtained:

1. Different CR/FA (M1 and M2) and CR/LFS (M3 and M4) ratios were prepared and tested for the purpose. The UCS test was performed for each specimen after 1, 14, 28, and 90 days to determine the efficiency of the blends. The highest compressive strength (59.95 MPa) was reached by the combination of 75CR-25 LFS/SS at 90 days of curing. It can be stated that this resulting material is stiffer compared to the CR-FA/SH or SS mixture, where the highest strength in the same conditions was 20.26 MPa;

2. M1-M2 and M3-M4 mixtures are calcium-poor or calcium-rich aluminosilicates, respectively, which are basically determined by the starting materials. Higher calcium content positively affects the strength of the mixture. As was evidenced throughout the UCS results;

3. The combination of the CR+FA precursors, regardless of the alkaline solution (SH or SS), enabled the formation of a cementitious gel-type, namely, N-A-S-H. On the other hand, NC-A-S-H or C-A-S-H gels are identified, when CR+LFS is activated whether SH or SS, respectively.

ACKNOWLEDGMENTS

REFERENCES

[1]   C.-L. Hwang, M. Damtie Yehualaw, D.-H. Vo, and T.-P. Huynh, "Development of high-strength alkali-activated pastes containing high volumes of waste brick and ceramic powders," *Constr. Build. Mater.*, vol. 218, pp. 519–529, Sep. 2019.

[2]   Eurostat, "Waste statistics - Statistics Explained," 2018. [Online]. Available: http://ec.europa.eu/eurostat/statistics-explained/index.php/Waste_statistics. [Accessed: 03-May-2018].

[3]   Cerame-Unie, "Ceramic industry | Cerame-Unie - The European Ceramic Industry Association." [Online]. Available: http://cerameunie.eu/ceramic-industry/. [Accessed: 08-May-2018].

[4]   M. S. Khan, M. Sohail, N. S. Khattak, and M. Sayed, "Industrial ceramic waste in Pakistan, valuable material for possible applications," *J. Clean. Prod.*, vol. 139, pp. 1520–1528, Dec. 2016.

[5]   H.-J. Chen, T. Yen, and K.-H. Chen, "Use of building rubbles as recycled aggregates," *Cem. Concr. Res.*, vol. 33, no. 1, pp. 125–132, Jan. 2003.

[6]   A. Jindal and G. D. Ransinchung R.N., "Behavioural study of pavement quality concrete containing construction, industrial and agricultural wastes," *Int. J. Pavement Res. Technol.*, Apr. 2018.

[7]   N. Cristelo, A. Fernández-Jiménez, T. Miranda, and Á. Palomo, "Sustainable alkali activated materials: Precursor and activator derived from industrial wastes," *J. Clean. Prod.*, vol. 162, pp. 1200–1209, 2017.

[8]   H. R. Gavali, A. Bras, P. Faria, and R. V. Ralegaonkar, "Development of sustainable alkali-activated bricks using industrial wastes," *Constr. Build. Mater.*, vol. 215, pp. 180–191, Aug. 2019.

[9]   S. K. Amin, S. A. El-Sherbiny, A. A. M. A. El-Magd, A. Belal, and M. F. Abadir, "Fabrication of geopolymer bricks using ceramic dust waste," *Constr. Build. Mater.*, vol. 157, pp. 610–620, Dec. 2017.

[10]   L. M. Murillo, S. Delvasto, and M. Gordillo, "A study of a hybrid binder based on alkali-activated ceramic tile wastes and portland cement," in *Sustainable and Nonconventional Construction Materials using Inorganic Bonded Fiber Composites*, Elsevier Inc., 2017, pp. 291–311.

[11]   M. A. Villaquirán-Caicedo and R. M. de Gutiérrez, "Synthesis of ceramic materials from ecofriendly geopolymer precursors," *Mater. Lett.*, vol. 230, pp. 300–304, Nov. 2018.

[12]   A. R. G. Azevedo, C. M. F. Vieira, W. M. Ferreira, K. C. P. Faria, L. G. Pedroti, and B. C. Mendes, "Potential use of ceramic waste as precursor in the geopolymerization reaction for the production of ceramic roof tiles," *J. Build. Eng.*, vol. 29, May 2020.

[13]   Z. Sun *et al.*, "Synthesis and thermal behavior of geopolymer-type material from waste ceramic," *Constr. Build. Mater.*, vol. 49, pp. 281–287, Dec. 2013.

[14]   G. F. Huseien, A. R. M. Sam, K. W. Shah, M. A. Asaad, M. M. Tahir, and J. Mirza, "Properties of ceramic tile waste based alkali-activated mortars incorporating GBFS and fly ash," *Constr. Build. Mater.*, vol. 214, pp. 355–368, Jul. 2019.

[15]   L. Reig, M. A. Sanz, M. V. Borrachero, J. Monzó, L. Soriano, and J. Payá, "Compressive strength and microstructure of alkali-activated mortars with high ceramic waste content," *Ceram. Int.*, vol. 43, no. 16, pp. 13622–13634, Nov. 2017.

[16]   N. R. Rakhimova and R. Z. Rakhimov, "Alkali-activated cements and mortars based on blast furnace slag and red clay brick waste," *Mater. Des.*, vol. 85, pp. 324–331, Nov. 2015.

[17]   G. F. Huseien, A. R. M. Sam, K. W. Shah, J. Mirza, and M. M. Tahir, "Evaluation of alkali-activated mortars containing high volume waste ceramic powder and fly ash replacing GBFS," *Constr. Build. Mater.*, vol. 210, pp. 78–92, Jun. 2019.

[18]   G. F. Huseien *et al.*, "Waste ceramic powder incorporated alkali activated mortars exposed to elevated Temperatures: Performance evaluation," *Constr. Build. Mater.*, vol. 187, pp. 307–317, Oct. 2018.

[19]   N. Cristelo, P. Tavares, E. Lucas, T. Miranda, and D. Oliveira, "Quantitative and qualitative assessment of the amorphous phase of a Class F fly ash dissolved during alkali activation reactions – Effect of mechanical activation, solution concentration and temperature," *Compos. Part B Eng.*, vol. 103, pp. 1–14, Oct. 2016.

[20]   CCP14, "CCP14 Homepage - Tutorials and Examples - Powder Cell for Windows, Structure Visualisation/Manipulation, Powder Pattern Calculation and Profile Fitting by Werner Kraus and Gert Nolze." [Online]. Available: http://www.ccp14.ac.uk/tutorial/powdcell/. [Accessed: 17-Jan-2020].

[21]   A. Le Bail, "Modelling the silica glass structure by the Rietveld method," *J. Non. Cryst. Solids*, vol. 183, no. 1–2, pp. 39–42, Apr. 1995.

[22]   N. Cristelo, J. Coelho, T. Miranda, Á. Palomo, and A. Fernández-Jiménez, "Alkali activated composites – An innovative concept using iron and steel slag as both precursor and aggregate," *Cem. Concr. Compos.*, vol. 103, pp. 11–21, Oct. 2019.

[23]   C. Ruiz-Santaquiteria, A. Fernández-Jiménez, and A. Palomo, "Alternative prime materials for developing new cements: Alkaline activation of alkali aluminosilicate glasses," *Ceram. Int.*, vol. 42, no. 8, pp. 9333–9340, Jun. 2016.

[24]   A. Fernández-Jiménez, M. Monzó, M. Vicent, A. Barba, and A. Palomo, "Alkaline activation of metakaolin-fly ash mixtures: Obtain of Zeoceramics and Zeocements," *Microporous Mesoporous Mater.*, vol. 108, no. 1–3, pp. 41–49, Feb. 2008.

[25]   I. Garcia-Lodeiro, A. Fernandez-Jimenez, and A. Palomo, "Hydration kinetics in hybrid binders: Early reaction stages," *Cem. Concr. Compos.*, vol. 39, pp. 82–92, 2013.

[26]   F. Puertas, M. Palacios, H. Manzano, J. S. Dolado, A. Rico, and J. Rodríguez, "A model for the C-A-S-H gel formed in alkali-activated slag cements," *J. Eur. Ceram. Soc.*, vol. 31, no. 12, pp. 2043–2056, Oct. 2011.

[27]   H. Schneider, J. Schreuer, and B. Hildmann, "Structure and properties of mullite-A review," *J. Eur. Ceram. Soc.*, vol. 28, no. 2, pp. 329–344, 2008.

[28]   J. F. Rivera, N. Cristelo, A. Fernández-Jiménez, and R. Mejía de Gutiérrez, "Synthesis of alkaline cements based on fly ash and metallurgic slag: Optimisation of the SiO 2 /Al 2 O 3 and Na 2 O/SiO 2 molar ratios using the response surface methodology," *Constr. Build. Mater.*, vol. 213, pp. 424–433, Jul. 2019.

<div align="right">Chapter IV:</div>

Effect of fiber reinforcement in alkali-activated ceramic/slag-based mortar under thermal curing

Since the source and the origin of the ceramic waste is different from the preceding chapter (i.e., from the ceramic industry), first, its fundamental properties were determined to assess its potential in the development of alkali-activated materials. Afterward, the mixture composition was refined to allow the incorporation of polyacrylonitrile (PAN) fibers aiming to enhance the physical and mechanical properties. Thus, the influence of PAN fibers of two different content was evaluated, 0.5% and 1% in volume, to be compared with the control paste, 0%.

Effect of polyacrylonitrile fiber on the properties of alkali-activated ceramic/slag-based mortar

Norma Gaibor [a, *], Dinis Leitão [b], Tiago Miranda [c], Nuno Cristelo [d], Eduardo N.B. Pereira [c], Vítor M.C.F. Cunha [c]

a. School of Engineering of the University of Minho, Azurem Campus, 4800-058, Guimarães, Portugal

b. CTAC, Department of Civil Engineering, University of Minho, 4800-058, Guimarães, Portugal

c. ISISE, Institute for Science and Innovation for Bio-Sustainability (IB-S), Department of Civil Engineering, University of Minho, 4800-058, Guimarães, Portugal

d. CQ-VR, Centro de Química – Vila Real, Department of Engineering, University of Trás-os-Montes e Alto Douro, 5001-801, Vila Real, Portugal

*Corresponding author: normygaibor@gmail.com

Abstract

This study aims to optimize the mechanical behavior of alkali-activated mortar reinforced with polyacrylonitrile fibers. In order to accomplish this, ceramic waste from clay bricks and roof tiles was used as the primary precursor, which was then combined with ladle furnace slag and activated with sodium silicate. Thereby, fibers were added to improve its brittle behavior, namely its toughness and the residual flexural strength of the material, thus enabling its use in a myriad of applications within the construction sector. So, an extensive experimental campaign was carried out to assess the influence of polyacrylonitrile fibers content (0%, 0.5%, and 1% in volume) and the curing time (14, 28, and 90 days) on the main physical and mechanical properties, including capillarity, porosity, uniaxial compressive, and flexural strength. Microstructural analysis was accomplished with Scanning Electron Microscopy, X-ray Energy Dispersive Analyzer, X-ray diffraction, and Fourier Transform Infrared Spectroscopy. Experimental results of the developed mortars showed satisfactory mechanical properties, enhanced by the fibers, regardless of the fiber ratio added, attaining compressive and tensile under flexural strengths' values up to 47 Mpa and 7 N/mm^2, respectively, after 90 days of curing. Compared to non-reinforced mortars, these values represent an improvement of about 20% in both cases, thus justifying the addition of fibers.

Keywords: Ceramic waste Slag Alkali-activation PAN fibers Mechanical properties Microstructural characterization

4.1. INTRODUCTION

Worldwide, Ordinary Portland Cement (OPC) is the most used binder within structural materials for the construction sector [1,2]. However, the production of OPC epitomizes significant pollution levels in terms of the greenhouse gas (GHG) volumes that are released into the atmosphere, representing 6 to 7% of the global CO_2 emissions to the atmosphere [3] and around 36% of the global energy consumption [4]. Recently, alkali-activated mortars (Aam) and concretes have been introduced as a new sustainable construction material to replace the traditional OPC-based cement mortars and concrete. It has been estimated that the production of these alternatives could allow the decrease of greenhouse gas emissions by nearly 70%, in comparison to the production of OPC, which undoubtfully constitutes an environmentally friendlier approach [5].

The ceramic industry encompasses very significant financial resources worldwide and generates a large number of jobs, thus being an essential part of the production chain within the Construction Sector [6]. On the other hand, it is also known that the ceramic industry generates and disposals to landfill significant amounts of waste without any further treatment. In 2009, the global production of ceramic tiles was about 10 million square meters. But, this generation has significant growth to reach about 11,980 and 13,552 million square meters in 2013 and 2017, respectively [4]. China and Spain are among the largest ceramic producers in the world, with a production of 10.23 billion m^2 in 2015, encompassing more than half of total worldwide ceramic production [7], which represented over 600 million m^2 in the last ten years and ranked them among the top four producers in the world [8]. A survey within the ceramic industry [9] estimated that about 15–30% of the total production is waste. Thus, the safe use of ceramic wastes is suggested without any significant changes [10] by recycling these wastes in the development of novel sustainable materials for the construction sector, e.g., through alkali activation of ceramic wastes, can convert large-scale waste streams into sustainable materials and at the same time relieve the ceramic industry waste disposal problem, suggesting a win-win situation from both the sustainable and economic point of views [3].

For alkali-activated mortars, ceramic waste (CW) has been suggested as a significant silica and alumina source, which plays an essential role in gel configuration and strengthening [11]. Some advantages of using CW as a precursor, alone or in combination with other materials or wastes, are the reduction in the depletion of natural resources and energy consumption, the lower economic cost,

and the decrease in the emissions of CO_2 and other greenhouse gases. On the other hand, it is also known that Aam with a high calcium content ($CaO + SiO_2 > 70\%$) will generate a calcium aluminum silicate hydrate (C-A-S-H) gel as the main reaction product [12], resulting in a dense matrix with good mechanical properties in terms of what is usually required by the construction industry [13]. Therefore, ladle furnace slag (LFS), a calcium-rich aluminosilicate, has been incorporated in the present work as a complementary precursor. Furthermore, the inclusion of the LFS includes further advantages, like enhanced durability (particularly against acid and sulfate attack), fast setting and hardening, low heat of hydration, and high-temperature resistance, among others [14]. Currently, binders based on this type of industrial by-products have boosted greater interest due to their low carbon footprints in contrast to cement [15].

Several authors have studied the development of sustainable alkali-activated building materials and the possible use of ceramic waste from different sources, such as construction and demolition waste (CDW) [16] and ceramic industry waste. Among those can be enunciated studies related to roof tiles production [6], [17]; bricks manufacturing [18]–[20]; ceramic materials from eco-friendly geopolymer precursors [5]; development of high-strength alkali-activated pastes [21]; alkali-activated mortars exposed to elevated temperatures [22], among others. The construction sector is the primary customer of ceramic products (e.g., sanitaryware, tiles, bricks, and others); for this reason, it plays an essential role in overcoming some of the consequent environmental issues. Nonetheless, there is still a long way to systematically introduce different types of industrial wastes and by-products into the material supply chain of this sector.

Hwang [21] studied the development of high-strength alkali-activated pastes in two groups of mixtures using two different main precursors, either waste red clay brick powder (WBP) or waste ceramic powder (WCP). The control samples were made with 100% WBP and 100% WCP. The other mixtures contained about 60% of the composition's total weight of the main starting materials (WBP or WCP), while the remaining 40% was completed with fly ash and slag by a varied ratio in 10% increments. Each group contained a set of four different blend compositions. Sodium silicate (Na_2SiO_3) and sodium hydroxide (NaOH) were used as the alkali activator. The alkali-activated pastes were cured at ambient temperature for 3, 7, 28, and 56 days. Workability and compressive strength were some of the studied parameters. Slump flow table values were measured by the horizontal free flow in perpendicular directions, resulting in 235–285 mm and 245-300 mm for WCP and WBP, respectively, showing

highly workable pastes in both cases. Compressive strength values from 36 to 70 Mpa were registered after 56 days of curing. In general, the alkali-activated pastes specimens with WBP showed better mechanical strength performance and denser morphology than those with WCP, determined by the finer particle size and higher calcium oxide (CaO) content of the WBP compared to the WCP. The latter results demonstrate the potential of using recycled WBP and WCP in the production of enhanced- or high-strength alkali-activated pastes. Huseien [3] studied the performance of waste ceramic powder (WCP) with different contents (i.e., 50, 60, and 70%) mixed with ground blast furnace slag (GBFS) and fly ash (FA) as a binder on the mechanical and microstructure properties of alkali-activated mortars. The specimens were cured at the ambient temperature of (27 ±1.5) °C and relative humidity of 75%, showing that a high volume of WCP produced an environmentally friendly Aam with compressive strengths higher than 70 Mpa at the age of 28 days. The results also showed that increasing the WCP content leads to an increase in workability. The work presented by Ameri [23] also reports that the waste ceramic powder (WCP) and waste clay brick powder (WCBP) based geopolymer mortars showed higher workability than other mortar mixes when slag (GGBFS) and metakaolin (MK) are used as aluminosilicate sources. The GGBFS-based alkali-activated mortar reached the highest strength value (82.5 Mpa) at 28 days, which was about 29% higher than Portland's (OPC) cement mortar. On the other hand, WCBP exhibited a lower reactivity than WCP, which lead to obtaining the lowest mechanical strength (~38Mpa). Besides, the author stated the studied alkali-activated mortars as an eco-friendly material since it was showed a carbon footprint and energy consumption of approximately 50% and 25% lower than OPC, respectively. Obaid Mahmoodi [24] studied the development of optimized binary use of ceramic tile waste (CTW) and concrete waste (CW) in geopolymer binders prepared and cured at normal laboratory temperature for in-situ applications. The results showed that the optimal binary CTW + CW composition can be achieved at 40% CTW + 60% CW and SiO_2/Al_2O_3 and Na_2O/SiO_2 of 12.3 and 0.18, respectively. The addition of 45% of ground granulated blast furnace slag content in ternary mixtures helped to reach very high strength binders of more than 100 Mpa under normal conditions.

Fiber incorporation in the composition can help mitigate the shrinkage problems and improve the mortar's post-cracking mechanical properties. It is worth mentioning that the capacity of fibers to counteract strain localization depends largely on the type, volume, mechanical properties, geometrical configuration, length, orientation, and the bond properties of the fiber/matrix interface [25], [26]. Based on shape, either man-made or natural fibers, are categorized into four groups, i) continuous

fibers, i.e. tows or monofilament; ii) discontinuous fibers, i.e. short fibers with a diameter of 3–5 µm; iii) whiskers, with diameter less than 1 µm or high aspect ratio; iv) particulates [27]. In general, several works have been conducted on studying the fiber reinforcement of alkali-activated materials with different fibers such as polypropylene [28], [29], [30], Polyvinyl alcohol (PVA) [31], basalt [32], carbon [32], among others. More related to CW use, the feasibility of using fiber-reinforced alkali-activated blast furnace slag and ceramic binders was assessed by Abdollahnejad et al. [25]. Besides, one-part alkali-activated slag/fly ash binders containing ceramic aggregates to be reinforced with different fiber types (PVA, PP, basalt) and combinations (single and hybrid) [33] were also studied by this author. However, specifically regarding the use of ceramic wastes and polyacrylonitrile fiber reinforcement in alkali-activated materials systems, no information was found, which justifies the originality of this research.

This study addresses the feasibility of developing an enhanced-strength ceramic-based mortar reinforced with polyacrylonitrile fibers (PAN) within the scope of novel composite mortars based on alkaline activation. Moreover, it aims to characterize ceramic waste's (CW) fundamental properties and assess its potential in the development of Aam. For this purpose, a CW from a company that produces clay bricks and roof tiles was used as the primary precursor in combination with ladle furnace slag (LFS) as a complementary starting material in the presence of sodium silicate (SS). Furthermore, the influence of different fiber dosages, i.e., 0.5% and 1%, and the curing age (14, 28, and 90 days) on the main mechanical and physical properties were also assessed. Additionally, it was performed a microstructural analysis, including Scanning Electron Microscopy (SEM), X-ray Energy Dispersive Analysis (EDX), X-ray diffraction (XRD), and Fourier Transform Infrared Spectroscopy (FTIR).

4.2. MATERIALS AND METHODS

4.2.1. Materials

The materials used in this study as precursors were ceramic waste (CW) rich in both silicon dioxide (54.9%) and aluminum oxide (26.3%), and ladle furnace slag (LFS) that is a calcium-rich aluminosilicate (64.2%), see Table 4-1. Sodium silicate (Na_2SiO_3) was used as an alkaline activator in the solution form. The CW was provided by a brick manufacturing company located near Braga, in the northwestern region of Portugal. The LFS from melting scrap in an electric arc furnace was supplied

by the Portuguese ironwork company *Megasa*, located in Maia. For the mortar's reinforcement, discrete PAN fibers with an 8 mm length and an approximate diameter of 20 μm were used. The latter was adopted due to its availability and chemical (good in alkaline medium) and thermal resistance (good in short-term processing temperature up to 220°C), as can be corroborated in the corresponding technical sheet [34].

Table 4-1. Chemical composition of the ceramic waste (CW), and ladle furnace slag (LFS), % wt

Precursor	Na_2O	MgO	Al_2O_3	SiO_2	P_2O_5	SO_3	Cl_2O	K2O	CaO	TiO_2	Cr_2O_3	MnO	Fe_2O_3	ZnO
CW	0.13	1.30	26.28	54.89	0.42	0.59	0.12	3.97	0.64	1.40	0.30	0.86	9.10	-
LFS	0.31	3.54	4.86	19.68	-	4.69	-	-	64.23	0.31	-	0.35	1.39	0.64

The CW (i.e., before and after grinding) and the LFS are presented in Figure 4-1. It can be observed that about 80% of the CW particles had a diameter within the 2 – 18 cm range. It is known that for alkali activation purposes, the particle size of precursors is important since the coarser particles are less involved in the geopolymerization process [35]. Therefore, CW was ground in a ball mill, using 12 steel balls of 0.41 kg each for 0.33 h at 50.50 rpm. The original LFS (i.e., as received in the laboratory) was sieved in a nominal mesh opening of 250 μm, and only the passing fraction was used.

The particle size distribution (PSD) of both precursors (CW and LFS) was determined in two stages. For the coarse particles (granulometry above 63 μm, i.e., sieve no. 200) standardized ASTM sieves were used, arranged in a column with ½ phi intervals, according to the modified Wentworth scale and agitation intervals of 5 minutes. As for the finer particle sizes (i.e., < 63μm), the PSD was determined by X-ray on a Sedigraph analyzer to measure particles up to 0.15μm. Figure 4-2 shows the PSD curves of the final materials, where it can be seen that the milling of the CW produced a well-graded material, with a fine fraction of about 38%.

Figure 4-1. Precursors used in the mixture: (a) ceramic waste (CW) before grinding; (b) CW after gridding; (c) ladle furnace slag (LFS) before sieving; and (d) after sieving
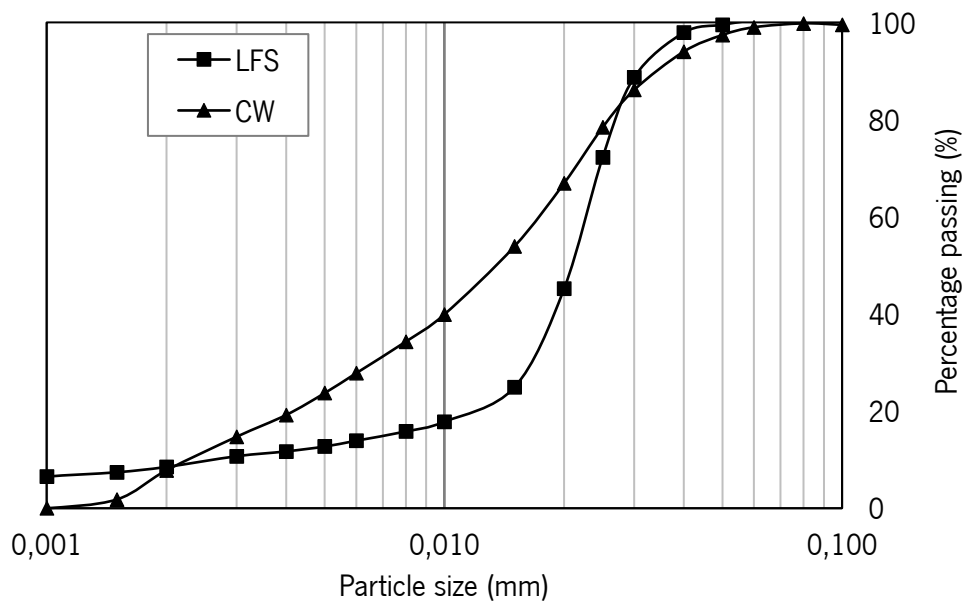
Figure 4-2. Particle size distribution (PSD) of precursors (ceramic waste (CW) after gridding and ladle furnace slag (LFS) after sieving)

4.2.2. Alkali activated mortar compositions

In a previous work [36], CW from CDW was studied in different CW/LFS ratios, namely, 75:25, 50:50, and 25:75, in weight (wt%), in which were alkali-activated either with sodium hydroxide (SH) or sodium silicate (SS). In total, ten different mix compositions were prepared and reviewed, including the reference samples (100 wt% for CW and LFS). Based on the results from this latter work, the composition 75 CW + 25 LFS, activated with SS, was used as the reference paste since it reached the highest compressive strength values. However, for the present study, the proportions of the precursors and activating solution were slightly modified, i.e., CW + LFS/SS equal to 0.72:0.28/ 0.48 for each formulation. Additionally, in the attempt to obtain better workability of the mortar, polycarboxylate-based superplasticizer (SP) [37] was also added (2% in wt) to the precursors, thus facilitating the incorporation of the fibers and their subsequent dispersion. This adjustment was necessary because the origin and type of the present waste are different from the waste used in the mentioned previous study [36]. Based on the results of preliminary tests related to the improvement workability of the developed mortars, as well as available literature (e.g., [30], [38]) where a fiber content in the range of 0.2%-2% for geopolymers is suggested, it was determined to use 0.5% and 1% fibers´ content. Table 4-2 shows the compositions of the alkali-activated mortars developed in the present work.

Table 4-2. Composition of the alkali-activated mortars

Paste ID	Precursor (wt. ratio)		Activator/ Precursor (wt. ratio)	SP/ precursor (wt. ratio)	PAN fiber (vol. fraction)	CaO / SiO_2	Na_2O / Al_2O_3	SiO_2 / Al_2O_3	SiO_2 / Na_2O
	CW	LFS	SS						
M1					0				
M2	72	28	0.48	0.02	0.5	0.32	0.32	2.84	8.96
M3					1				

Preparation of the blends occurred as follows; in the batching process, the CW, LFS, SS, and the SP were added to the mixer bucket, in this order, and mixed for 1-minute. The mixture procedure was executed in an industrial mixer at the minimum speed (i.e., 140 ±5 rpm). Subsequently, PAN fibers were incorporated and stirred again for 2 min to guarantee a homogeneous distribution. Promptly, after the mixing process (3 minutes total), the homogenized mortar was poured inside of stainless-steel prisms molds and mechanically compacted for 1 minute on a shaking table. The flow properties of the fresh mortar were characterized by the slump-flow test [39]. During this test, for the three studied blends, the initial diameter was 100 mm, and after 15 strokes, the spread of the diameter

passed to 150 mm, 135mm, and 125mm, for mortars with 0%, 0.5%, and 1% of fiber content (C f), respectively. There was no significant evidence of segregation. It can be ascribed to applying an adequate precursor/activator ratio, beyond using the superplasticizer, which originally acts as a micro-rollers and significantly reduces the paste's friction and flow resistance [40]. However, the influence of the superplasticizer in the mixture was not very significant since there are several compatibility issues as reported in the literature [41]. Afterward, the curing was performed in two phases; first, the mortar was subjected to a curing temperature of 70°C during the early 24 hours, then the specimens were demoulded and cured at ambient temperature (20-23 °C) and humidity of around 60% HR ± 5% for the remaining of the 14-, 28-, and 90-days period. For each studied series with different fiber content (unreinforced – 0, 0.5, and 1%) and curing time (14, 28, and 90 days), five prismatic specimens were prepared to be conducted the compression test, and four specimens for each of the physical and other mechanical tests.

4.3. FABRICATION AND TESTING OF THE SPECIMENS

4.3.1. Mechanical properties

After the corresponding curing period and before mechanical testing, each specimen was rectified, weighed, and each edge of the cubes was measured for further calculations. The main mechanical properties of the M1, M2, and M3 series were assessed through experimental tests. The Young's modulus (E_{cm}) was determined according to the EN 12390-13 standard [42], and a customized procedure obtained the compressive stress-strain relationship and the uniaxial compressive strength (UCS) based on the adaptation of recommendations from [43]. Five specimens with a dimension of 50×50×100 mm^3 were used for the abovementioned tests. The tests were performed on a servo-hydraulic testing rig with a load actuator of 300 kN. Tests were carried out under closed-loop displacement control at a rate of 0.002 mm/min. Figure 4-3 shows the adopted test set-up for obtaining the elasticity modulus and the compressive stress-strain relationships.

(a)   (b)
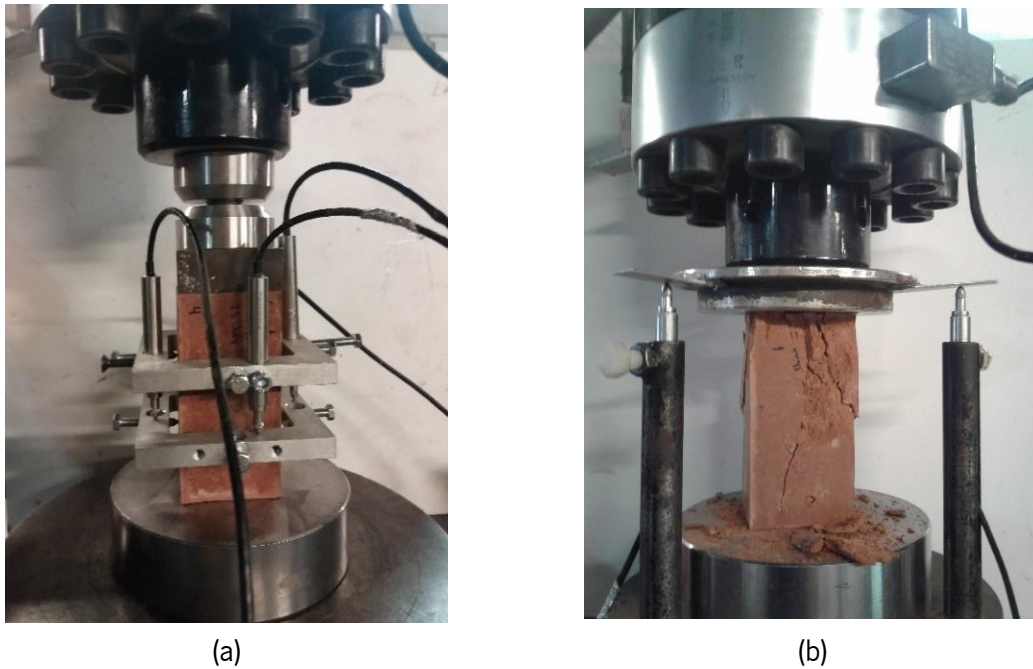
Figure 4-3. Test set-up for (a) the elasticity modulus; (b) the uniaxial compressive stress-strain

The tensile behavior under flexure was assessed through three-point bending tests. The test set-up was adapted from the recommendations of the standards BS EN 1015-11:1999 [44] and EN 14651:2005 [45], respectively, for plain mortars and fiber-reinforced concretes. Each series comprised four notched prismatic specimens of 40x40 mm^2 cross-section and 160 mm length with a span of 100 mm. An electromechanical universal testing rig, LLOYD LR50K, fitted with a 50 kN load cell, was used. The tests were performed under displacement control with a rate of 0.002 mm/min.

4.3.2. Physical properties

The physical properties were obtained from the fractured halves of the flexural specimens (i.e., 40x40x80 mm^3) after 28 days of curing; four specimens were used per test and series. The open porosity (P), which translates the absorption of water by immersion under vacuum, as well as the water absorption (C) due to capillary action, were determined according to the procedures prescribed by the standards LNEC E 395 [46] and BS EN1015-18:2002 [47], respectively.

4.3.3. Microstructural and chemical analysis

The microstructural analysis was performed on both the original materials' precursors and some selected samples of the developed alkali-activated mortars (i.e., mix M2, at 14-, 28-, and 90-days

curing). The Scanning Electron Microscopy (SEM) analyses were carried out on an FEI Quanta 400 scanning electron microscope, at 30 kV, in low vacuum mode, with partial pressure inside the chamber (1.3 mbar), avoiding the deposition of a conductive layer. An EDS analyzer from EDAX allowed a chemical analysis of the elements present in each sample, using the same spectrum acquisition time and a ZAF correction model. The XRD was assessed on a PANalytical X'Pert Pro diffractometer, fitted with an X'Celerator detector and a secondary monochromator, using CuKα radiation at 40 kV and 30 mA. The scans were acquired with Bragg-Brentano geometry, covering a 2θ range between 7 and 85°, with a nominal step size of 0.017 and 100 s/step. In the case of the CW, LFS, and resulting pastes, phase quantification was performed on diffraction patterns applying Rietveld [48], with the code Highscore Plus 4.8. Table 4-5 presents the values in weight percentage. The amorphous phase was simulated through the Le Bail model [49]. Volume percentages were converted into weight percentages using the respective density.

Finally, the FTIR spectra were acquired using a Thermo Scientific Nicolet iS50 FTIR spectrometer, resorting to an ATR (Attenuated Total Reflectance) accessory with a diamond crystal. The instrument was controlled by the Omnic software package, version 9.2.28, from Thermo Fisher Scientific Inc. A spectrum range of 400 to 4000 cm^{-1} was defined, with 4 cm^{-1} and 64 scan resolution during 90 seconds for each sample. The material was previously milled with the aid of a laboratory mortar and pestle for 20 min.

4.4. RESULTS AND DISCUSSION

4.4.1. Mechanical behavior

4.4.1.1. Compressive behavior

Table 4-3 presents the average uniaxial compressive strength (UCS) and the coefficient of variation of the alkali-activated mortars reinforced with distinct PAN fiber contents (i.e., 0, 0.5, and 1% in volume) after curing periods of 14, 28, and 90 days. In general, the curing age increased the compressive strength values, irrespective of the fiber ratio added, ranging from approximately 27 to 47 MPa, respectively, at 14 and 90 days. It is in agreement with the results of other studies where the waste ceramic brick was used as a precursor [23], [50], [51], since it presents a relatively lower reactivity in

comparison with other CW with different compositions, e.g., ceramic wastes from the floor and wall tiles and sanitaryware furniture [16], [36]. The series reinforced with PAN fibers exhibited higher UCS than the one unreinforced.

The effects of moderate fiber content on the compressive strength can be either negative or positive. The compressive strength can decrease the UCS when fibers originate more air voids and a less compact matrix. In contrast, it may improve when fibers counteract micro-cracking propagation and delay its coalescence into macro-cracks [33]. In the present study, it was observed that fiber addition enhanced the compressive strength of the studied Aam (Table 4-3). In particular, it may be attributed to the fiber geometry used in the present study, namely small dimension and high aspect ratio (length/diameter) that favors the micro-cracking arrestment during the pre-peak stage under compression [52], and therefore the increase in the compressive strength.

The post-peak behavior, i.e., after reaching the maximum load, at all curing ages and notwithstanding the fiber content, was not possible to obtain due to problems controlling the test because of the brittle nature of the material even when reinforced. This can be associated with the relatively high porosity of the alkali-activated matrix, later explained in section 4.4.2.1, and some problems with the closed-loop displacement control of the servo-hydraulic equipment. The M2 series (0.5% fibers) registered an increase of approximately 17% in strength at 90 days of curing, Figure 4-5(c), compared to the reference series (M1_0% of fibers), Figure 4-4(c). However, a different behavior was observed on M3 (1% fibers) at 14- and 90-days curing (see Figure 4-6(a) and 6(c), and the UCS values were slightly lower (nearby 5% and 12%, respectively) in comparison to M2 Figure 4-5(a) and 5(c). It can be attributed to the mixing process. As it is explained by Ranjbar [38], the order of fiber addition into the blend is important to obtain uniform fiber dispersion. For multifilament fibers, e.g., PAN fibers, the author recommends mixing with the alkali activator solution in advance to separate the fiber bunches and then mixing with dry aluminosilicates and other fillers. As was not the case, PAN fibers were not homogeneously distributed in the mortar, and they formed clumps or balls (see Figure 4-7, c), plus the relatively low workability of the fresh paste affected the mechanical properties of the whole matrix.

Table 4-3. Uniaxial compressive strength (UCS), Elasticity modulus (E), and flexural strength (f) of the alkali-activated mortar after 14, 28, and 90 days of curing

	M1 (0% Cf)			M2 (0.5% Cf)			M3 (1% Cf)		
	14d	28d	90d	14d	28d	90d	14d	28d	90d
UCS (MPa)	26.90	34.44	39.30	41.31	40.69	46.92	39.43	46.79	41.52
(CoV, %)	(10.1)	(9.7)	(8.2)	(5.1)	(0.8)	(3.6)	(5.2)	(11.8)	(6.1)
E_{cm} (GPa)	6.72	8.21	10.88	9.94	11.16	12.2	9.21	12.38	10.75
(CoV, %)	(5.2)	(8.3)	(1.3)	(6.7)	(4.2)	(2.8)	(5.6)	(13.9)	(2.3)
f_{ct}^{f} (N/mm²)	5.19	4.44	5.39	5.89	4.28	3.90	4.59	7.58	6.47
(CoV, %)	(9.1)	(8.0)	(8.3)	(7.1)	(15.7)	(24.1)	(7.4)	(2.1)	(6.8)
$f_{R0.3mm}$ (N/mm²)	-	-	-	1.73	0.87	0.33	2.38	4.10	5.63
(CoV, %)				(63.2)	(57.2)	(126.2)	(33.8)	(13.8)	(13.5)
$f_{R0.5mm}$ (N/mm²)	-	-	-	0.55	0.14	0.05	1.03	2.74	2.82
(CoV, %)				(83.3)	(200)	(173.2)	(46.8)	(36.7)	(12.8)
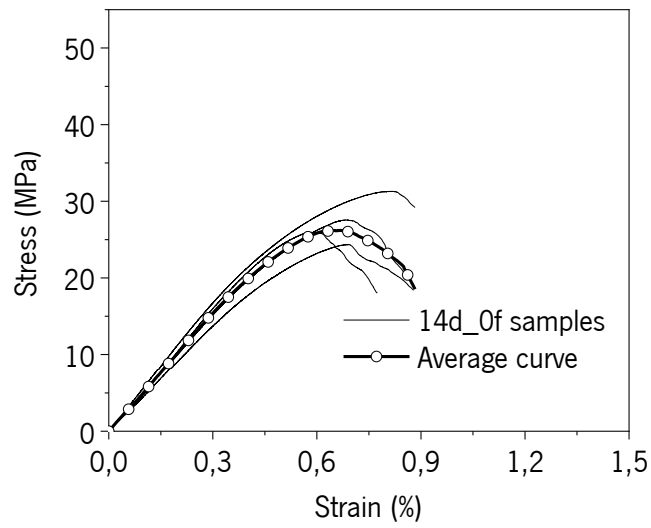
(a)
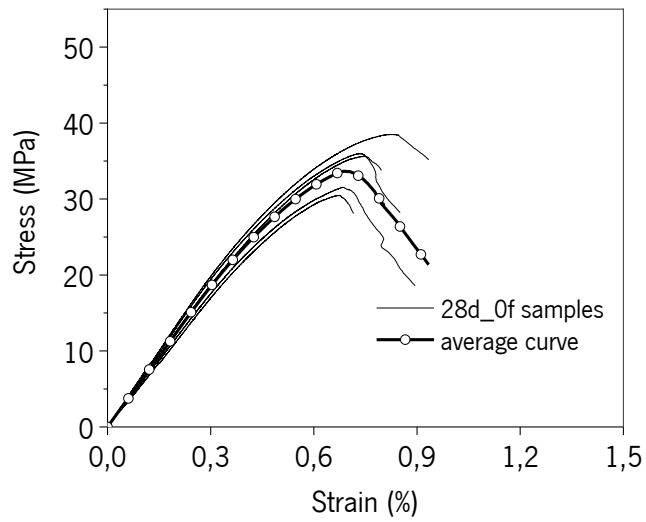
(b)
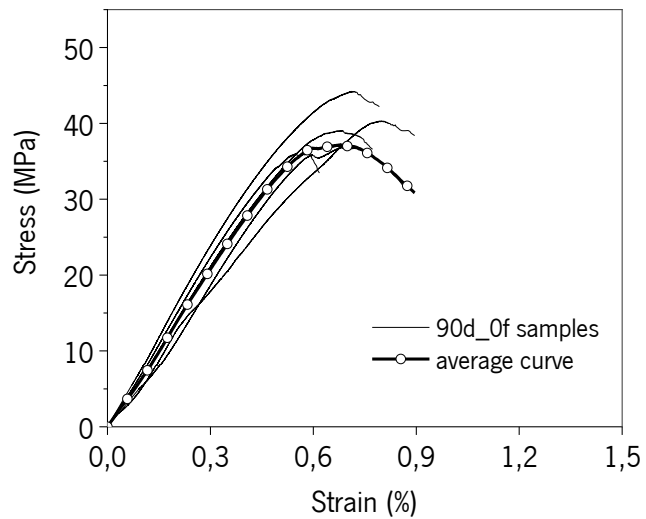
(c)

Figure 4-4. Compressive stress-strain relationships of the M1 (0% fibers) alkali-activated mortar after: (a) 14, (b) 28, and (c) 90 days of curing
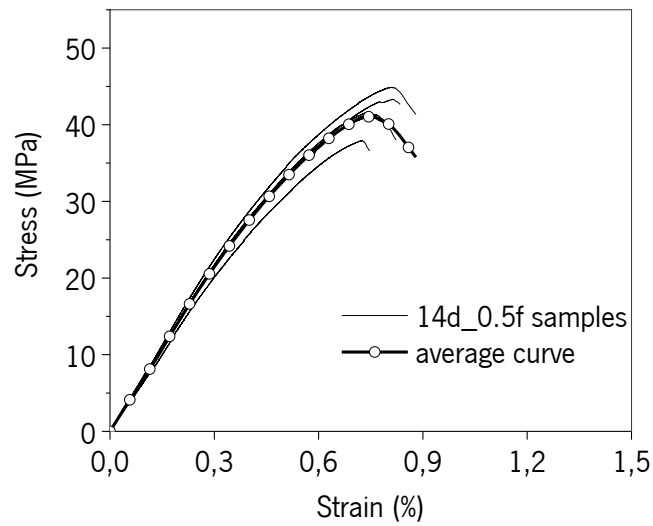
(a)
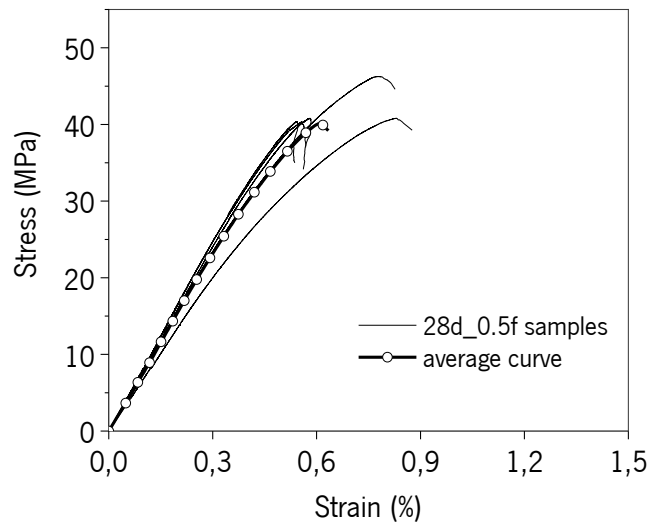
(b)
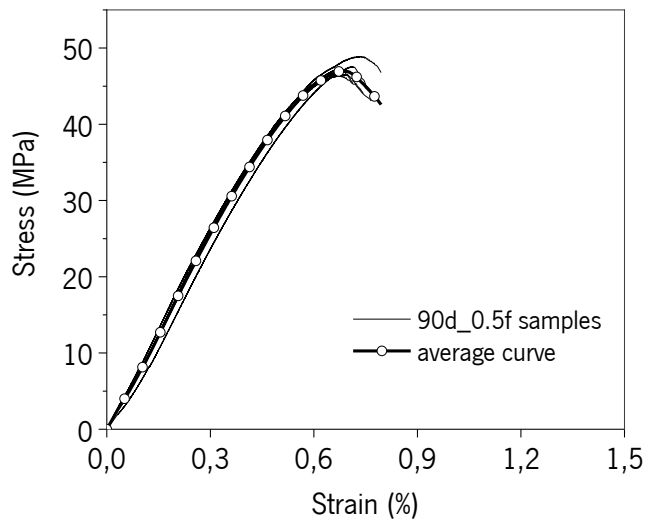
(c)

Figure 4-5. Compressive stress-strain relationships of the M2 (0.5% fibers) alkali-activated mortar after: (a)14; (b) 28; and (c) 90 days of curing
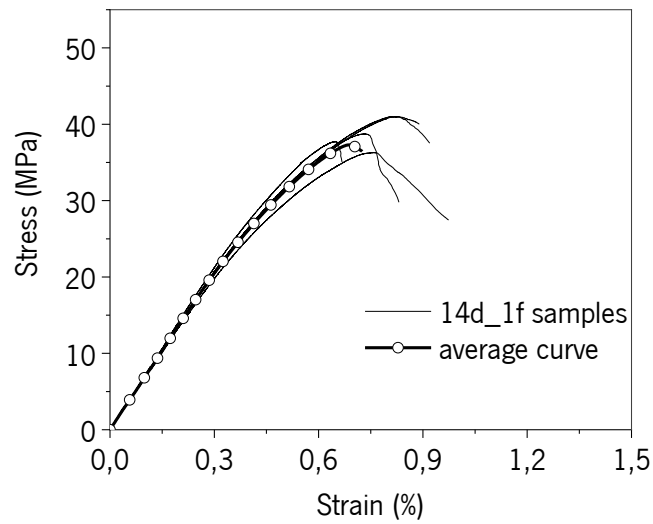
(a)
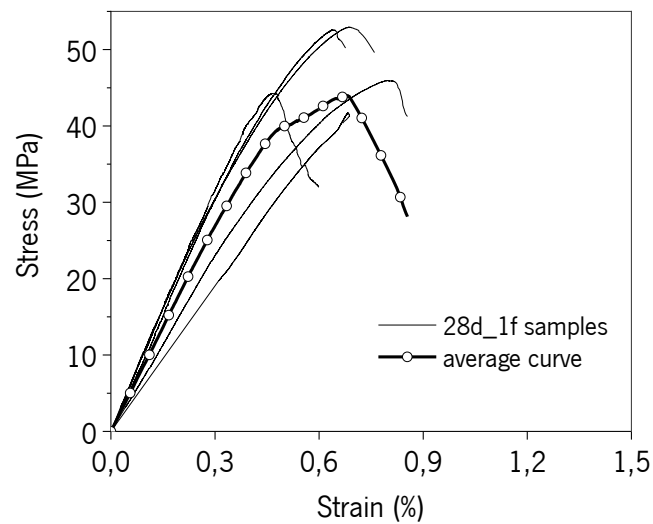
(b)
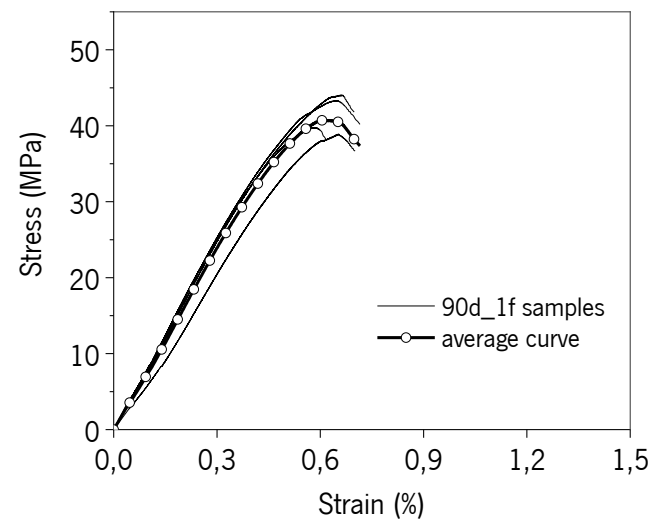
(c)

Figure 4-6. Compressive stress-strain relationships of the M3 (1% fibers) alkali-activated mortar after: (a)14; (b) 28; and (c) 90 days of curing

4.4.1.2. Elasticity modulus

Table 4-3 includes the average values of the elasticity modulus (E_{cm}) and the corresponding coefficient of variation (CoV). In general, the E_{cm} increased with the age of curing. It is worth mentioning that the M1, M2, and M3 series had an average elasticity modulus of 8.2, 11.2, and 12.4 GPa, respectively, at 28 days of curing, which in all cases concur with the available results in the bibliography (i.e., 3.8 to 15 GPa) for alkaline mortars [53]–[55].

The reinforced series, i.e., M2 and M3, exhibited a higher elasticity modulus when compared to the unreinforced one (M1), this is in agreement with section 4.4.1.1., i.e., the elastic modulus of AAm with/without fibers is increased with the increase of compressive strength [38]. Nonetheless, at the stress level in which the elasticity modulus is assessed, no significant micro-cracking is expected. Thus, the increase observed in the elasticity modulus was not ascribed to the mobilization of the fibers but rather to a more compact and stiffer matrix of the M2 and M3 compositions. It can be noticed from the SEM images (Figure 4-13), in fact, fibers are adhered to the matrix, improving the interfacial bond strength and rose the energy consumption during the fiber pulling process, which leads to the enhancement of some mechanical properties such as compressive and flexural strengths [38], [56]. The E_{cm} of the M3 series at 90 days of curing also exhibited a similar trend to the one observed for UCS, i.e., it slightly decreased (approximately 13.2%) compared to the 28 days series, in the presence of 1% of fibers.

4.4.1.3. Flexural behavior

The flexural strength (f_{ct}^{f}) and the residual flexural tensile strengths computed respectively for crack mouth opening displacements of 0.3 mm ($f_{R0.3mm}$), and 0.5 mm ($f_{R0.5mm}$) for the developed AAm are listed in Table 4-3. In the case of the unreinforced mixture, M1, it can be observed that the obtained values for f_{ct}^{f} did not significantly increase concerning the age of curing, nearby 3% at 90 days. Even more, M2 showed a decreasing tendency, which was not expectable, for f_{ct}^{f} at 28 and 90 days, with a decrease of 27.3% and 33.8%, respectively, in comparison to f_{ct}^{f} at 14 days (5.89 N/mm²). This peculiar behavior can be attributed to the non-uniform fiber distribution (see, e.g., Figure 4-7) due to the low workability of the paste and the relatively high porosity (section 4.4.2.1) [38], [56], [57]. The

highest increase in f_{ct}^f with the curing age was observed for the M3 series at 28- and 90-days curing, respectively, of about 65% and 40%. It is worth noting that all blends used in this study have the same mix components, and the effect of fiber addition is analyzed below.

a)   b)   c)
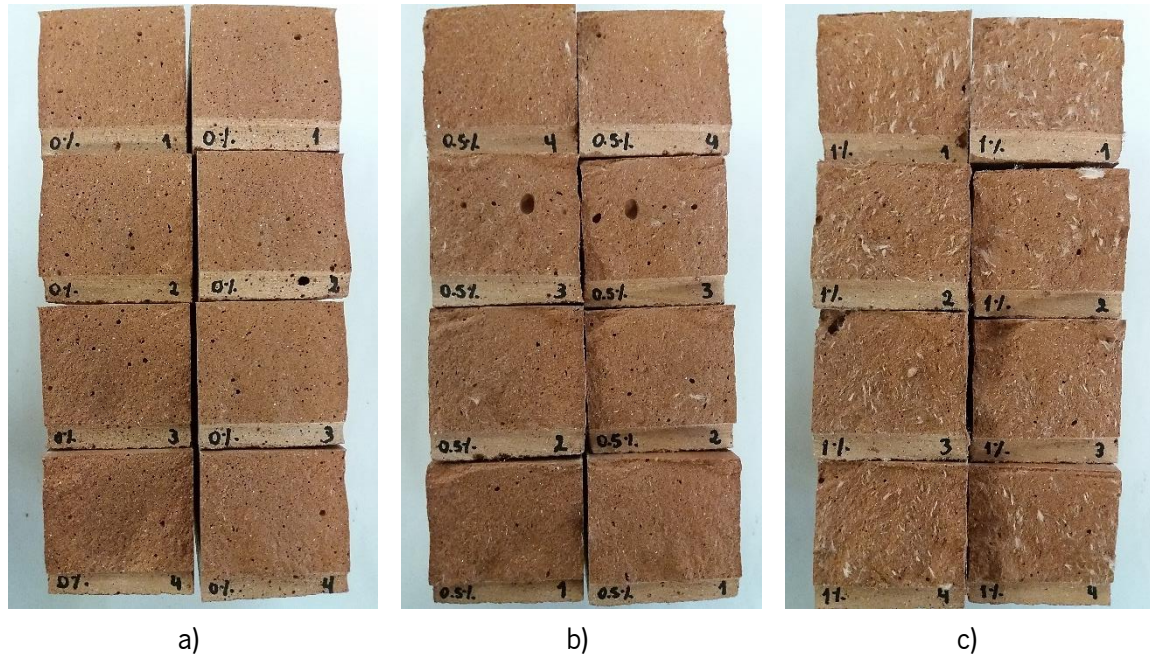
Figure 4-7. a) M1; b) M2; and c) M3 specimens after flexural strength test at 28 days curing

The flexural load-displacement curve for control (M1),0.5% (M2), and 1% (M3) addition of PAN fibers to AAm are shown in Figure 4-8, 4.9, and 4.10, respectively. As can be seen from Figure 4-8, at all ages, the reference specimens cracked suddenly at peak load, representing a typical brittle failure because of the small aggregate size and sudden release of the elastic energy accumulated during the cracking process, a similar observation was registered by Ranjbar et al., [38]. In contrast, with the addition of fibers in mixtures M2 and M3, it was possible to obtain the post-peak stage. In general, a sharp softening branch after peak load was observed, followed by a more gradual softening stage.

The increase in the fiber content produced an increase in the post-peak residual force, as expected (Figure 4-9 and 4.10). Similar behavior was observed in another study where the material with low fiber content experienced a sharp-brittle post-cracking behavior [58]. In some series, such as M3 at 90 days, a small deflection-hardening behavior was observed after the peak.

The addition of a fiber ratio of 1% lead to a significant increase in the residual strengths, moreover, leads to an increase in the ultimate crack opening width [38]. The comparison of the ultimate crack opening width series M2 and M3 results, i.e., 0.5 and 1% of fibers, may suggest that fiber rupture was

predominant in series M2, while fiber pullout was more prone in series M3. Note that the ultimate crack opening width, w_u, may be estimated through $w_u = L_{b,proj} = \eta \cdot l_f / 2$ [59], where η is an orientation factor ranging from 0.5 to 1.0, respectively, for a 3D isotropic uniform random fiber distribution (IURD) and 1D IURD; whereas $L_{b,proj}$ is the average fiber projected embedded length in an active crack and l_f is the fiber length. Therefore, having in mind the adopted fiber length, the w_u should at least be around 2 mm if fiber pullout was the predominant fracture mode.

For the series M2, 0.5% of fibers, it was no observed apparent increase in flexure strength compared to the reference series [38], [60]. On the other hand, for higher fiber reinforcement ratios, i.e., 1%, already it is seen an increase in the flexural strength. The influence of the fiber addition was more visible on the residual flexural strengths since for moderate fiber reinforcing ratios, the reinforcement role of the fibers is more critical after the coalescence of the micro-cracking into the macro-crack, i.e., in the post-cracking stage [61], [62], [63] [64].
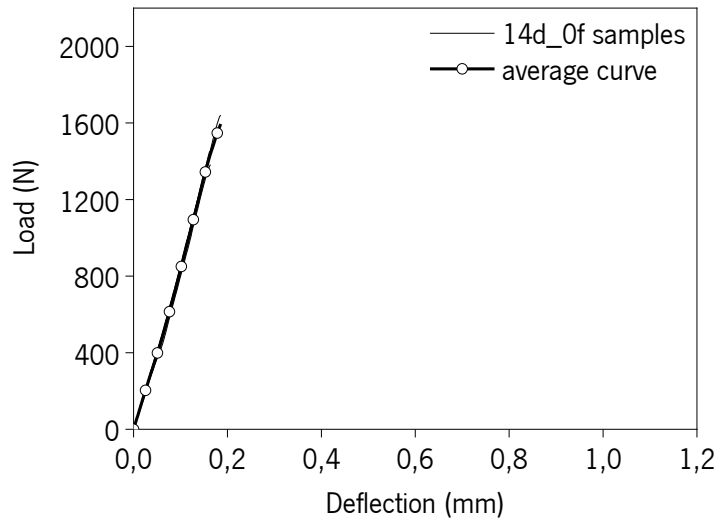
(a)
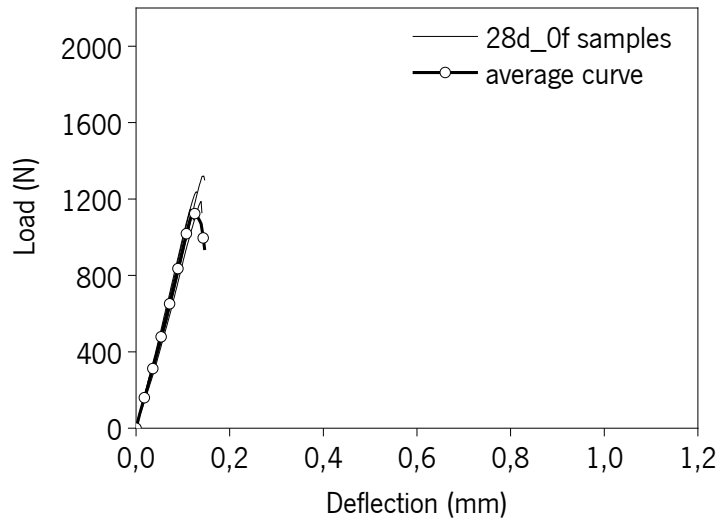
(b)
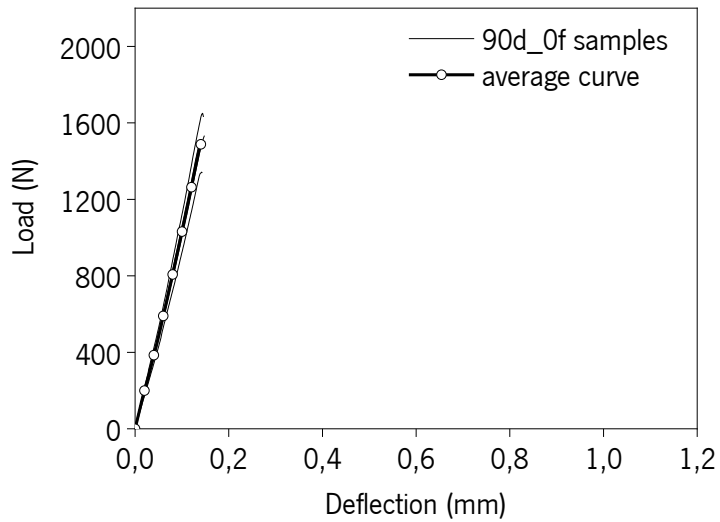
(c)

Figure 4-8. Average curves of flexural strength of M1 (0% fiber) alkali-activated mortar after: (a)14; (b) 28; and (c) 90 days of curing
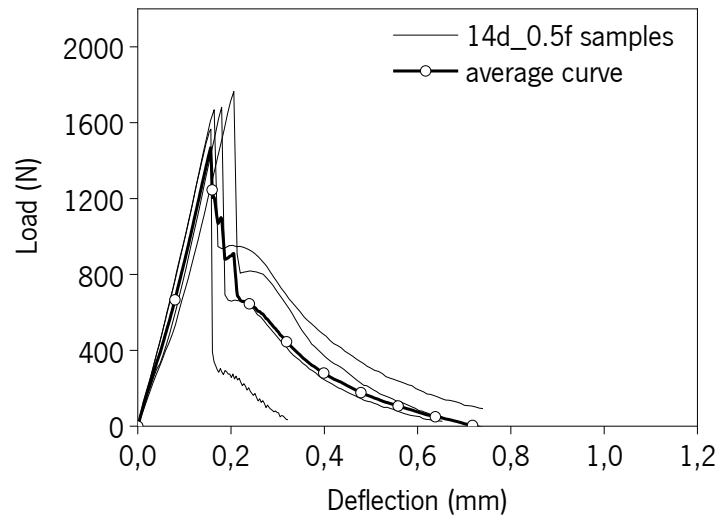
(a)
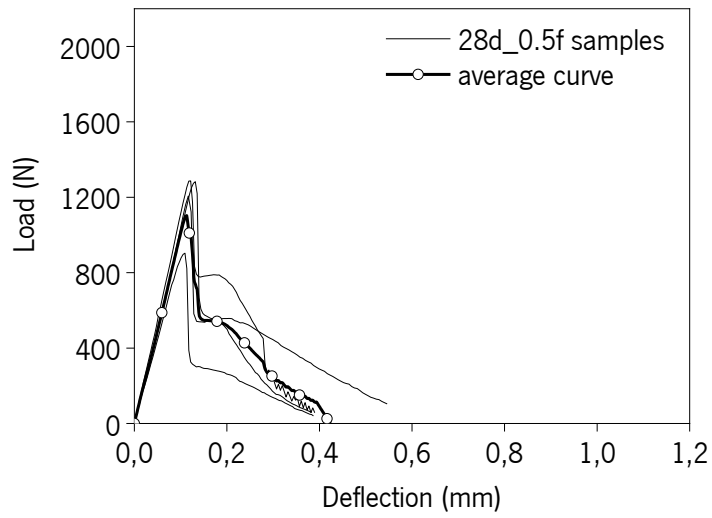
(b)
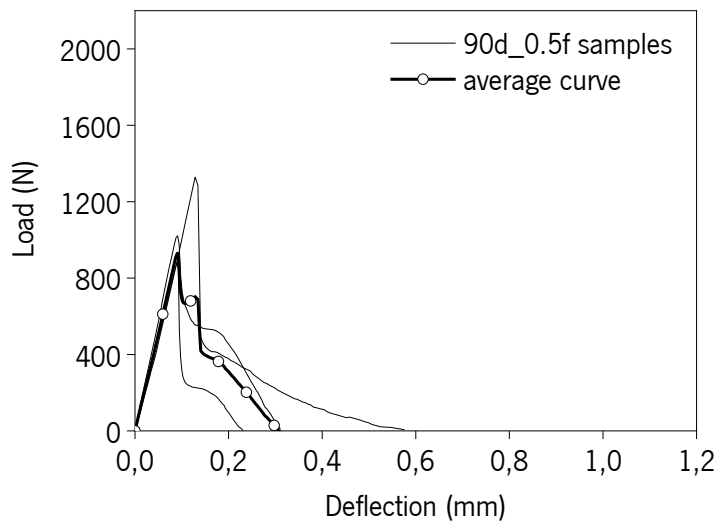
(c)

Figure 4-9. Average curves of flexural strength of M2 (0.5% fiber) alkali-activated mortar after (a) 14; (b) 28; and (c) 90 days of curing
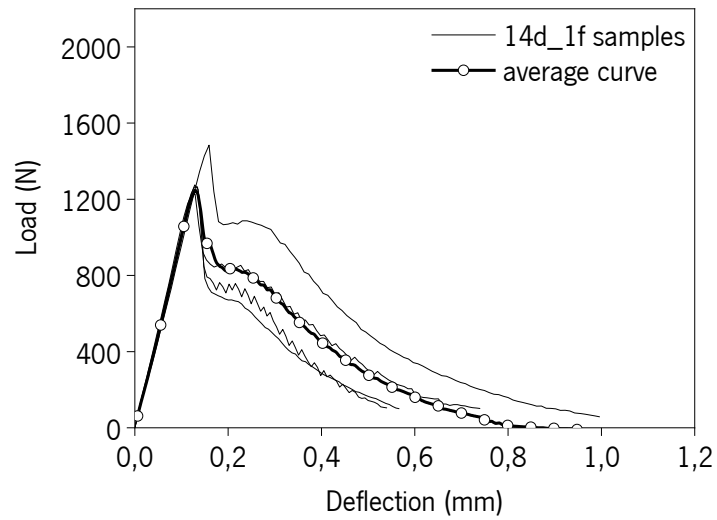
(a)
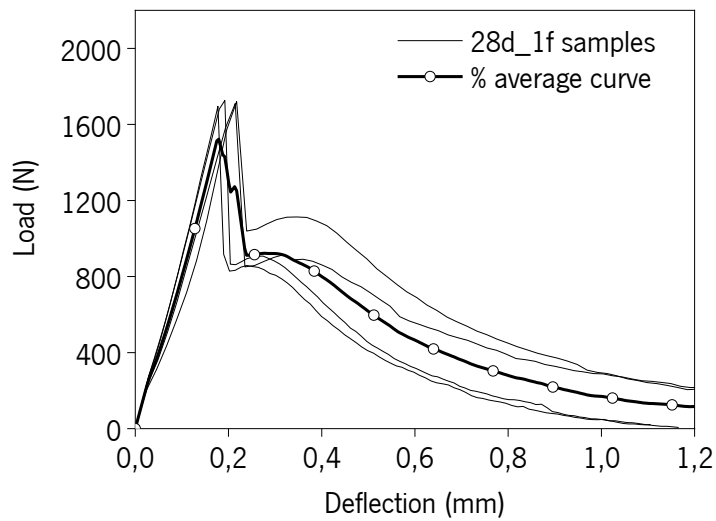
(b)
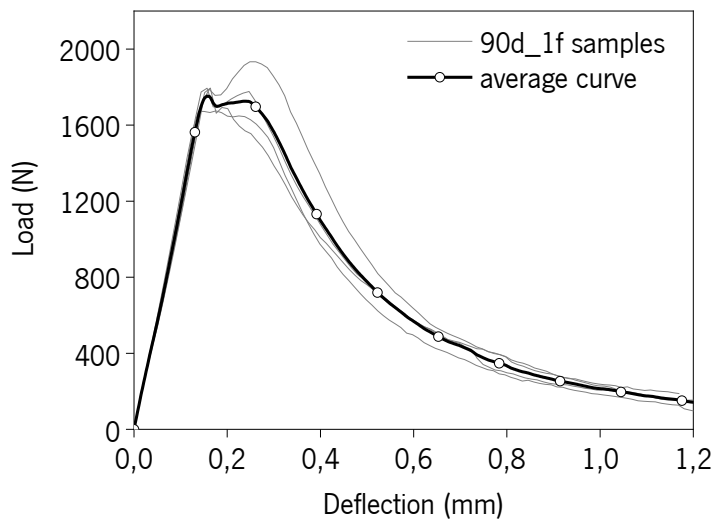
(c)

Figure 4-10. Average load-deflection curves for M3 (1% fiber) alkali-activated mortar after: (a)14; (b) 28; and (c) 90 days of curing

4.4.2. Physical properties

4.4.2.1. Open Porosity

Generally, water absorption by capillarity (C) and immersion (P) could be affected by adding fibers [52]; therefore, the assessment of those parameters was carried out for all the series, and the results are reported in Table 4-4. According to the test results, tested specimens showed relatively high porosity values regardless of the fiber content, above 20%, for all compositions (i.e., M1, M2, and M3). Then, using PAN fibers did not lead to tortuosity or larger pores than the control sample (M1). Similar behavior was found in a study related to alkali-activated mortars for bricks with cellulose and basalt fibers, where it was reported porosity values of about 25% [65]. Pore formation, size, and distribution can be attributed to the high CaO content of the precursors due to the formation of calcium silicate hydrates [66], [67], in this case, ascribed to the presence of LFS (Table 4-1).

Table 4-4. Open porosity of the alkali-activated mortar after 28 days of curing, (%)

	M1 (0% f)	M2 (0.5% f)	M3 (1% f)
Porosity (%)	23.26	23.51	21.71
(CoV)	(1.22)	(1.59)	(1.44)

4.4.2.2. Water absorption (Capillarity)

Water absorption due to capillary action (C) is directly related to material porosity since more porous materials with open and interconnected pores lead to larger water absorption [68],[69]. Thus, C of the studied alkali-activated mortars was influenced by the pore structure of mortar specimens prepared with high CW content and LFS, where the capillary pores are a consequence of the chemical reactions and the remaining water in the system, which is evaporated due to the hardening of the matrix through the curing time [70]. The precursors' chemical composition also restricted the C-A-S-H gel formulation and exhibited higher porosity and permeability to water. In all series, the capillarity coefficients were nearby 0.0002 kg / (m². min$^{0.5}$) (Figure 4-11), which is significantly lower than 0.53-0.62 kg/m².min$^{0.5}$ reported in [65] for cellulose and plain alkali-activated desulfurization slag-based mortars. The reported C coefficient also suggests that C was not governed by the addition of fibers, consistent with the open porosity results (section 4.4.2.1).
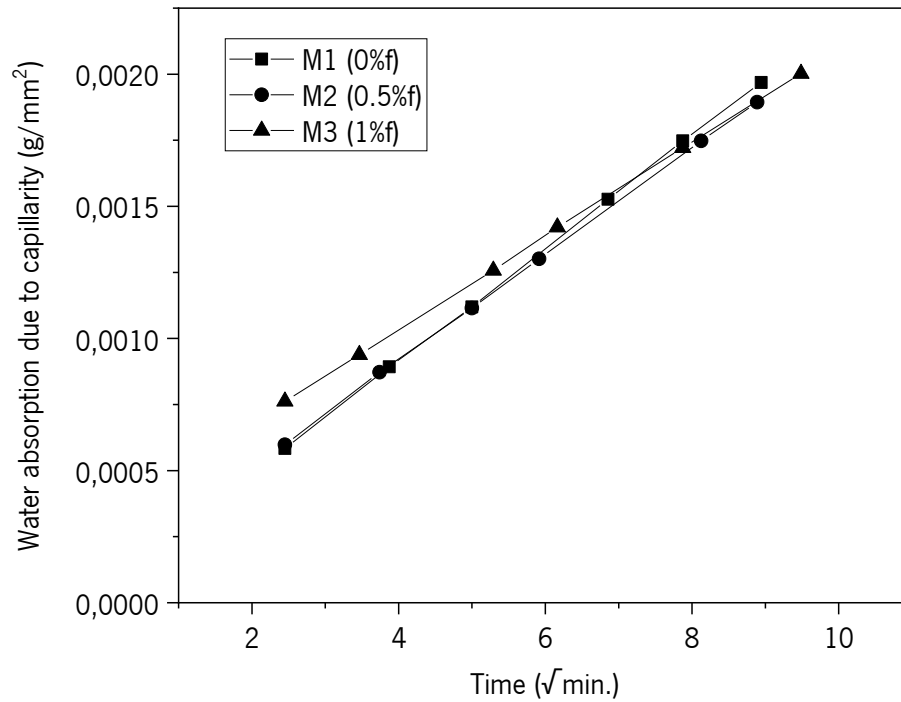
Figure 4-11. Dependence of the mass increase on the suction surface $\Delta m_t / F$, concerning the square root of time $\sqrt{t}$ for samples of the alkali activated mortar after 28 days of curing

4.4.3. Mineralogical and microstructural characterization

To characterize the reaction products developed after 14, 28, and 90 days of curing and considering that the composition of the pastes was identical (only the fiber content was modified), samples from the M2 series were randomly selected. They were subjected to microstructural analyses, i.e., X-ray diffraction (XRD), Electron Microscopy (SEM), X-ray Energy Dispersive Analyzer (EDX), and Fourier Transform Infrared Spectroscopy (FTIR).

4.4.3.1.XRD

Figure 4-12 plots the XRD diffractograms of the original precursors (i.e., LFS and CW) and the AAm (M2) paste. It can be observed that LFS presents a tenuous halo between 28 and 38°(2θ), characteristic of amorphous materials [71], as well as some crystalline phases, such as calcium olivine (highest content at 48.5%), cuspidine, mayenite, lime, and larnite. By contrast, the CW is fundamentally quartz (81.1%, Table 4-1), even though other phases were also identified, namely muscovite, hematite, and garronite. This precursor also shows a halo between 25 and 30°(2θ). The

presence of these halos in the precursors indicates the existence of a vitreous phase, which is fundamental for the alkaline activation reactions [3], [36], [72]. After curing for 14, 28, and 90 days, these halos became less intense and shifted in range, translating into a formation of an amorphous gel.

The ceramic waste evidently influenced the diffraction peaks and the developed crystallinity phases in the resulting paste. However, some peaks in the reaction products were also identified in the LFS, revealing that some phases are basically inert to the alkali activation process.

An increase in crystallinity can either increase or decrease certain mechanical properties, depending on the space available in the paste to be filled with crystals. Besides, the transition of amorphous gels to ordered structures can originate from internal stresses due to inevitable microstructure variations [33],[73].

Although the resulting gel is mostly amorphous, some new semi-crystalline clusters were detected in the M2 paste, such as enstatite, illite, phengite, calcite, and feldspar. These observations are in line with findings in Huseien et al. [22], where it is shown that these semi-crystalline phases are observed in alkali-activated mortars containing ceramic wastes, GGBFS, and FA.

The XDR patterns of the M2 mixtures throughout the curing time show a decrease of the characteristic quartz peaks (Table 4-5), accompanied by a slight increase of mullite (90 days), obtained from the Al_2O_3 in the CW. Moreover, the newly formed crystalline Mg- and silicate-based phase, enstatite, which showed a significant content increase with curing time (reaching 30.3% after 90 days, Table 4-5), suggests that the phase composition of the studied samples may be affected by the available soluble SiO_2 content provided by the alkali-activator solution. [74].
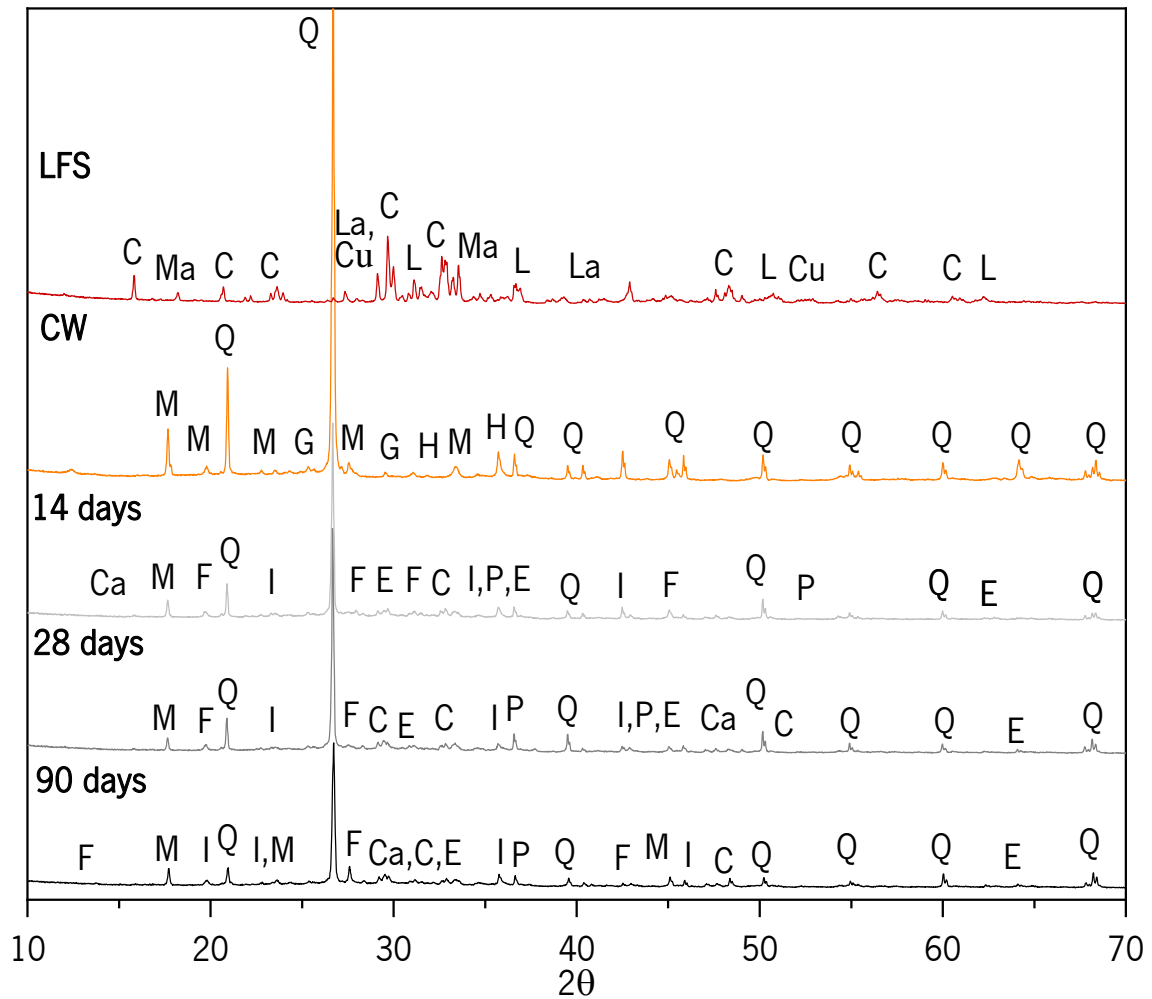
(Q: quartz; M: muscovite; C: calcium olivine; E: enstatite; I: Illite; P:Phengite; Ca: Calcite; F: Feldspar; Cu: Cuspidine; Ma: Mayenite; L: Lime; La: Larnite; H: Hematite; G: Garronite)

Figure 4-12. XRD patterns of starting materials (CW and LFS), and M2 (0.5% fiber) mortar at 14, 28 and 90 days curing time

Table 4-5. Mineral's quantification in starting materials (CW and LFS), and M2 (0.5% fiber) mortar at 14-, 28 and 90 days curing time, (% wt)

Material	Q	H	M	G	C	Cu	Ma	L	La	E	Ca	P	F	I
CW	81.1	4.4	13.8	0.6	-	-	-	-	-	-	-	-	-	-
LFS	-	-	-	-	48.5	18.5	6.7	2.1	24.2	-	-	-	-	-
M2_14 days	44.1	2.5	12.1	-	10.1	-	-	-	-	9.8	0.1	0	15.7	5.5
M2_28 days	26.1	1.7	4.4	-	7.7	-	-	-	-	8.2	12.4	0	23.8	15.1
M2_90 days	12.4	0.4	12.7	-	13.2	-	-	-	-	30.3	6.2	0.5	18.9	5.3

Q: Quartz; H: Hematite; M: Muscovite; G: Garronite; C: Calcio Olivine; Cu: Cuspidine; Ma: Mayenite; L: Lime; La: Larnite; E: enstatite; Ca: Calcite; P:Phengite; F: Feldspar; I: Illite

1.   SEM micrographs

The same samples from the M2 series were analyzed through SEM / EDX to perform a thorough qualitative analysis of the developed microstructure of the reaction products, which is illustrated in Figure 4-13. The effect of the curing time on the M2 AAm is evident; at 14 days, mostly unreacted particles (points 1 and 2 correspondings to CW and LFS, respectively) are still visible with some precipitated hydrates on their surface, this suggests the first signs of activation but a still small amount, Figure 4-13, (a). After 28 days of curing, hydration is not complete since CW and LFS particles are still detected. However, their surface is greater covered with reaction products, denoting a better extent of reaction, Figure 4-13, (b). After 90 days, most of the particles show an apparently higher reaction degree than in the previous curing stages, and the mass of aluminosilicate gel seams is more scattered in the structure of the paste. However, still, CW larger particles (Figure 4-13,c. point 1) were only partially reacted [50]. SEM micrographs also demonstrated the high-water absorption of this AAm. The observations were corroborated by previous findings [51], [75], where it was detected unreacted brick residue powder particles and pores in SEM images of alkaline activated mortar based on powdered brick waste. Regarding the type of gel produced, it can be classified as C-A-S-H due to the combination of the specific compositions of CW and LFS, with a significant content of calcium. This finding is in line with the results obtained by [76], [77].

As for the fiber reinforcement, the SEM images (Figure 4-13, points 3) show that hydrated particles are attached to the surface of PAN fibers, which evidence their good embeddedness in the matrix, thus enhancing the mechanical properties of the mortar, especially the flexural strength. The good adhesion of PAN fibers explains the increase in strength of M2 and M3, as fiber can act as a bridge when an external load is applied. Similar results concerning good adhesion in the case of PVA fibers in AAms are reported in [25], [62].

a)

b)

c)
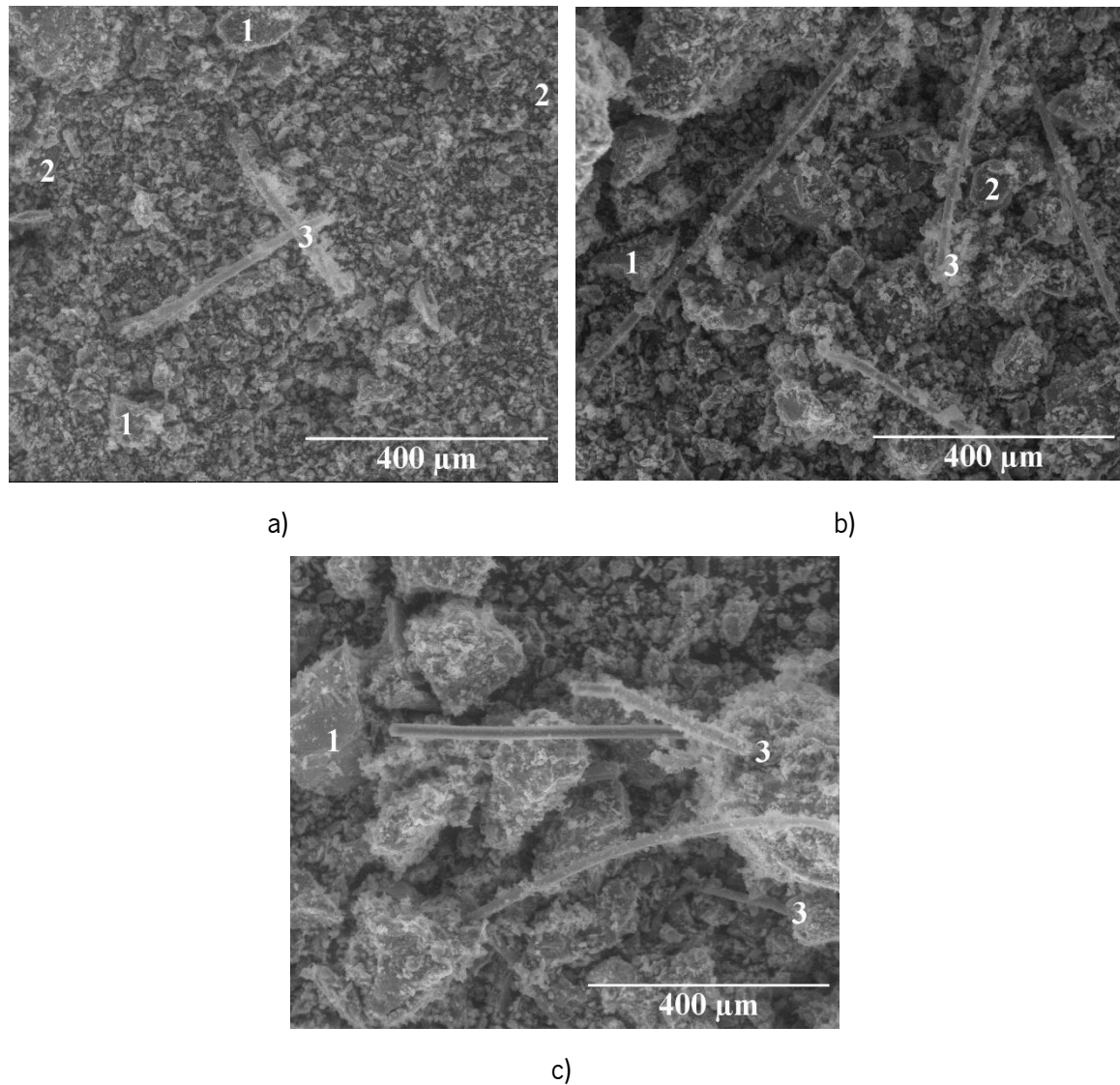
Figure 4-13. SEM images of M2 (0.5% fiber content) after a) 14 days, b) 28 days, and c) 90 days curing time. Points 1 and 2) ceramic waste and ladle furnace slag particles, respectively; point 3) PAN fibers"

2. FTIR spectra of precursors and AAm

Figure 4-14 displays the FTIR spectra of the initial materials (LFS and CW) and the M2 mixture after 14, 28, and 90 days of curing, which shows a set of bands positioned in the frequency range within [400 - 1800] cm^{-1}. The LFS spectrum presents a wideband between 1550 and 1420 cm^{-1}, centered at 1475 cm^{-1}, associated with CO_3^{2-} vibrations in different configurations [78], denoting the existence of carbonated compounds. The deep cupula perceptible between 1050 and 750 cm^{-1} is mainly assigned to silico-aluminate groups, among the main components of the slag structure (Table 4-1).

Finally, the 560 cm^{-1} band is associated with the Al-O-Al, while the bands at 490 cm^{-1} and 440 cm^{-1} are associated with the O-Si-O bonds. The CW exhibits an intense and broad main band around 1015 cm^{-1}. This band is characteristic of the asymmetric tension vibration related to Si-O-Si or Si-O-Al bonds [79], confirming the material's crystallinity. The bands at 420 and 440 cm^{-1} represent the O-Si-O bonds, mostly from the quartz.

Some modifications in the microstructure of the M2 AAm paste can be detected, relatively to the original precursors. Such adjustments depend on several factors, including the composition of the precursor, the type of alkaline activator, and the curing conditions [78]. One of the most significant was the shift of the main band of the original CW to lower wavelengths (1000 cm^{-1}), translating a structural reordination motivated by the precipitation of the reaction products, where the C-A-S-H type gel has been identified as the primary phase. This observation is in agreement with the findings reported by Hwang [72].

Comparing the three spectra of M2, it is possible to assume that the new band formed after 14 days, located at 1480 cm^{-1}, is mainly attributed to the inclusion of soluble silicon (from the sodium silicate), suggesting that the 14-day period was not long enough to dissolve the precursor and start the nucleation process (when the silicon ions from the activator would be required). At 90 days, this band practically disappeared, as these additional ions are now combined with other species. This behavior confirms that the original quartz and mullite bands (690, 540, 440 cm^{-1}) did not present any meaningful changes after 14 days, relatively to the original materials. In the 14-, 28-, and 90-day spectra are also visible the formation and growth of new bands, namely at 875 and 1410 cm^{-1}, which are usually assigned with C-O functional groups [79], possibly result from the development of different types of carbonate minerals, like calcite. This agrees with the XRD results, which are illustrated in Figure 4-12.
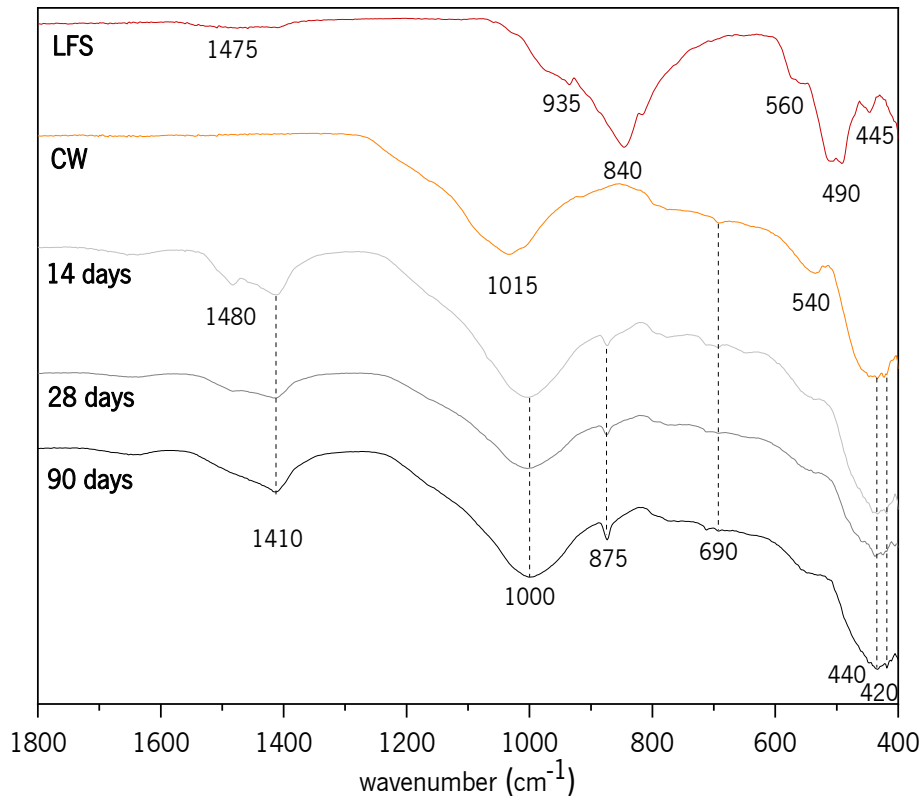
Figure 4-14. FTIR spectra of starting materials, the ladle furnace slag (LFS); ceramic waste (CW) – after milled, and M2 blend (0.5% fiber content) after 14-, 28-, and 90-days curing time.

4.5. CONCLUSIONS

The development of enhanced-strength alkali-activated mortars reinforced with different percentages of polyacrylonitrile (PAN) fibers was carried out in this research. Ceramic waste from a company that produced clay bricks and roof tiles was used as the main precursor in combination with ladle furnace slag (LFS) in the presence of sodium silicate (SS) as an activator. The main conclusions obtained in this work are:

— The efficiency of fiber addition, i.e., 0.5% and 1%, of the developed AAm was determined by the mechanical and physical properties. It exhibited an improvement of nearly 12% in elasticity modulus and about 20% in compressive and flexural strength with values up to 47 MPa and 7 N/mm², respectively, at 90 curing days, compared to plain AAm;

— As expected, the main benefits of the fiber reinforcement were observed at the post-cracking stage of the flexural responses, with the toughness and residual strengths increased for increasing fiber content. Fiber rupture was predominant in the series with 0,5% of fiber, while fiber pullout

was more prone in series of a fiber ratio of 1%, which also showed a significant increase in the ultimate crack opening width in contrast with the first series. Residual stresses nearby 5.6 and 2.8 MPa were obtained for crack mouth openings of 0.3 and 0.5 mm;

— Mortar flowability decreased as fiber content increased, which caused a poor fiber distribution in the AAm. This could have affected the mechanical test results. However, physical properties (open porosity and capillarity) were not significantly influenced by fiber incorporation;

— As specified by the XRD, SEM, and FTIR microstructure findings, the formulated AAm with a high CW (72%) the content in combination with LFS (28%) enabled the formation of a cementitious gel-type so-called C-A-S-H, as the main product of the alkali-activated reaction;

— The SEM results showed a good interfacial bond between PAN fibers with the CW+LFS based alkali-activated matrix at 28 days of curing.

In general conclusion, the present work is a contribution to the dissemination and development of the application of fiber reinforcement in alkali-activated pastes and mortars and, in particular, alkali-activated mortars based on ceramic waste. The reinforcement with PAN fibers can now be seen as a promising and environmentally friendly alternative to similar products based on conventional Portland. There were still significant doubts, given the scarce studies on fiber reinforcement of alkali-activated materials, regarding the viability and technical effectiveness of this solution (which is already widespread in Portland cement-based materials) when applied in alkali-activated systems, but the present study helped to mitigate some legitime concerns, by showing significant improvements of the fiber-reinforced alkali-activated mortar, in terms of mechanical properties. However, intensive research is still needed if this combination of alkali matrixes and PAN fibers will ever become a common alternative. Several aspects, from actual problems to simpler indications on how to design, fabricate and apply the material, have yet to be addressed. Based on the presented findings, some of those aspects were identified, from which it is possible to highlight the issue of the workability of the paste. Detailed experimental work is now required, in the very near future, to improve the fiber distribution in the matrix, which would allow the increase in fiber content.

ACKNOWLEDGMENTS

REFERENCES

[1]   P. Duxson, J. L. Provis, G. C. Lukey, and J. S. J. van Deventer, "The role of inorganic polymer technology in the development of 'green concrete,'" *Cem. Concr. Res.*, vol. 37, no. 12, pp. 1590–1597, Dec. 2007, doi: 10.1016/j.cemconres.2007.08.018.

[2]   A. M. Rashad, Y. Bai, P. A. M. Basheer, N. B. Milestone, and N. C. Collier, "Hydration and properties of sodium sulfate activated slag," *Cem. Concr. Compos.*, vol. 37, no. 1, pp. 20–29, Mar. 2013, doi: 10.1016/j.cemconcomp.2012.12.010.

[3]   G. F. Huseien, A. R. M. Sam, K. W. Shah, M. A. Asaad, M. M. Tahir, and J. Mirza, "Properties of ceramic tile waste based alkali-activated mortars incorporating GBFS and fly ash," *Constr. Build. Mater.*, vol. 214, pp. 355–368, Jul. 2019, doi: 10.1016/j.conbuildmat.2019.04.154.

[4]   A. M. Rashad and G. M. F. Essa, "Effect of ceramic waste powder on alkali-activated slag pastes cured in hot weather after exposure to elevated temperature," *Cem. Concr. Compos.*, vol. 111, p. 103617, Aug. 2020, doi: 10.1016/J.CEMCONCOMP.2020.103617.

[5]   M. A. Villaquirán-Caicedo and R. M. de Gutiérrez, "Synthesis of ceramic materials from ecofriendly geopolymer precursors," *Mater. Lett.*, vol. 230, pp. 300–304, Nov. 2018, doi: 10.1016/j.matlet.2018.07.128.

[6]   A. R. G. Azevedo, C. M. F. Vieira, W. M. Ferreira, K. C. P. Faria, L. G. Pedroti, and B. C. Mendes, "Potential use of ceramic waste as precursor in the geopolymerization reaction for the production of ceramic roof tiles," *J. Build. Eng.*, vol. 29, May 2020, doi: 10.1016/j.jobe.2019.101156.

[7]   H. Wang, Z. Chen, L. Liu, R. Ji, and X. Wang, "Synthesis of a foam ceramic based on ceramic tile polishing waste using SiC as foaming agent," *Ceram. Int.*, vol. 44, no. 9, pp. 10078–10086, Jun. 2018, doi: 10.1016/J.CERAMINT.2018.02.211.

[8]   F. Puertas, A. Barba, M. F. Gazulla, M. P. Gómez, M. Palacios, and S. Martínez-Ramírez, "Ceramic wastes as raw materials in Portland cement clinker fabrication. Characterization and alkaline activation," vol. 56, no. 281, pp. 73–84, 2006, Accessed: Apr. 23, 2018. [Online]. Available: http://digital.csic.es/bitstream/10261/26676/1/134.pdf.

[9]   R. M. Senthamarai and P. Devadas Manoharan, "Concrete with ceramic waste aggregate," *Cem. Concr. Compos.*, vol. 27, no. 9–10, pp. 910–913, Oct. 2005, doi: 10.1016/j.cemconcomp.2005.04.003.

[10]   K. W. Shah and G. F. Huseien, "Bond strength performance of ceramic, fly ash and GBFS ternary wastes combined alkali-activated mortars exposed to aggressive environments," *Constr. Build. Mater.*, vol. 251, p. 119088, Aug. 2020, doi: 10.1016/J.CONBUILDMAT.2020.119088.

[11]   L. Reig, M. M. Tashima, L. Soriano, M. V. Borrachero, J. Monzó, and J. Payá, "Alkaline

Activation of Ceramic Waste Materials," *Waste Biomass Valor*, vol. 4, pp. 729–736, 2013, doi: 10.1007/s12649-013-9197-z.

[12] M. Sarkar and K. Dana, "Partial replacement of metakaolin with red ceramic waste in geopolymer," *Ceram. Int.*, vol. 47, no. 3, pp. 3473–3483, Feb. 2021, doi: 10.1016/J.CERAMINT.2020.09.191.

[13] F. Collins and J. G. Sanjayan, "Microcracking and strength development of alkali activated slag concrete," *Cem. Concr. Compos.*, vol. 23, no. 4–5, pp. 345–352, Aug. 2001, doi: 10.1016/S0958-9465(01)00003-8.

[14] K. Arbi, M. Nedeljković, Y. Zuo, and G. Ye, "A Review on the Durability of Alkali-Activated Fly Ash/Slag Systems: Advances, Issues, and Perspectives," *Industrial and Engineering Chemistry Research*, vol. 55, no. 19. American Chemical Society, pp. 5439–5453, May 18, 2016, doi: 10.1021/acs.iecr.6b00559.

[15] M. Tuyan, L. V. Zhang, and M. L. Nehdi, "Development of sustainable preplaced aggregate concrete with alkali-activated slag grout," *Constr. Build. Mater.*, vol. 263, p. 120227, Dec. 2020, doi: 10.1016/j.conbuildmat.2020.120227.

[16] P. Shoaei, H. R. Musaeei, F. Mirlohi, S. Narimani zamanabadi, F. Ameri, and N. Bahrami, "Waste ceramic powder-based geopolymer mortars: Effect of curing temperature and alkaline solution-to-binder ratio," *Constr. Build. Mater.*, vol. 227, p. 116686, Dec. 2019, doi: 10.1016/j.conbuildmat.2019.116686.

[17] G. F. Huseien, A. R. M. Sam, K. W. Shah, M. A. Asaad, M. M. Tahir, and J. Mirza, "Properties of ceramic tile waste based alkali-activated mortars incorporating GBFS and fly ash," *Constr. Build. Mater.*, vol. 214, pp. 355–368, Jul. 2019, doi: 10.1016/J.CONBUILDMAT.2019.04.154.

[18] A. Seco, J. Omer, S. Marcelino, S. Espuelas, and E. Prieto, "Sustainable unfired bricks manufacturing from construction and demolition wastes," *Constr. Build. Mater.*, vol. 167, pp. 154–165, Apr. 2018, doi: 10.1016/J.CONBUILDMAT.2018.02.026.

[19] H. R. Gavali, A. Bras, P. Faria, and R. V. Ralegaonkar, "Development of sustainable alkali-activated bricks using industrial wastes," *Constr. Build. Mater.*, vol. 215, pp. 180–191, Aug. 2019, doi: 10.1016/J.CONBUILDMAT.2019.04.152.

[20] S. K. Amin, S. A. El-Sherbiny, A. A. M. A. El-Magd, A. Belal, and M. F. Abadir, "Fabrication of geopolymer bricks using ceramic dust waste," *Constr. Build. Mater.*, vol. 157, pp. 610–620, Dec. 2017, doi: 10.1016/j.conbuildmat.2017.09.052.

[21] C.-L. Hwang, M. Damtie Yehualaw, D.-H. Vo, and T.-P. Huynh, "Development of high-strength alkali-activated pastes containing high volumes of waste brick and ceramic powders," *Constr. Build. Mater.*, vol. 218, pp. 519–529, Sep. 2019, doi: 10.1016/J.CONBUILDMAT.2019.05.143.

[22] G. F. Huseien *et al.*, "Waste ceramic powder incorporated alkali activated mortars exposed to elevated Temperatures: Performance evaluation," *Constr. Build. Mater.*, vol. 187, pp. 307–317, Oct. 2018, doi: 10.1016/j.conbuildmat.2018.07.226.

[23] F. Ameri, S. A. Zareei, and B. Behforouz, "Zero-cement vs. cementitious mortars: An experimental comparative study on engineering and environmental properties," *J. Build. Eng.*, vol. 32, p. 101620, Nov. 2020, doi: 10.1016/j.jobe.2020.101620.

[24] O. Mahmoodi, H. Siad, M. Lachemi, S. Dadsetan, and M. Sahmaran, "Development of optimized binary ceramic tile and concrete wastes geopolymer binders for in-situ applications," *J. Build. Eng.*, vol. 43, p. 102906, Nov. 2021, doi: 10.1016/J.JOBE.2021.102906.

[25] Z. Abdollahnejad, M. Mastali, T. Luukkonen, P. Kinnunen, and M. Illikainen, "Fiber-reinforced one-part alkali-activated slag/ceramic binders," *Ceram. Int.*, vol. 44, no. 8, pp. 8963–8976, Jun. 2018, doi: 10.1016/j.ceramint.2018.02.097.

[26] M. J. Khalaj, A. Khoshakhlagh, S. Bahri, M. Khoeini, and M. Nazerfakhari, "Split tensile strength of slag-based geopolymer composites reinforced with steel fibers: Application of Taguchi method in evaluating the effect of production parameters and their optimum condition," *Ceram. Int.*, vol. 41, no. 9, pp. 10697–10701, Nov. 2015, doi: 10.1016/j.ceramint.2015.05.002.

[27] K. Z. Farhan, M. A. M. Johari, and R. Demirboğa, "Impact of fiber reinforcements on properties of geopolymer composites: A review," *J. Build. Eng.*, vol. 44, p. 102628, Dec. 2021, doi: 10.1016/J.JOBE.2021.102628.

[28] A. Bhutta, M. Farooq, and N. Banthia, "Matrix hybridization using waste fuel ash and slag in alkali-activated composites and its influence on maturity of fiber-matrix bond," *J. Clean. Prod.*, vol. 177, pp. 857–867, Mar. 2018, doi: 10.1016/j.jclepro.2018.01.001.

[29] X. Guo and X. Pan, "Mechanical properties and mechanisms of fiber reinforced fly ash–steel slag based geopolymer mortar," *Constr. Build. Mater.*, vol. 179, pp. 633–641, Aug. 2018, doi: 10.1016/j.conbuildmat.2018.05.198.

[30] S. Rajaei *et al.*, "Rubberized alkali-activated slag mortar reinforced with polypropylene fibres for application in lightweight thermal insulating materials," *Constr. Build. Mater.*, vol. 270, p. 121430, Feb. 2021, doi: 10.1016/j.conbuildmat.2020.121430.

[31] X. Guo and J. Yang, "Intrinsic properties and micro-crack characteristics of ultra-high toughness fly ash/steel slag based geopolymer," *Constr. Build. Mater.*, vol. 230, p. 116965, Jan. 2020, doi: 10.1016/j.conbuildmat.2019.116965.

[32] H. Funke, S. Gelbrich, and L. Kroll, "The Durability and Performance of Short Fibers for a Newly Developed Alkali-Activated Binder," *Fibers*, vol. 4, no. 4, p. 11, Mar. 2016, doi: 10.3390/fib4010011.

[33] Z. Abdollahnejad, M. Mastali, B. Woof, and M. Illikainen, "High strength fiber reinforced one-part alkali activated slag/fly ash binders with ceramic aggregates: Microscopic analysis, mechanical properties, drying shrinkage, and freeze-thaw resistance," *Constr. Build. Mater.*, vol. 241, Apr. 2020, doi: 10.1016/j.conbuildmat.2020.118129.

[34] Composites - Fibers & Materials | SGL Composites, "Binder+-3D-reinforcement solutions," 2019. www.sglcarbon.com (accessed Jan. 30, 2020).

[35] V. Pommer, E. Vejmelková, R. Černý, and M. Keppert, "Alkali-activated waste ceramics: Importance of precursor particle size distribution," *Ceram. Int.*, Aug. 2021, doi: 10.1016/J.CERAMINT.2021.08.037.

[36] N. Gaibor, J. Coelho, D. Leitão, T. Miranda, P. Tavares, and N. Cristelo, "Alkali activation of recycled ceramic aggregates from construction and demolition wastes," *Mater. Construcción*, vol. 70, no. 339, p. 222, Jul. 2020, doi: 10.3989/mc.2020.13619.

[37] Sika Portugal, "Sika® ViscoCrete®-5501 SUPERPLASTIFICANTE DE ELEVADO DESEMPENHO DESCRIÇÃO DO PRODUTO | HIGH PERFORMANCE SUPERPLASTICIZER," *Sika Portugal, SA*, 2020. https://prt.sika.com/content/dam/dms/pt01/q/sika_viscocrete_-5501.pdf (accessed Sep. 02, 2021).

[38] N. Ranjbar and M. Zhang, "Fiber-reinforced geopolymer composites: A review," *Cem. Concr. Compos.*, vol. 107, p. 103498, Mar. 2020, doi: 10.1016/j.cemconcomp.2019.103498.

[39] "BS EN 12350-8. Testing Fresh Concrete. Self-compacting Concrete. Slump-flow Test.," 2010. Google Scholar.

[40] F. Soltanzadeh, V. M. C. F. Cunha, and J. A. O. Barros, "Assessment of different methods for characterization and simulation of post-cracking behavior of self-compacting steel fiber reinforced concrete," *Constr. Build. Mater.*, vol. 227, p. 116704, Dec. 2019, doi: 10.1016/j.conbuildmat.2019.116704.

[41] L. Lei and H. K. Chan, "Investigation into the molecular design and plasticizing effectiveness

of HPEG-based polycarboxylate superplasticizers in alkali-activated slag," *Cem. Concr. Res.*, vol. 136, p. 106150, Oct. 2020, doi: 10.1016/j.cemconres.2020.106150.

[42] "BS EN 12390-13. Testing Hardened Concrete-Part 13: Determination of Secant Modulus of Elasticity in Compression, 2014.," 2014. [Online]. Available: https://scholar.google.com/scholar_lookup?title=Testing Hardened Concrete - Part 13%3A Determination of Secant Modulus of Elasticity in Compression&author=UNE%2C EN 12390-13%3A2014&publication_year=2014.

[43] "ASTM C39 / C39M - 18. Standard test method for compressive strength of cylindrical concrete specimens. Active Standard ASTM C39 / C39M," 2018. [Online]. Available: Google Scholar.

[44] "BS EN 1015-11:1999. Methods of test for mortar for masonry Part 11: Determination of flexural and compressive strength of hardened mortar," 1999. [Online]. Available: Google Scholar.

[45] "UNE-EN 14651:2005 Test method for metallic fibered concrete - Measuring the flexural tensile strength (limit of proportionality (LOP), residual)," 2006. Accessed: Sep. 29, 2020. [Online]. Available: https://www.en.une.org/encuentra-tu-norma/busca-tu-norma/norma?c=N0036878.

[46] LNEC, "LNEC E 398 (1993) - Concrete: calculation of drying shrinkage and expansion (in Portuguese)," Lisbon, 1993.

[47] "BS EN 1015-18:2002. Determination of water absorption coefficient due to capillary action of hardened mortar," 2002. [Online]. Available: Google Scholar.

[48] N. Cristelo, P. Tavares, E. Lucas, T. Miranda, and D. Oliveira, "Quantitative and qualitative assessment of the amorphous phase of a Class F fly ash dissolved during alkali activation reactions – Effect of mechanical activation, solution concentration and temperature," *Compos. Part B Eng.*, vol. 103, pp. 1–14, Oct. 2016, doi: 10.1016/J.COMPOSITESB.2016.08.001.

[49] A. Le Bail, "Modelling the silica glass structure by the Rietveld method," *J. Non. Cryst. Solids*, vol. 183, no. 1–2, pp. 39–42, Apr. 1995, doi: 10.1016/0022-3093(94)00664-4.

[50] L. Reig, M. M. Tashima, M. V. Borrachero, J. Monzó, C. R. Cheeseman, and J. Payá, "Properties and microstructure of alkali-activated red clay brick waste," *Constr. Build. Mater.*, vol. 43, pp. 98–106, Jun. 2013, doi: 10.1016/j.conbuildmat.2013.01.031.

[51] M. Tuyan, Ö. Andiç-Çakir, and K. Ramyar, "Effect of alkali activator concentration and curing condition on strength and microstructure of waste clay brick powder-based geopolymer," *Compos. Part B Eng.*, vol. 135, pp. 242–252, Feb. 2018, doi: 10.1016/j.compositesb.2017.10.013.

[52] S. Aydin and B. Baradan, "The effect of fiber properties on high performance alkali-activated slag/silica fume mortars," *Compos. Part B Eng.*, vol. 45, no. 1, pp. 63–69, Feb. 2013, doi: 10.1016/j.compositesb.2012.09.080.

[53] M. Kheradmand, Z. Abdollahnejad, and F. Pacheco-Torgal, "Shrinkage Performance of Fly Ash Alkali-activated Cement Based Binder Mortars," *KSCE J. Civ. Eng.*, vol. 22, no. 5, pp. 1854–1864, May 2018, doi: 10.1007/s12205-017-1714-3.

[54] N. Cristelo, A. Fernández-Jiménez, C. Vieira, T. Miranda, and Á. Palomo, "Stabilisation of construction and demolition waste with a high fines content using alkali activated fly ash," *Constr. Build. Mater.*, vol. 170, pp. 26–39, May 2018, doi: 10.1016/J.CONBUILDMAT.2018.03.057.

[55] R. Robayo-Salazar, C. Jesús, R. Mejía de Gutiérrez, and F. Pacheco-Torgal, "Alkali-activated binary mortar based on natural volcanic pozzolan for repair applications," *J. Build. Eng.*, vol. 25, Sep. 2019, doi: 10.1016/j.jobe.2019.100785.

[56] R. F. Zollo, "Fiber-reinforced concrete: An overview after 30 years of development," *Cement*

and Concrete Composites, vol. 19, no. 2. Elsevier Ltd, pp. 107–122, Jan. 01, 1997, doi: 10.1016/s0958-9465(96)00046-7.

[57] N. Ranjbar, S. Talebian, M. Mehrali, C. Kuenzel, H. S. Cornelis Metselaar, and M. Z. Jumaat, "Mechanisms of interfacial bond in steel and polypropylene fiber reinforced geopolymer composites," *Compos. Sci. Technol.*, vol. 122, pp. 73–81, Jan. 2016, doi: 10.1016/j.compscitech.2015.11.009.

[58] N. Ranjbar *et al.*, "A comprehensive study of the polypropylene fiber reinforced fly ash based geopolymer," *PLoS One*, vol. 11, no. 1, Jan. 2016, doi: 10.1371/journal.pone.0147546.

[59] V. Cunha, J. Barros, and J. Sena-Cruz, "Numerical simulation of indirect tensile tests – Two distinct approaches."

[60] A. Koenig *et al.*, "Flexural behaviour of steel and macro-PP fibre reinforced concretes based on alkali-activated binders," *Constr. Build. Mater.*, vol. 211, pp. 583–593, Jun. 2019, doi: 10.1016/j.conbuildmat.2019.03.227.

[61] A. Abrishambaf, V. M. C. F. Cunha, and J. A. O. Barros, "A two-phase material approach to model steel fibre reinforced self-compacting concrete in panels," *Eng. Fract. Mech.*, vol. 162, no. Pergamon, pp. 1–20, 2016, doi: 10.1016/j.engfracmech.2016.04.043.

[62] S. F. A. Shah, B. Chen, S. Y. Oderji, M. Aminul Haque, and M. R. Ahmad, "Comparative study on the effect of fiber type and content on the performance of one-part alkali-activated mortar," *Constr. Build. Mater.*, vol. 243, p. 118221, May 2020, doi: 10.1016/j.conbuildmat.2020.118221.

[63] N. A. Farhan, M. N. Sheikh, and M. N. S. Hadi, "Engineering Properties of Ambient Cured Alkali-Activated Fly Ash–Slag Concrete Reinforced with Different Types of Steel Fiber," *J. Mater. Civ. Eng.*, vol. 30, no. 7, p. 04018142, Jul. 2018, doi: 10.1061/(ASCE)MT.1943-5533.0002333.

[64] J. Qin *et al.*, "Mechanical properties of basalt fiber reinforced magnesium phosphate cement composites," *Constr. Build. Mater.*, vol. 188, pp. 946–955, Nov. 2018, doi: 10.1016/j.conbuildmat.2018.08.044.

[65] M. Mastali, K. M. Shaad, Z. Abdollahnejad, M. Falah, P. Kinnunen, and M. Illikainen, "Towards sustainable bricks made with fiber-reinforced alkali-activated desulfurization slag mortars incorporating carbonated basic oxygen furnace aggregates," *Constr. Build. Mater.*, vol. 232, Jan. 2020, doi: 10.1016/j.conbuildmat.2019.117258.

[66] R. Sobott, K. Bente, and M. Kittel, "Comparative porosity measurements on ceramic materials," *Old Potter's Alm.*, vol. 19, no. 1, pp. 18–25, Jun. 2014, doi: 10.11588/opa.2014.1.14853.

[67] M. Keppert *et al.*, "Red-clay ceramic powders as geopolymer precursors: Consideration of amorphous portion and CaO content," *Appl. Clay Sci.*, vol. 161, pp. 82–89, Sep. 2018, doi: 10.1016/j.clay.2018.04.019.

[68] G. F. Huseien, A. R. M. Sam, K. W. Shah, J. Mirza, and M. M. Tahir, "Evaluation of alkali-activated mortars containing high volume waste ceramic powder and fly ash replacing GBFS," *Constr. Build. Mater.*, vol. 210, pp. 78–92, Jun. 2019, doi: 10.1016/j.conbuildmat.2019.03.194.

[69] Y. Ma, J. Hu, and G. Ye, "The pore structure and permeability of alkali activated fly ash," *Fuel*, vol. 104, pp. 771–780, Feb. 2013, doi: 10.1016/j.fuel.2012.05.034.

[70] W. Chen and H. J. H. Brouwers, "The hydration of slag, part 1: Reaction models for alkali-activated slag," *J. Mater. Sci.*, vol. 42, no. 2, pp. 428–443, Jan. 2007, doi: 10.1007/s10853-006-0873-2.

[71] N. Cristelo, J. Coelho, T. Miranda, Á. Palomo, and A. Fernández-Jiménez, "Alkali activated composites – An innovative concept using iron and steel slag as both precursor and

aggregate," *Cem. Concr. Compos.*, vol. 103, pp. 11–21, Oct. 2019, doi: 10.1016/j.cemconcomp.2019.04.024.

[72]   C. L. Hwang, M. Damtie Yehualaw, D. H. Vo, and T. P. Huynh, "Development of high-strength alkali-activated pastes containing high volumes of waste brick and ceramic powders," *Constr. Build. Mater.*, vol. 218, pp. 519–529, Sep. 2019, doi: 10.1016/j.conbuildmat.2019.05.143.

[73]   Z. Abdollahnejad, T. Luukkonen, M. Mastali, P. Kinnunen, and M. Illikainen, "Development of One-Part Alkali-Activated Ceramic/Slag Binders Containing Recycled Ceramic Aggregates," *J. Mater. Civ. Eng.*, vol. 31, no. 2, p. 04018386, Feb. 2019, doi: 10.1061/(ASCE)MT.1943-5533.0002608.

[74]   T. Yang, Q. Wu, H. Zhu, and Z. Zhang, "Geopolymer with improved thermal stability by incorporating high-magnesium nickel slag," *Constr. Build. Mater.*, vol. 155, pp. 475–484, Nov. 2017, doi: 10.1016/j.conbuildmat.2017.08.081.

[75]   F. Ameri, P. Shoaei, S. A. Zareei, and B. Behforouz, "Geopolymers vs. alkali-activated materials (AAMs): A comparative study on durability, microstructure, and resistance to elevated temperatures of lightweight mortars," *Constr. Build. Mater.*, vol. 222, pp. 49–63, Oct. 2019, doi: 10.1016/j.conbuildmat.2019.06.079.

[76]   F. Pacheco-Torgal, J. Castro-Gomes, and S. Jalali, "Alkali-activated binders: A review. Part 2. About materials and binders manufacture," *Construction and Building Materials*, vol. 22, no. 7. Elsevier, pp. 1315–1322, Jul. 01, 2008, doi: 10.1016/j.conbuildmat.2007.03.019.

[77]   F. Pacheco-Torgal, J. Castro-Gomes, and S. Jalali, "Alkali-activated binders: A review. Part 1. Historical background, terminology, reaction mechanisms and hydration products," *Construction and Building Materials*, vol. 22, no. 7. Elsevier, pp. 1305–1314, Jul. 01, 2008, doi: 10.1016/j.conbuildmat.2007.10.015.

[78]   U. De Filippis, E. Prud'homme, and S. Meille, "Relation between activator ratio, hydration products and mechanical properties of alkali-activated slag," *Constr. Build. Mater.*, vol. 266, p. 120940, Jan. 2021, doi: 10.1016/j.conbuildmat.2020.120940.

[79]   M. F. Zawrah, R. A. Gado, N. Feltin, S. Ducourtieux, and L. Devoille, "Recycling and utilization assessment of waste fired clay bricks (Grog) with granulated blast-furnace slag for geopolymer production," *Process Saf. Environ. Prot.*, vol. 103, pp. 237–251, Sep. 2016, doi: 10.1016/j.psep.2016.08.001.

Effect of non-thermal curing on alkali-activated ceramic/slag-based cement reinforced with fibers

Research regarding ceramic wastes/slag-based material for geopolymer production cured at ambient conditions is scarce. Even more so when it comes to the incorporation of fibers in this material. Here we focused on improving the workability of the developed alkali-activated cement presented in the previous chapter to improve both, the fiber distribution (maintaining the same PAN fiber content, i.e., 0%; 0.5%, and 1% in volume) and consequently their mechanical performance. Also, a more sustainable way to produce activated alkaline cement was considered, therefore, ambient curing (20°C and 60% HR ± 5%) was experienced.

Fiber Reinforced Alkali Activated Cements from Ceramic Waste and Ladle Furnace Slag cured at ambient temperature

Norma Gaibor [a]; Dinis Leitão [b]; Tiago Miranda [c]; Nuno Cristelo [d]; Lisete Fernandes [d]; Eduardo N.B. Pereira [c]; Vítor M.C.F. Cunha [c]

a. School of Engineering of the University of Minho, Azurem Campus, 4800-058, Guimarães, Portugal

b. CTAC, Department of Civil Engineering, University of Minho, 4800-058, Guimarães, Portugal

c. ISISE, Institute for Science and Innovation for Bio-Sustainability (IB-S), Department of Civil Engineering, University of Minho, 4800-058, Guimarães, Portugal

d. CQ-VR, Centro de Química - Vila Real, Department of Engineering, University of Trás-os-Montes e Alto Douro, 5001-801, Vila Real, Portugal

*Corresponding author: normygaibor@gmail.com

Abstract

The development of new alkaline-activated materials, as an alternative to Portland cement and conventional concrete, using different industrial by-products or wastes is getting considerable attention from the scientific community. This study aims to investigate the potential of ceramic waste, specifically from brick and tile production, and ladle furnace slag (for composition correction) as precursors in alkaline activated cement reinforced with polyacrylonitrile fibers. Sodium silicate, in solution form, was used to activate the precursors, and three different fiber contents were tested, namely 0, 0.5, and 1%, by volume. The cements were cured at 20°C and tested after 14, 28, and 90 days. Physical and mechanical properties were assessed, such as capillarity, porosity, uniaxial compressive strength, flexural strength, and elasticity modulus. In addition, microstructural analysis was also carried out, namely, Scanning Electron Microscopy, X-ray Energy Dispersive Analyzer, X-ray diffraction, and Fourier Transform Infrared Spectroscopy. The results revealed that environmentally friendly alkali-activated binders were produced from wastes with very few industrial recycling possibilities, and the addition of 0.5% fibers was able to potentiate its performance, up to a flexural strength of 8.84 N/mm^2 and compressive strength of 29 MPa. The mechanical performance presented by this material is relevant, especially when considering that two abundant and less-common wastes were used (avoiding more frequent precursors, like coal fly ash or ground blast furnace slag, which are becoming scarce in Europe) and, also, considering that no thermal curing was applied. Calcium aluminum silicate hydrate (C-A-S-H) was detected as the main reaction product.

Keywords: Ambient curing; ceramic waste; alkali activation; polyacrylonitrile fiber; physical and mechanical properties.

5.1. INTRODUCTION

The production of ordinary Portland cement (OPC) is associated with high amounts of greenhouse gas emissions, which is significantly contributing to serious environmental issues [1]. About one ton of CO_2 is released per ton of OPC produced, which means that the Portland cement industry alone is responsible for approximately 8% of the total global CO_2 emissions to the earth's atmosphere [2], and it is predicted that this value will increase up to 10% in the short term. Moreover, the production of OPC is also responsible for 36% of the global energy consumption, especially due to the calcination step [3]. These environmental concerns about OPC have encouraged researchers to look for sustainable alternatives. Over the last few years, alkali-activated materials (AAM) have appeared as a promising alternative to OPC, mainly due to its substantially lower CO_2 emissions [4], as well as to some of its specific characteristics, like the faster setting, the high early-age strength and the enhanced durability [5]. The use of inorganic industrial wastes or residual products in the production of concrete and/or mortar can contribute towards a more sustainable building design and a greener environment.

AAMs are developed by the reaction between aluminosilicate-based powders, usually referred to as "precursors", and an alkaline solution. Depending on the nature of the starting materials, namely its calcium content, the reaction products can be classified as a sodium aluminosilicate gel (N-A-S-H), or a calcium aluminosilicate gel (C-A-S-H), or under very specific conditions, as a combination of the above mentioned (N-C-A-S-H) [6]. The mechanical behavior and durability performance of the AAM is mainly reliant on the gel type and volume that the alkali-activated system is able to develop [7]. Various authors have studied different types of industrial wastes and by-products, in the way to create sustainable alkali-activated building materials, to later be incorporated into civil construction. This development in introducing an alternative to OPC has drawn the attention of professionals in the commercial and academic sectors [8]. However, so far, the spotlights have been set on coal fly ash and blast furnace slag [9], which are two wastes that are becoming scarcer in Europe, as more efficient and/or cleaner alternatives for the production of power or steel, respectively, are optimized and installed. Viable alternatives, like construction and demolition waste [10] or different types of ceramic waste have also been tested as precursors in alkaline activated systems [11], especially for non-structural applications, such as embankments or fills, road, and railway pavement foundations, among others.

In 2017, the overall production of ceramic waste (CW) exceeded 25 million tons, assuming that 1 m² of ceramic can produce 1.9 kg of waste [12]. Therefore, it has been estimated that approximately 30% of the production within the ceramic industry goes to waste [13], while ceramic materials represent around 45% of construction and demolition waste [14]. As CW is amassing every day, there is a concern in the ceramic industries to find out an alternative solution for its disposal. Despite the recycling and reusing of several kinds of CW, the total amount used in the construction sectors in general and concrete industries are still irrelevant, which represents a very significant possibility to apply, with direct or indirect strategies, substantial percentages of this waste [15]. Thereby, the use of these materials in the construction sector relieves various environmental problems, such as, reducing the total demand and consumption of natural resources and raw materials, saving energy, and costs concerning waste disposal in landfills [16]. It is worthy to note that ceramic wastes can be used safely without any significant processing and be properly recycled for the construction sector. Furthermore, CW usually has an important aluminosilicate content, constituting an appropriate supplement for cement materials, by enhancing their mechanical strength and durability performance [11].

Regarding the use of CW as a precursor, Keppert et al. [17] used two different red-clay ceramic powders, with both producing satisfactory mechanical properties. However, their rheological performance hindered its use in applications requiring pumping or spraying, because of their high viscosity. It was concluded that, when the Ca content is above a specific threshold, it induces a broader pore size distribution and an overall higher porosity on the geopolymer, due to the formation of calcium silicate hydrates. Reig et al. [11] also studied CW materials of different origins (red clay brick and porcelain stoneware) to analyze the properties and microstructure of alkali-activated pastes and mortars. The resulting mortars developed a compressive strength ranging between 22 and 41 MPa, after 7 days of curing at 65 °C, based on the sodium concentration in the solution and the water/binder ratio. Azevedo et al. [18] characterized clay bricks' waste to be used as an alternative precursor to produce roof tiles for buildings. It was proved that the waste has high silica and alumina content, which are fundamental compounds for the geopolymers synthesis. It also has fine particles and high pozzolanic reactivity. Hence, this waste has excellent potential to be applied as a raw material for getting ceramic roof tiles through geopolymeric reactions. Sun et al. [19] worked with ceramic waste (CW) derived from municipal waste collection, i.e. a combination of tiles, pan forms, blocks, etc., activated by sodium/potassium hydroxide and/or silicate solutions. Maximum compressive

strength of 71.1 MPa, after 28 days, was obtained, while its thermal resilience was also enhanced, showing a compressive strength of 75.6 MPa after heat treatment up to 1000 °C.

On the other hand, a specific type of slag is discharged from the production of steel, very common and abundant in most European countries, is the so-called "ladle furnace slag" (LFS), resulting from the metallurgical secondary and the steel refining process [20]. According to statistics, 30 - 60 Kg of LFS for each ton of molten steel is generated [21]. The chemical and mineralogical composition of LFS is largely different from those of ordinary steel slag and blast furnace slag. Even more, the components of the LFS differ owing to many factors in the refining process, even within the same plant [22]. Regarding the mineralogical composition, LFS is mainly characterized by the presence of phases with cementing or low/non-reactive activity, generally $C_{12}A_7$ with a fast hydration rate and a small portion of the C_2S, which is one of the main crystal mineral phases keeping the later performance of hardened cement paste. Its chemical components are calcium and silicon oxide and alumina [23]. As it is known, AAMs with a high calcium content (CaO + SiO_2 > 70%) will produce a calcium aluminum silicate hydrate (C-A-S-H) gel as the major reaction product promoting the enhancement of the mechanical properties of the matrix [24]. Therefore, LFS (rich in calcium sources) has been used in the present research as a complementary precursor.

In general, several studies have proved that the mixture of a high-calcium-level precursor (e.g. slag) with another low-calcium-level precursor (e.g. fly ash, ceramic wastes) reduces shrinkage compared to alkali-activated binders containing slag only [25]. In contrast, the analysis of the particular combination of CW and LFS cured at ambient temperature, as an alternative cement, is less known, but it is expected that this blended system could reduce or mitigate the cracking proneness of AAM due to shrinkage. Furthermore, one possible effective technological solution and relatively simple way, compared to other methods, to reduce the cracks caused by shrinkage and other disadvantages previously mentioned, is the incorporation of reinforcement fibers into the mix. That said, the level of cement improvement depends on the nature and type, content, and mechanical properties of the fibers, bond properties at the interface of the fiber and the matrix, and properties of the cement itself [26]. Some works have observed the effects of using different fibers in alkali-activated materials such as carbon fibers [27], polypropylene and basalt [28], and Polyvinyl alcohol [29], among others. Few studies were found regarding the fiber-reinforced cement prepared with ceramic wastes and slag. Abdollahnejad et al. [30] developed an experimental and numerical investigation, observing that,

124

regardless of the fiber type and curing method, increasing the fiber content increased the compressive and flexural strengths. However, the enhancement level was determined by fiber type and curing conditions (sealing and water bath).

Several works regarding the alkali activation of different materials at room temperature are available in the literature, such as different combinations of slag with fly ash [31], glass powder [32], and silica fume [33], among others. Nonetheless, research concerning ceramic wastes/slag-based material for geopolymer production cured at ambient conditions is scarcer. Hwang et al. [14] studied the alkali activation with curing at 25 °C of the waste brick powder and waste ceramic sand used as a precursor and fine aggregate, respectively, and also the blend of waste red clay brick powder and ceramic from construction and demolition waste together [34], in both cases combined with slag. Room temperature cured alkali-activated materials have demonstrated their advantages in field applications [35] while at the same time, providing a promising alternative to reduce energy consumption due to heat-curing [24]. Nevertheless, limited studies about the combined influence of the development of alkali-activated ceramic/slag cements with fiber addition are available in the literature.

Therefore, having in mind the previous considerations, the present study aimed at the application of two abundant industrial wastes – ladle furnace slag and ceramic waste from a ceramic brick industry in Portugal – as a combined precursor to produce alkali-activated cement. The use of such materials, which are known to possess lower reactivity than other, more common precursors (namely coal fly ash and blast furnace slag), allowed ambient curing conditions (20°C), with inevitable financial and environmental benefits. It should also be highlighted that these are two valuable examples of industrial wastes with a very significant and increasing production rate, especially in Europe, for which a sustainable solution needs to be developed, thus avoiding their landfilling. Sodium silicate solution was used as the activator and, for a broader application range, and to mitigate the lower reactivity of the precursors, polyacrylonitrile fibers (0, 0.5, and 1% contents) were also included in the cements. The final products were assessed in terms of axial stiffness and compressive and flexural strength, physical behavior (capillarity and porosity), and microstructural analyses, which included Scanning Electron Microscopy (SEM), X-ray Energy Dispersive Analysis (EDX), X-ray diffraction (XRD) and Fourier Transform Infrared Spectroscopy (FTIR).

5.2. MATERIALS AND MIXTURES

5.2.1. Materials

Wastes from a ceramic brick (CBW) manufacturing company located nearby the city of Braga (northwestern Portugal) were used to develop the alkali-activated cements in this study, Figure 5-1(a). The ladle furnace slag (LFS), which is the result of scrap melting in an electric arc furnace, was supplied by the ironwork company *Megasa*, located near the city of Maia (northwestern Portugal), Figure 5-1(b). Both were used as the main and secondary precursor materials, respectively. The general characterization of these starting materials, i.e., the particle size distribution and chemical composition were described in the work by Gaibor et al. [36]. In which, the gradation curve showed that the grinding process of CW generated a well-graded material with a fine fraction of around 60%. In addition, it was determined that CBW mainly consists of silica (54.89 wt.%) and alumina (26.28 wt.%), while the LFS was characterized by a significant percentage of CaO (64.23 wt.%) and silica content of 19.68 wt.%. The sodium silicate (Na_2SiO_3) was the alkaline activator solution employed in the reaction process. The developed cement was reinforced with polyacrylonitrile fibers (PANf) of 8 mm in length and ˜20 µm in diameter. PANf was chosen due to its properties, specifically the chemical (good in alkaline medium) and thermal resistance (good in short-term processing temperature up to 220°C) as it is shown in the corresponding technical sheet [37].

(a)

(b)

Figure 5-1. Original materials in situ: (a) ceramic bricks waste (CBW); and (b) ladle furnace slag (LFS)

5.2.2. Alkali-activated cement mixture and production

The present experimental work is the continuation of previous work, namely, Gaibor et al. [38], which was selected from a set of ten different mix compositions, including the reference samples (100 wt.% for CBW and LFS), the mixture with the best mechanical performance. The criteria for this selection were compressive strength. The mix with 75% of ceramic waste plus 25% of ladle furnace slag alkali-activated with sodium silicate (SS) leads to the highest compressive strength i.e., nearby 60 MPa. Secondly, having into consideration some issues regarding the workability of these alkali-activated cements [36], the referred blend composition [38] was modified by adding a polycarboxylate-based superplasticizer [39] with a specific density of 1.03 ± 0.05 and a pH of 7 ± 1 and a small amount of water, in order to make the AAm workable and homogeneous [40] and consequently to improve the incorporation and distribution of fibers in these mixtures. Also, based on the available literature [41] stating that a cement design can be optimized by using up to 2% fiber by volume, it was determined to carry out this experimental work with 0, 0.5, and 1% of volume ratio of PAN. Table 5-1 shows the characterization of the developed cements.

127

Table 5-1. Identification and characterization of the tested cements

Cement ID	Precursor (wt. ratio)		Activator/ Precursor (wt. ratio)	SP/ precursor (wt. ratio)	Water/SS (wt. ratio)	PAN fiber (vol. fraction)	CaO / SiO$_2$	Na$_2$O / Al$_2$O$_3$	SiO$_2$ / Al$_2$O$_3$	SiO$_2$ / Na$_2$O
	CBW	LFS	SS							
M1						0				
M2	75	25	0.45	0.02	0.05	0.5	0.29	0.29	2.76	9.59
M3						1.0				

For alkali activation purposes, the time and order of adding the precursors, alkali activator, and fibers are important [42]. The mixing process occurred in two stages, first, the homogenization of the solid phase and the activator solution for 1 minute in an industrial mixer at the minimum speed (i.e., 140±5 rpm). Afterward, the SP and water were added and mixed for two more minutes at maximum speed (i.e., 285±10 rpm). Finally, the fibers were slowly incorporated into the cement and mixed again for 3 minutes at maximum speed to guarantee uniform distribution of PANf. Thus, the blend was mixed for a total of 6 continuous minutes. The flowability of the cement blending was measured through the flow table test, following the specifications of BS EN 12350-8. During the fresh state, no segregation was observed, this can be attributed to the correct precursor/activator ratio. The slump-flow test, after 15 strokes, yielded a result of the opened out diameter of 165 mm, 145 mm, and 133 mm, for cements with 0%, 0.5, and 1% of PANf content, respectively. Even though the reasonably low workability, an improvement can be noticed when comparing with results obtained by Gaibor et al. [36]. It is worth mentioning that the superplasticizer utilization, which originally plays the role of micro-rollers [43], did not significantly affect the friction and the flow resistance of this alkali-activated cement. Further research is needed to find a more suitable plasticizer in these highly alkaline mediums. Immediately after the slump-flow test, the cement was placed inside stainless-steel prisms molds and vibrated for 2 minutes to remove air bubbles. Samples were cured in a climatic chamber (Fitoclima 28000 EDTU) with constant environmental conditions of 20°C (±0.5°C) and 60% (±5%) relative humidity (RH). After the first 24 hours, specimens were unmolded and left to cure in the same terms till the testing time, i.e., 14, 28, and 90 days. As one of the main aims of this work was not to use thermal curing conditions, this curing method was not employed. Each set of blends (M1, M2, and M3) had five samples for the uniaxial compressive test and four samples to perform the other mechanical and physical tests, respectively, elasticity modulus, flexural tests, porosity, and capillarity tests.

5.3. TEST SET-UP

5.3.1. Physical characterization

The physical properties were obtained from the portions of prisms ruptured during the flexural tests at 28 days of curing. The open porosity (P) was determined based on the Portuguese standard LNEC E 395, while the determination of the water absorption (C) due to capillary action followed the recommendations of BS EN1015-18:2002. The lateral surfaces of the cubic specimens were covered by a silicone layer to avoid water evaporation and humidity transportation through them, the bottom surface was placed in contact with about 10 mm of water, and the mass of the absorbed water by capillary rise was measured over 192 h until the curve has stabilized. More detailed information about the test setup performed can be found in our previous work, [36].

5.3.2. Mechanical behavior

The Young's modulus (E_{cm}) was determined accordingly to method B comprised in BS EN 12390-13 standard, while the uniaxial compressive behavior was obtained through a customized test set-up using a servo-hydraulic testing machine with a 300 kN load capacity actuator and monotonic displacement control rate of 0.002 mm/min. Before the execution of the tests at 14, 28, and 90 days, each specimen with nominal dimensions of $50 \times 50 \times 100$ mm^3 was rectified to guarantee smooth parallel surfaces for the load application. The flexural behavior, namely, tensile strength under flexure and post-cracking residual strengths of each series were assessed by testing four prismatic beams of $40 \times 40 \times 160$ mm^3 with a notch depth of 8 mm. A three-point bending test was used, which was adapted from the recommendations of the standards BS EN 1015-11:1999 and EN 14651:2005. A LLOYD LR50K universal press fitted with a 50 kN load cell was used for the flexural tests. A constant displacement control rate of 0.002 mm/min was adopted.

5.3.3. Mineralogical and microstructural characterization

Both the two used precursors and the resulting reaction products were characterized regarding their mineralogy and microstructure. After the completion of the mechanical tests, a hardened small portion of a randomly selected specimen from each batch was immersed in acetone to stop the chemical

reactions. Later on, these samples were milled with the traditional cement and pestle for 20 min, to get a fine powder (< 0.45 mm) to be analyzed by X-ray diffraction (XRD). The results were obtained from a PANalytical X'Pert Pro diffractometer, fitted with an X'Celerator detector and a secondary monochromator, with a CuKα radiation setting of 40kV and 30mA, a nominal step size of 0.017°, a rate of 100 s/step, and a 2θ range between 10 and 85°. The chemical compounds and energy dispersion were ascertained by employing an FEI Quanta 400 scanning electron microscopy (SEM) and X-ray spectroscopy (EDS) from EDAX, respectively, using the same spectrum acquisition time and a ZAF correction model.

For the FTIR analysis, a Thermo Scientific Nicolet iS50 FTIR spectrometer, recourse to an ATR (Attenuated Total Reflectance) accessory with a diamond crystal was used. The instrument was controlled by the Omnic software package, version 9.2.28, from Thermo Fisher Scientific Inc., spectra were recorded between 400 and 4000 cm^{-1} with a resolution of 4 cm^{-1} and 64 scan readouts during 90 seconds on each sample.

5.4. RESULTS AND DISCUSSION

5.4.1. Physical properties

5.4.1.1. Open Porosity

Table 5-2 includes the open porosity values, ranging from 21 to 23% for the studied AAm (M1, M2, M3). No significant differences were observed between these series, therefore the water absorption by immersion was not governed by the addition of fibers. It is worth mentioning that relatively high porosity in alkali-activated materials was also observed by other researchers, e.g. [44], [45]. Furthermore, the LFS influenced the chemical reactions through the alkali activation process, since this precursor had high calcium content (Table 1, [36]). Higher content of CaO in the starting materials is found to cause a broader pore size distribution and higher porosity of the resulting AAm, due to the expectable formation of calcium silicate hydrates [17]. On the other hand, the fact of adding extra water to the blend composition results in larger amounts of "free" water that perhaps is confined in the intergranular area or broad pores after geopolymerization, which evaporates through the curing time, causing significant quantities of intergranular pores in the microstructure [46]. Additionally, the

irregular shape of the crushed ceramic wastes [47] (the major component in the mixture), could also be another factor that conducts to higher porosity.

Table 5-2. Open porosity of the alkali-activated cement after 28 days of curing, (%)

	M1 (0%f)	M2 (0.5%f)	M3 (1%f)
Porosity (%)	23.26	23.51	21.71
(CoV)	1.22	1.59	1.44

5.4.1.2. Capillarity

Water absorption by capillarity was performed to interpret the connectivity of pores and it can also denote an estimation of pore tortuosity and the capillary network. According to the results, the incorporation of fibers did not considerably affect water sorptivity by capillarity. It can be observed in Figure 5-2, that the time-related capillarity coefficient variation in AAm with low fiber content (0.5% fiber - M2) was not significant, obtaining a capillary coefficient of 3.00E-01 $kg/m^2.min^{0.5}$, the same value as the cement M1 (without fiber reinforcement). The obtained value is within the range, of 0.18–0.62 $kg/m^2.min^{0.5}$ [44], of capillary coefficients registered in other studies for plain slag or fly ash-based alkali-activated cements. In contrast, it was observed that with a higher amount of PAN fibers, i.e., 1% in the M3 series, the alkali-activated mixtures presented a threefold increase in the capillarity coefficient (9.00E-01 $kg/m^2.min^{0.5}$) in comparison to plain AAm (M1), which is higher than 0.53 $kg/m^2.min^{0.5}$ and 0.61 $kg/m^2.min^{0.5}$ reported in other AAm reinforced with cellulose or basalt fibers [44], respectively. In this case, the uptake of water can be associated with perhaps a continuous capillary network which also may explain the lower compressive strength observed for M3 (Figure 5-3).
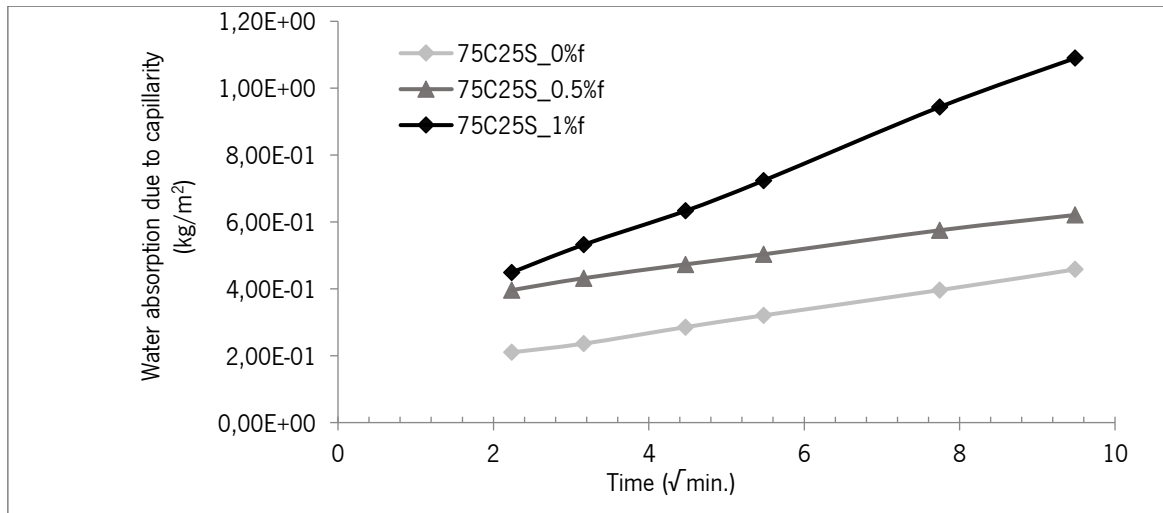
Figure 5-2. Dependence of the mass increase on the suction surface $\Delta m_t/F$, about the square root of time $\sqrt{t}$ for samples of the alkali-activated cement after 28 days of curing

5.4.2. Mechanical behavior

5.4.2.1. Compressive strength

Figure 5-3 displays the uniaxial compressive strength (UCS) of the studied AAms, respectively, M1, M2, and M3 determined at the age of 14, 28, and 90 days. The fact of adding fibers to the compressive strength can be either positive or negative. The compressive strength rises when fibers stop crack propagation, but it drops when fibers cause more air voids [30], [47]. In general, results showed that the curing time increased the UCS, regardless of the percentage of fibers added. The UCS of the M2 series with 0.5% PANf increased about 7.7% (29.2 MPa) when compared to the control series i.e., M1. On the other hand, the UCS of the M3 series with 1% of PANf decreased by approximately 7% at 90 days of curing age when compared to the same reference mix i.e., M1.

The relatively low compressive strength values in this research, in comparison to other AAm, using ceramic wastes and slag cured at ambient temperature found in literature, e.g. 24–93 MPa (23 ± 2°C and RH of 50%) [14], 36–70 MPa (25 °C and RH of 65%) [48], and 25-70 MPa (room temperature) [49], could be related to several factors. First, the difference in the chemical composition of precursors, i.e., as CBW is the major constituent in the mixture (75%), the low content of calcium (0.64 %wt.) and high content of silica (54.89 %wt.) led to less production of C-(A)-S-H gels, which negatively affect the strength of AAm [50], despite the contribution of Ca^{2+}, Si^{4+}, and Al^{3+} ions from the LFS into the alkali

132

activation system. Second, the somewhat high porosity found in the AAms, as was explained in section 5.4.1.1. Finally, the third factor could be associated with the curing conditions. It has been stated that alkaline-activated systems are sensitive to temperature and relative humidity (RH) [51]. It is well known that when used at elevated temperatures (30–90 °C) in the early curing hours, it catalyzes the reactions of alkali-activated binders and facilitates them to form a strong network of hydrates and increased the number of Si-O-Al which in turn substantially enhances their compressive strengths [52]. Therefore, curing under ambient conditions restricts alkaline-activated binders to obtain higher strength. In this case, the curing at the climatic chamber (20 °C ±0.5 and 60% ±5 RH) may not allow the evaporation of the excess water, thus not enough monolithic geopolymer was formed. On the other hand, it has been reported that room temperature is more propitious to the development of interfacial bond strength between fibers and matrix. That is, ambient temperature curing can play a better role in bridging fibers to matrix [29]. Concluding, the developed AAMs showed acceptable compressive strength, 27 MPa at 90 days (M1), which could be used for several applications in the construction industry.
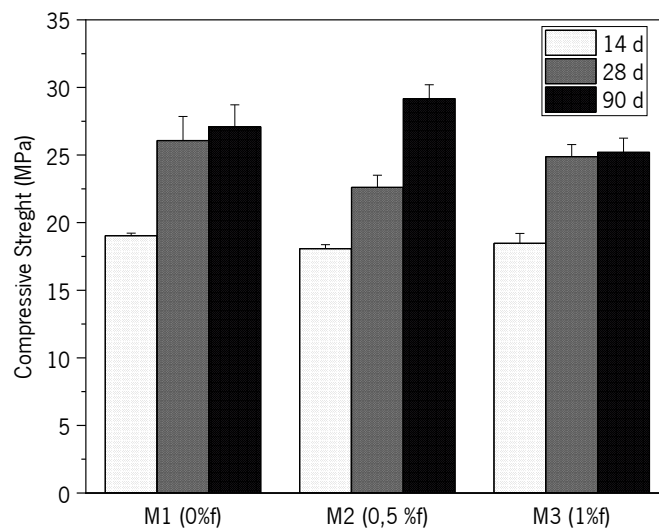
Figure 5-3. Uniaxial Compressive Strength (UCS) obtained for 0% (M1), 0,5% (M2) and 1% (M3) fibers contents after 14, 28 and 90 days curing

5.4.2.2. Elasticity modulus

The modulus of elasticity is considered to be an important property since it does not only influence the stiffness of a certain element but also the elastic deformations of an AAm element [53]. The Young's modulus (E_{cm}) of alkali-activated materials with/without fibers generally increases with the increase of the compressive strength [42], as it also occurs in this case. Figure 5-4 includes the

average value of E_{cm} for the studied blends cured under ambient conditions, at 14, 28, and 90 days of curing. The plain cement series (M1) attained an average elasticity modulus of 7.76 GPa at 28 days of curing. Whereas, an improvement in the E_{cm} was observed by the gradual addition of fibers (M2 and M3), which agrees with the findings of Behfarnia et al., [54] and Alomayri [55] for polypropylene and micro-glass fibers incorporation, respectively. This was expected accordingly to the mixtures law theory since the PAN fibers have a higher elasticity modulus, i.e., 10.6 GPa, than the plain cement mixture. This can be also related to the optimal fiber content and its homogenous distribution [42], thereby, it might show that PAN fibers are well-dispersed into the CBW/LFS-based Aam. The highest E_{cm} value (11.86 GPa) was obtained for 1% fiber volume content (M3) at 90 days representing an increment of about 23% compared to the unreinforced control sample i.e., M1. While the addition of 0.5% of PANf (M2) did not represent such a significant increase in E_{cm} (~8%) compared to M1.
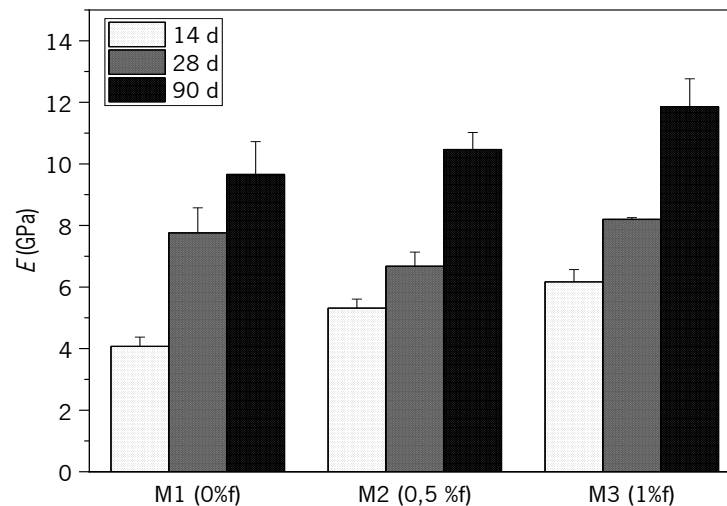
Figure 5-4. Young's modulus (E_{cm}) obtained for 0% (M1), 0,5% (M2) and 1% (M3) fibers contents after 14, 28 and 90 days curing.

5.4.2.3. Stress-strain relationships

Figure 5-5, 5.6, and 5.7 depict the stress-strain relationships for the M1, M2, and M3 series, respectively. Besides the increase in the compressive strength previously discussed, it is visible that the strain at peak stress decreases with the increase of age due to the increase in the specimens' stiffness. Even though the post-peak behavior was not fully assessed, for the M3 series with a volumetric ratio reinforcement of 1%, it is visible the increase in the energy absorption energy capacity, when compared with the other two series. Note that the main benefits of discrete fiber reinforcement arise under tensile behavior and shear [56], [57], [58].

134
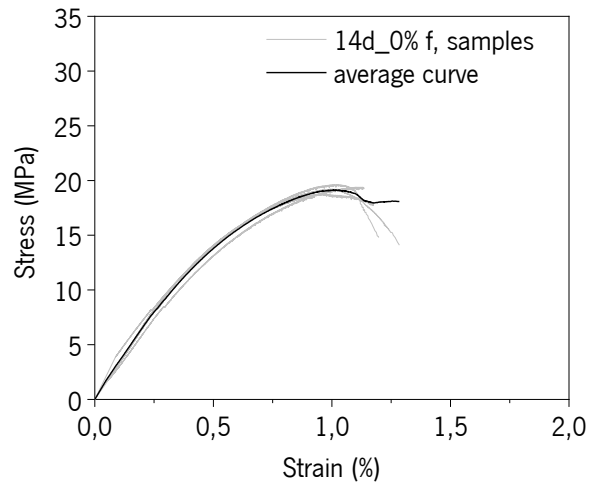
(a)
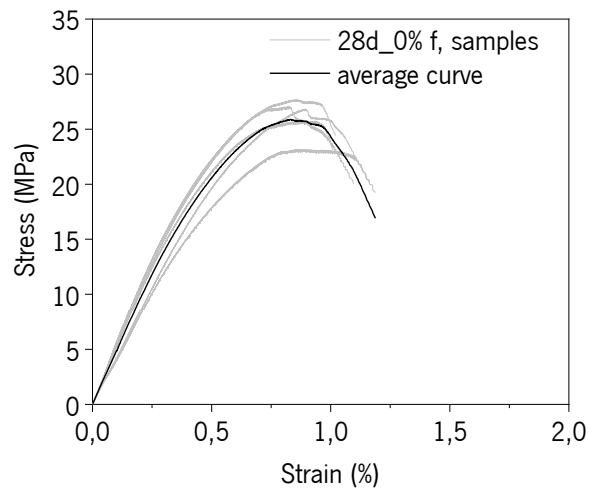
(b)
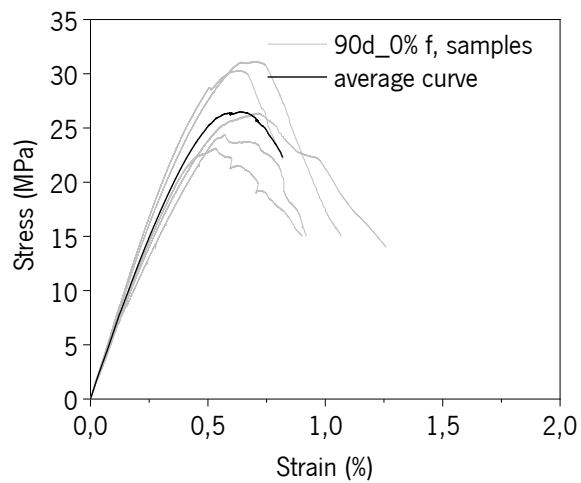
(c)

Figure 5-5. Stress-strain curves for AAm control samples, M1_0% fibers, after (a) 14, (b) 28, and (c) 90 days curing
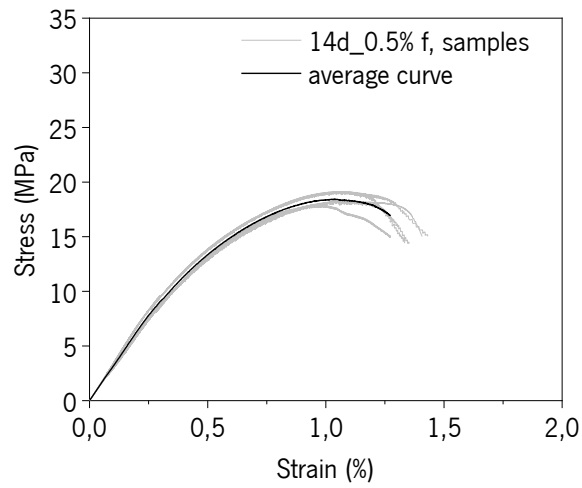
(a)
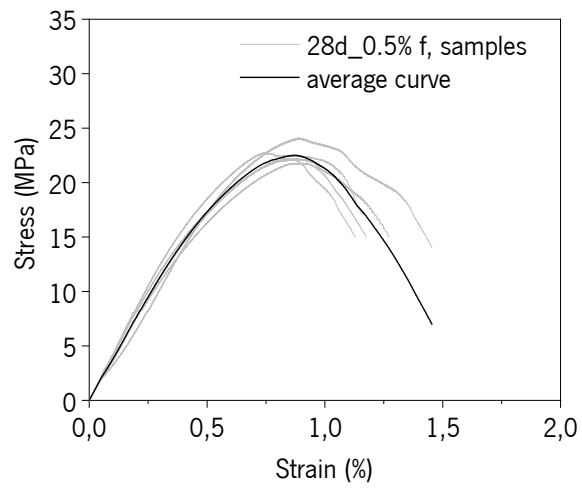
(b)
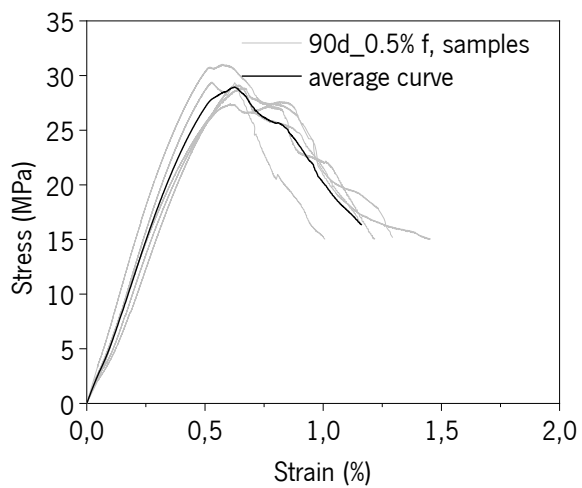
(c)

Figure 5-6. Stress-strain curves for AAM reinforced with 0.5% PAN fibers after a) 14, b) 28, and c) 90 days curing.
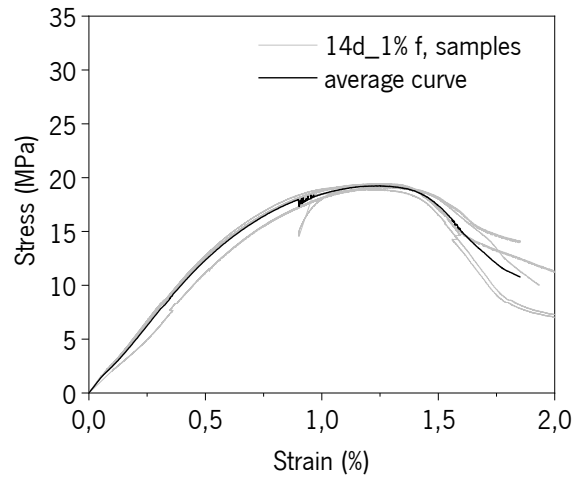
(a)
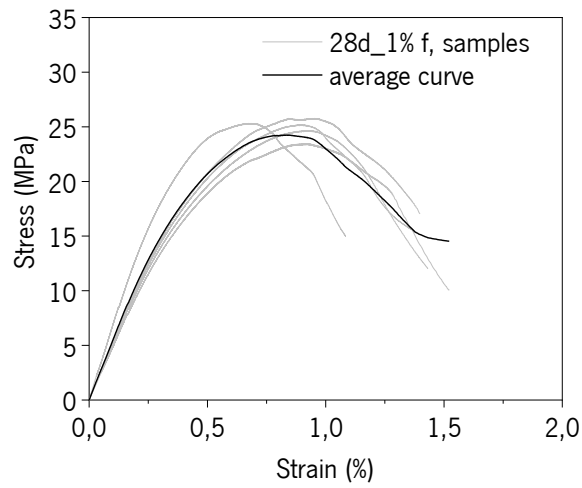
(b)
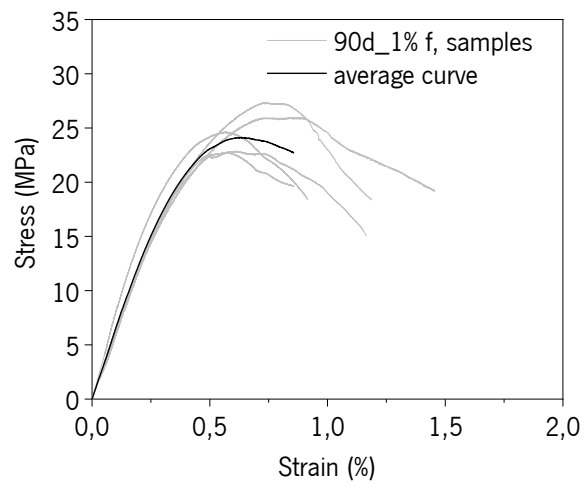
(c)

Figure 5-7. Stress-strain curves for AAM reinforced with 0.5% PAN fibers after (a) 14, (b) 28, and (c) 90 days curing.

5.4.2.4. Flexural behavior

The tensile strength under flexure (f_{ct}^{f}), as well as the residual flexural tensile strengths for crack mouth opening displacements of 0.3 mm ($f_{R0.3mm}$) and 0.5 mm ($f_{R0.5mm}$) of all mixtures tested in this research, are presented in Figure 5-8. In general, f_{ct}^{f} increased with the curing age, regardless of the fiber content (Figure 5-8 (a)). The strength development in AAm reinforced with PANf is attributed to the effect of the matrix itself rather than the fiber contribution, due to the progressive dissolution and hydration reactions that occur at early ages in the alkaline matrix [59]. However, it can be observed, that at 14 days there was an increase of f_{ct}^{f} in about 18 and 25% with the incorporation of 0.5 and 1% of PANf, respectively, demonstrating the ability of the fibers to transfer the developed stress levels along the micro-cracks. At 28 days, results of f_{ct}^{f} for the three different cements do not display significant variations. At 90 days there is not a clear trend, but it was identified that increasing the percentage of fiber by 1% resulted in slight strength reduction showing a similar behavior as for compression strength, which was assigned to the relatively high porosity detected in the AAm. Similar results were found by Puertas et al. [60] with the introduction of polypropylene fibers up to 1% dosage, while the study of Alomayri et al. [61] exhibited an improvement in the flexural strength up to a dosage of 0.5% before the flexural strength starts to fade.

Figure 5-9, 5.10, and 5.11 show the load-deflection curves obtained for all specimens up to a 2 mm deflection. As illustrated in Figure 5-9, the control sample (M1) exhibits brittle failure at all ages. On the other hand, M2 and M3 have increased the energy absorption capacity, in particular for the highest fiber content i.e., 1%. In both cases, the highest flexural load was observed at the crack onset and then decreased during loading, which can be referred to as a classical softening behavior [62]. At 90 days, it was possible to draw the load-deflection curve only for one sample of the series with a 0.5% fiber content (Figure 5-10 (c)), since the other specimens had a brittle failure. The latter occurred on specimens that exhibited a higher peak load than the other specimens that exhibited a ductile post-cracking behavior.

In general, the increase in the residual strengths and energy absorption capacity was more significant for the series with lower compressive strength, i.e., at younger ages. This may indicate that for the older series the bond strength between fiber/matrix is higher leading to a predominant fiber rupture failure mode. Consequently, as curing time increases the $f_{R0.3mm}$ and $f_{R0.5mm}$ values decrease, Figure 5-8

138

(b) and (c), respectively. Besides, in Figure 5-11 (a), for the series with 1% of PANf, can be observed an increase in the residual strengths with increasing deformation, which does not exceed the first crack load, corresponding to a post-hardening behavior that is more visible at 14 days.
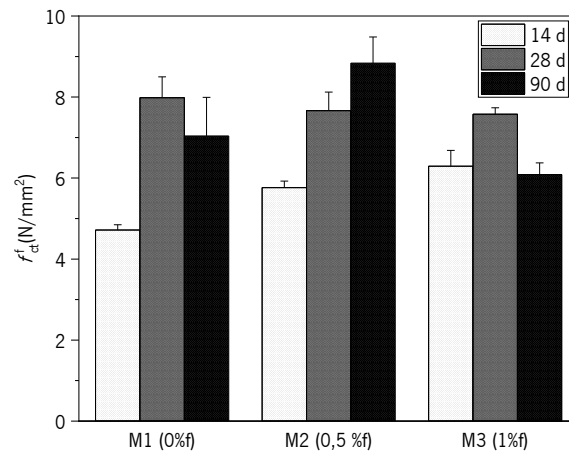
(a)
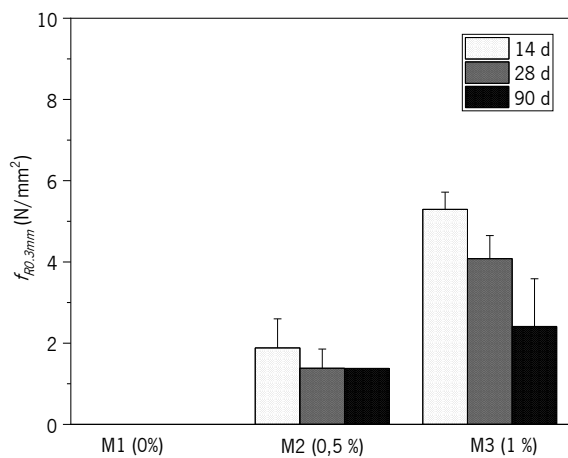
(b)
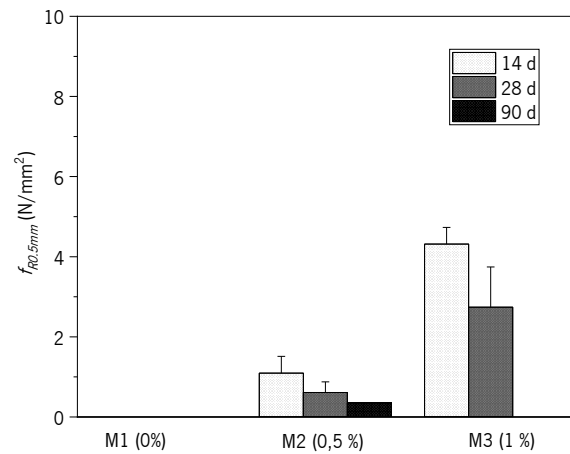
(c)

Figure 5-8. Flexural strength and residual flexural tensile strengths for crack mouth opening displacements of 0.3 mm ($f_{R0.3mm}$) and 0.5 mm ($f_{R0.5mm}$) of the alkali-activated cement after 14, 28, and 90 days of curing
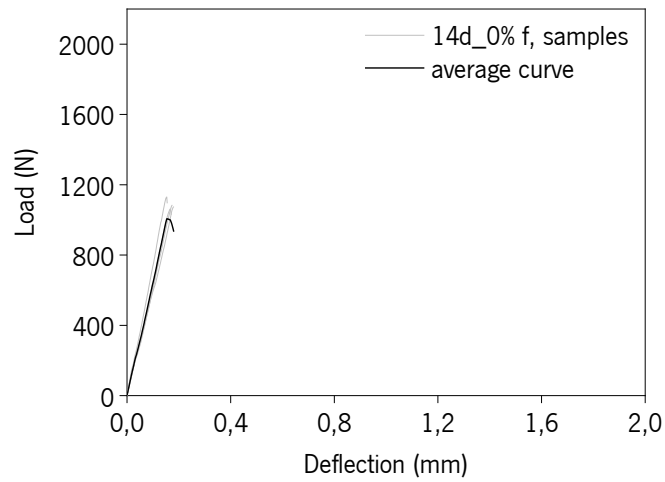
(a)
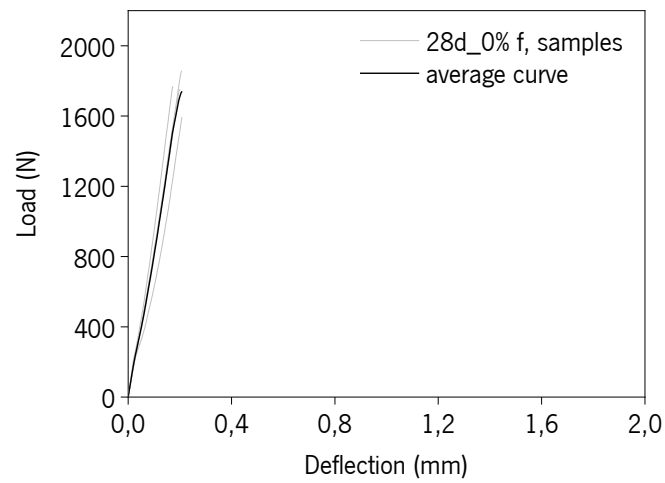
(b)
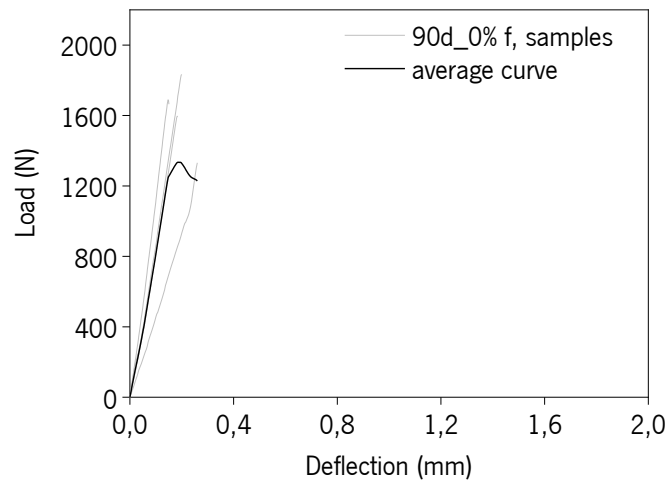
(c)

Figure 5-9. Load displacement curves under flexural loading for AAm control samples, M1_0% fibers, after a) 14, b) 28, and c) 90 days of curing
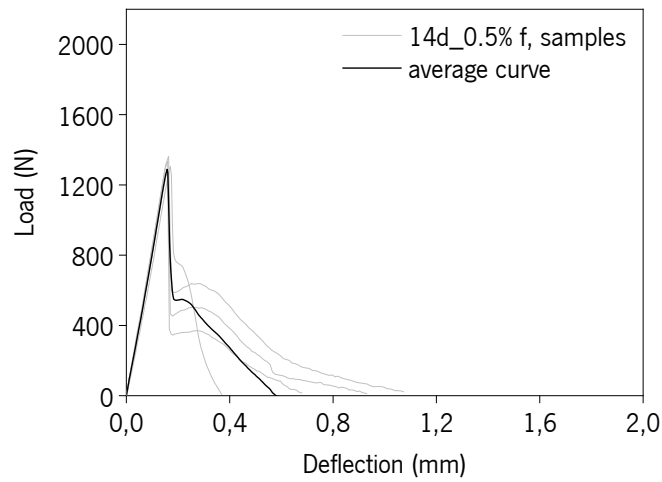
(a)
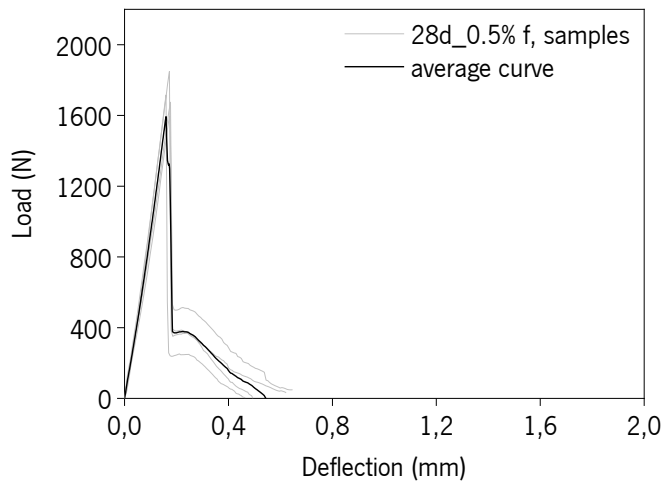
(b)
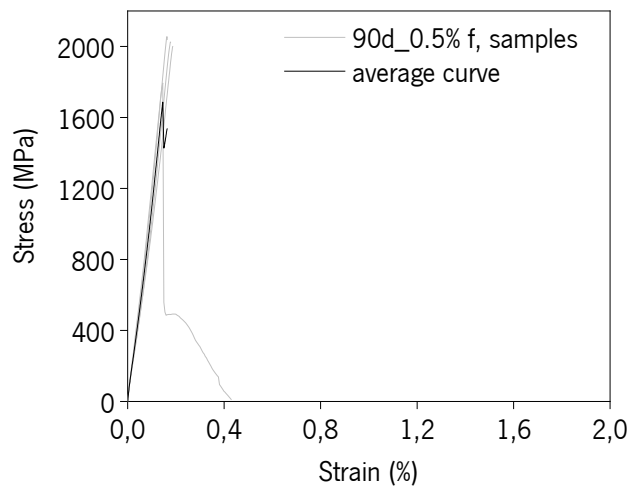
(c)

Figure 5-10. Load displacement curves under flexural loading for AAM reinforced with 0.5% PAN fibers, M2, after a) 14, b) 28, and c) 90 days of curing
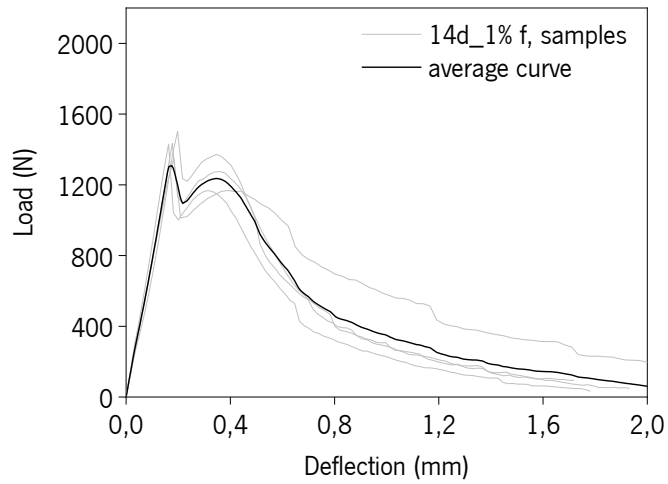
(a)
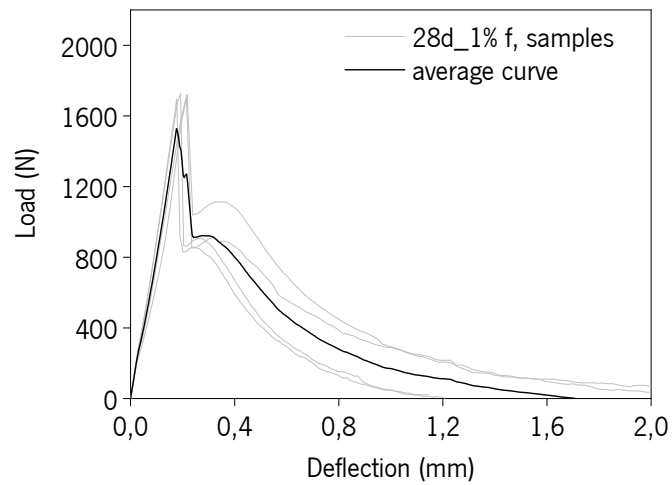
(b)
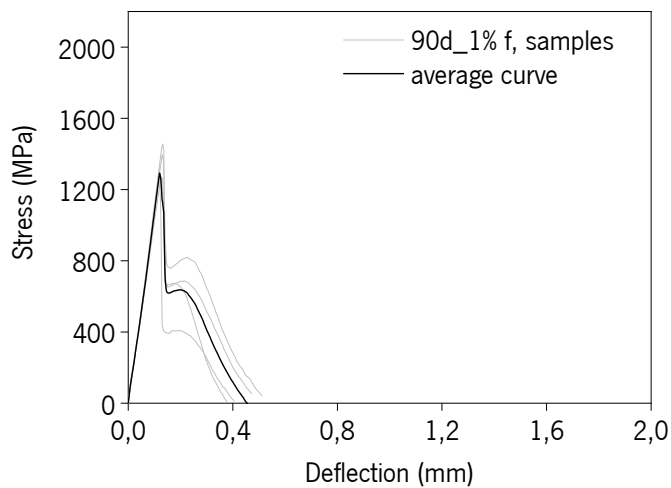
(c)

Figure 5-11. Load displacement curves under flexural loading for AAm reinforced with 1% PAN fibers, M3, after a) 14, b) 28, and c) 90 days of curing

5.4.3. Mineralogical and microstructural characterization

The mineralogical and microstructural analyses were conducted on randomly selected M3 specimens considering that the blended compositions only differed on the fiber content. Therefore, the selected samples were submitted to X-ray diffraction (XRD), Scanning Electron Microscopy (SEM), X-ray Energy Dispersive Analysis (EDX), and Fourier Transform Infrared Spectroscopy (FTIR) to investigate the crystalline phases, the morphology and identify the chemical compounds of the reaction products at 14, 28 and 90 curing days.

5.4.3.1. X-ray analysis

The X-ray diffractograms (XRDs) of the raw precursors (CBW and LFS) and the selected mixture, i.e., M3, are exhibited together in Figure 5-12 to facilitate the direct comparison. The slight amorphous hump between 25 and 30°2θ reveals some amorphous content on the LFS. However, in general, it lacks long-range order, illustrating a complex structure with several crystalline phases, translated by the many peaks. Short reflections for calcium olivine, mayenite, cuspidine, lime, and larnite were identified.

Regarding the CBW, a broader hump was detected, which reveals a higher amorphous content than that found in the LFS. The main crystalline phase documented was quartz (SiO_2) which represents 81.1 %wt. (Table 5-3). The same finding was reported by Zawrah et al. [63] for waste-fired clay bricks. Some peaks revealing the presence of muscovite, hematite, and garronite were also found, though these peaks were significantly less intense.

It is known that curing conditions, such as temperature and humidity, play a key role in the development of microstructure and, thus, in the final properties of the AAm [64]. The majority of the studies found in the literature regarding this particular type of alkaline cements (i.e. based on ceramic waste or ladle furnace slag) used high temperatures and/or humidity for curing [11], [38]. Therefore, the present work, aiming at a more economically viable application of this material, focused on the effects of ambient temperatures (below 25 °C) on microstructural development.

In general terms, the diffraction patterns of the materials resulting from the activation reactions were governed by the ceramic waste. Curing time and temperature, i.e., 14, 28 90 days at 20°C, did not change the mineralogical phases significantly. Most of the crystalline phases present in the starting materials were also distinguished in the hydrated mixtures. But the diffractograms of the activated blend (M3) exposed smaller peaks of some of the main phases, like quartz (Q), Calcio olivine (C), and hematite (H), thus indicating some reaction of these phases, even considering the normal intensity decrease produced by the mixture with another precursor (LFS).

The alkaline activation reaction was responsible for the slight translation and distribution of their humps towards 2θ angle positions between 18° and 65°. This translation denotes the formation of the amorphous calcium aluminosilicate gel [65]. Furthermore, the formation of new crystalline phases was also detected, namely enstatite (E), phengite (P), feldspar (F), and illite (I). The content of Fe_2O_3 and MgO in the CBW and LFS, respectively, plus the soluble SiO_2 content incorporated through the alkaline activator may have led to the formation of E, suggesting that the latter could influence the resulting materials of the studied AAm. The P is a high silica variety of muscovite [66] that was present in CBW. It is persistent during the curing time at ~20° (2θ). The presence of silica in the CBW was translated as the crystalline phase in feldspars or as free quartz, whereas alumina was detected on feldspars only. This explains the approach of the F peak at ~24° and ~26° at 14 and 28 days, respectively, towards the chief peak of quartz until getting disappeared at 90 days. The F peak at 28° (2θ) remains constant through the curing time. Illite is a mineral phase usually found in soils-quartz [65] which is associated with the presence of CBW as a major precursor. It is also visible at all curing ages close to the main halo of quartz.

The evolution of the mineralogy and, in particular, its quantification, influences the compressive strength of the alkali-activated materials produced. The values presented in Table 5-3 were normalized. Content variation of crystalline phases could be attributed to the impacts of curing conditions on the chemical reactions. For instance, from 14 to 90 days, C and F phases decrease by 25% and 34%, respectively, whereas the Q phase increases by about 43% during the same period. The increase of the quartz content can also help explain the strength gained with curing time [51].
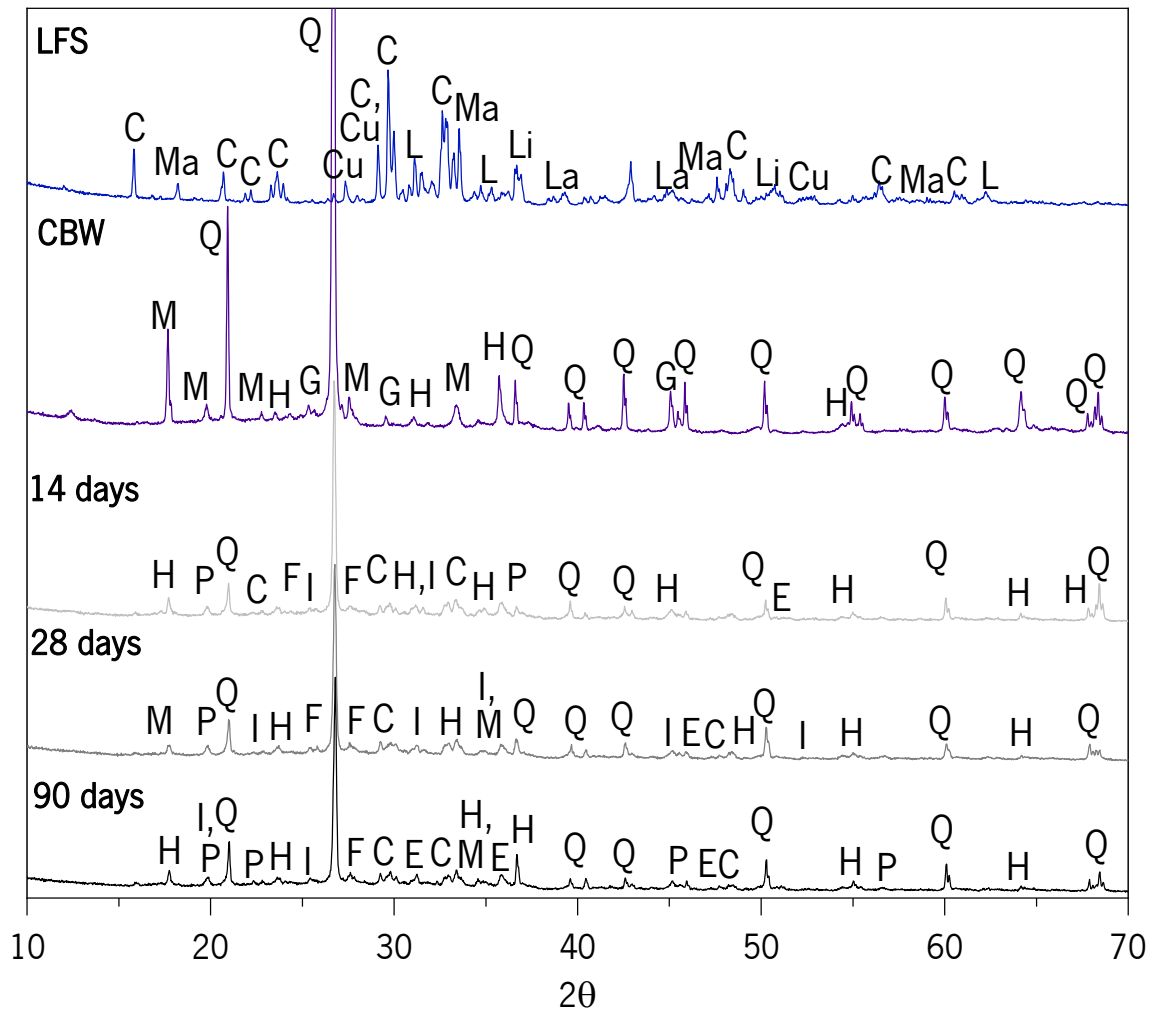
(Q: quartz; M: muscovite; C: calcium olivine; E: enstatite; I: Illite; P: Phengite; F: Feldspar; Cu: Cuspidine; Ma: Mayenite; L: Lime; La: Larnite; H: Hematite; G: Garronite)

Figure 5-12. X-ray diffractograms (XRDs) of the precursors (CBW and LFS) and the AAm reinforced with 1% of PAN fibers (M3), at 14, 28, and 90 days of curing time

Table 5-3. Minerals´ quantification of the precursors (CBW and LFS) and the AAm reinforced with 1% of PAN fibers (M3), at 14, 28 and 90 days curing time, (% wt)

Material	Q	H	M	G	C	Cu	Ma	L	La	E	P	F	I
CBW	81.1	4.4	13.8	0.6	-	-	-	-	-	-	-	-	-
LFS	-	-	-	-	48.5	18.5	6.7	2.1	24.2	-	-	-	-
M3_14 days	13.9	3.1	19.3	-	21.7	-	-	-	-	12.4	2.1	22.4	5.0
M3_28 days	12.9	2.3	6.6	-	18.6	-	-	-	-	37.9	9.5	10.8	1.5
M3_90 days	24.3	1	14.3	-	16.3	-	-	-	-	27.9	0.6	14.8	14.3

Q: Quartz; H: Hematite; M: Muscovite; G: Garronite; C: Calcio Olivine; Cu: Cuspidine; Ma: Mayenite; L: Lime; La: Larnite; E: enstatite; Ca: Calcite; P: Phengite; F: Feldspar; I: Illite

5.4.3.2. SEM/EDS analysis

SEM micrographs on M3 samples were taken after 14, 28, and 90 days (Figure 5-13). Generally, the matrix can be described as a compact microstructure, with some unreacted and partially reacted CBW particles with an irregular and angular shape (points 1). However, the effect of the curing time is very clear in terms of the number and extension of the unreacted particles, with both decreasing significantly (Figure 5-13 (c)). At the same time, as can be seen from the images, the fibers have been effectively incorporated into the matrix (points 2), as the gel phase (points *) surrounded and connected them, improving the interfacial bond strength and increasing the potential during the fiber pulling process, which translates in overall improved mechanical properties [28], mainly in terms of the flexural strength.

Moreover, since the alkali-activated mixtures partly consisted of slag (25%) and this amorphous precursor is rich in calcium (64.23% wt.), it is accordingly expected to form a calcium silicate hydrate gel in the matrix, possibly with a significant aluminum content (from the slag). The presence of high content of Ca in the AAm accelerates the initial stages of the reaction, enabling the rapid formation of a C-A-S-H type gel (Figure 5-13, points *), potentiated by the presence of soluble silica in the activator. Such a mechanism could explain the relatively high strength reached at 28 days, considering the curing developed at 20°C. However, after the initial formation of this primary gel, further evolution of the reactions is residual [65], in a process similar to that observed for the Portland cement, which reaches between 85 to 90% of its maximum compressive strength in this timeframe. As a result, similar strength values were obtained after 28 and 90 days.

a)

b)

c)
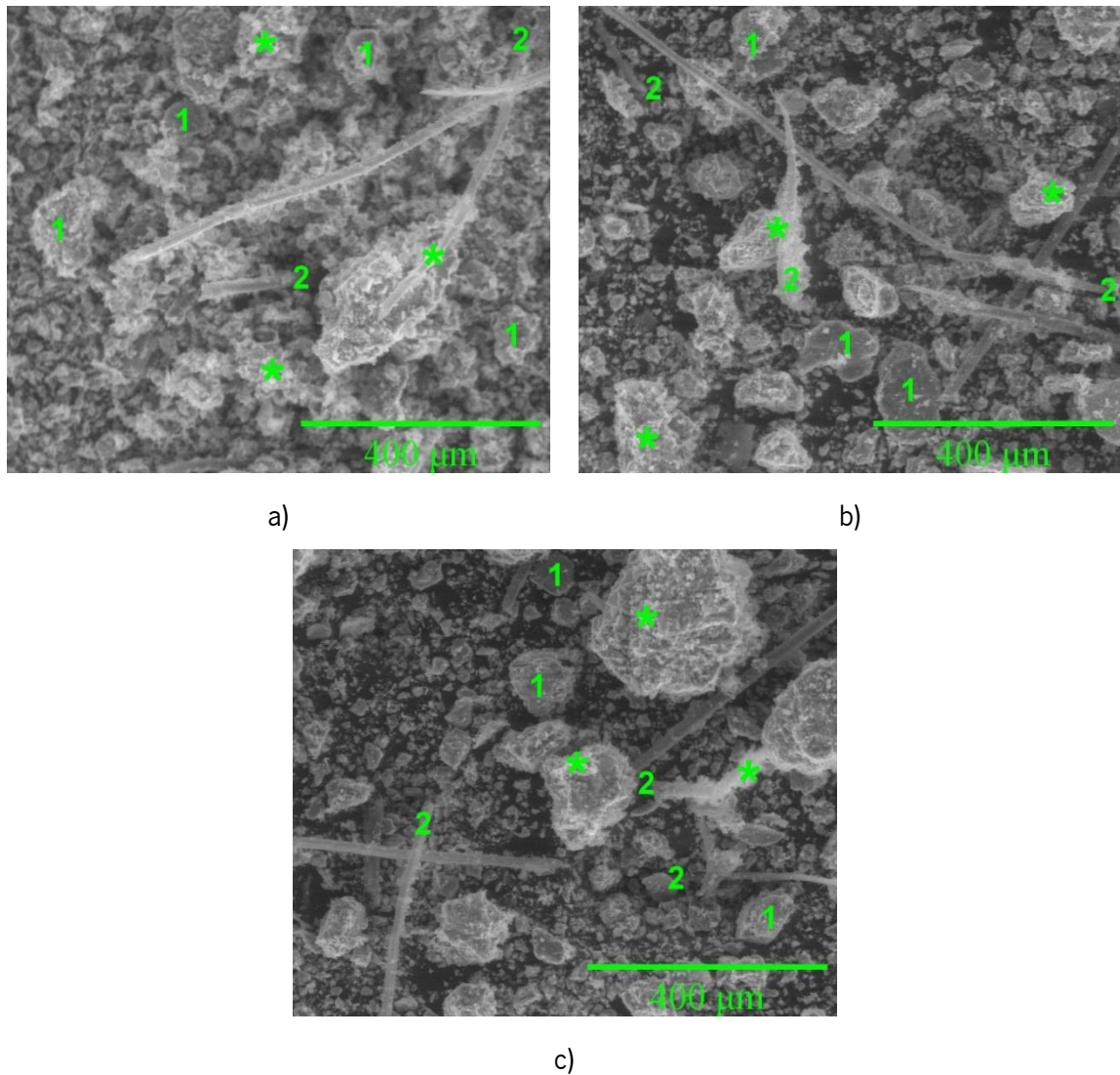
Figure 5-13. SEM images of the AAm reinforced with 1% of PAN fibers (M3), after a) 14 days, b) 28 days, and c) 90 days curing time. Point 1) ceramic waste particles; Point 2) PAN fibers; Point *) C-A-S-H type gel.

5.4.3.3. FTIR spectra of starting materials and mixtures

FTIR spectrum of original materials and the AAm of the studied mixtures after 14, 28, and 90 days are plotted in the wavenumber range of 400-1800 cm^{-1} and are exposed in Figure 5-14. The FTIR pattern of the LFS shows two bands set at 445 and 490 cm^{-1} which belong to the O-Si-O ($v4$ O-Si- O) vibration, while the 540 cm^{-1} band is related to the Al-O-Al bond. The bands distinguished at 840 and 1475 cm^{-1} are typically linked to the deformation vibration of carbonates (CO_3^{2-}), C-O. For the CBW spectra, there is the main broadband at 1270-900 cm^{-1}, with a deeper frequency at 1035 cm^{-1}, corresponding to Si-O and Al-O bonds. The band at 774 and 690 cm^{-1} belong to the Al-O stretching

vibration in AlO_4 groups and Si-O, respectively. And the absorbance bands at 440 and 420 cm^{-1} reflect the stretching vibration of quartz, O–Si–O bonds.

Regarding FTIR spectral analysis for the alkali-activated mixtures, the weak band placed around 1650 cm^{-1} reflects the stretching and bending of O–H, denoting the water absorption associated with the developed hydrated gels [67]. The two bands located at 1480 and 1415 cm^{-1} are attributed to the presence of $[CO_3]^{2-}$ demonstrating the O-C-O stretching and vibration bond due to atmospheric carbonation [68] which is slightly deeper at 90 days of curing. The main band for hydrated alkali-activated gel was shaped at about 1000 cm^{-1} which is associated with the asymmetric stretching vibration mode of Si-O-T (T: tetrahedral Si or Al). This is in agreement with the results of other studies [48], [69]. Besides, the decrease in wavelengths of these bands, compared to CBW (1035 cm^{-1}), refers to the gradual formation of tetrahedral C-A-S-H gel since the Al^{4+} atoms penetrate the original configuration of Si-O-Si skeletal structure occurred during the polycondensation process [19]. The bands at 875 cm^{-1} belong to the $v2$ $[CO3]^{2-}$ carbonate vibration. Undissolved quartz particles are traced at 692, 440, and 420 cm^{-1}. Results are consistent with the compressive strength and SEM findings.
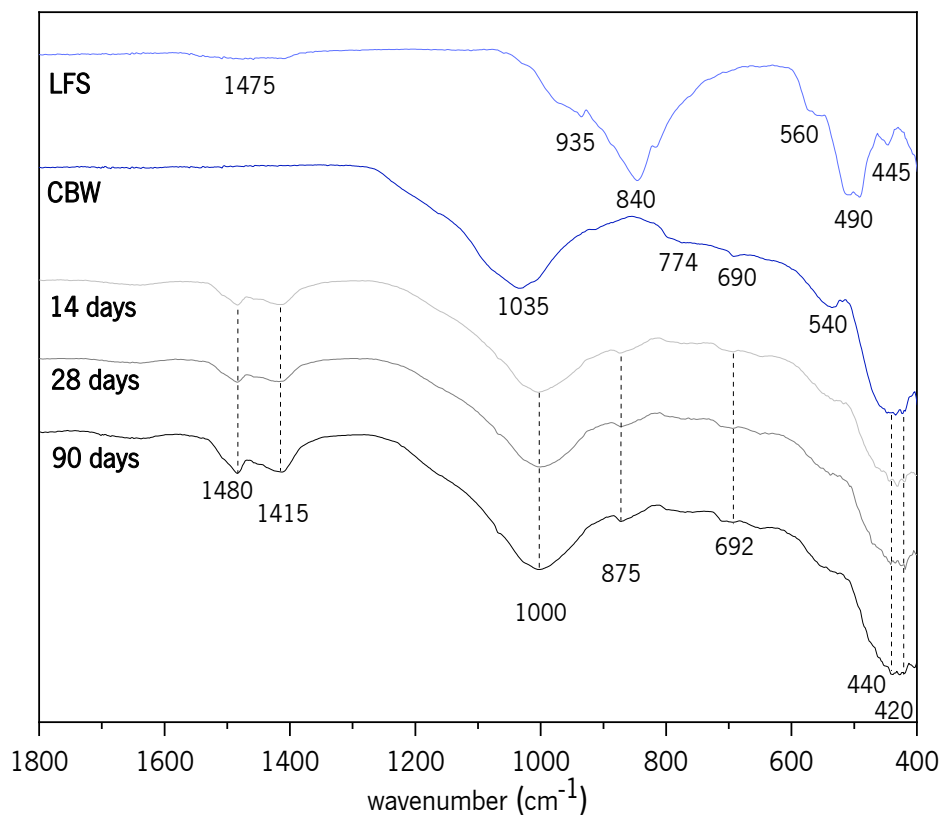
Figure 5-14. FTIR spectra for precursors ceramic bricks waste (CBW), ladle furnace slag (LFS), and the studied cement.

5.5. CONCLUSIONS

This paper aimed to study the matrix and composite of ambient-cured (20°C) alkali-activated cements (AAm) with high content of ceramics bricks waste (CBW) and ladle furnace slag (LFS) as a complementary precursor and reinforced with the polyacrylonitrile fibers (PANf) in varying proportions up to 1% by volume. The conclusions from the findings reported and analyzed above are as follows.

1. Curing conditions determine the water available during alkali-activated CBW/LFS matrix hardening. Consequently, it plays a crucial role in the development of microstructural characteristics of the material, kinetics, degree of reaction, and their respective macroscopic properties. Regarding physical properties of the developed AAm, i.e., water absorption by immersion and capillarity was not substantially affected by fibers incorporation. However, the high content of CaO, due to the LFS presence, performs a key leader in the formation of the hydrated gel, which causes a greater pore formation;

2. The nature of the matrix was the most important factor in strength development, more than fiber content. Compressive strengths ranging from 25 to 29 MPa were registered at 90 days for the studied series with distinct fiber reinforcement contents. This outcome suggests a satisfactory compressive strength since the specimens were cured without high-temperature levels (20°C), opposite to what is typically employed in other studies, minimizing energy consumption, cost, and CO_2 emissions. Besides, the acquired mechanical properties are appropriated for several applications and open a possibility to use it as an alternative material within the construction industry. Notwithstanding, further investigations into durability performance are still needed;

3. The reinforcement with PANf (0.5 and 1%) led to an improvement in the flexural strength performance, more visible at the 14 days, basically owing to lower matrix strength. But in general, it was associated with the enhancement of workability of the cement and consequently the homogeneous dispersion of the fibers in the matrix which ends in the adequate fiber bridging and stress transfer in the composite throughout the micro-cracks. However, at the curing ages of 28 and 90 days, there are no significant variations, and a clear trend was not identified, respectively. Regarding the residual flexural tensile strength, as was expected, the greater effect on increasing it was for crack mouth opening displacements of 0.3 mm ($f_{R0.3mm}$) and 0.5 mm ($f_{R0.5mm}$) was determined when 1% of fiber content.

149

4. The general properties exhibited by alkaline cements in this study are directly related to the nature and structure of its main reaction product, which has been identified as C-A-S-H gel.

In a general conclusion, the present study suggests that ambient curing can be used in developing more cost-effective AAMs since it does not require energy treatment to improve the reaction process, which makes it practical also for on-site works. Besides, the reinforcement with PAN fibers of alkali-activated cements based on the combination of ceramic waste/ladle furnace slag seems to be a promising alternative to conventional Portland cement-based materials, nonetheless, they have been scarce reported.

DATA AVAILABILITY STATEMENT

All data, models, and code generated or used during the study appear in the submitted article.

ACKNOWLEDGMENTS

REFERENCES

[1] A. Galvão Souza Azevedo and K. Strecker, "Kaolin, fly-ash and ceramic waste based alkali-activated materials production by the 'one-part' method," *Constr. Build. Mater.*, vol. 269, p. 121306, Feb. 2021, doi: 10.1016/J.CONBUILDMAT.2020.121306.

[2] G. F. Huseien, A. R. M. Sam, K. W. Shah, J. Mirza, and M. M. Tahir, "Evaluation of alkali-activated mortars containing high volume waste ceramic powder and fly ash replacing GBFS," *Constr. Build. Mater.*, vol. 210, pp. 78–92, Jun. 2019, doi: 10.1016/j.conbuildmat.2019.03.194.

[3] K. Kermeli *et al.*, "The scope for better industry representation in long-term energy models: Modeling the cement industry," *Appl. Energy*, vol. 240, pp. 964–985, Apr. 2019, doi: 10.1016/J.APENERGY.2019.01.252.

[4] A. S. Ouda and M. Gharieb, "Behavior of alkali-activated pozzocrete-fly ash paste modified with ceramic tile waste against elevated temperatures and seawater attacks," *Constr. Build. Mater.*, vol. 285, p. 122866, May 2021, doi: 10.1016/J.CONBUILDMAT.2021.122866.

[5] K. Arbi, M. Nedeljković, Y. Zuo, and G. Ye, "A Review on the Durability of Alkali-Activated Fly Ash/Slag Systems: Advances, Issues, and Perspectives," *Industrial and Engineering Chemistry Research*, vol. 55, no. 19. American Chemical Society, pp. 5439–5453, May 18, 2016, doi: 10.1021/acs.iecr.6b00559.

[6] G. F. Huseien, A. R. M. Sam, K. W. Shah, M. A. Asaad, M. M. Tahir, and J. Mirza, "Properties of ceramic tile waste based alkali-activated mortars incorporating GBFS and fly ash," *Constr. Build. Mater.*, vol. 214, pp. 355–368, Jul. 2019, doi: 10.1016/J.CONBUILDMAT.2019.04.154.

[7] S. Çelikten, M. Sarıdemir, and İ. Özgür Deneme, "Mechanical and microstructural properties of alkali-activated slag and slag + fly ash mortars exposed to high temperature," *Constr. Build. Mater.*, vol. 217, pp. 50–61, Aug. 2019, doi: 10.1016/j.conbuildmat.2019.05.055.

[8] G. F. Huseien and K. W. Shah, "Performance evaluation of alkali-activated mortars containing industrial wastes as surface repair materials," *J. Build. Eng.*, vol. 30, p. 101234, Jul. 2020, doi: 10.1016/j.jobe.2020.101234.

[9] N. Marjanović, M. Komljenović, Z. Baščarević, V. Nikolić, and R. Petrović, "Physical-mechanical and microstructural properties of alkali-activated fly ash-blast furnace slag blends," *Ceram. Int.*, vol. 41, no. 1, pp. 1421–1435, Jan. 2015, doi: 10.1016/j.ceramint.2014.09.075.

[10] R. Mejía de Gutiérrez, A. R. Robayo-Salazar, and J. F. Rivera, "Alkali-activated building materials made with recycled construction and demolition wastes," *Constr. Build. Mater.*, vol. 149, pp. 130–138, Sep. 2017, doi: 10.1016/J.CONBUILDMAT.2017.05.122.

[11] L. Reig, M. M. Tashima, L. Soriano, M. V. Borrachero, J. Monzó, and J. Payá, "Alkaline Activation of Ceramic Waste Materials," *Waste Biomass Valor*, vol. 4, pp. 729–736, 2013, doi: 10.1007/s12649-013-9197-z.

[12] A. M. Rashad and G. M. F. Essa, "Effect of ceramic waste powder on alkali-activated slag pastes cured in hot weather after exposure to elevated temperature," *Cem. Concr. Compos.*, vol. 111, p. 103617, Aug. 2020, doi: 10.1016/J.CEMCONCOMP.2020.103617.

[13] R. M. Senthamarai and P. Devadas Manoharan, "Concrete with ceramic waste aggregate," *Cem. Concr. Compos.*, vol. 27, no. 9–10, pp. 910–913, Oct. 2005, doi: 10.1016/j.cemconcomp.2005.04.003.

[14] C. L. Hwang, M. D. Yehualaw, D. H. Vo, T. P. Huynh, and A. Largo, "Performance evaluation of alkali activated mortar containing high volume of waste brick powder blended with ground

granulated blast furnace slag cured at ambient temperature," *Constr. Build. Mater.*, vol. 223, pp. 657–667, Oct. 2019, doi: 10.1016/j.conbuildmat.2019.07.062.

[15] H. Mohammadhosseini, N. H. A. S. Lim, M. M. Tahir, R. Alyousef, H. Alabduljabbar, and M. Samadi, "Enhanced performance of green mortar comprising high volume of ceramic waste in aggressive environments," *Constr. Build. Mater.*, vol. 212, pp. 607–617, Jul. 2019, doi: 10.1016/j.conbuildmat.2019.04.024.

[16] K. W. Shah and G. F. Huseien, "Bond strength performance of ceramic, fly ash and GBFS ternary wastes combined alkali-activated mortars exposed to aggressive environments," *Constr. Build. Mater.*, vol. 251, p. 119088, Aug. 2020, doi: 10.1016/j.conbuildmat.2020.119088.

[17] M. Keppert *et al.*, "Red-clay ceramic powders as geopolymer precursors: Consideration of amorphous portion and CaO content," *Appl. Clay Sci.*, vol. 161, pp. 82–89, Sep. 2018, doi: 10.1016/j.clay.2018.04.019.

[18] A. R. G. Azevedo, C. M. F. Vieira, W. M. Ferreira, K. C. P. Faria, L. G. Pedroti, and B. C. Mendes, "Potential use of ceramic waste as precursor in the geopolymerization reaction for the production of ceramic roof tiles," *J. Build. Eng.*, vol. 29, May 2020, doi: 10.1016/j.jobe.2019.101156.

[19] Z. Sun *et al.*, "Synthesis and thermal behavior of geopolymer-type material from waste ceramic," *Constr. Build. Mater.*, vol. 49, pp. 281–287, 2013, doi: 10.1016/j.conbuildmat.2013.08.063.

[20] K. Fang, J. Zhao, D. Wang, H. Wang, and Z. Dong, "Use of ladle furnace slag as supplementary cementitious material before and after modification by rapid air cooling: A comparative study of influence on the properties of blended cement paste," *Constr. Build. Mater.*, vol. 314, p. 125434, Jan. 2022, doi: 10.1016/J.CONBUILDMAT.2021.125434.

[21] M. Skaf, V. Ortega-López, J. A. Fuente-Alonso, A. Santamaría, and J. M. Manso, "Ladle furnace slag in asphalt mixes," *Constr. Build. Mater.*, vol. 122, pp. 488–495, Sep. 2016, doi: 10.1016/J.CONBUILDMAT.2016.06.085.

[22] P. Araos Henríquez, D. Aponte, J. Ibáñez-Insa, and M. Barra Bizinotto, "Ladle furnace slag as a partial replacement of Portland cement," *Constr. Build. Mater.*, vol. 289, p. 123106, Jun. 2021, doi: 10.1016/J.CONBUILDMAT.2021.123106.

[23] K. Fang, D. Wang, J. Zhao, and M. Zhang, "Utilization of ladle furnace slag as cement partial replacement: Influences on the hydration and hardening properties of cement," *Constr. Build. Mater.*, vol. 299, p. 124265, Sep. 2021, doi: 10.1016/J.CONBUILDMAT.2021.124265.

[24] M. Sarkar and K. Dana, "Partial replacement of metakaolin with red ceramic waste in geopolymer," *Ceram. Int.*, vol. 47, no. 3, pp. 3473–3483, Feb. 2021, doi: 10.1016/J.CERAMINT.2020.09.191.

[25] X. Gao, Q. L. Yu, and H. J. H. Brouwers, "Assessing the porosity and shrinkage of alkali activated slag-fly ash composites designed applying a packing model," *Constr. Build. Mater.*, vol. 119, pp. 175–184, Aug. 2016, doi: 10.1016/j.conbuildmat.2016.05.026.

[26] N. Ranjbar, S. Talebian, M. Mehrali, C. Kuenzel, H. S. Cornelis Metselaar, and M. Z. Jumaat, "Mechanisms of interfacial bond in steel and polypropylene fiber reinforced geopolymer

composites," *Compos. Sci. Technol.*, vol. 122, pp. 73–81, Jan. 2016, doi: 10.1016/j.compscitech.2015.11.009.

[27] J. S. Alcaide, E. G. Alcocel, F. Puertas, R. Lapuente, and P. Garcés, "Carbon fibre-reinforced, alkali-activated slag mortars," *Mater. Constr.*, vol. 57, no. 288, pp. 33–48, Oct. 2007, doi: 10.3989/mc.2007.v57.i288.63.

[28] X. Guo and X. Pan, "Mechanical properties and mechanisms of fiber reinforced fly ash–steel slag based geopolymer mortar," *Constr. Build. Mater.*, vol. 179, pp. 633–641, Aug. 2018, doi: 10.1016/j.conbuildmat.2018.05.198.

[29] X. Guo and J. Yang, "Intrinsic properties and micro-crack characteristics of ultra-high toughness fly ash/steel slag based geopolymer," *Constr. Build. Mater.*, vol. 230, p. 116965, Jan. 2020, doi: 10.1016/j.conbuildmat.2019.116965.

[30] Z. Abdollahnejad, M. Mastali, T. Luukkonen, P. Kinnunen, and M. Illikainen, "Fiber-reinforced one-part alkali-activated slag/ceramic binders," *Ceram. Int.*, vol. 44, no. 8, pp. 8963–8976, Jun. 2018, doi: 10.1016/j.ceramint.2018.02.097.

[31] G. Fang, W. K. Ho, W. Tu, and M. Zhang, "Workability and mechanical properties of alkali-activated fly ash-slag concrete cured at ambient temperature," *Constr. Build. Mater.*, vol. 172, pp. 476–487, May 2018, doi: 10.1016/J.CONBUILDMAT.2018.04.008.

[32] M. N. N. Khan, J. C. Kuri, and P. K. Sarker, "Effect of waste glass powder as a partial precursor in ambient cured alkali activated fly ash and fly ash-GGBFS mortars," *J. Build. Eng.*, vol. 34, p. 101934, Feb. 2021, doi: 10.1016/J.JOBE.2020.101934.

[33] S. V. Dave, A. Bhogayata, and N. K. Arora, "Mix design optimization for fresh, strength and durability properties of ambient cured alkali activated composite by Taguchi method," *Constr. Build. Mater.*, vol. 284, p. 122822, May 2021, doi: 10.1016/J.CONBUILDMAT.2021.122822.

[34] C.-L. Hwang, M. Damtie Yehualaw, D.-H. Vo, and T.-P. Huynh, "Development of high-strength alkali-activated pastes containing high volumes of waste brick and ceramic powders," *Constr. Build. Mater.*, vol. 218, pp. 519–529, Sep. 2019, doi: 10.1016/J.CONBUILDMAT.2019.05.143.

[35] X. Gao, Q. L. Yu, and H. J. H. Brouwers, "Reaction kinetics, gel character and strength of ambient temperature cured alkali activated slag–fly ash blends," *Constr. Build. Mater.*, vol. 80, pp. 105–115, Apr. 2015, doi: 10.1016/J.CONBUILDMAT.2015.01.065.

[36] N. Gaibor, D. Leitão, T. Miranda, N. Cristelo, E. N. B. Pereira, and V. M. C. F. Cunha, "Effect of polyacrylonitrile fiber on the properties of alkali-activated ceramic/slag-based mortar," *J. Build. Eng.*, vol. 44, p. 103367, Dec. 2021, doi: 10.1016/J.JOBE.2021.103367.

[37] Composites - Fibers & Materials | SGL Composites, "Binder+-3D-reinforcement solutions," 2019. www.sglcarbon.com (accessed Jan. 30, 2020).

[38] N. Gaibor, J. Coelho, D. Leitão, T. Miranda, P. Tavares, and N. Cristelo, "Alkali activation of recycled ceramic aggregates from construction and demolition wastes," *Mater. Construcción*, vol. 70, no. 339, p. 222, Jul. 2020, doi: 10.3989/mc.2020.13619.

[39] Y. Alrefaei, Y. S. Wang, and J. G. Dai, "The effectiveness of different superplasticizers in ambient cured one-part alkali activated pastes," *Cem. Concr. Compos.*, vol. 97, pp. 166–174, Mar. 2019, doi: 10.1016/j.cemconcomp.2018.12.027.

[40] N. Ranjbar *et al.*, "A comprehensive study of the polypropylene fiber reinforced fly ash based geopolymer," *PLoS One*, vol. 11, no. 1, Jan. 2016, doi: 10.1371/journal.pone.0147546.

[41] A. Adesina, "Performance of fibre reinforced alkali-activated composites – A review," *Materialia*, vol. 12, p. 100782, Aug. 2020, doi: 10.1016/j.mtla.2020.100782.

[42] N. Ranjbar and M. Zhang, "Fiber-reinforced geopolymer composites: A review," *Cem. Concr. Compos.*, vol. 107, p. 103498, Mar. 2020, doi: 10.1016/j.cemconcomp.2019.103498.

[43] F. Soltanzadeh, V. M. C. F. Cunha, and J. A. O. Barros, "Assessment of different methods for characterization and simulation of post-cracking behavior of self-compacting steel fiber reinforced concrete," *Constr. Build. Mater.*, vol. 227, p. 116704, Dec. 2019, doi: 10.1016/j.conbuildmat.2019.116704.

[44] M. Mastali, K. M. Shaad, Z. Abdollahnejad, M. Falah, P. Kinnunen, and M. Illikainen, "Towards sustainable bricks made with fiber-reinforced alkali-activated desulfurization slag mortars incorporating carbonated basic oxygen furnace aggregates," *Constr. Build. Mater.*, vol. 232, Jan. 2020, doi: 10.1016/j.conbuildmat.2019.117258.

[45] I. Balczár, T. Korim, and A. Dobrádi, "Correlation of strength to apparent porosity of geopolymers - Understanding through variations of setting time," *Constr. Build. Mater.*, vol. 93, no. 93, pp. 983–988, Jul. 2015, doi: 10.1016/j.conbuildmat.2015.05.059.

[46] M. Criado, A. Fernández Jiménez, I. Sobrados, A. Palomo, and J. Sanz, "Effect of relative humidity on the reaction products of alkali activated fly ash," *J. Eur. Ceram. Soc.*, vol. 32, no. 11, pp. 2799–2807, Aug. 2012, doi: 10.1016/j.jeurceramsoc.2011.11.036.

[47] Z. Abdollahnejad, M. Mastali, B. Woof, and M. Illikainen, "High strength fiber reinforced one-part alkali activated slag/fly ash binders with ceramic aggregates: Microscopic analysis, mechanical properties, drying shrinkage, and freeze-thaw resistance," *Constr. Build. Mater.*, vol. 241, Apr. 2020, doi: 10.1016/j.conbuildmat.2020.118129.

[48] C. L. Hwang, M. Damtie Yehualaw, D. H. Vo, and T. P. Huynh, "Development of high-strength alkali-activated pastes containing high volumes of waste brick and ceramic powders," *Constr. Build. Mater.*, vol. 218, pp. 519–529, Sep. 2019, doi: 10.1016/j.conbuildmat.2019.05.143.

[49] G. F. Huseien, A. R. M. Sam, K. W. Shah, and J. Mirza, "Effects of ceramic tile powder waste on properties of self-compacted alkali-activated concrete," *Constr. Build. Mater.*, vol. 236, p. 117574, Mar. 2020, doi: 10.1016/j.conbuildmat.2019.117574.

[50] G. F. Huseien, J. Mirza, M. Ismail, S. K. Ghoshal, and M. A. M. Ariffin, "Effect of metakaolin replaced granulated blast furnace slag on fresh and early strength properties of geopolymer mortar," *Ain Shams Eng. J.*, vol. 9, no. 4, pp. 1557–1566, Dec. 2018, doi: 10.1016/j.asej.2016.11.011.

[51] Z. Abdollahnejad *et al.*, "Microstructural Analysis and Strength Development of One-Part Alkali-Activated Slag/Ceramic Binders Under Different Curing Regimes," *Waste Biomass Valorization 2019 116*, vol. 11, no. 6, pp. 3081–3096, Feb. 2019, doi: 10.1007/S12649-019-00626-9.

[52] N. Ghafoori, M. Najimi, and B. Radke, "Natural Pozzolan-based geopolymers for sustainable construction," *Environ. Earth Sci. 2016 7514*, vol. 75, no. 14, pp. 1–16, Jul. 2016, doi: 10.1007/S12665-016-5898-5.

[53] R. Robayo-Salazar, C. Jesús, R. Mejía de Gutiérrez, and F. Pacheco-Torgal, "Alkali-activated

binary mortar based on natural volcanic pozzolan for repair applications," *J. Build. Eng.*, vol. 25, Sep. 2019, doi: 10.1016/j.jobe.2019.100785.

[54]   K. Behfarnia and M. Rostami, "Mechanical Properties and Durability of Fiber Reinforced Alkali Activated Slag Concrete," *J. Mater. Civ. Eng.*, vol. 29, no. 12, p. 04017231, Dec. 2017, doi: 10.1061/(asce)mt.1943-5533.0002073.

[55]   T. Alomayri, "The microstructural and mechanical properties of geopolymer composites containing glass microfibres," *Ceram. Int.*, vol. 43, no. 5, pp. 4576–4582, Apr. 2017, doi: 10.1016/j.ceramint.2016.12.118.

[56]   V. M. C. F. Cunha, J. A. O. Barros, and J. Sena-Cruz, "Modelling the influence of age of steel fibre reinforced self-compacting concrete on its compressive behaviour," *Mater. Struct. Constr.*, vol. 41, no. 3, pp. 465–478, Apr. 2007, doi: 10.1617/S11527-007-9259-4.

[57]   M. D. E. Teixeira, J. A. O. Barros, V. M. C. F. Cunha, B. N. Moraes-Neto, and A. Ventura-Gouveia, "Numerical simulation of the punching shear behaviour of self-compacting fibre reinforced flat slabs," *Constr. Build. Mater.*, vol. 74, pp. 25–36, Jan. 2015, doi: 10.1016/J.CONBUILDMAT.2014.10.003.

[58]   V. M. C. F. Cunha, J. A. O. Barros, and J. M. Sena-Cruz, "An integrated approach for modelling the tensile behaviour of steel fibre reinforced self-compacting concrete," *Cem. Concr. Res.*, vol. 41, no. 1, pp. 64–76, May 2010, doi: 10.1016/J.CEMCONRES.2010.09.007.

[59]   S. A. Bernal, R. M. De Gutierrez, and E. D. Rodríguez, "Alkali-activated materials : cementing a sustainable future," *Ing. y Compet.*, vol. 15, no. 2, pp. 211–223, 2013.

[60]   F. Puertas, T. Amat, A. Fernández-Jiménez, and T. Vázquez, "Mechanical and durable behaviour of alkaline cement mortars reinforced with polypropylene fibres," *Cem. Concr. Res.*, vol. 33, no. 12, pp. 2031–2036, Dec. 2003, doi: 10.1016/S0008-8846(03)00222-9.

[61]   T. Alomayri, F. U. A. Shaikh, and I. M. Low, "Characterisation of cotton fibre-reinforced geopolymer composites," *Compos. Part B Eng.*, vol. 50, pp. 1–6, Jul. 2013, doi: 10.1016/j.compositesb.2013.01.013.

[62]   A. Koenig *et al.*, "Flexural behaviour of steel and macro-PP fibre reinforced concretes based on alkali-activated binders," *Constr. Build. Mater.*, vol. 211, pp. 583–593, Jun. 2019, doi: 10.1016/j.conbuildmat.2019.03.227.

[63]   M. F. Zawrah, R. A. Gado, N. Feltin, S. Ducourtieux, and L. Devoille, "Recycling and utilization assessment of waste fired clay bricks (Grog) with granulated blast-furnace slag for geopolymer production," *Process Saf. Environ. Prot.*, vol. 103, pp. 237–251, Sep. 2016, doi: 10.1016/j.psep.2016.08.001.

[64]   G. Kovalchuk, A. Fernández-Jiménez, and A. Palomo, "Alkali-activated fly ash: Effect of thermal curing conditions on mechanical and microstructural development - Part II," *Fuel*, vol. 86, no. 3. Elsevier, pp. 315–322, Feb. 01, 2007, doi: 10.1016/j.fuel.2006.07.010.

[65]   N. Cristelo, A. Fernández-Jiménez, C. Vieira, T. Miranda, and Á. Palomo, "Stabilisation of construction and demolition waste with a high fines content using alkali activated fly ash," *Constr. Build. Mater.*, vol. 170, pp. 26–39, May 2018, doi: 10.1016/J.CONBUILDMAT.2018.03.057.

[66]   A. P. Willner, S. Pawlig, H. J. Massonne, and F. Hervé, "Metamorphic evolution of spessartine

quartzites (coticules) in the high-pressure, low-temperature complex at Bahia Mansa, Coastal Cordillera of South-Central Chile," *Canadian Mineralogist*, Dec. 01, 2001. .

[67]   K. Somna, C. Jaturapitakkul, P. Kajitvichyanukul, and P. Chindaprasirt, "NaOH-activated ground fly ash geopolymer cured at ambient temperature," *Fuel*, vol. 90, no. 6, pp. 2118–2124, Jun. 2011, doi: 10.1016/j.fuel.2011.01.018.

[68]   G. F. Huseien, A. R. M. Sam, K. W. Shah, M. A. Asaad, M. M. Tahir, and J. Mirza, "Properties of ceramic tile waste based alkali-activated mortars incorporating GBFS and fly ash," *Constr. Build. Mater.*, vol. 214, pp. 355–368, Jul. 2019, doi: 10.1016/j.conbuildmat.2019.04.154.

[69]   Z. Y. Qu, Q. Yu, Y. D. Ji, F. Gauvin, and I. K. Voets, "Mitigating shrinkage of alkali activated slag with biofilm," *Cem. Concr. Res.*, vol. 138, p. 106234, Dec. 2020, doi: 10.1016/j.cemconres.2020.106234.

Mechanical and thermal performance analysis of alkali-activated ceramic waste-based panel

The developed alkali-activated cement could be used for various applications in the construction industry. In this section, the feasibility of using the optimal mixture defined in the previous chapter for the manufacture of two non-structural panels with different conventional insulating materials, either extruded polystyrene or cork cardboard, was analyzed. Functional tests related to mechanical and thermal behavior were performed for each solution.

Development of half-sandwich panels with alkali-activated ceramic and slag wastes: Mechanical and thermal characterization

Norma Gaibor [a*]; Dinis Leitão [b]; Tiago Miranda [c]; Nuno Cristelo [d]; Eduardo N.B. Pereira [c]; Ana Briga-Sá [d]; Vítor M.C.F. Cunha [c]

a. School of Engineering of the University of Minho, Azurém Campus, 4800-058, Guimarães, Portugal

b. CTAC, Department of Civil Engineering, University of Minho, 4800-058, Guimarães, Portugal

c. ISISE, Institute for Science and Innovation for Bio-Sustainability (IB-S), Department of Civil Engineering, University of Minho, 4800-058, Guimarães, Portugal

d. CQ-VR, Centro de Química - Vila Real, Department of Engineering, University of Trás-os-Montes e Alto Douro, 5001-801, Vila Real, Portugal

*Corresponding author: normygaibor@gmail.com

ABSTRACT

This paper presents the development of two solutions for sandwich panels, composed of a slender layer formed by an alkali-activated composite, based on ceramic waste and ladle slag (AAc), and a thicker insulation layer, formed by extruded polystyrene (panel named, AP_{XPS}) foam or expanded cork agglomerate (panel named, AP_{ICB}). The AAc combined ceramic waste from clay bricks and roof tiles (75%) with ladle furnace slag (25%), activated with sodium silicate. The AAc layer was further reinforced with polyacrylonitrile fibers (1% content). The mechanical behavior was assessed by uniaxial compressive strength (AAc pastes), shear bond strength between the layers, pull-off strength of the layer between the AAc and the insulation material, and global flexural testing. The thermal performance was characterized by heat flux, inner surface temperatures, thermal transmission coefficient, thermal resistance, and thermal conductivity. The results of the mechanical behavior indicated clear differences between the two proposed solutions, for instance, although higher tensile bond strength values were reported for AP_{XPS} panels, a better interlayer bond strength of the AP_{ICB} was detected. Findings were similar for the shear bond strength where it was observed that the irregular surface of the ICB board, positively affected the adhesion with the AAc layer. Concerning the flexural strength, after the first peak load, the AP_{XPS} continued increasing the flexural load reaching a higher load-bearing capacity and energy absorption capacity compared to the AP_{ICB}. Also, thermal resistance values of 1.02 m²°C/W and 1.14 m²°C/W for AP_{ICB} and AP_{XPS} were estimated, respectively, showing promising results in comparison to currently available building materials.

Keywords: Half-sandwich panels; Industrial wastes; Alkali activation; Mechanical behavior; Thermal performance

6.1. INTRODUCTION

This work aims to contribute, based on an extensive experimental campaign, to the development and characterization of two distinct sandwich panel solutions, focusing on their thermal performance, but without minimizing the importance of their mechanical behavior. They are composed of a thin alkali-activated ceramic waste/slag cement layer and a thicker insulation layer made either from extruded polystyrene (XPS) foam or expanded cork agglomerate (ICB) as insulation materials. Ceramic waste (CW) and ladle furnace slag (LFS) were used in the present work, since they are two abundant industrial wastes and their production rate is increasing, especially in Europe. Thus, alternatives need to be found for these wastes, hence avoiding their landfilling, and promoting a potential circular economy model. The use of alkali-activated cement (AAc) seeks to achieve a low-carbon environmentally friendly solution while having a similar or even better mechanical performance to ordinary Portland cement (OPC) composites. Sodium silicate solution (Na_2SiO_3) was used as the activator, the thin alkali-activated ceramic layer was reinforced with polyacrylonitrile (PAN) fibers (1% content) and cured at ambient temperature. The ambient-temperature curing of the developed AAc contributed to increasing its eco-friendliness. The uniaxial compressive strength of the AAc, the direct shear behavior between the layers, the pull-off strength of the interfacial layer between the AAc and the insulation material, the flexural behavior of the panel, and the thermal parameters, such as heat fluxes, inner surface temperatures, thermal transmission coefficient, thermal resistance, and thermal conductivity, were measured and analyzed. Subsequently, a thorough literature review is presented and critically discussed in order to highlight the novelty of this work.

The cement and concrete industry, as a whole, may be responsible for as much as 10% of global anthropogenic CO_2 emissions [1], [2], [3]. Therefore, nowadays the development of sustainable construction and building materials with a lowered environmental footprint over both manufacturing and operational stages is a key point in the global housing and construction industry. Alkali-activated materials are seen as promising candidates for partially replacing OPC, as their production allows up to 70% reduction in greenhouse gas emissions [4], but also due to its remarkable mechanical and durability characteristics [5].

Globally, in 2017, the generation of ceramic wastes (CW) registered about 25.75 million tons, based on that 1.9 kg of waste is produced per 1 square meter of ceramic [6]. Where a significant number of

ceramic wastes corresponds to ceramic manufacture and another important part comes from the demolition and construction wastes, representing about 30% [7] and 45% [8], respectively. Even so, it is expected to increase due to the rapid growth in worldwide demand. Research aiming at the reuse of industrial waste is highly focused on cementitious materials, being a useful way to help in the conservation of natural resources and reduce environmental impacts. In terms of alkali activation, CW presents very favorable physical and chemical properties (most notably the amorphization degree and the aluminosilicate content) [9], [10].

Ladle furnace slag (LFS) has been also incorporated in the present work as a complementary precursor, as an important source of calcium and silicon oxide and alumina [11], resulting in a cementitious calcium-silicate hydrate (C–S–H) or calcium aluminum silicate hydrate (C-A-S-H) promoting the enhancement of the mechanical properties of the matrix [12].

In general, several works have been conducted on studying the development of sustainable alkali-activated building materials using industrial ceramic wastes [13], [14], [15] and the incorporation of different types of slag mainly in civil engineering, [16], [17], [18]. But research about the combination of those two industrial wastes in alkali activation systems is still scarce, the available findings are presented in Table 6-1. Moreover, information concerning the feasibility of the PAN fiber reinforcement of AAc is very limited, to the authors' knowledge a couple of works on this topic are available [19], [20].

Table 6-1 Alkali-activated materials based on ceramic wastes (CW) and slag (S)

Ceramic waste type	Precursor (wt. ratio), CW:S	Alkali activator	Compressive strength, 28 days, MPa	Curing conditions	Reference
Tile waste	50:50 60:40 70:30	NaOH (4M)[2]: Na$_2$SiO$_3$, mass % 0.75	Up to ~ 73 Up to ~ 68 Up to ~ 32	ambient T, 27°C	[21]
	70:30	NaOH (2M)[2]: Na2SiO3, mass % 0.75	Up to ~ 34	Cured in air	[22]
	50:50 60:40 70:30	NaOH (4M)[2]: Na$_2$SiO$_3$	Up to ~ 73 Up to ~ 68 Up to ~ 32	ambient T, 25°C	[23]
Red clay brick waste from the brick-making plant	20:80 40:60 60:40 80:20	Na$_2$SiO$_3$ + Na$_2$CO$_3$ (SiO2/Na2O, sílica modulus of 1.5)	Up to ~ 100 Up to ~ 96 Up to ~ 70 Up to ~ 40	room T, or steam curing	[24]

160

Table 6.1. (*continued*) Alkali-activated materials based on ceramic wastes (CW) and slag (S)

Ceramic waste type	Precursor (wt. ratio), CW:S	Alkali activator	Compressive strength, 28 days, MPa	Curing conditions	Reference
Waste brick powder	100-50[1]	NaOH (10M)[2] + Na₂SiO₃	Ranged from 24 to 93 MPa.	ambient T, 25°C	[8]
Ceramic waste and red clay brick waste	10:90	Na₂SiO₃ + Na₂CO₃	Up to ∼ 80 Up to ∼ 83	37 ± 2 °C for 24 h, then tap water at 23 ± 2 °C	[25]
Ceramic waste from CDW	75:25 50:50 25:75	NaOH (8M)[2] [SH] or Na₂SiO₃ [SS]	[SH]; [SS] ∼ 18; ∼ 50 ∼ 15; ∼ 50 ∼ 5; ∼ 38	70 ± 2 °C for 24h, then ambient T, 21 ± 2 °C	[26]

[1] 0–50% at increments of 10% by volume; [2] molar concentration of alkaline solution; T: temperature

At the EU level, the building sector represents more than 40% of the total energy consumption [27], and half of that is utilized in space acclimatization and lost to the environment [28], [29]. Hence, having in mind the enhancement of the energy efficiency and decrease of the environmental impact of building operation, the importance of insulation materials for buildings and industrial facilities is growing [30]. Insulation materials are classified by their chemical or their physical structure as illustrated in Figure 6-1. In the European market, the dominant isolation materials are the inorganic fibrous materials (e.g., stone wool and glass wool) and organic foamy materials (e.g., expanded polystyrene, followed by extruded polystyrene and polyurethane). Each group represents about 60% and 30%, respectively, while all other materials accounted for less than 13%, the corkboard insulation included [27].

The extruded polystyrene (XPS) consists of polyester grains (polymerized polystyrol, 1.5–2%) into an extruder, with the addition of a blowing agent expanded polystyrene (air, 98–98.5%) [31]. XPS is characterized to have higher specific heat in comparison to expanded polystyrene (between 1.3 and 1.7 kJ/kg K). Moisture negatively affects the values of thermal conductivity. The biopersistence of the XPS as waste is lengthy, thus it cannot be disposed of as common demolition waste, and specialized industries are needed for the recycling process due to their easily flammable and burning releases dangerous gases into the atmosphere [32].

In contrast, the agglomerated cork is a material that comes from the bark of the cork oak tree (*Quercus Suber* L.) [33]. It is typically reaped from the Southern Mediterranean countries, where Portugal is the

main producer, holding about 1/3 of the total cork tree area and representing 50% of the worldwide production [34]. Cork is a common material used in the building sector due to its excellent thermal and acoustic performance, chemical stability, and durability [35]. Some of the main cork physical-mechanical properties are the thermal conductivity, density, and specific heat whose values are ranged from 0.037 to 0.050 W/m K, 110 to 170 kg/m³, to 1.5 and 1.7 kJ/kg K, respectively [36]. In terms of ecological features, it is a 100% natural product, therefore, easily recycled [37]. Tártaro et al. [30] concluded that it is the only insulation material present in the market with a negative carbon footprint, mainly because cork is a renewable raw material and biomass is used for its production.

Figure 6-1. Classification of the dominant insulating materials in the European Market, [31]
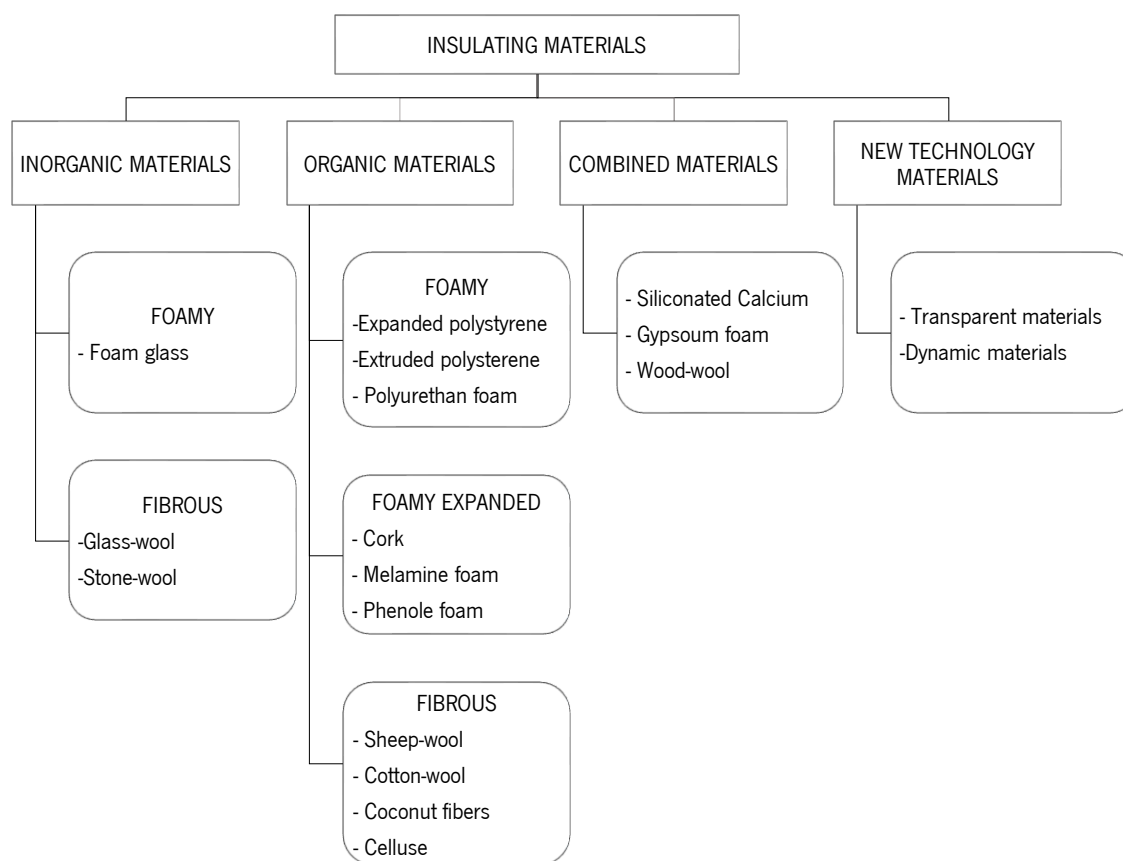
Limited research about using AAc based on industrial wastes for the development of sandwich panels was found. In all the cases presented below, fly ash and slag were the main precursors of the geopolymer binder. The available studies were focused on investigating the structural behavior and vibration characteristics [38], [39], flexural behavior, and failure mechanism [40], [41], [42] of fiber-reinforced geopolymer sandwich wall panels enabled with FRP connectors. In general, it was concluded that the obtained results can be validated with the development of a finite element model,

and further, experimental, and numerical investigations are needed to understand the general mechanical behavior of the developed panels and the connectors' behavior at different loading stages.

6.2. MATERIALS AND METHODS

This research campaign was carried out in three main stages, namely, i) the panels' production, ii) mechanical, and iii) thermal testing of specimens. The studied panels were composed of one layer (or skin) of alkali-activated ceramic waste/slag-based cement, as an element that will contribute to the stiffness and strength of the solution, bonded with either extruded polystyrene (XPS) foam or expanded cork agglomerate (ICB) boards mainly contributing to the insulation performance.

6.2.1. Materials

In the present work, wastes from Portuguese industries were used as precursors of the developed alkali-activated cement (AAc), specifically, ceramic wastes (CW) from a brick manufacturing company in Braga and ladle furnace slag (LFS) from melting scrap in an electric arc furnace from the ironwork company Megasa, placed in Maia. The matrix was reinforced with polyacrylonitrile (PAN) fibers with an 8 mm length and a diameter of 20 μm. For the reaction process, sodium silicate Na_2SiO_3 (SS) was used as an alkaline activator in the solution form. Water and polycarboxylate-based superplasticizers were also part of the blend. The detailed characterization of the physical, chemical, mechanical, as well microstructure, of the developed alkali-activated cement, can be found elsewhere [20], which corresponds to Chapter V of the present thesis.

In this study, two different thermo-insulating materials of 30 mm thicknesses each were analyzed, the rigid extruded polystyrene foam (XPS) board with a grooved surface finish on one face and expanded cork agglomerate (ICB), standardized according to EN 13164:2013 [44] and EN 13170:2013+A1:2015 [45], respectively. Based on their corresponding technical sheets, the main properties of the insulation materials used for this study are displayed in Table 6-2.

163

Table 6-2. Technical specification according to supplier datasheet for extruded polystyrene (XPS) [46] foam and expanded cork agglomerate (ICB) [47].

	XPS	ICB
Density (kg/m³)	30 to 33	+/- 110
Compressive strength (kPa) At 10% deformation	300	≥ 100
Tensile strength (kN/m²)	50 to 80	≥ 600
Thermal Conductivity (W/m.K)	0.033	0.039
Water permeability	High resistance to water absorption Satisfactory diffusion of water vapor	Water absorption Permeability to water vapor
Reaction to fire	Euroclass E	Euroclass E
Environmental Properties	100% recyclable 50 years durability Produced without CFC'S and HCFC'S GWP: 2.57 kg CO_2-Eq /1 m² XPS board, [48]	100% natural and fully recyclable Almost unlimited durability CO_2 sink (Carbon Negative)

6.2.2. Mixture and panels manufacture

A mixture composition of 75% CW + 25% LFS /SS-based, reinforced with 1% in volume of PAN fibers, and ambient cured (20°C and 60% HR ± 5%) [19] was used for the development of the present non-structural panels. Therefore, two sets of half-sandwich panels were manufactured, the first set comprised of the AAc + XPS and the second set constituted of the AAc + ICB. The composition of the rigid layer for each of the panels is displayed in Table 6-3.

For easier reference, the panels' nomenclature for the tests specimens is as follows: the first two letters "AP" are consistent all through the tests indicating the use of the developed AAc; the next letters denote the type of isolation, XPS, or ICB, thus the panels are identified as AP_{XPS} and AP_{ICB}, respectively. In the case of the AP_{XPS}, when the direction of the grooves was considered, the following designation was used when parallel ($AP_{XPS}^{\parallel}$) and when perpendicular ($AP_{XPS}^{\perp}$).

Table 6-3. Non-structural panels based on alkali-activated cement with high ceramic waste, composition in kg/m³

Precursor		Activator	SP	Water	PANf
CW	LFS	SS			
499.2	166.4	299.5	13.3	15.0	6.7

For the production of the alkali-activated cement (AAc), the mixing process was carried out in an industrial mixer with a capacity of 50 l. A low mixing speed, i.e., at a rate of 40 ± 3 rpm, was used.

Each production batch was at least 15 l to guarantee constant cement properties and control the standard variation on results of the tested specimens. Firstly, the dry components (CW and LFS) were mixed for three minutes. Then, the activator (SS) was added to the mixture, and it was stirred for two more minutes, followed by the incorporation of the water and SP for a further one min. As it is known, the order of fiber incorporation during the mixing is important to have a uniform fiber dispersion [49]. Consequently, in the last step, PAN fibers were gradually added to the fresh mix composition to avoid fiber balling and it was mixed for a further 3 min to ensure a homogeneous distribution of fibers. Thus, the blend was mixed for a total of 9 uninterrupted minutes. The workability of the fresh alkali-activated cement was verified using the slump flow test following the specifications of BS EN 12350-8 [50]. It was conducted by measuring the average horizontal free flow of the AAc in a perpendicular direction using a steel scale and no segregation was observed. The workability of AAc measured an average opened-out diameter from 100mm to 135 mm, Figure 6-2, (a), where it is noticed an improvement of about 1.5% in comparison with the reference sample in Gaibor et al. (2022), [20].

Finally, one layer of 10 mm of the fresh AAc was cast directly over the isolation materials, being 40 mm of the total height of the panel. Each specimen was framed with PVC profiles, in which dimensions varied according to the test performed, Figure 6-2 (b), either mechanical or thermal tests, as detailed in sections 6.3 and 6.4. Finally, specimens were vibrated for 2 min to release entrapped air. All panel samples were left for 28 days in a climatic chamber (Fitoclima 28000 EDTU) with constant environmental conditions of 20°C (±0.5°C) and under HR of 60% ± 5%. or until the tests were performed.

(a)

(b)

Figure 6-2. (a) Flowability test, (f) Preparation of isolation materials for casting

6.3. MECHANICAL TESTING PROCEDURES

6.3.1. Compressive strength

The uniaxial compressive strength (UCS) was assessed on four cubic specimens per batch, with nominal dimensions of $50 \times 50 \times 50 mm^3$. The tests were performed at 28 days, Figure 6-3. The UCS was determined by adapting the methodology proposed by ASTM C39/C39M-18 [51]. A monotonic displacement rate of 0.002 mm/min and an actuator of load capacity of 300 kN, Figure 6-3.

(a)
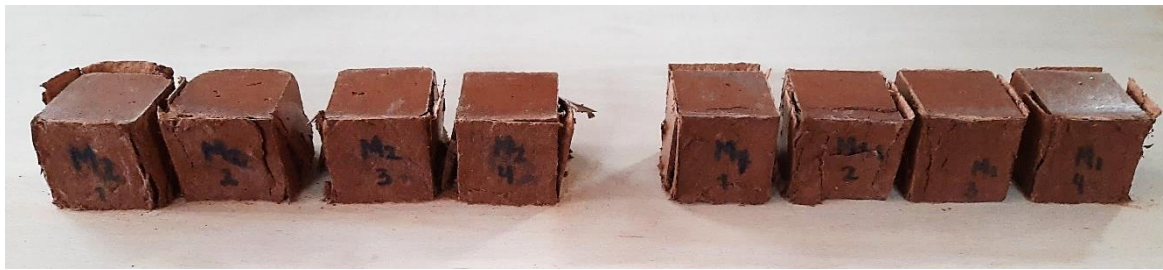
(b)

Figure 6-3. (a) Uniaxial Compressive Test performance; (b) Cubic specimens of $50 \times 50 \times 50mm^3$ after test execution.

6.3.2. Pull-off

In the present work, the bond strength performance of the AAc matrix with the isolation material, either the XPS or the ICB, was investigated using the pull-off tests. A sample was manufactured for each half sandwich panel (AP_{XPS} and AP_{ICB}) with dimensions of $600 \times 150 \times 40mm$ (length × width × height), and, as mentioned in section 6.2.2, the AAc panels were cast immediately after completing the mixing process. The PVC profiles of 40 mm in height were glued to the isolation material to ensure a final thickness of 10 mm of AAc and by the aid of a plain spatula the excess mixture was removed, and consequently, a smooth surface was achieved. Before the test, circular cuts perpendicular to the surface of 50 mm diameter and 10 mm deep were executed on the AAc face of the panel. A total of five equidistant circular cuts (with 50 mm of space in-between, equal to the diameter of each cylindrical sample) were made per specimen (Figure 6-4 (a)). A Sika Icosit® K 101 N epoxy resin was used to glue a metal disk (dolly) to the circular AAc surface of each cut (Figure 6-4 (b)). This step was

167

made 24 hours before the test to ensure that the cutting procedure would not induce significant damage that could decrease the interfacial strength.

The pull-off test (Figure 6-4 (c)) was carried out in a servo-hydraulic testing machine with a load capacity of 25 kN, where a tensile force was applied at a constant rate of 0.003 mm/s. To calculate the bond stress (MPa), the ratio between the maximum pull-off load (kN) and the loading area (mm^2) was considered. The average of five results per AAc/ XPS or ICB system is presented.

(a)

(b)

(c)
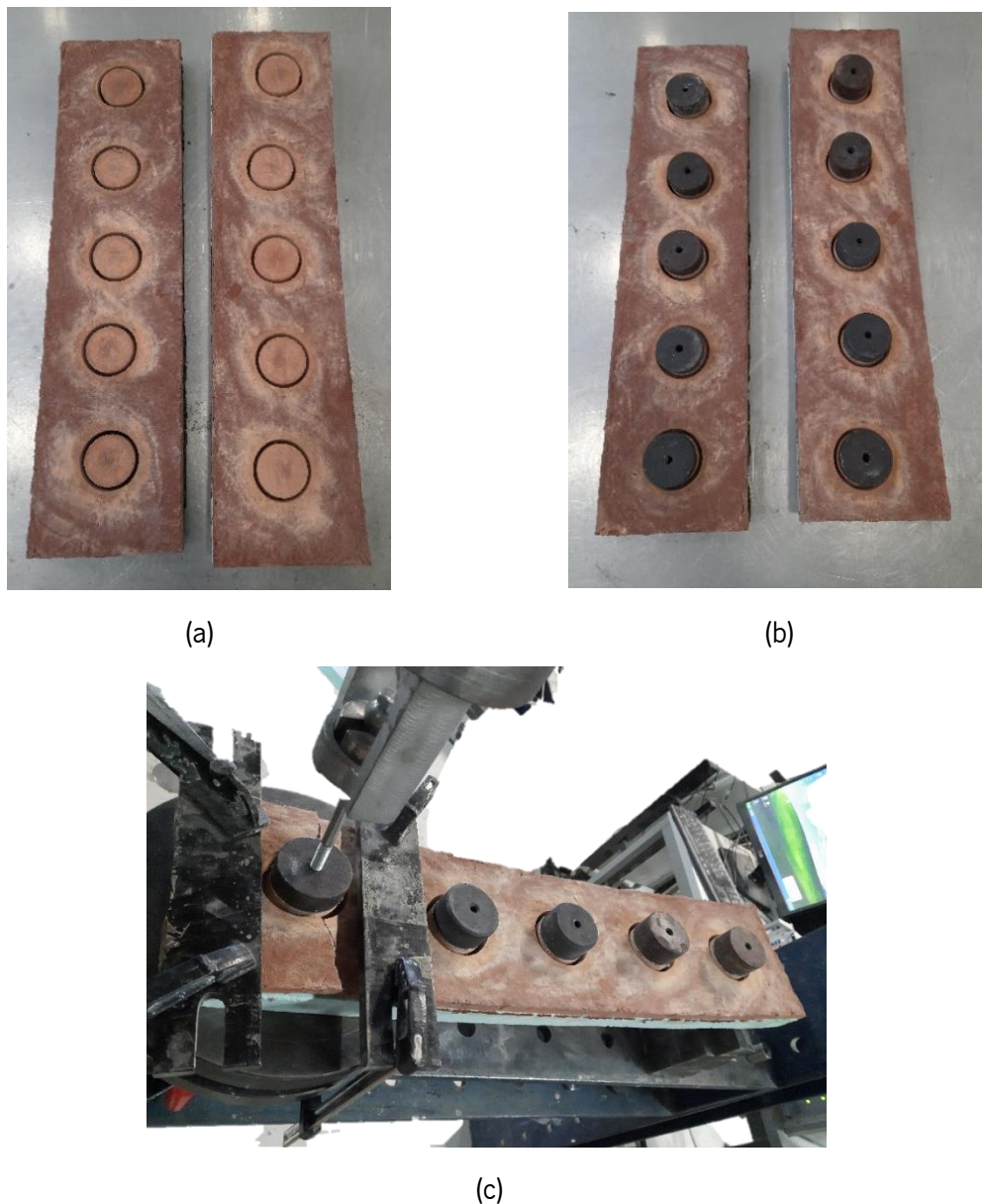
Figure 6-4. (a) sample preparation; (b) bond of the metal disk to the samples' outer surface; (c) Pull-off tests set-up, real apparatus

6.3.3. Direct shear

Four panels with $120 \times 120 \times 50$ mm were used for each composite solution, i.e., AAc + XPS or ICB, in order to assess the shear bond behavior (τ_s – s). The τ_s – s of the composite panel made with XPS were assessed through two distinct directions, i.e., along the parallel ($AP_{XPS}^{\parallel}$) and perpendicular ($AP_{XPS}^{\perp}$) direction of the grooves, Figure 6-5, (a). A total of 12 samples were tested for the three series. The load was applied on the lateral surface of the AAc and the insulation material was fixed to the testing rig. Servo-hydraulic testing with a load capacity of 25 kN was used. The tests were carried out under displacement control at a rate of 0.005 mm/s. Before starting the test, a plate of the same height for the AAc layer (20 mm) and another for the insulating material (30 mm) was placed along the specimen to distribute the load and avoid deformation of the XPS or ICB plate, respectively, and evaluate the bond between the two layers of the panel. Linear variable differential transformers (LVDTs) were also employed to measure the relative displacement between the two layers, hereinafter designated by slip (s). LVDTs were attached on small aluminum plates placed next to the actuator or on the AAc face layer of the specimen and the other two directly on the cross-section of the AAc on the opposite side, as shown in Figure 6-5 (b).

(a)   (b)
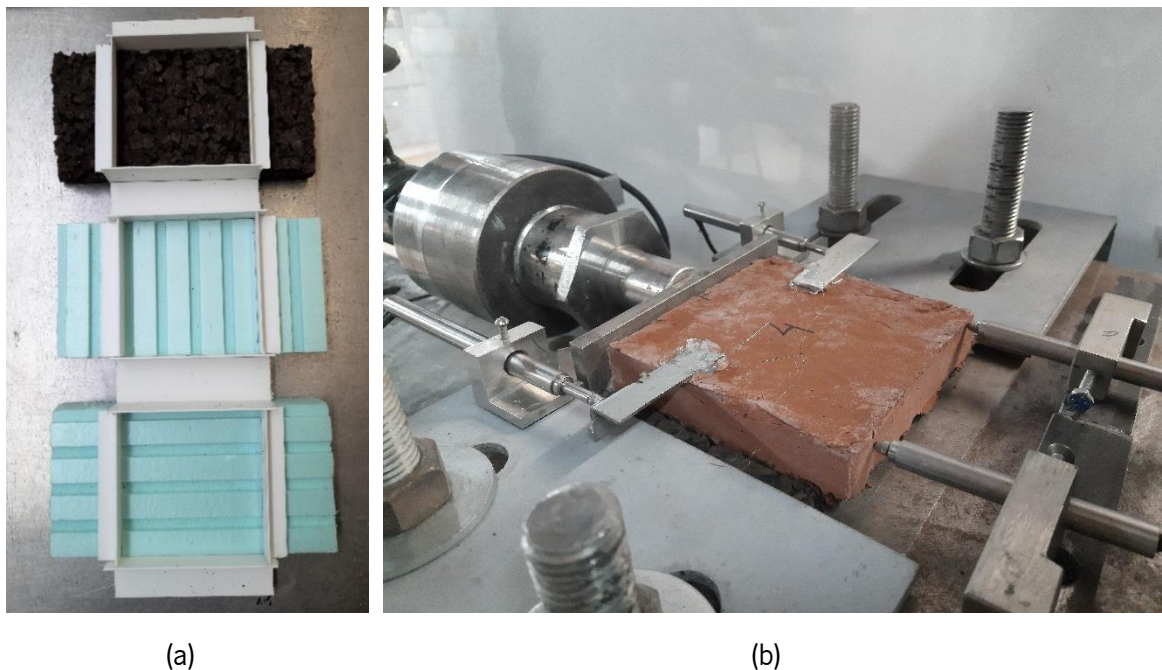
Figure 6-5. (a) Preparations samples before casting; (b) Set up for the direct shear test

6.3.4. Flexural behavior

The flexural behavior of the two studied panel systems (AP$_{XPS}$ and AP$_{ICB}$) was determined through a three-bending point test setup. For each series, four specimens of 600 mm × 150 mm × 40 mm were manufactured. A servo-hydraulic testing rig with a 100 kN load cell was used. The tests were performed under displacement control at a rate of 0.005 mm/s. The panels were tested with a 500 mm span. Prior to the test, low-density polyester putty was put on in the center of the specimen to hold a metallic roll to distribute the load, which was applied at the mid-span. The deflection at the mid-span was assessed by linear variable differential transformers (LVDTs), as shown in Figure 6-6.

(a)   (b)

Figure 6-6. Set-up of the three-point bending test on half-sandwich AAc panels with different thermo-insulating materials: (a) extruded polystyrene (XPS) and (b) Insulation corkboard (ICB)

6.4. THERMAL TESTING PROCEDURES AND ANALYSIS

6.4.1. Experimental Set-up

The evaluation of the thermal behavior was performed following the experimental procedure indicated in ISO 9869 (1994) [52]. Two half-sandwich panels of 600 × 500 × 40 mm (width × height × thickness) were manufactured, each comprising a 30 mm thick of XPS or ICB as thermal insulation material, and 10 mm of AAc, identified as AP$_{XPS}$ and AP$_{ICB}$, respectively. Additionally, for comparison purposes, a panel of alkali-activated cement based on ceramic wastes and slag only (ACP), with

equivalent layer thickness (10 mm) was fabricated, therefore a total of 3 panels were tested simultaneously.

This experimental test was carried out in a test room with dimensions of 4.0 m × 3.0 m × 2.5 m (length × width × height). The setup preparation includes first the replacement of the existing windows on the test room facade by an XPS board with dimensions of 3 cm × 76 cm × 64 cm (thickness × width × height) which framed and held the AP_{XPS}, the AP_{ICB}, and the AAc uninsulated panel. Next, the panels were positioned on the north-facing of the test room and were simultaneously analyzed, allowing to compare the thermal performance of the three different samples. The alkali-activated cement layer of the panels was placed towards the interior of the room Figure 6-7 (a) and consequently, the face of the insulation materials was exposed to the exterior environment Figure 6-7 (b). Then, each sample was meticulously sealed with the aid of polyurethane foam (PU) to avoid thermal bridges and non-insulated headers to ensure the absence of leaks and the experimental test reliability.

(a)   (b)

Figure 6-7. Thermal Experimental Setup of the half-sandwich panels, AAc + extruded polystyrene (AP_{XPS}), AAc + Insulation corkboard (AP_{ICB}), and the uninsulated panel (ACP): (a) sealed interior view; (b) sealed exterior view.

The equipment used for the experimental work includes three heat flux systems, each one comprised of a datalogger, two Hukseflux HFP01SC plate sensors (HF_1 and HF_2), and four inner surface temperature sensors (Tsi_{11}, Tsi_{12}, Ts_{21}, and Tsi_{22}), which were fixed on the inner surface of each panel to measure the heat flux (q_1 and q_2) and the inner surface temperatures, respectively, Figure 6-8.

Two Hanna Instrument HI 91610C Thermo hygrometers composed of a datalogger and a temperature probe were employed to ensure the measurement of the temperature inside (Ti) and outside (Te) the test room. The information acquired and stored by the different dataloggers using Softwares LoggerNet and PC208W3.3 for the heat flux systems and 92000-16 for the Thermo hygrometers was then transferred to a computer for further analysis and thermal parameters estimation.

According to ISO 9869 [52], the maintenance of a high thermal gradient between the interior and the exterior environments is needed to ensure a significant heat flux through the panels with the same signal during the measurement period. So, the test room was thermally controlled by a heating system that was successfully employed in previous studies [53], [54]. An interior temperature of 32°C ± 1°C throughout the measurement period was guaranteed as can be observed in the following sections. The experiment was carried out for 15 consecutive days in the early autumn, that is, the measurement period was from September 12th to the 28th. The parameters $q_{1(n)}$ and $q_{2(n)}$; $Tsi_{(n)}$; $Ti_{(n)}$ and $Te_{(n)}$ were continuously obtained in 10-minute intervals.
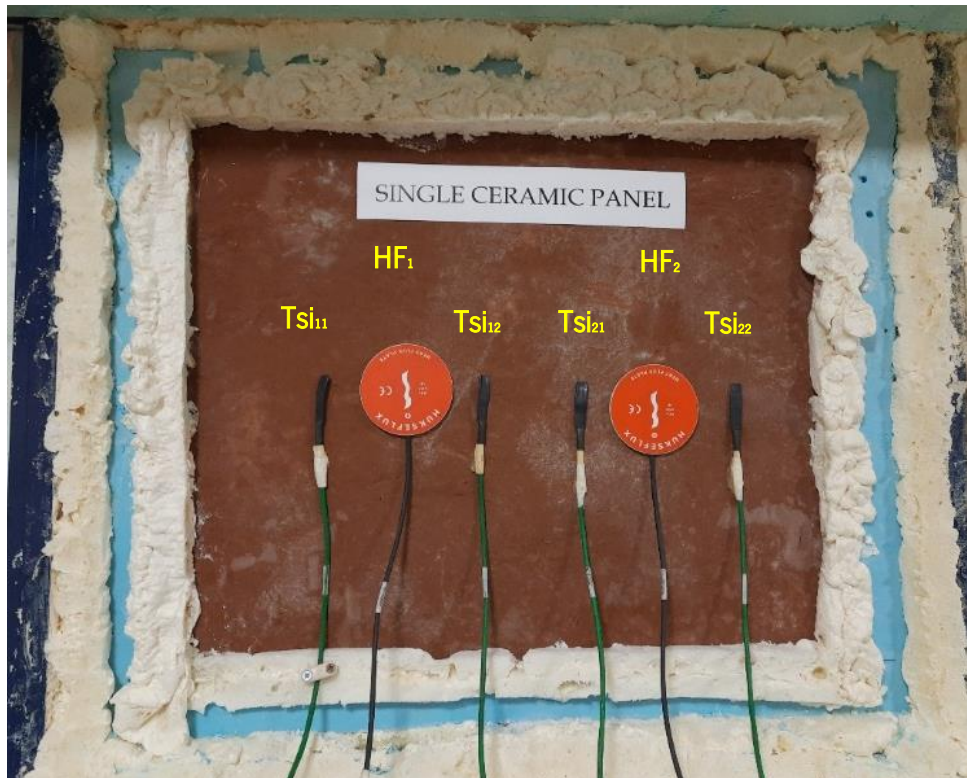
(a)

Figure 6-8. Utilized equipment for thermal performance analysis, Heat flux sensors, HF_1 and HF_2, and inner surface temperature sensors, Tsi_{11}, Tsi_{12}, Ts_{21}, and Tsi_{22}.

6.4.2. Analysis procedure

For a multi-layer panel, thermal properties can be represented by thermal transmission coefficient (U), defined as the heat flow that passes through a unit area of a complex component or inhomogeneous material due to a temperature gradient equal to 1 K [36]. For the assessment of U values for AP_{XPS}, AP_{ICB}, and ACP panels, guidelines of ISO 9869 [52] were followed. Thereby, some assumptions have been considered to characterize the thermal performance of the investigated panels using a heat flow meter. Firstly, assessing the temperature values on both sides of the sample and the average of the heat flow rate over an adequately long time provides an acceptable estimate of the steady-state conditions. The measurement period is defined based on the thermal inertia of the element under analysis, stating that for high inertia elements a measurement period of 14 days is required while for low thermal inertia ones a minimum of 72 hours is acceptable. Given that a measurement period of 15 days was considered for the panels with low thermal inertia, the steady-state conditions are guaranteed. Secondly, the thermal properties and the heat transfer coefficient of the studied materials do not vary through the range of temperature fluctuation that takes place over the experimental test. Thirdly, the difference in the amount of the stored heat in the building element or material is insignificant in comparison with the amount of heat going across it. Moreover, the use of interior (Ti) and exterior (Te) temperatures rather than surface temperatures is recommended to determine the thermal transmission coefficient (U). Finally, with the above-mentioned considerations, the calculation of U was based on the dynamic or average method applying **¡Error! No se encuentra el origen de la referencia.** from Table 6-4.

In this case, as two heat flux sensors (HF_1 and HF_2) with their corresponding pair of temperature sensors ($Tsi_{11(n)}$ and $Tsi_{12(n)}$; $Tsi_{21(n)}$ and $Tsi_{21(n)}$) were used on each studied element, two heat flux values ($q_{1(n)}$ and $q_{2(n)}$) were obtained. Therefore, applying **¡Error! No se encuentra el origen de la referencia.**, resulted in two U values ($U_{1(ntotal)}$ and $U_{2(ntotal)}$) where their average, as defined in **¡Error! No se encuentra el origen de la referencia.**, was designated as the final $U´$ value for each panel.

The inverse of the thermal transmission coefficient is the thermal resistance (R). Thus, the thermal resistance ($R´_{(ntotal)}$) of the proposed solutions was estimated using **¡Error! No se encuentra el origen de la referencia.**. Given that the ACP solution is a single panel, it is possible to estimate the thermal

resistance value of the ACP layer considering the external and the internal superficial thermal resistances, *Rse* and *Rsi*, respectively, as indicated in Equation 4.

Finally, by estimating the thermal resistance value for the ACP layer (R'_{ACP}) of 10 mm thickness, the theoretical value of the thermal conductivity (λ) can be computed by applying Equation 5. Thus, the conductibility of the alkali-activated cement based on ceramic wastes and slag can be estimated and compared with currently available materials such as ceramic, and other traditional construction materials.

Table 6-4. List of equations for the thermal performance assessment

	Parameter	Units	Equation	Description
Equation 1	Thermal transmission coefficient, *(U)*	W/m²°C	$U_{(ntotal)}$ $= \dfrac{\sum_{n=1}^{ntotal} q(n)}{\sum_{n=1}^{ntotal}(Ti(n) - Te(n))}$	$q_{(n)}$: heat flow across the sample for the instant n $Ti_{(n)}$: interior temperature $Te_{(n)}$: exterior temperature *ntotal*: total number of instants of registered data during the experiment Applied for each *HFi* data set
Equation 2	Thermal transmission coefficient of each panel *(U´)*	W/m²°C	$U'_{(ntotal)}$ $= \dfrac{U_{1(ntotal)} + U_{2(ntotal)}}{2}$	Use $U_{(ntotal)}$ values from Equation 1 Applied for *HF₁* and *HF₂* data set
Equation 3	Thermal resistance, *(R')* for each panel	(m²°C/W)	$R'_{(ntotal)}$ $= \dfrac{1}{U'_{(ntotal)}}$	Use $U'_{(ntotal)}$ value from Equation 2
Equation 4	Thermal resistance of the ACP layer, *(R´_{ACP})*	(m²°C/W)	$R'_{(ACP)}$ $= R'_{(ntotal)} - R_{se} - R_{si}$	Use $R'_{(ntotal)}$ value from Equation 3 R_{se}: 0.04 m²°C/W, [55] R_{si}: 0.13 m²°C/W, [55] R'_{ACP} is estimated for the ACP layer
Equation 5	Thermal conductivity (λ)	(W/m°C)	$\lambda_{ACP} = \dfrac{e_{ACP}}{R'_{ACP}}$	e_{ACP}: thickness of the ACP R_{ACP}: ACP thermal resistance from Equation 4

6.5. RESULTS AND DISCUSSION

6.5.1. Mechanical behavior

In this section, the experimental results of the two proposed half-sandwich panels, AP_{XPS} and AP_{ICB}, are presented and analyzed. The compressive strength value outcome of the AAc consisted of the average of all sample measurements resulting in 37.23 MPa (CoV 10.61%) at 28 days of curing.

On the other hand, the nature and design of the insulating board used for each building solution must be considered when interpreting the results. For instance, the grooved XPS insulation board used is a rigid foam material. In contrast, the ICB is an all-natural material acquired by expanding the cork granulates by steam-heating them. This feature makes the ICB panel has an irregular surface.

6.5.1.1. Pull-off tests

The tensile bond strength between the AAc and the insulation layer was determined based on five pull-off tests, Table 6-5. Figure 6-9 shows the force-displacement curves for each composite panel. A relatively high scatter of the responses was observed for AP_{XPS}, this could be ascribed to the non-uniform distribution of the grooves within the circular area where the test was performed, Figure 6-10 (a). The highest tensile bond strength values were reported for AP_{XPS} panels, which were about 80% higher than for AP_{ICB}. The values for the latter can be regarded as the tensile strength of the cork particle board itself due to the observed failure mechanism since two different types of failures were observed for the panels with AP_{XPS} and AP_{ICB}. In the first, for the AP_{XPS} panels, it was observed the debonding at the interface between the AAc and the insulation layer, Figure 6-10 (a). The second type of failure occurred outside the interface region, i.e., occurred within the bulk of the cork particleboard layer, indicating that the tensile bond strength between the AAc and the ICB exceeds the tensile strength of the ICB itself, revealing a weak internal structure of ICB, Figure 6-10 (b). The latter can be related to the high porosity of the cork particle board used.

Table 6-5. Basic mechanical properties of the developed panels

Panel ID		Shear bond strength [kPa], (CoV, %)	Interfacial tensile strength [kPa], (CoV, %)
AP$_{XPS}$	$AP_{XPS}^{\perp}$	88.97 (13.75)	86.42 (29.84)
	$AP_{XPS}^{\parallel}$	79.32 (8.61)	
AP$_{ICB}$		46.45 (1.05)	52.42 (15.18)
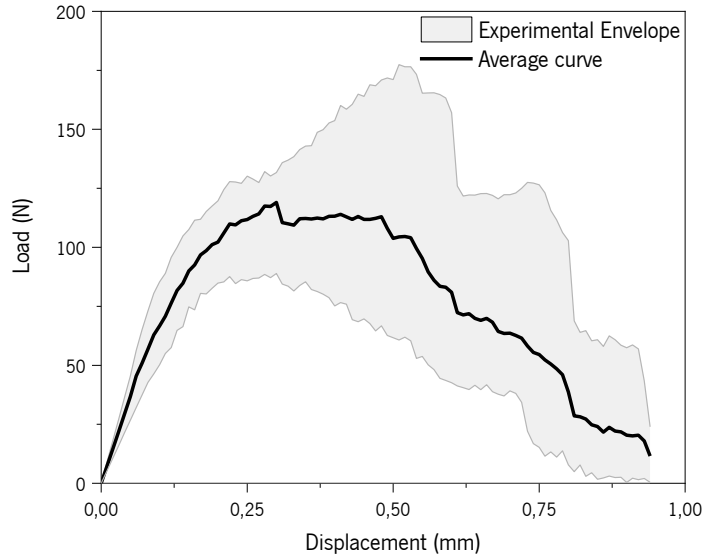
(a)
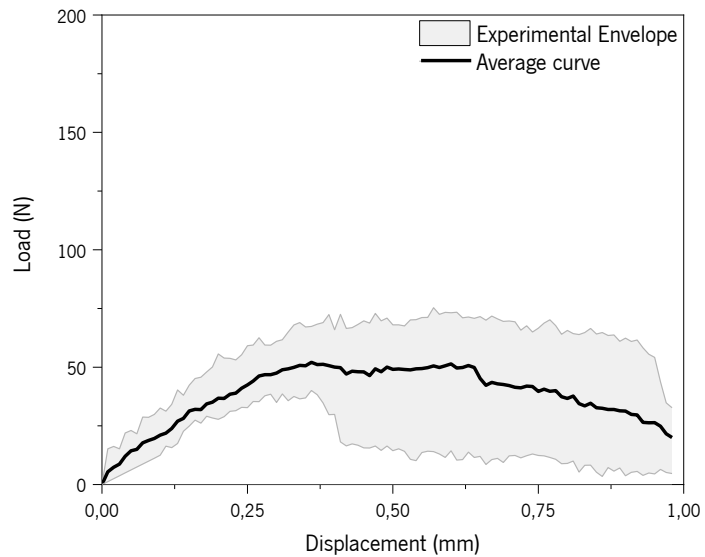
(b)

Figure 6-9. Force-displacement graph based on test results (a) AP$_{XPS}$ and (b) AP$_{ICB}$

(a)

(b)

Figure 6-10. Failure modes obtained on the pull-off tests (a) AP$_{XPS}$ and (b) AP$_{ICB}$

6.5.1.2. Direct shear test

The average shear bond strength (τ_s) values of the AP$_{XPS}$ and the AP$_{ICB}$ were computed based on the maximum load and area of the interfacial surface. In general, τ_s of the AP$_{XPS}$ series, loaded parallel ($AP^{\parallel}_{XPS}$) or perpendicular ($AP^{\perp}_{XPS}$) to the direction of the grooves, were higher than the AP$_{ICB}$ tested specimens, which represented an increase of about 90% and 70%, respectively, Table 6-5. Moreover, as expected, the bond strength obtained for the $AP^{\perp}_{XPS}$ was slightly higher ($\sim$12%) than the $AP^{\parallel}_{XPS}$. The load-slip average curve for each type of the investigated half-sandwich panel is depicted in Figure 6-11. Figure 6-12 shows a collection of photos taken during and after testing all specimen typologies.

In a general view, when the load was applied in the perpendicular direction to the grooves of the XPS, it was distinguished as an initial linear branch followed by a nonlinear section up to the peak load,

Figure 6-11 (a). The test was stopped when the load remained more or less constant at an average slip of 8.5 mm, and a displacement of the AAc layer of about 2 mm was observed, Figure 6-12 (a). In this case, the perpendicular grooves of the XPS interlocked the top layer of the panel mitigating its splitting. On the other hand, when the load was applied in the parallel direction of the grooves of the XPS, a first linear phase which is most probably due to the auto-alignment of the load line is also exhibited. However, the peak load occurred at the average relative displacement of ~ 3 mm, Figure 6-11 (b), and it was followed by a short parallel displacement and a slight softening branch attributed to the unstable debonding process at the interfacial layer. The load was removed when the skin layer of the $AP_{XPS}^{\parallel}$ slipped approximately 5 mm, Figure 6-12 (b).

Specimens with ICB isolation layer did not show a peak, but a continuous deformation with increasing resistance to the point that the resistance became constant was registered instead, Figure 6-11 (b). Besides, the AP_{ICB} panel layers did not debond due to chemical bond/friction between the ICB and the AAc, when the test was finished and the load was removed, the AAc layer returned to its original position Figure 6-12 (c). This also confirms that the surface roughness of the insulation board provides a better bond [56] between the ICB and the AAc, opposite to the AP_{XPS} shear behavior. Nevertheless, during casting there is a possibility that may be trapped air between the XPS and the AAc interface, causing the reduction of the bond and consequently the overall shear flow strength.

Direct shear results are in accordance with Pull-off findings, Table 6-5, i.e., in general, the values acquired for the behavior of the AP_{XPS} almost double the results of the AP_{ICB}.
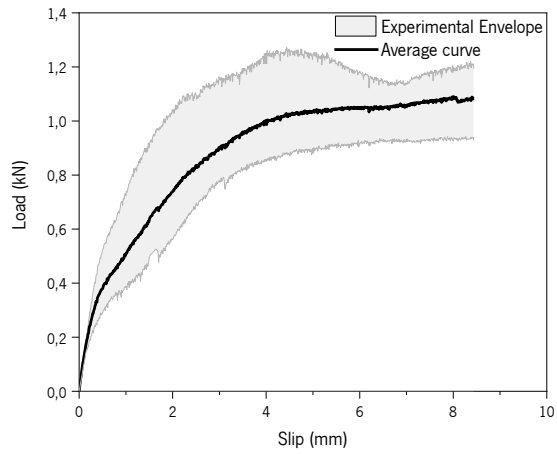
(a)
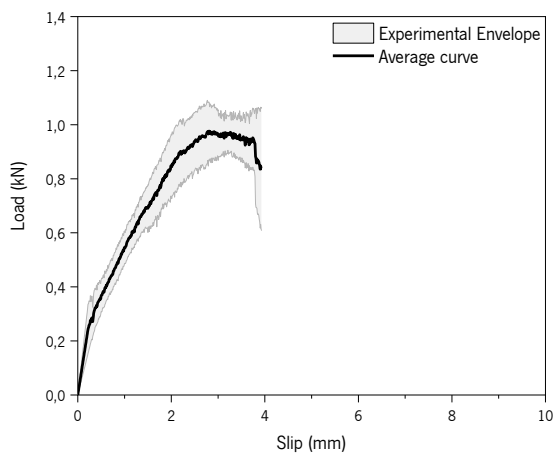
(b)
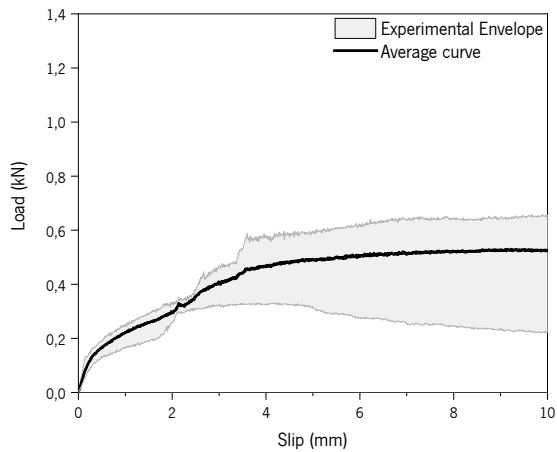
(c)

Figure 6-11. Mechanical shear behavior of panels with (a) XPS parallel groves ($AP_{XPS}^{\parallel}$); (b) XPS perpendicular groves ($AP_{XPS}^{\perp}$); and (a) ICB

(a)

(a)
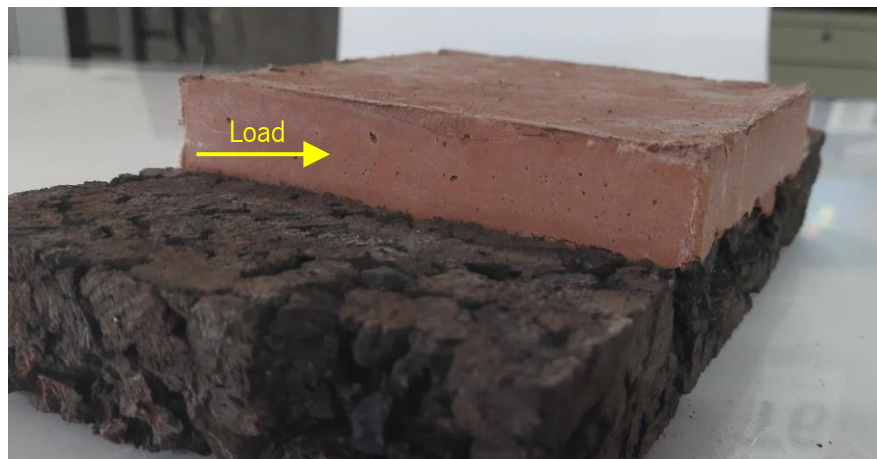
(c)

Figure 6-12. Specimens after direct shear tests (a) AP$_{XPS}$ with XPS perpendicular groves ($AP_{XPS}^{\perp}$); (b) AP$_{XPS}$ with XPS parallel groves ($AP_{XPS}^{\parallel}$); (c) AP$_{ICB}$

6.5.1.3. Flexural behavior

Figure 6-14 displays the plotted load-deflection curves and the failure mode of the two types of half-sandwich panels are shown in Figure 6-15. In general, the two tested half-sandwich panels exhibited a different flexural behavior, which can be ascribed to distinct mechanical properties of the insulation materials, but mostly due to the distinct equivalent height of the AAc reinforced layer of the panel's cross-section that will consequently translate on a higher inertia moment.

Regarding the flexural behavior of the AP_{XPS}, in the beginning, the skin layer (AAc) and the isolation material (XPS) act in a linear-elastic mode until the first peak. Since the cross-section flexural stiffness of the panel with XPS is considerably higher than the one from ICB (see Figure 6-13) this first peak which is quite similar in both panels should be related to the interfacial shear bond stress between the AAc reinforced layer and the insulation material. Afterward, a higher load-carrying capacity after first cracking is registered, which is categorized as deflection-hardening, Figure 6-14 (a). Still, the emergence of sudden small drops in force along the curves is observed, it may be associated with the action of the PAN fibers of the AAc layer. In contrast, three phases were identified for the bending behavior of the AP_{ICB}. It starts with a linear ramp-up until the interfacial cracking point. In the second stage, a sharp softening branch after peak load was observed. Finally, the tension that was resisted by the AAc is transferred to the reinforcement, i.e., to the PAN fibers but also the ICB isolation material, Figure 6-14 (b). Eventually, the system fails when the fibers pull out is ended and the capacity of the ICB layer is exhausted.

The contrast between the flexural behavior of the two studied systems supports the hypothesis that the performance discrepancy between both panels is mainly due to differences in the cross-section of the AAc layer, as well to a lesser extent due to the isolation material strength.

Concerning failure mode, in the case of AP_{XPS} panels, the formation of several shear cracks in the AAc layer was visible, while in XPS the most tensioned zone was inside the XPS groves.

(a)

(b)
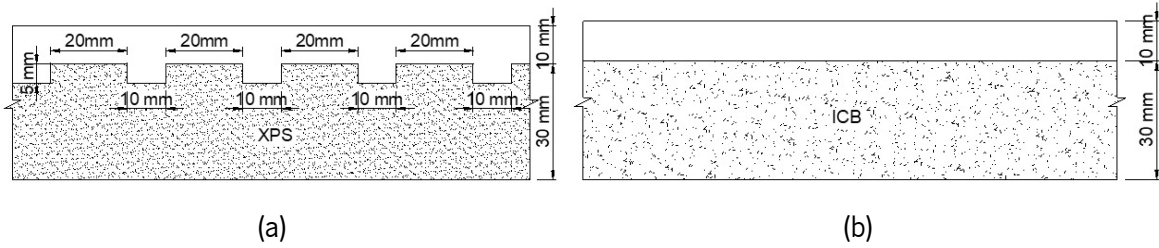
Figure 6-13. Vertical cross-section of semi-sandwich AAc panels with different thermo-insulating materials: (a) extruded polystyrene (AP$_{XPS}$) and (b) Insulation corkboard (AP$_{ICB}$)
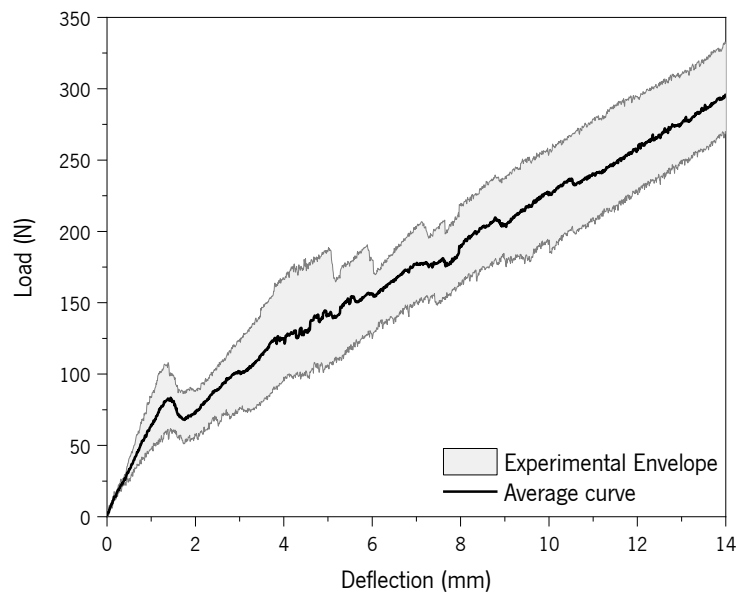
(a)
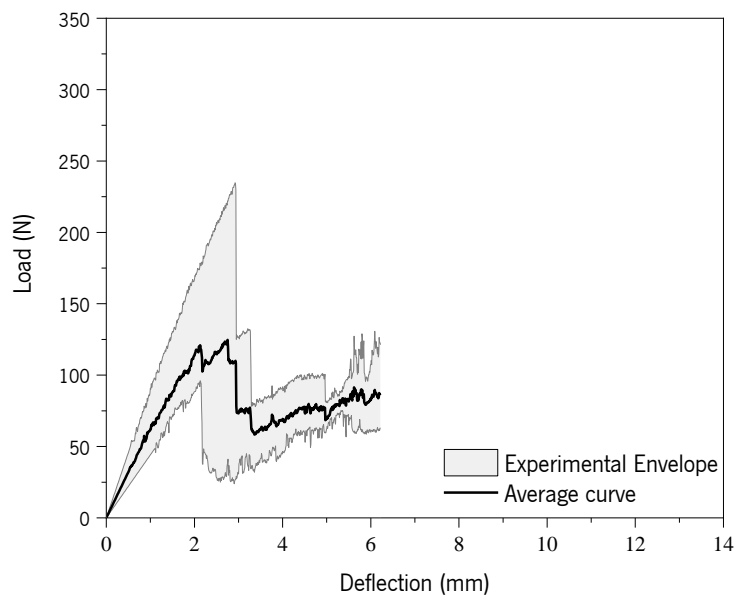
(b)

Figure 6-14. Load displacement curves under flexural loading for (a) AP$_{XPS}$; (b) AP$_{ICB}$, at 28 days of curing
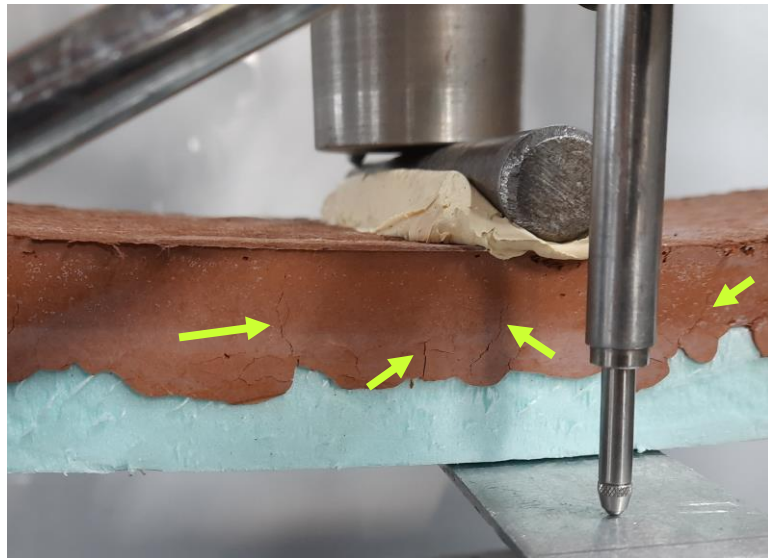
(a)

(b)

Figure 6-15. Failure types in the panels (a) AP$_{XPS;}$ (b) AP$_{ICB}$

6.5.2. Thermal performance

The temperature conditions and the thermal parameters of the AP$_{XPS}$, AP$_{ICB,}$ and ACP panels resulting from the experimental tests are presented in Table 6-6. As mentioned before, measured data was registered at a 10 min timing interval for fifteen days, therefore the mean values of the different variables recorded for each sample are displayed in Table 6-6 and will be discussed in the following sections.

Table 6-6. Experimental conditions and thermal parameters of ACP, AP_{ICB}, and AP_{XPS} panels

Panel ID	Ti (°C)	Te (°C)	Tsi (°C)	qi (W/m²)	$U'_{(total)}$ (W/m²°C)	$R'_{(total)}$ (m²°C/W)	R'_{ACP} (m²°C/W)	λ_{ACP} (W/m°C)
ACP			26.15	65.94	3.91	0.26	0.09	0.12
AP_{ICB}	32.04	15.37	30.14	16.64	0.98	1.02	-	-
AP_{XPS}			29.62	14.86	0.88	1.14	-	-

6.5.2.1. Heat flux

It can be observed from Figure 6-16 that during the measurement period, the test room indoor temperature (Ti) was nearly constant and always higher than the outdoor temperature (Te), which ensured the requirements specified in the ISO 9869 [52] regarding the maintenance of the heat flux signal, in this case occurring from the interior of the test room to the exterior environment. The Ti values stabilized at an average of 32.04°C, while Te fluctuated naturally since it is not possible to be controlled, recording 7.35°C and 24.52°C as the minimum and the maximum values, respectively. During the execution of the experimental test, a positive differential between Ti and Te was corroborated, and consequently, positive curves of $q_{1(n)}$ and $q_{2(n)}$ also resulted.

Regarding heat flux curves, higher values of $q_{1(n)}$ and $q_{2(n)}$ were observed for the non-insulated panel (ACP) compared to AP_{ICB} and AP_{XPS}, as expected, with significant peak variation related to diurnal and nocturnal periods. An average differential of about 1.43 W/m², 0.23 W/m² and 0.08 W/m² were registered between $q_{1(n)}$ and $q_{2(n)}$ for ACP, AP_{ICB}, and AP_{XPS}, respectively, demonstrating that the heat flux sensors HF_1 and HF_2 were correctly placed at points where a uniform composition of the analyzed panels is reflected. It was also noted that no significant difference existed between the heat flux values of AP_{ICB} and AP_{XPS} panels, since almost overlapping curves can be seen in Figure 6-16. Nevertheless, the heat flux curves of the AP_{ICB} sample showed slightly larger fluctuations that can be attributed to voids present in the expanded agglomerated cork insulation panel due to the nature of its composition, which also explains a higher average differential value between $q_{1(n)}$ and $q_{2(n)}$ in comparison to AP_{XPS}. Furthermore, it is also known that ICB is characterized by a higher thermal conductivity value compared to XPS, which confirms the differential verified in the heat flux curves. Besides, when comparing the reference panel (ACP) with the two other solutions, AP_{ICB} and AP_{XPS}, a reduction of 74.54% and 76.10% in the heat flux values were detected, respectively.
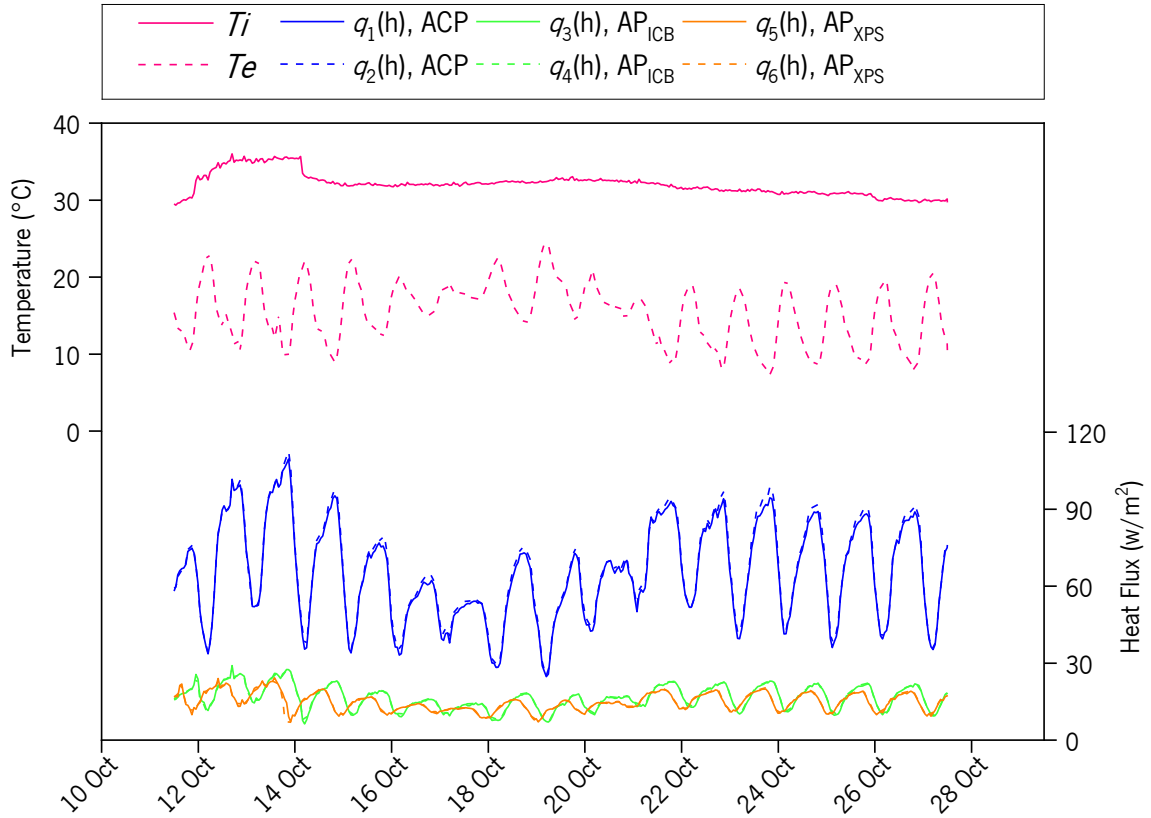
Figure 6-16. Indoor (Ti_n), outdoor (Te_n) temperatures, and heat flux ($qi_{(n)}$).

6.5.2.2. Inner surface temperatures

The inner surface temperature curves obtained by the $Tsi_{11(n)}$ and $Tsi_{21(n)}$ sensors, for each panel sample studied, are shown in Figure 6-17, while the average values are given in Table 6-6. The reference sample (ACP) recorded a mean value of 26.16°C, a minimum of 22.55°C, and a maximum of 30.76°C. Thus, concerning ACP, an increase of 15.44% and 13.51% in the mean surface temperatures was verified for AP_{ICB} and AP_{XPS}, respectively. In both cases, a minimum of around 26°C and a slightly higher maximum value for AP_{ICB} (33.67°C vs. 32.90°C) were registered. It is worth mentioning that the greater oscillation detected in the ACP curve is an evident thermal behavior in the absence of an insulation layer in this sample.

The present results are consistent with the previous section in terms of heat flux variation. A similar oscillation pattern can be evidenced in the three panels studied. Moreover, the inner surface temperature curves of AP_{ICB} and AP_{XPS} are also nearly overlaid, as was expected given the results obtained for the heat flux curves. For the same indoor and outdoor temperature conditions, higher surface temperature values are obtained for panel solutions with higher thermal resistance values.
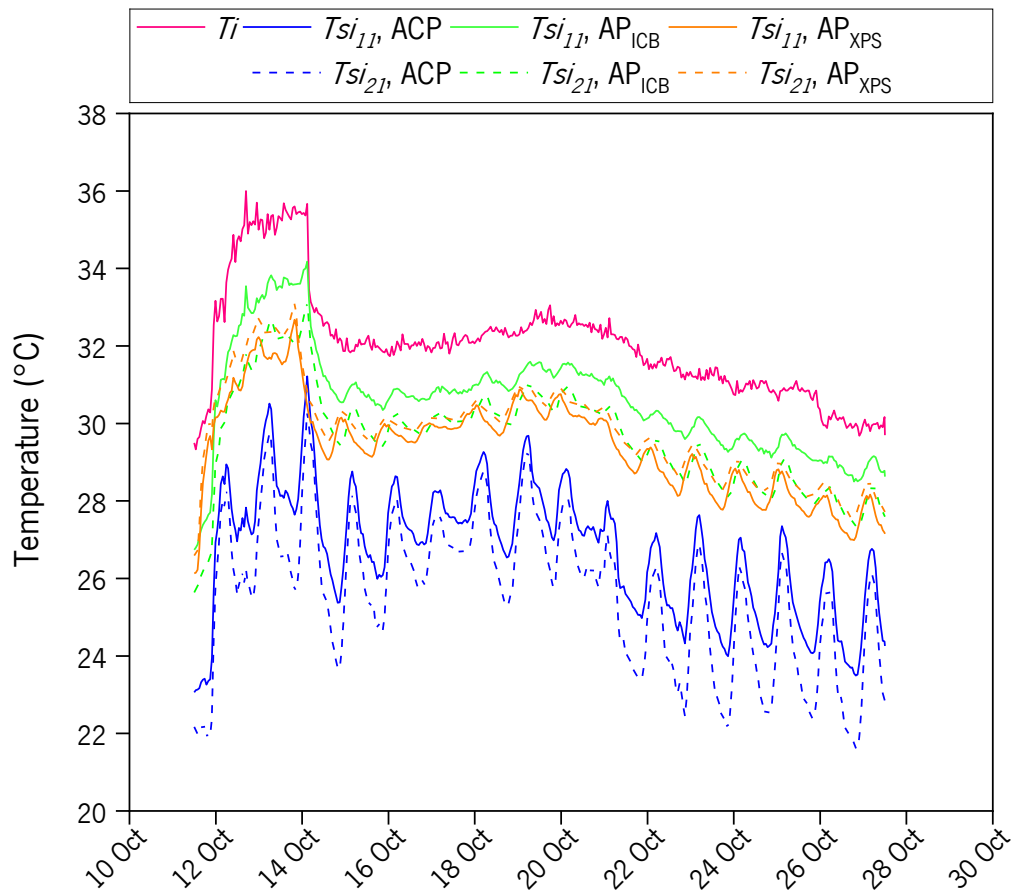
Figure 6-17. Interior ($Ti_{(n)}$) and inner surface temperatures ($Tsi_{(n)}$)

6.5.2.3. Thermal transmission coefficient

Considering that two heat flux sensors were used to define $q_{1(n)}$ and $q_{2(n)}$), it was also possible to estimate two heat transfer coefficients, $U_{1(ntotal)}$ and $U_{2(ntotal)}$, as illustrated in Figure 6-18. It is worth mentioning that $U_{(ntotal)}$ values were calculated five days after the start of the experimental test. In this way, the stabilization of the system is guaranteed. However, in the period from October 16 to 22, a slight depression can be observed in the heat transfer coefficient curves for the ACP sample. This can be explained by the fact that for the same period, shorter Te peaks were identified in Figure 6-16, as outdoor conditions cannot be controlled, the differential of temperature was altered and, consequently, heat fluxes were also affected. Since the other two panels, AP_{ICB} and AP_{XPS}, are composed of the thermal insulation layer, this change was not so perceptible.

Besides, the thermal transmission coefficient of each sample ($U'_{(ntotal)}$) resulted from the average of $U_{1(ntotal)}$ and $U_{2(ntotal)}$, Table 6-6. It can be seen that the reference sample (ACP) is characterized to have significantly higher $U'_{(ntotal)}$ values in comparison to AP_{ICB} and AP_{XPS}, where a decrease of 74.97% and 77.58% of the thermal transmission coefficient were found, respectively. In contrast, an increment of 11.67% on the $U'_{(ntotal)}$ of the AP_{ICB} was identified compared to AP_{XPS}, which was also expected given the higher density and the higher thermal conductivity of the expanded cork agglomerate board against the extruded polystyrene foam.

Additionally, the thermal resistance ($R'_{(ntotal)}$) of each studied panel was also computed (Table 6-6), which shows an approximately threefold increase in the value of $R'_{(ntotal)}$ for AP_{ICB} (1.02 m²°C/W) and AP_{XPS} (1.14 m²°C/W) with respect to ACP (0.26 m²°C/W). It evidenced an inverse ratio between the $U'_{(ntotal)}$ and $R'_{(ntotal)}$, where the ACP was demonstrated to have the lowest thermal resistance. Since the ACP is composed of a single layer of alkali-activated ceramic wastes and slag, these results were expected as mentioned in the previous sections. Regarding the two insulated solutions, the AP_{XPS} panel exhibited a slightly higher resistance, about 12%, than the $AP_{ICB,}$ which is in line with the $U_{(ntotal)}$ results. Furthermore, comparing the calculated thermal resistance values of the three studied panels with the available values for simple masonry walls with 10 - 11 cm of thickness [57], it can be determined that the reference panel (ACP) exhibited values of the same magnitude, being even higher in the most of the cases. Besides, the proposed insulated panels, AP_{ICB} and AP_{XPS}, showed a considerably higher thermal resistance, i.e., about 2.7 and 3.2 times higher than the common hollow ceramic brick wall and the lightweight concrete blocks, respectively. In addition, considering a conventional solution of ceramic solid brick, significantly higher $R'_{(ntotal)}$ values were achieved for the AP_{ICB} and AP_{XPS} panels, resulting in approximately 6.8 and 7.8 times higher, for each case. Thus, an improvement in the thermal performance can be achieved for the two insulated panels when compared to conventional wall solutions, as displayed in Table 6-7. Moreover, considering Equation 4, the thermal resistance of the ACP layer was determined, obtaining a R'_{ACP} value of 0.09 m²°C/W, which allowed calculating λ_{ACP} as described below.

The thermal conductivity (λ) of a material can be quantified by knowing its thermal transmission coefficient. Therefore, a theoretical λ_{ACP} value of 0.12 W/m°C was estimated for the developed ACP, when compared to other traditional construction materials, it presents significantly lower λ for its relatively high-density value (~1950 kg/m³) as shown in Table 6-7. For instance, the thermal

conductivity of traditional ceramic materials is at least five times higher than the ACP. When comparing other conventional materials, such as the standard concrete and the "resistant" insulating concrete, λ values of around tenfold and fivefold higher were found. It was also detected that the λ_{ACP} is 90% and 88% lower than the traditional and non-traditional mortars and renders or plasters, respectively. On the other hand, in the literature, limited studies about the thermal conductivity λ of alkali-activated ceramic wastes were found. Hwang et al. [58], studied alkali-activated pastes made of waste red clay brick powder and waste ceramic powder from contraction and demolition wastes and reported that the λ value is affected by the microstructure of the hardened paste and the thermal characteristics of its constituents, also mentioned that for alkali-activated materials the thermal conductivity showed a decreasing trend with increasing curing age. But still, λ values ranged between 0.72 and 0.87 W/m°C at 56 days of curing were registered, which are higher than the λ_{ACP}.

Porosity also plays an important role, since a high porosity and a closed pore structure are positive factors to decrease the thermal conduction, thus enhancing the thermal insulation performance [59]. Thereby, the outstanding thermal conductivity found in the present work can be ascribed to the relatively high porosity (21.71%, [20]) of the alkali-activated cement used for the manufacturing of the ACP. This finding is in line with the results found by Pommer et al. [60], who concluded that higher porosity (22-24%) led to lower thermal conductivity, after measuring the heat transport expressed by the thermal conductivity of alkali-activated ceramic wastes of four different particle sizes. However, higher λ values were reported, ranging between 1.49 and 1.89 W/m°C. These findings suggest that the alkali-activation processing technology improves the thermal conductivity of the developed ceramic waste/slag-based cement.

Table 6-7. Thermal conductivity (λ) of the ACP vs. traditional construction materials and thermal insulators [57].

Building solution		ρ (kg/m³)	$R'_{(total)}$ (m²°C/W)	λ (W/m°C)
Developed alkali-activated material	ACP	1950	0.26	0.12
	AP_{ICB}		1.02	-
	AP_{XPS}		1.14	-
Traditional masonry elements (0.10 – 0.11) m	Hollow ceramic brick	-	0.27	-
	Solid ceramic brick	-	0.13	-
	Concrete blocks	-	0.16	-
	Lightweight concrete blocks	-	0.27	-

Table 6.7 (*continued*). Thermal conductivity (λ) of the ACP vs. traditional construction materials and thermal insulators [57]

	Ceramic materials used for bricks, blocks, roof tiles, and tiles,	1800 - 2000	-	0.77
	Standard concrete	2000 - 2300	-	1.65
	Conventional cavernous concrete	1800 - 2000	-	1.35
	Cavernous concrete, with expanded clay aggregate, light sand, and no river sand	800 - 1000	-	0.33
	"Resistant" insulating concrete, with expanded clay aggregate, light sand, and no river sand	1200	-	0.46
Traditional construction materials	With light sand and river sand (≤10%)	1200-1400		0.70
	Perlite or expanded vermiculite aggregate concrete	400 - 600 600 - 800	-	0.24 0.31
	Traditional mortars and renders or plasters	1800 - 2000	-	1.3
	Non - traditional mortars and renders or plasters	1600 - 1800	-	1.0
	Fiber cement boards with asbestos fibers	1800 - 2200	-	0.95
	Fiber cement boards with cellulosic fibers	1400 - 1800	-	0.46
	Plywood panels	1000	-	0.24
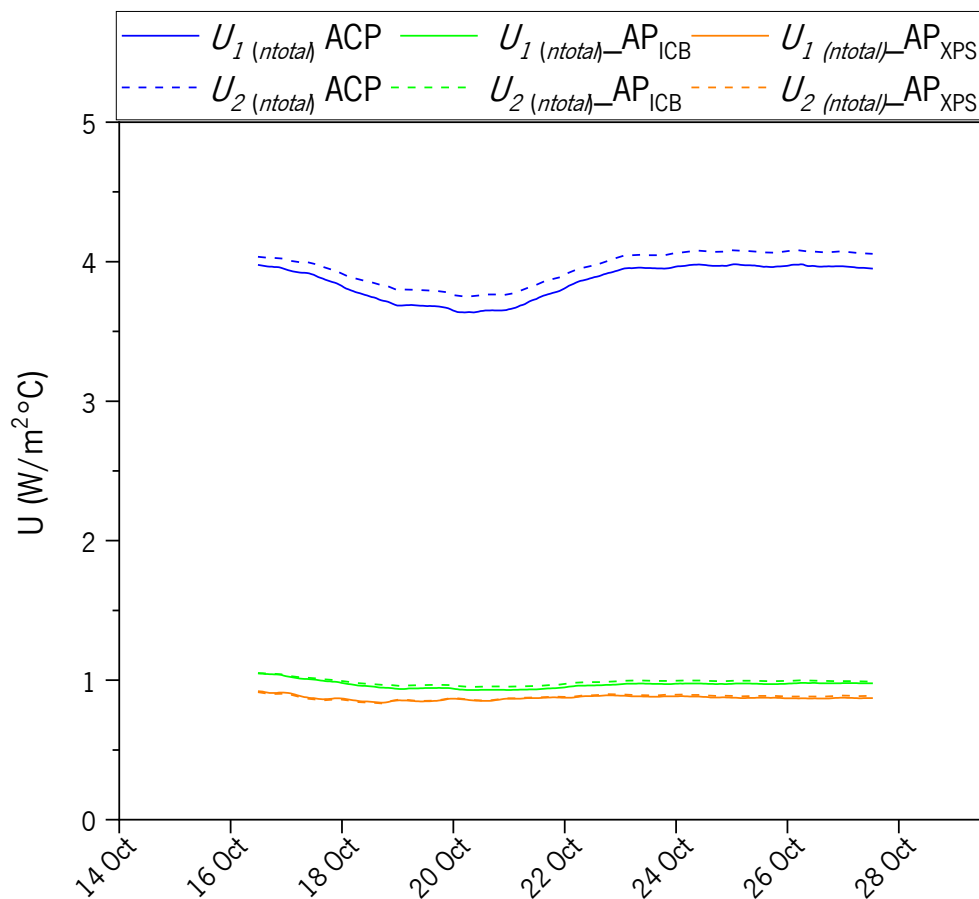
Figure 6-18. Thermal transmission coefficients, $U_{1(ntotal)}$ and $U_{2\ (ntotal)}$

6.6. CONCLUSIONS

In this research, an experimental campaign was carried out that aimed to characterize two half-sandwich panel solutions composed of a thin layer of alkali-activated slag cement/ceramic residue and a thicker insulating layer of either, extruded polystyrene foam (XPS) or expanded cork agglomerate (ICB) as insulation materials. Based on the experimental mechanical and thermal results, the following main conclusions can be drawn. From the mechanical behavior point of view:

1. The AAc exhibited satisfactory performance in terms of compressive strength, up to around 37 MPa. It has been demonstrated that AAc is a viable solution for the development of building elements, e.g., non-structural panels while contributing to a circular economy and sustainability in the construction sector;

2. The Pull off test performed for the two proposed half-sandwich panels, AP$_{XPS}$ and AP$_{ICB}$, revealed clear differences regarding the type of failure for the specimens with different insulation material typologies. That is, although higher tensile bond strength values were reported for AP$_{XPS}$ panels, better bond strength was observed between AAc and ICB. It is explained because the failure occurred outside of the AP$_{ICB}$ interface region, indicating a weak internal structure of ICB. As opposed to AP$_{XPS}$ where the XPS completely debonded at the interface with the AAc. Therefore, the obtained value for AP$_{ICB}$ can be attributed rather to the tensile strength of the expanded cork agglomerate board itself;

3. The direct shear tests showed that AP$_{ICB}$ specimens, although having lower bond strength values, behaved better under shear loading when compared to the AP$_{XPS}$ series with grooved surface finishing. Therefore, it is highlighted that the irregular surface of the ICB board, due to the cork granules, had a positive influence on the adhesion with the AAc layer, which avoided the interfacial slip (debonding) between both panel layers. In contrast to the AP$_{XPS}$ series, when the load was applied parallel ($AP_{XPS}^{\parallel}$) or perpendicular ($AP_{XPS}^{\perp}$) to the direction of the grooves almost two-folded the results of the AP$_{ICB}$. However, a full debonding between XPS and AAC layer was detected;

4. Different flexural behavior was identified for the two studied systems, i.e., after the first cracking, the AP$_{XPS}$ exhibited a deflection-hardening phase while for the AP$_{ICB}$ a sharp softening branch was observed. This might be attributed mostly to the differences in the cross-section of the AAc layer and, to a lesser extent, to the isolation material strength. The failure mode was also different, in

the case of AP_{XPS} multiple cracks in the AAc layer were detected, while the most tensioned zone was inside the XPS groves. In contrast, for the APICB, only a macro-crack near the loading point was visible.

Regarding the thermal performance:

5. The thermal performance of the three studied panels was achieved by analyzing heat fluxes, inner surface temperatures, and thermal transmission coefficients. The results of the experimental work showed that the highest oscillation patterns of the heat flux and inner surface temperature curves correspond to the non-insulated panel (APC), as expected, while no significant differences were detected between the heat flux values of AP_{ICB} and AP_{XPS}. However, slightly larger fluctuations of the heat flux curves of the AP_{ICB} sample were observed, ascribed to the existing voids in the expanded agglomerated cork insulation panel (due to the origin of its composition) and its higher thermal conductivity value compared to XPS;

6. Thermal resistance values of 1.02 m²°C/W and 1.14 m²°C/W for AP_{ICB} and AP_{XPS} were registered, respectively, which are about three times higher than ACP (0.26 m²°C/W). It was also observed a slight increase (~12%) in the $R'_{(ntotal)}$ for AP_{XPS} with respect to AP_{ICB}, as expected, given that XPS presents a lower thermal conductivity value. The obtained results of the proposed insulated panels revealed that an improvement in the thermal properties can be achieved since a thermal resistance of about 2.7 and 3.2 times higher than the common hollow ceramic brick wall and the lightweight concrete blocks were detected, respectively, and at least 7 times higher when compared to a conventional solution of ceramic solid brick;

7. A theoretical value of 0.12 W/m°C was calculated for the thermal conductivity of ACP solution, which is significantly lower than the specified λ of traditional construction materials, such as ceramic materials, standard concrete, the "resistant" insulating concrete, the traditional and non-traditional mortars, and renders or plasters, among others. This may suggest that the alkali-activation technology enhances the thermal conductivity of the developed ceramic waste/slag-based cement.

REFERENCES

[1]   M. Elchalakani, T. Aly, and E. Abu-Aisheh, "Sustainable concrete with high volume GGBFS to build Masdar City in the UAE," *Case Stud. Constr. Mater.*, vol. 1, pp. 10–24, Jan. 2014, doi: 10.1016/J.CSCM.2013.11.001.

[2]   Z. Zhang, J. L. Provis, A. Reid, and H. Wang, "Geopolymer foam concrete: An emerging material for sustainable construction," *Constr. Build. Mater.*, vol. 56, pp. 113–127, Apr. 2014, doi: 10.1016/J.CONBUILDMAT.2014.01.081.

[3]   G. M. Zannerni, K. P. Fattah, and A. K. Al-Tamimi, "Ambient-cured geopolymer concrete with single alkali activator," *Sustain. Mater. Technol.*, vol. 23, p. e00131, Apr. 2020, doi: 10.1016/J.SUSMAT.2019.E00131.

[4]   M. A. Villaquirán-Caicedo and R. M. de Gutiérrez, "Synthesis of ceramic materials from ecofriendly geopolymer precursors," *Mater. Lett.*, vol. 230, pp. 300–304, Nov. 2018, doi: 10.1016/j.matlet.2018.07.128.

[5]   J. L. Provis, A. Palomo, and C. Shi, "Advances in understanding alkali-activated materials," *Cem. Concr. Res.*, vol. 78, pp. 110–125, 2015, doi: 10.1016/j.cemconres.2015.04.013.

[6]   A. M. Rashad and G. M. F. Essa, "Effect of ceramic waste powder on alkali-activated slag pastes cured in hot weather after exposure to elevated temperature," *Cem. Concr. Compos.*, vol. 111, p. 103617, Aug. 2020, doi: 10.1016/J.CEMCONCOMP.2020.103617.

[7]   R. M. Senthamarai and P. Devadas Manoharan, "Concrete with ceramic waste aggregate," *Cem. Concr. Compos.*, vol. 27, no. 9–10, pp. 910–913, Oct. 2005, doi: 10.1016/j.cemconcomp.2005.04.003.

[8]   C. L. Hwang, M. D. Yehualaw, D. H. Vo, T. P. Huynh, and A. Largo, "Performance evaluation of alkali activated mortar containing high volume of waste brick powder blended with ground granulated blast furnace slag cured at ambient temperature," *Constr. Build. Mater.*, vol. 223, pp. 657–667, Oct. 2019, doi: 10.1016/j.conbuildmat.2019.07.062.

[9]   L. Reig, M. M. Tashima, L. Soriano, M. V. Borrachero, J. Monzó, and J. Payá, "Alkaline Activation of Ceramic Waste Materials," *Waste Biomass Valor*, vol. 4, pp. 729–736, 2013, doi:

10.1007/s12649-013-9197-z.

[10] G. F. Huseien, A. R. M. Sam, K. W. Shah, J. Mirza, and M. M. Tahir, "Evaluation of alkali-activated mortars containing high volume waste ceramic powder and fly ash replacing GBFS," *Constr. Build. Mater.*, vol. 210, pp. 78–92, Jun. 2019, doi: 10.1016/j.conbuildmat.2019.03.194.

[11] K. Fang, D. Wang, J. Zhao, and M. Zhang, "Utilization of ladle furnace slag as cement partial replacement: Influences on the hydration and hardening properties of cement," *Constr. Build. Mater.*, vol. 299, p. 124265, Sep. 2021, doi: 10.1016/J.CONBUILDMAT.2021.124265.

[12] M. Sarkar and K. Dana, "Partial replacement of metakaolin with red ceramic waste in geopolymer," *Ceram. Int.*, vol. 47, no. 3, pp. 3473–3483, Feb. 2021, doi: 10.1016/J.CERAMINT.2020.09.191.

[13] A. R. G. Azevedo, C. M. F. Vieira, W. M. Ferreira, K. C. P. Faria, L. G. Pedroti, and B. C. Mendes, "Potential use of ceramic waste as precursor in the geopolymerization reaction for the production of ceramic roof tiles," *J. Build. Eng.*, vol. 29, May 2020, doi: 10.1016/j.jobe.2019.101156.

[14] S. K. Amin, S. A. El-Sherbiny, A. A. M. A. El-Magd, A. Belal, and M. F. Abadir, "Fabrication of geopolymer bricks using ceramic dust waste," *Constr. Build. Mater.*, vol. 157, pp. 610–620, Dec. 2017, doi: 10.1016/j.conbuildmat.2017.09.052.

[15] J. P. Mendes, F. Elyseu, L. J. J. Nieves, A. Zaccaron, A. M. Bernardin, and E. Angioletto, "Synthesis and characterization of geopolymers using clay ceramic waste as source of aluminosilicate," *Sustain. Mater. Technol.*, vol. 28, p. e00264, Jul. 2021, doi: 10.1016/J.SUSMAT.2021.E00264.

[16] M. Skaf, V. Ortega-López, J. A. Fuente-Alonso, A. Santamaría, and J. M. Manso, "Ladle furnace slag in asphalt mixes," *Constr. Build. Mater.*, vol. 122, pp. 488–495, Sep. 2016, doi: 10.1016/J.CONBUILDMAT.2016.06.085.

[17] Z. Sun, X. Lin, P. Liu, D. Wang, A. Vollpracht, and M. Oeser, "Study of alkali activated slag as alternative pavement binder," *Constr. Build. Mater.*, vol. 186, pp. 626–634, Oct. 2018, doi: 10.1016/J.CONBUILDMAT.2018.07.154.

[18] M. Shojaei, K. Behfarnia, and R. Mohebi, "Application of alkali-activated slag concrete in railway sleepers," *Mater. Des.*, vol. 69, pp. 89–95, Mar. 2015, doi: 10.1016/J.MATDES.2014.12.051.

[19] N. Gaibor, D. Leitão, T. Miranda, N. Cristelo, E. N. B. Pereira, and V. M. C. F. Cunha, "Effect of polyacrylonitrile fiber on the properties of alkali-activated ceramic/slag-based mortar," *J. Build. Eng.*, vol. 44, p. 103367, Dec. 2021, doi: 10.1016/J.JOBE.2021.103367.

[20] N. Gaibor *et al.*, "Fiber Reinforced Alkali Activated Cements from Ceramic Waste and Ladle Furnace Slag cured at ambient temperature (under review since 04-23-2022)," *J. Mater. Civ. Eng.*, no. Manuscript number: MTENG-14776, 2022.

[21] G. F. Huseien, A. R. M. Sam, K. W. Shah, M. A. Asaad, M. M. Tahir, and J. Mirza, "Properties of ceramic tile waste based alkali-activated mortars incorporating GBFS and fly ash," *Constr. Build. Mater.*, vol. 214, pp. 355–368, Jul. 2019, doi: 10.1016/j.conbuildmat.2019.04.154.

[22] G. F. Huseien, A. R. M. Sam, K. W. Shah, and J. Mirza, "Effects of ceramic tile powder waste

on properties of self-compacted alkali-activated concrete," *Constr. Build. Mater.*, vol. 236, p. 117574, Mar. 2020, doi: 10.1016/j.conbuildmat.2019.117574.

[23] K. W. Shah and G. F. Huseien, "Bond strength performance of ceramic, fly ash and GBFS ternary wastes combined alkali-activated mortars exposed to aggressive environments," *Constr. Build. Mater.*, vol. 251, p. 119088, Aug. 2020, doi: 10.1016/J.CONBUILDMAT.2020.119088.

[24] N. R. Rakhimova and R. Z. Rakhimov, "Alkali-activated cements and mortars based on blast furnace slag and red clay brick waste," *Mater. Des.*, vol. 85, pp. 324–331, Nov. 2015, doi: 10.1016/J.MATDES.2015.06.182.

[25] S. R. Zedan, M. R. Mohamed, D. A. Ahmed, and A. H. Mohammed, "Effect of demolition/construction wastes on the properties of alkali activated slag cement," *HBRC J.*, vol. 13, no. 3, pp. 331–336, Dec. 2017, doi: 10.1016/J.HBRCJ.2015.12.001.

[26] N. Gaibor, J. Coelho, D. Leitão, T. Miranda, P. Tavares, and N. Cristelo, "Alkali activation of recycled ceramic aggregates from construction and demolition wastes," *Mater. Construcción*, vol. 70, no. 339, p. 222, Jul. 2020, doi: 10.3989/mc.2020.13619.

[27] J. Sierra-Pérez, J. Boschmonart-Rives, and X. Gabarrell, "Environmental assessment of façade-building systems and thermal insulation materials for different climatic conditions," *J. Clean. Prod.*, vol. 113, pp. 102–113, Feb. 2016, doi: 10.1016/J.JCLEPRO.2015.11.090.

[28] DIRECTIVE 2010/31/EU, *Directive 2010/31/EU of the European Parliament and of the Council of 19 May 2010 on the energy performance of buildings*. 2010.

[29] DIRECTIVE (EU) 2018/844, *DIRECTIVE (EU) 2018/844 OF THE EUROPEAN PARLIAMENT AND OF THE COUNCIL of 30 May 2018 amending Directive 2010/31/EU on the energy performance of buildings and Directive 2012/27/EU on energy efficiency (Text with EEA relevance)*. 2018.

[30] A. S. Tártaro, T. M. Mata, A. A. Martins, and J. C. G. Esteves da Silva, "Carbon footprint of the insulation cork board," *J. Clean. Prod.*, vol. 143, pp. 925–932, Feb. 2017, doi: 10.1016/J.JCLEPRO.2016.12.028.

[31] A. M. Papadopoulos, "State of the art in thermal insulation materials and aims for future developments," *Energy Build.*, vol. 37, no. 1, pp. 77–86, Jan. 2005, doi: 10.1016/J.ENBUILD.2004.05.006.

[32] N. Llantoy, M. Chàfer, and L. F. Cabeza, "A comparative life cycle assessment (LCA) of different insulation materials for buildings in the continental Mediterranean climate," *Energy and Buildings*, vol. 225. Elsevier Ltd, p. 110323, Oct. 15, 2020, doi: 10.1016/j.enbuild.2020.110323.

[33] M. Palahí, Y. Birot, F. Bravo, and E. Gorriz, "Modelling, Valuing and Managing Mediterranean Forest Ecosystems for Non-Timber Goods and Services."

[34] L. Gil, "New Cork-Based Materials and Applications," *Mater. 2015, Vol. 8, Pages 625-637*, vol. 8, no. 2, pp. 625–637, Feb. 2015, doi: 10.3390/MA8020625.

[35] O. Anjos, H. Pereira, and M. E. Rosa, "Tensile properties of cork in the tangential direction: Variation with quality, porosity, density and radial position in the cork plank," *Mater. Des.*, vol. 31, no. 4, pp. 2085–2090, Apr. 2010, doi: 10.1016/J.MATDES.2009.10.048.

[36]   S. Schiavoni, F. D'Alessandro, F. Bianchi, and F. Asdrubali, "Insulation materials for the building sector: A review and comparative analysis," *Renew. Sustain. Energy Rev.*, vol. 62, pp. 988–1011, Sep. 2016, doi: 10.1016/J.RSER.2016.05.045.

[37]   T. Dickson and S. Pavía, "Energy performance, environmental impact and cost of a range of insulation materials," *Renew. Sustain. Energy Rev.*, vol. 140, p. 110752, Apr. 2021, doi: 10.1016/J.RSER.2021.110752.

[38]   S. Kumar, B. Chen, Y. Xu, and J. G. Dai, "Structural behavior of FRP grid reinforced geopolymer concrete sandwich wall panels subjected to concentric axial loading," *Compos. Struct.*, vol. 270, p. 114117, Aug. 2021, doi: 10.1016/J.COMPSTRUCT.2021.114117.

[39]   Y. Cui, H. Hao, J. Li, W. Chen, and X. Zhang, "Structural behavior and vibration characteristics of geopolymer composite lightweight sandwich panels for prefabricated buildings," *J. Build. Eng.*, vol. 57, no. April, p. 104872, 2022, doi: 10.1016/j.jobe.2022.104872.

[40]   S. Kumar, B. Chen, Y. Xu, and J. G. Dai, "Axial-flexural behavior of FRP grid-reinforced geopolymer concrete sandwich wall panels enabled with FRP connectors," *J. Build. Eng.*, vol. 47, p. 103907, Apr. 2022, doi: 10.1016/J.JOBE.2021.103907.

[41]   Y. Cui, H. Hao, J. Li, and W. Chen, "Failure mechanism of geopolymer composite lightweight sandwich panel under flexural and edgewise compressive loads," *Constr. Build. Mater.*, vol. 270, p. 121496, 2021, doi: 10.1016/j.conbuildmat.2020.121496.

[42]   J. Q. Huang and J. G. Dai, "Flexural performance of precast geopolymer concrete sandwich panel enabled by FRP connector," *Compos. Struct.*, vol. 248, no. June, p. 112563, 2020, doi: 10.1016/j.compstruct.2020.112563.

[43]   J. Q. Huang and J. G. Dai, "Flexural performance of precast geopolymer concrete sandwich panel enabled by FRP connector," *Compos. Struct.*, vol. 248, p. 112563, Sep. 2020, doi: 10.1016/J.COMPSTRUCT.2020.112563.

[44]   E. 13164:2012, "EN 13164:2012 - Thermal insulation products for buildings - Factory made extruded polystyrene foam." https://standards.iteh.ai/catalog/standards/cen/529f73f8-a7e5-447f-9fd3-a923c7ac58bf/en-13164-2012 (accessed Nov. 23, 2021).

[45]   EN13170:2012+A1:2015, "EN 13170:2012+A1:2015 - Thermal insulation products for buildings - Factory made products of," 2015. https://standards.iteh.ai/catalog/standards/cen/49ba9cdb-6a4b-424a-9d4c-741cea3f2d43/en-13170-2012a1-2015 (accessed Nov. 23, 2021).

[46]   IBERFIBRAN, "FIBRANxps 300 C. Ficha Técnica," Ovar, Portugal, 2021. [Online]. Available: https://fibran.pt/wp-content/uploads/sites/10/2021/10/FT_300C_PT.pdf.

[47]   C. I. Amorim, "Expanded insulation corkboard. Technical Sheet," Mozelos, Portugal, 2021. Accessed: Nov. 22, 2021. [Online]. Available: www.amorimcorkinsulation.com.

[48]   B. together danosa, "ENVIRONMENTAL PRODUCT DECLARATION: FOAMULAR Extruded Polystyrene (XPS) Insulation," 2013. [Online]. Available: https://www.danosa.com/global/wp-content/uploads/sites/9/2021/12/Danosa_EDP_danopren.pdf.

[49]   N. Ranjbar and M. Zhang, "Fiber-reinforced geopolymer composites: A review," *Cem. Concr. Compos.*, vol. 107, p. 103498, Mar. 2020, doi: 10.1016/j.cemconcomp.2019.103498.

[50]   "BS EN 12350-8. Testing Fresh Concrete. Self-compacting Concrete. Slump-flow Test.," 2010. Google Scholar.

[51]   "ASTM C39 / C39M - 18. Standard test method for compressive strength of cylindrical concrete specimens. Active Standard ASTM C39 / C39M," 2018. [Online]. Available: Google Scholar.

[52]   ISO 9869, *ISO 9869. Thermal insulation – building elements – in-situ measurement of thermal resistance and thermal transmittance. International Organization for Standardization (ISO)*. 1994.

[53]   D. Leitão, J. Barbosa, E. Soares, T. Miranda, N. Cristelo, and A. Briga-Sá, "Thermal performance assessment of masonry made of ICEB's stabilised with alkali-activated fly ash," *Energy Build.*, vol. 139, pp. 44–52, Mar. 2017, doi: 10.1016/j.enbuild.2016.12.068.

[54]   A. Ramos *et al.*, "Thermal performance and life cycle assessment of corn cob particleboards," *J. Build. Eng.*, vol. 44, p. 102998, Dec. 2021, doi: 10.1016/J.JOBE.2021.102998.

[55]   L. M. C. Santos, "Coeficientes de Transmisssão Térmica de Elementos da Envolvente dos Edifícios Colecção Edifícios – ITE 50," Lisbon, 2006. Accessed: Jan. 19, 2022. [Online]. Available: http://home.fa.utl.pt/~lcaldas/LNEC_ITE_50.pdf.

[56]   H. Kazem, W. G. Bunn, H. M. Seliem, S. H. Rizkalla, and H. Gleich, "Durability and long term behavior of FRP/foam shear transfer mechanism for concrete sandwich panels," *Constr. Build. Mater.*, vol. 98, pp. 722–734, Nov. 2015, doi: 10.1016/J.CONBUILDMAT.2015.08.105.

[57]   Santos C and Matias L., "Coeficientes de Transmissão Térmica de Elementos da Envolvente dos Edifícios Coleção Edifícios – ITE 50," Lisbon, ISBN: 978-972-49-2065-8, 2006. Accessed: Sep. 20, 2021. [Online]. Available: http://home.fa.utl.pt/~lcaldas/LNEC_ITE_50.pdf.

[58]   C. L. Hwang, M. Damtie Yehualaw, D. H. Vo, and T. P. Huynh, "Development of high-strength alkali-activated pastes containing high volumes of waste brick and ceramic powders," *Constr. Build. Mater.*, vol. 218, pp. 519–529, Sep. 2019, doi: 10.1016/j.conbuildmat.2019.05.143.

[59]   X. Li *et al.*, "Lightweight porous silica ceramics with ultra-low thermal conductivity and enhanced compressive strength," *Ceram. Int.*, vol. 48, no. 7, pp. 9788–9796, Apr. 2022, doi: 10.1016/J.CERAMINT.2021.12.180.

[60]   V. Pommer, E. Vejmelková, R. Černý, and M. Keppert, "Alkali-activated waste ceramics: Importance of precursor particle size distribution," *Ceram. Int.*, vol. 47, no. 22, pp. 31574–31582, Nov. 2021, doi: 10.1016/J.CERAMINT.2021.08.037.

Sustainability of sandwich panels developed based on alkali-activated ceramic/slag wastes

A sustainability analysis was conducted to understand the potential of the introduction of the studied industrial wastes into the proposed panels. The best solution was defined as the one that better combines the environmental, functional, and economic factors when compared to two conventional technologies, a heavyweight conventional partition wall and a lightweight gypsum panels wall, also a conceptual design of a lightweight sandwich wall was taken as reference. A sensitivity analysis was also performed to validate the interpretation results.

Sustainability assessment of half-sandwich panels based on alkali-activated ceramic/slag wastes cement versus conventional technologies

Norma Gaibor [a*]; Ricardo Mateus [b]; Nuno Cristelo [c]; Tiago Miranda [b]; Eduardo N.B. Pereira [b]; Vítor M.C.F. Cunha [b]; Dinis Leitão [d]

a. School of Engineering of the University of Minho, Azurem Campus, 4800-058, Guimarães, Portugal

b. ISISE, Institute for Science and Innovation for Bio-Sustainability (IB-S), Department of Civil Engineering, University of Minho, 4800-058, Guimarães, Portugal

c. CQ-VR, Centro de Química - Vila Real, Department of Engineering, University of Trás-os-Montes e Alto Douro, 5001-801, Vila Real, Portugal

d. CTAC, Department of Civil Engineering, University of Minho, 4800-058, Guimarães, Portugal

*Corresponding author: normygaibor@gmail.com

ABSTRACT

This study assessed the sustainability of two partition walls and intended to contribute to the Circular Economy in the construction sector. A life cycle approach and a multi-criteria decision support method were applied to know the environmental, functional, and economic performances of the production process of half-sandwich panels based on alkali-activated ceramic waste/slag cement, choosing as system boundary the method "cradle to gate". The proposed building solutions differ from each other in the type of insulating material used, either extruded polystyrene foam (AP_{XPS}) or expanded cork agglomerate board (AP_{ICB}). Besides, a comparative analysis of the developed building solutions versus three reference constructive solutions: i) a conventional heavyweight partition wall, ii) a lightweight gypsum wall panel, and iii) a conceptual lightweight sandwich membrane building technology was performed. Results showed that the two proposed half-sandwich wall panels (AP_{XPS} and AP_{ICB}) resulted in the most sustainable alternatives, of which the AP_{XPS} obtained the best overall results since it combined the best the environmental, functional, and economic behavior. Besides, the environmental contribution analysis determined that the greatest environmental burden to the Global Warming Potential (GWP), in the case of the AP_{XPS} was associated with the XPS (57%), being the alkali activator (23%) placed as the second major contributor. When the ICB was used as the insulation layer, the energy used (nearly 38%) and the sodium silicate (about 17%) were the larger contributors to CO_2 emissions. It is worth mentioning that the use of ICB represented a negative contribution (of about -34%) to the GWP category.

Keywords: Sustainability assessment; partition walls; Cradle to gate; alkali-activation; ceramic wastes

7.1. INTRODUCTION

Worldwide, concrete is the most common building material. More recent data (2020) showed that the yearly global production of the Ordinary Portland Cement (OPC) reached 4.1 billion tones, where the top three world cement producers are China which still produces roughly 56%, India, and the European Union (EU28) representing the 7.8% and 4.4%, respectively, [1]. However, OPC production is responsible for 8% of the global CO_2 emissions [2], and it is expected that this value will boost up to 10% in the short term. The OPC is an energy-intensive process, also its production requires an important quantity of natural resources, and their extraction is faster than the sustainability of the system. Moreover, as the world's population increases, the demand for housing materials and the increasing volume of industrial waste also grow. Thus, alkali-activated materials (AAM) are considered the most promising substitutes for OPC, since this technology might address the mentioned problems by using wastes to develop new construction materials. This may lead to a reduction of over 80% of the emissions and up to 40% less embodied energy than OPC [3]. On the other hand, the development and application of prefabricated concrete sandwich panels in building construction is an increasing trend in the industry, especially, because of the structural and thermal efficiency that can be acquired with this technology [4]. Environmental awareness and a growing concern with the greenhouse effect have promoted the construction industry to seek sustainable materials and the incorporation of different types of industrial waste and residues as alternative materials in the construction industry can contribute in an efficient way to such sustainability.

AAM (occasionally mentioned as "geopolymers", even though this term should apply only for low calcium binding systems) can be described as a reaction between amorphous aluminosilicate materials (precursors) and alkali-based chemicals (activators), such as hydroxides and silicates, to produce a solid dense binding matrix. In general, the physical properties of AAM depend on precursor and activator composition and the curing method of the synthesized material. Precursors can be from different sources, (i) directly quarried from nature (e.g., volcanic ash); (ii) by-products (e.g., fly ash, blast furnace slag, calcined clays); and (iii) wastes (e.g., construction and demolition wastes). Secondary products (group ii) are no longer considered waste due to their successful and extensive application as pozzolanic materials in standard concrete and blended PC production [5]. From the sustainability point of view, the alkaline activation of wastes is a favored alternative. Evidently, wastes

that none or minor treatment are required to be used as precursors are preferred, as is the case of ceramic wastes (CW).

The annual production of ceramic tiles represents more than 10 million square meters, of which about 30% end up as waste [6]. The construction sector is the main customer of ceramics, however, only a small amount of its waste is reused by them. Therefore, aiming to improve the sustainability of this sector, it is essential to find alternatives for the recycling of ceramic wastes (CW) in different building applications. CW can be transformed into useful products by exploiting their chemical reactivity. As CW is rich in silica and alumina, essential compounds for the geopolymers synthesis, are suitable precursors to improve the mechanical and durability properties of concrete [7]. Moreover, another less commonly used industrial waste, ladle furnace slag (LFS, a calcium-rich aluminosilicate), has been incorporated as a complementary precursor. The addition of LFS represents some advantages like improved durability (especially against acid and sulfate attack), low heat of hydration, fast setting and hardening, and high-temperature resistance, among others, [8].

AAM based on industrial wastes, such as CW and LFS, has been studied from the mechanical, physical, and chemical perspective [9], [10], [11]. However, its evaluation from an environmental point of view is crucial, as the environmental factor is important in decision-making and research at the building material level. Life Cycle Assessment (LCA) is an analytical and systematic methodology for identifying, quantifying, and assessing the potential environmental burdens related to products or processes during their lifetime (i.e., from cradle to grave) from raw material extraction to production, use, and its final disposal [12]. Environmental assessments of AAM through LCA have been performed largely to prove its advantages over conventional concrete. Several studies have concluded that the capacity to reduce the Global Warming Potential strongly depends on the origin and type of the alkali activator [3], [13], as well as the type of energy utilized for its production [14]. Joudah et al [15], studied the alkali-activated mortars (AAMs) synthesized from waste ceramic tile powder (WCP), ground blast furnace slag (GBFS), and fly ash (FA). Results found that AAMs were cost-effective, and more efficient with lesser CO_2 emission, lower production costs, and lesser fuel consumption when compared to the traditional OPC mortars. Moreover, higher sustainable performance was obtained when the WCP based AAMs were produced by substituting GBFS with FA. Ramagiri et al. [16], conducted a life cycle assessment of six different mixes of alkali-activated mortar made from industrial waste as precursors and activators through ReCiPe methodology. Traditional precursor (fly ash and

slag) was replaced by waste ceramic powder and red mud (RM) and conventional alkali-activators (sodium silicate (SS) and sodium hydroxide (SH)) with RM, desulfurization dust, and silica fume (SF). It was determined that, the SS contributed 50–59% of climate change for blends with traditional activator and the substitution by SF presented the least negative effects on ecosystem quality and human health.

Sandwich panels generally are composed of a two-layer element, thin outer layers (skins) of high-strength material, and a lightweight thicker core of moderately low average strength. Commonly, the structural performance of sandwich panels depends on several factors, such as the properties of the skins and the core, their bonding performance, as well as the geometric dimensions of the components, in special the thicknesses of the skins and core [4]. On the other hand, studies on the environmental benefits of the use of AAM on the development of a particular building element are limited. To the authors' knowledge, to date, no research exists on the evaluation of the sustainability of the application of alkali-activated ceramic waste/slag-based cement for partition wall manufacture. Hossain et al. [17], designed cement-free partition wall blocks entirely with recycled materials (recycled glass aggregate (RGA); concrete slurry waste (CSW); fine recycled concrete aggregate (FRCA); granulated blast furnace slag (GBFS); fly ash (FA)). Four different mixtures for the wall block production were studied. The LCA showed that the most sustainable strategy was the partition wall blocks produced with CSW, FA, and FRCA since it resulted in a reduction of up to 82% of the total carbon emission in comparison to the other blend compositions. In addition, the reuse of CSW was found to represent a potential annual savings of 80,000 m³ of landfill area and about US$4 million in costs related to landfill disposal. Fernando et al. [18] studied the LCA, from cradle to grave, considering the environmental and economic factors of alkali-activated bricks based on low calcium fly ash (FA) and rice husk ash (RHA). The functional unit was defined as the "one square meter of a brick wall (m²)" and "one cubic meter of brick mixture" for the environment and the life cycle cost analysis, respectively. Results determined slightly higher impacts (5.40 kg CO2 eq/m²) for the FA-RHA bricks in comparison to the Portland cement concrete brick, which is attributed to the electricity generation when using renewable sources. It was found that the manufacturing of the alkali activators contributed around 62% - 90% to the total impact for all environmental impact categories. A savings of 30.36$ per cubic meter of concrete for brick production was registered when considering the cost of dry raw materials/binders in the brick mix by avoiding PC.

The present work aims to assess the sustainability of half-sandwich panels developed based on alkali-activated ceramic/slag wastes composed of different conventional thermo-insulating materials, either the rigid extruded polystyrene foam (XPS) or expanded cork agglomerate (ICB). The analysis of these novelty solutions intended to contribute to the Circular Economy in the construction sector, as well as to the development of the state-of-art since no similar ones have been found. Within this scope, the main objective is to evaluate the environmental, functional, and economic performances of the proposed alternatives and compared them with three reference technologies for partition walls. That is two conventional solutions, i.e., a heavyweight and a lightweight, and one conceptual design for a lightweight sandwich. The comparative analysis of these technologies will be based on a standard Life Cycle Analysis method and on a multi-criteria decision support method to allow the integrated study of the selected sustainability indicators.

7.2. STUDIED PARTITION WALLS TECHNOLOGIES

This study evaluates the sustainability of the two panel solutions proposed, which are composed of one face layer (or skin) of alkali-activated ceramic waste/slag-based cement (AAc), as a rigid surface layer, bonded to either extruded polystyrene foam or expanded cork agglomerate boards insulation. The production of these building solutions was developed at a laboratory scale. Furthermore, they are compared with two other conventional solutions: i) heavyweight reference masonry partition wall (HWR), ii) lightweight reference plasterboard partition wall (LWR), and for the third solution to be compared, a constructive solution proposed by Mateus et al. [19] was utilized as reference iii) lightweight sandwich solution (LWS). The analyzed technologies differ mainly in the type and origin of the materials used.

7.2.1. Reference solutions

Data of all parameters considered for the sustainability assessment of the three reference technologies used in the present study, either the traditional building solutions or the partition wall developed under the *AdjustMembrane* research project were taken from the research of Mateus et al. [19]. This was due to the object of the study being comparable (partition walls), the mentioned author used the same multicriteria decision-making support method (i.e., MARS-SC), and the same production site for the prototype solutions was considered, i.e., the University of Minho, Guimaraes, Portugal. Below is a brief

202

description of the partition walls used as a reference, since more detailed information can be found in the cited work [19].

The heavyweight reference (HWR) is a single wall built with ceramic hollow bricks with nominal dimensions of $0.30 \times 0.20 \times 0.11$ m. The brick units were bonded with Portland cement-based mortar, and 0.02 m thick of Portland cement plaster is applied on each side of the wall as a render, resulting in a total wall thickness of 0.15 m and a mass per surface area of about 150 kg/m^2. Each unit of ceramic has a regular geometry with four striated sides. The horizontal grooves present on the brick´s face bring on a good bonding of any type of finishing. Alkyd paint is used for the wall finish.

The lightweight reference (LWR) is made-up of vertical profiles set every 1.5 m; a 50 mm thick rock wool blanket as filling; plasterboards of 15 mm thickness for each face; and alkyd paint on each surface is also used as finishing. The total wall thickness is 80 mm. This solution is commonly used as a substitute for traditional heavyweight technology.

Mateus et al. [19] studied with a conceptual approach ten design alternatives for lightweight sandwich walls (LWS). For comparison purposes, the best building technology in terms of sustainability performance was selected to be used in this study. The conceptual LWS consists of a modular core of sisal fibers (70 mm), a steel fixing structure in tensioned straps, a medium-density fiberboard structural coating (3mm), and a finishing over coating (1.5 mm) of a polyester membrane with a PVC coating. The total wall thickness is 79 mm.

7.2.2. Proposed alkali-activated ceramic wastes/slag based panels

Each of the half-sandwich panels was made up of 10 mm of an alkali-activated ceramic waste/slag-based cement (AAc) rigid face sheet and thermal insulation material of 40 mm thickness each, either extruded polystyrene foam (XPS) or expanded cork agglomerate boards (ICB). This results in a total wall panel thickness of 50 mm. Panels were referenced by the type of isolation, labeled as AP$_{XPS}$ and AP$_{ICB}$, respectively, Figure 7-1. Information regarding panels' manufacturing process and their mechanical and thermal performance were presented in section 6 of the thesis.

(a)   (b)
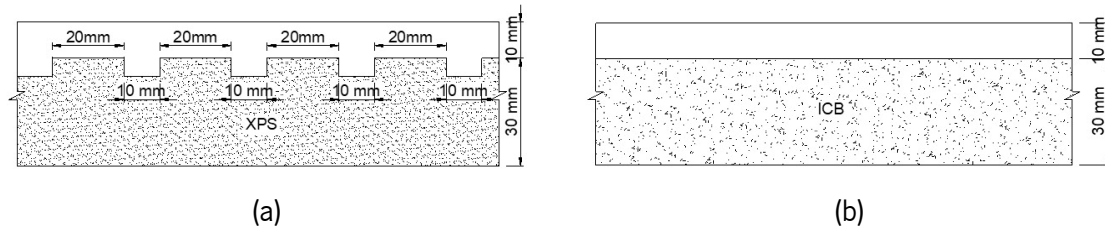
Figure 7-1. Vertical cross-section of semi-sandwich AAc panels with different thermo-insulating materials: (a) extruded polystyrene (AP$_{XPS}$) and (b) Insulation corkboard (AP$_{ICB}$).

For the alkali-activated ceramic waste/slag-based cement (AAc) manufacture, precursors utilized were ceramic wastes (CW) and ladle furnace slag (LFS) from a brick manufacturing industry and melting scrap in an electric arc furnace ironwork company, respectively, both located in Portugal. The matrix was reinforced with polyacrylonitrile fibers (PAN), and sodium silicate (SS) in the solution form was used as an alkaline activator. The mixture proportions in relation to total weight are shown in Table 7-1. The cured was under environmental conditions (20°C ± 0.5°C and 60% HR ± 5%). More details about the mix composition, mechanical, physical, and chemical properties of the developed AAc were reported earlier by Gaibor et al. (2022) [20] corresponding to Chapter 5 of this document.

Table 7-1. Half-sandwich panels composition, (wt.%)

Panel ID	Precursor		Activator	SP	Water	PANf	Insulation material
	CBW	LFS	SS				
AP$_{XPS}$	49.92	16.64	29.95	1.33	1.50	0.67	XPS
AP$_{ICB}$	49.92	16.64	29.95	1.33	1.50	0.67	ICB

7.3. LIFE CYCLE ASSESSMENT METHODOLOGY

The methodology applied in the present work to assess the sustainability of the described solutions for partition walls followed the cradle-to-gate Life Cycle Analysis (LCA) phases, that is, the impacts to produce each material used as an input in the life cycle inventory, the energy used for the production stage, and the transportation of the materials to the building site. Besides, the comparative analysis and aggregation of indicators were performed based on the multicriteria decision support Methodology for the Relative Sustainability Assessment of Building Technologies (MARS-SC) [21].

According to ISO 14040:2006 [22], the LCA includes four main phases as illustrated in Figure 7-2. The first phase (Goal and Scope) defines the purpose, objectives, the functional and system limits. The second phase (Inventory Analysis) consists of collecting all data related to inputs, processes, and emissions, among others, of the entire life cycle. In the third phase (Impact Assessment), environmental impacts and input resources are quantified based on the inventory analysis. The last phase (Interpretation) is to interpret the results calculated from the Impact Assessment phase and recommend improvement measures as appropriate.
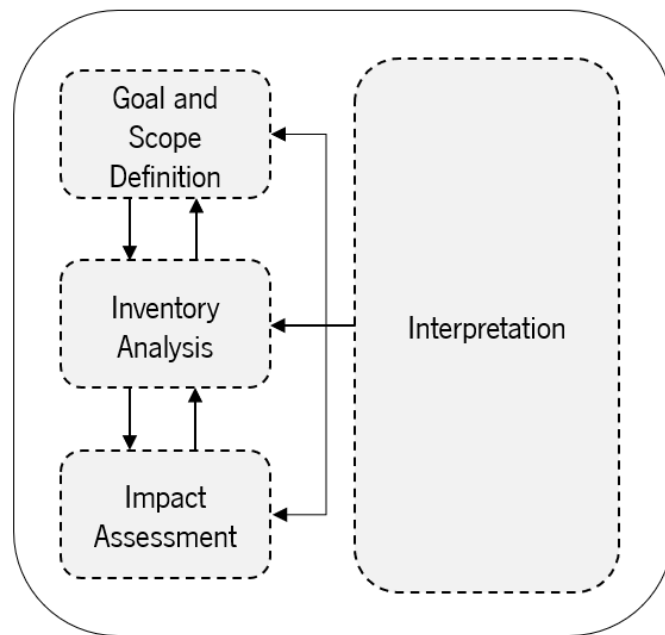
Figure 7-2. Life Cycle Assessment structure according to ISO 14040

The MARS-SC method was created to particularly address the sustainability of building elements. This method allows comparing the performance of the studied building solution with the locally most applied solution or conventional building element. It is based on three groups of sustainability categories: environmental, functional, and economic [19]. The five main steps that the MARS-SC methodology involves are presented in Figure 7-3.
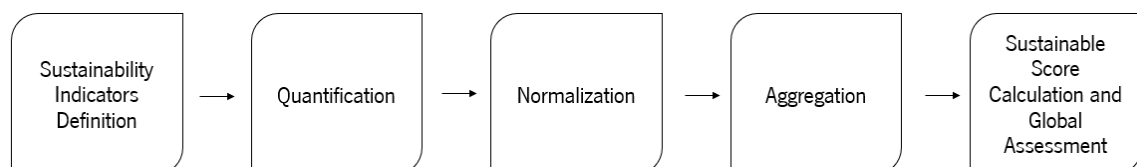
Figure 7-3. Structure and assessment steps of the MARS-SC methodology, [21]

7.3.1. Goal and Scope

The object of study is a building solution for a partition element without structural function and the declared unit is 1 m² of the studied solutions, which represents the basis for comparison throughout the study. Although the assessment of each stage of the life cycle of a building element can be performed by the MARS-SC, a comparison is made with the reference solutions using the cradle-to-gate approach due to a lack of data regarding the usage phase of the half-sandwich panels based on alkali-activated ceramic waste/slag-based cement. Thus, system boundaries encompass: i) the acquisition of raw materials (CW, LFS, PANf, SS, W, SP, XPS, ICB, and SM, Table 7-2) and preparation processes, ii) the transportation to the production site, and iii) the mixing process, Figure 7-4.
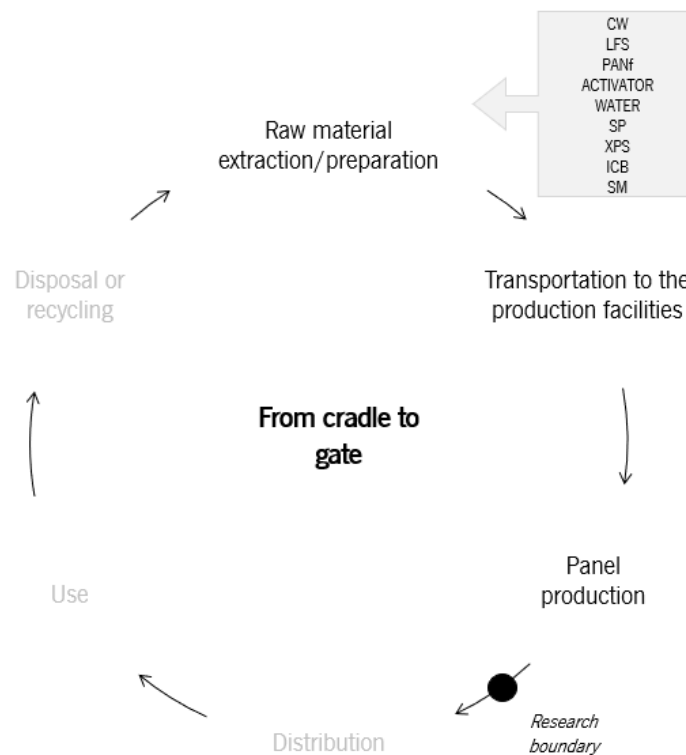
Figure 7-4. System boundaries of the study

Regarding the limitations of this evaluation, they are the geographic boundaries, since this study covers data that apply in large part to Portugal, namely, the obtaining and distribution of electric energy and the processing of the raw materials. It is worth mentioning that the AP_{XPS} and AP_{ICB} production was at a laboratory scale, so energy consumption may be different at an industrial scale. For the main precursor

of the alkali-activated cement, i.e., the ceramic wastes, the closest supplier to the production site (University of Minho) was selected.

7.3.2. Inventory Analysis

The inventory analysis is the first step in determining environmental impacts. Thus, the inputs (e.g., amount of energy and materials) and the outputs (e.g., emissions) of the different panel solutions studied were quantified. Considering that this study covers the life cycle from cradle to gate, the following three main steps were included in the inventory: i) the raw materials ii) the transportation of the materials to the production facilities, and iii) the energy used for the manufacturing process. Due to the lack of specific environmental information for all the materials utilized, in this work, the EcoInvent 3.7.1. [23] integrated into the SimaPro 7.3 software was used to obtain the data for the inventory, which is the most internationally recognized generic environmental database. Table 7-2 shows the inventory of the materials and the quantities needed for the manufacturing of each studied building element.

For the development of the inventory, the following assumptions were considered. The embodied impacts for the CW were not taken into account since it is a waste and therefore does not have allocated environmental impacts. Therefore, only the environmental burden regarding the transportation to the production site and the electricity needed for grinding (Los Angeles Ball mill – 0.0789 kWh/kg) the CW until to get a fine fraction of about 38% [24] to be utilized as a precursor in the alkali activation were included. A similar case occurred with the LFS since its supplier declared it as non-hazardous waste and it is currently deposited in a landfill. The LFS was manually sieved, thus, only the environmental load for the transportation was considered.

Concerning the inventory of the other used materials (PAN, SS, W, SP, HG), generic data was used. Data relating to the environmental impact categories of the insulation corkboard were obtained from an Environmental Product Declaration of a Portuguese ICB [25], while for the XPS insulating material, generic figures were considered.

The PVC profiles (PVC) and the hot melt glue (HG) are later referred to as secondary materials (SM) since they were not constituents of the panel itself. The PVC was used to frame the insulating material

to be used as a mold for casting the alkali-activated cement. Therefore, calculations were by assuming that the PVC profiles can be reused to produce at least 50 panels. The HG was used to bond the PVC with the insulating material.

Transportation inventory is essential to determine the actual environmental impacts caused by a specific product. In this study, lorry freight transportation type was considered to assess the potential environmental impacts of the transportation processes. Also, the production site of the prototype was assumed to be in the same spot as the university, i.e., the University of Minho, Guimaraes, Portugal. Thus, the suppliers closest to the production facility were selected and a map application (e.g., Google Maps) was used to calculate the distance, results are shown in Table 7-2.

Table 7-2 also contains the inventory data for the reference solutions (HWR, LWR, and LWS) that were taken from Mateus et al. [19]. To ensure a fair comparison, it was verified that the following conditions were similar as in this study: i) the declared unit, which is 1 m^2; ii) the location of the manufacturing site (Guimaraes, Portugal), therefore, transportation inventory was the same as reported.

Table 7-2. Inventory of the materials and supplies inputs for each analyzed building solution

Materials and Supplies		ID	Building solution					Units	Transport
			AP_{XPS}	AP_{ICB}	HWR	LWR	LWS		
Proposed solutions	Ceramic waste	CW	9.62	9.62	-	-	-	kg/m²	38.8
	Ladle Furnace Slag	LFS	3.21	3.21	-	-	-	kg/m²	49.7
	Polyacrylonitrile fiber	PANf	0.13	0.13	-	-	-	kg/m²	405
	Sodium silicate	SS	5.77	5.77	-	-	-	kg/m²	250
	Water	W	0.29	0.29	-	-	-	kg/m²	-
	Superplasticizer	SP	0.26	0.26	-	-	-	kg/m²	96.2
	Extruded polystyrene	XPS	0.99	-	-	-	-	kg/m²	91.6
	Insulation corkboard	ICB	-	3.30	-	-	-	kg/m²	71.6
	PVC profile	PVC	0.02	0.02	-	-	-	kg/m²	368
	Hot melt glue	HG	0.03	0.03	-	-	-	kg/m²	
Reference solutions	Brick (hollow)		-	-	-	61.4	-	-	kg/m²	208
	Cement mortar		-	-	-	117.8	-	-	kg/m²	10
	Gypsum plasterboard		-	-	-	-	26.3	-	kg/m²	188
	Medium-density Fiberboard		-	-	-	-	-	0.003	m³	190
	Paint (alkyd, white, and 60% in solvent)		-	-	-	0.6	0.6	-	kg/m²	48
	Polyester membrane		-	-	-	-	-	0.5	kg/m²	33
	Rock wool		-	-	-	-	1.6	-	kg/m²	33
	Sisal fibber		-	-	-	-	-	0.040	m³	33
	Steel (cold-formed)		-	-	-	-	2.6	0.400	kg/m²	92
Equipment	Hot melt glue gun	-	0.02	0.02	-	-	-	kWh/kg	-
	Ball mill (Los Angeles)	-	3.29	3.29	-	-	-	kWh/kg	-
	Mixer	-	0.10	0.10	-	-	-	kWh/kg	-
	Shaking Table	-	0.0003	0.0003	-	-	-	kWh/kg	-

7.4. IMPACT ASSESSMENT

7.4.1. Environmental, functional, and economic performance

The selected environmental, functional, and economic performance indicators are summarized in Table 7-3. For the *environmental performance*, SimaPro LCA software was used to calculate environmental impacts using two life cycle impact assessment methods: baseline CML 2001 for environmental impact assessment and Cumulative Energy Demand V1.08 for determining embodied primary energy. The impact categories considered for the analysis of the two studied half-sandwich panels (AP_{XPS} and AP_{ICB}) are: i) Global Warming Potential; ii) Ozone depletion; iii) Photochemical oxidation; iv) Acidification Potential; v) Eutrophication Potential; vi) Total Embodied energy; vii) Non-renewable Embodied energy. It is worth mentioning that the MARS-SC methodology does not consider the Total Embodied energy [19], therefore when the comparative analysis of sustainability was performed, this impact category was not included. For the reference panels (HWR, LWR, and LWS) used for comparison, results from the quantification of the impact categories defined were taken from Mateus et al. [19].

Regarding the *functional performance*, as the studied building solutions aim to be used as an interior partition element with and without thermal requirements, the thermal transmission coefficient (U) was considered an indicator to be analyzed. In the case of the proposed alkali-activated ceramic/slag wastes-based panels (AP_{XPS} and AP_{ICB}), the U value was experimentally determined under the guidelines of ISO 9869 [26], and the results were presented in chapter number six. The U values of the reference solutions were taken from the work carried out by de Mateus et al. [19], which was quantified based on the Portuguese thermal code, Decreto-Lei n.º 101-D/2020 [27].

The *economic performance* of the two proposed building technologies in this study was defined through the Construction Cost (CC) indicator that includes the average market price of the materials, the labor, and the energy used costs for the manufacturing. Regarding the CW and LFS, were declared as no hazardous wastes by their respective suppliers, so they do not afford an economic value. However, the freight charges to the production site were counted. The cost of the remaining materials, i.e., PAN, SS, W, SP, XPS, ICB, and SM were obtained from the corresponding vendors.

The sustainability assessment study of the reference solutions was published in 2013. Thus, to guarantee a fair comparison, the reported construction cost of each wall solution was adjusted considering the compound interest in the inflation rate determined by the National Statistics Institute of Portugal (INE) [28]. Accordingly, the applied update factor from January 2013 to April 2022 was 1.1344 and the corrected CC values are shown in Table 7-6.

Table 7-3. Indicators, units, and quantification methods

Dimensions	Indicators	Units	Methods
Environmental	Global Warming Potential (GWP)	[kg CO_2 eq]	CML 2 baseline 2001 V2.05
	Ozone layer depletion (ODP)	[kgCFC-11 eq]	CML 2 baseline 2001 V2.05
	Photochemical oxidation (POCP)	[kg C_2H_4 eq]	CML 2 baseline 2001 V2.05
	Acidification Potential (AP)	[kg SO_2 eq]	CML 2 baseline 2001 V2.05
	Eutrophication Potential (EP)	[kg PO_4 eq]	CML 2 baseline 2001 V2.05
	Total Embodied energy (EE_T)	[MJ]	Cumulative energy demand V1.08
	Non-renewable Embodied energy (EE_NR)	[MJ]	Cumulative energy demand V1.08
Functional	Thermal insulation (U)	[W/m^2°C]	Portuguese thermal code
Economic	Construction cost (CC)	[€/m^2]	Average market value

7.4.2. Comparative analysis of the sustainability of partition solutions

Following the main steps suggested by the MARS-SC methodology [21], the normalization, aggregation, and global assessment of the previously defined sustainability indicators were estimated. The normalization of the indicators attempts to prevent scale effects in the aggregation of parameters of the different indicators to facilitate results interpretation of the type "higher is better" and others "lower is better". Normalization provides dimensionless values and converts them into a limited scale between 0 (worst value) and 1 (best value). Normalization was done by applying *Equation 6* of Diaz-Balteiro [29], see Table 7-5.

Presenting the performance of a solution by listing the results obtained at the level of all the parameters considered, that is, environmental, functional, and economical, makes complex the understanding of the solution's overall performance. Therefore, a complete aggregation method for each sustainability dimension (ND$_A$) was used according to *Equation 7*, Table 7-5. The sum of all the weights must be

equal to 1 [19]. For the aggregation, the relative importance weights (Table 7-4) proposed by the US Environmental Protection Agency's Science Advisory Board (SAB) were used in this study [30]. The MARS-SC methodology [21] considers this approach appropriate for the Portuguese context since this system of weights is one of the most recognized by the international scientific community in the field. Regarding the functional and economic performance, the same values as the normalized functional and economic parameters were assumed since there is only one indication in these two dimensions.

Table 7-4. Weight for each sustainability indicator, [21]

Sustainability dimension	Indicator	Weight (%)
Environmental (ND$_A$)	GWP	38
	ODP	12
	POCP	14
	AP	12
	EP	12
	EE_NR	12
Functional (ND$_F$)	U	100
Economic (ND$_E$)	CC	100

The phase after the aggregation of each of the parameters consists of determining the global performance of the building solution by a single index. It is based on the quantification of the sustainability score (NS) that is calculated using *Equation 8*, Table 7-5. In the global assessment, the MARS-SC sets a default weight of 0.40 for the environmental and 0.30 for both functional and economic dimensions [19], respectively. The sum of the weights assigned to the three dimensions must be equal to 1, in order to obtain a sustainable score between 0 and 1.

Table 7-5. List of equations for the sustainability comparative analysis of the interior partition solutions

	Assessment steps	Equation	Description
Equation 6	Normalization	$$\bar{P}_i = \frac{P_i - P_{*i}}{P_i^* - P_{*i}} \; \forall_i$$	$\bar{P}_i$: value of the i sustainability indicator (SI) P_{*i}: The worst value of the SI among the analyzed building technologies P_i^*: The best value of the SI among the analyzed building technologies
Equation 7	Aggregation	$$ND_A = \sum_{i=1}^{n} w_i * \bar{P}_i$$	ND_A: global indicator w_i: weight of the ith indicators $\bar{P}_i$: normalized indicator
Equation 8	Sustainable score	$$NS = \sum_{j=1}^{n} ND_j * w_j$$	NS: sustainability score ND_j: performance at the level of the dimension j w_j: weight of the jth dimension

A sustainable profile is also presented as part of the results using a "radar" or Amoeba chart. In this chart, the plotted rays are equal to the number of indicators under study. Therefore, each sustainable profile monitored the global performance of the two proposed half-sandwich panels (AP$_{XPS}$ and AP$_{ICB}$) and compared with the performance of the reference solutions. In the radar chart, the closest to the center a solution is represented, the lowest its sustainability.

7.4.3. Sensitivity analysis

The sensitivity analysis lets review the effect of the most relevant assumptions in the global assessment. As suggested by Mateus et al. [19], it is based in the Hofstetter triangle [31]. In the present work, a sensitivity analysis of the effect of the weight for each sustainability dimension on the global sustainability score was made. In this context, each edge of the mixing triangle illustrates the weight of one sustainability dimension and each point inside the triangle represents a combination of weights of the three sustainability dimensions.

7.5. RESULTS AND DISCUSSION

7.5.1. Impacts Assessment

After applying the aforementioned methodology, the results obtained from the quantification of the environmental, functional, and economic indicators for the declared unit of the two studied half-sandwich solutions based on alkali-activated ceramic/slag residues are exhibited in Table 7-6. It also contains the quantification of the impact categories for the two selected conventional solutions to be compared, i.e., the heavyweight and lightweight partition walls, and the building solution proposed by Mateus et al. [19]. For the three reference solutions, there is no data related to the total embodied energy, therefore empty cells for that environmental parameter are observed. As this impact category is not considered by the used multi-criteria support decision method (MARS-SC), it does not affect the analysis.

In general, the heavyweight reference presented the highest values for all environmental impacts. It was expected since cement mortar was used to bind the brick units, which is characterized by high CO_2 emission and energy consumption during its production process [32],[33], therefore the

environmental burdens increased substantially. Thus, it can be noticed that the GWP value (44.3 kg CO_2 eq) for the HWR is significantly higher in comparison to all other solutions. In contrast, for the AP_{ICB} solution, a negative CO_2 emission (−5.10 kg CO_2 eq) was verified. This may be attributed to the use of ICB as insulating material. The cork tree is a long-lived species (250–300 years) with a great potential for CO_2 capture and sequestration. Cork is extracted from the tree, a method that does not damage the tree, therefore considered a carbon sink [34].

The figures displayed in Table 7-6 were used for the normalization of the parameters that are presented and discussed in the comparative analysis section.

Table 7-6. Quantification of Environmental, Functional, and Economic parameters for each studied partition walls technologies

	Impact category	Units	Building solution				
			AP_{XPS}	AP_{ICB}	HWR	LWR	LSW
Environmental	GWP	[kg CO_2 eq]	1,89E+01	-5,10E+00	4,43E+01	9,50E+00	6,75E+00
	ODP	[kgCFC-11 eq]	1,52E-04	7,97E-07	3,21E-06	1,38E-06	6,61E-07
	POCP	[kg C_2H_4 eq]	3,49E-03	3,95E-03	5,43E-03	4,49E-03	1,82E-03
	AP	[kg SO_2 eq]	6,28E-02	7,80E-02	1,12E-01	6,16E-02	3,26E-02
	EP	[kg PO_4 eq]	1,43E-02	2,14E-02	3,19E-02	1,66E-02	1,78E-02
	EE_NR	[MJ]	2,01E+02	1,24E+02	3,39E+02	1,33E+02	1,07E+02
	EE_T	[MJ]	2,20E+02	1,61E+02	-	-	-
Functional	U	[W/m²°C]	0.88	0.98	1.80	0.80	0.81
Economic	CC	[€]	24,40	32,30	30,13	42,72	42,90

7.5.2. Environmental contribution analysis

The objective of presenting the analysis of the contribution of environmental impacts for the two new proposed solutions (AP_{XPS} and AP_{ICB}) was to detect the most relevant processes of the life cycle that contribute to the impacts evaluated for each category. As can be seen in Figure 7-5 a), for the AP_{XPS} solution, the use of the extruded polystyrene foam (XPS) as insulating material made it the main contributor for the GWP, POCP, EE_NR, and EE_T with impacts accounting for about 57.02%, 38.66%, 49.54%, and 46.27%, respectively. Furthermore, XPS represents the highest impact for the ODP category, reaching 99.61%. This is due to the high energy requirements for the XPS manufacture and even more, the process itself uses carbon dioxide, consequently causing an increase in GHG emissions

[35]. The alkali activator (sodium silicate) was the largest contributor to the AP (38.95%) and the EP (49.75%) categories, while for Global Warming Potential (23.1%) it was ranked as the second important contributor. Other components such as energy use, PAN fibers, and the SP were less significant, representing 10.16%, 3.89%, and 2.55% respectively, and similar contributions were found in the EE_T and EE_NR.

In contrast, when the expanded cork agglomerate (ICB) was used as a thermal insulator of the half-sandwich panel, a negative contribution (-33.61%) to the GWP was determined. This is justified by the fact that the cork absorbs carbon during its growth, is a renewable material, and its production process is almost chemical-free, as stated by Tártaro et al. [34]. Therefore, the energy used (37.63%) and the sodium silicate (16.70%) was the dominant process in this category. The ODP, POCP, and AP primary contributors are also related to the ICB (24%–49%) and the SS (25%–39%). For the Total Embodied Energy and the Non-renewable Embodied Energy categories, it can be observed that the alkali activator (30.60% and 34.55%, respectively) represented the most significant environmental burden. This is in line with other LCA studies which involve alkali-activated materials, where an important bulk of the environmental impacts are attributed to the alkali-activator [16]. The relatively high contribution of the ICB to the EE_T (26.28%) and the EE_NR (17.59) may be related to pruning and cork extraction from tree's branches and the bonding process of the cork granules to become agglomerated since they are energy-intensive steps, [34]. Finally, the other contributors to these two environmental factors by order of weight are the PAN fibers (up to ~11 %), the SP (up to ~6.5 %), and the transportation of materials (up to ~4.2 %).
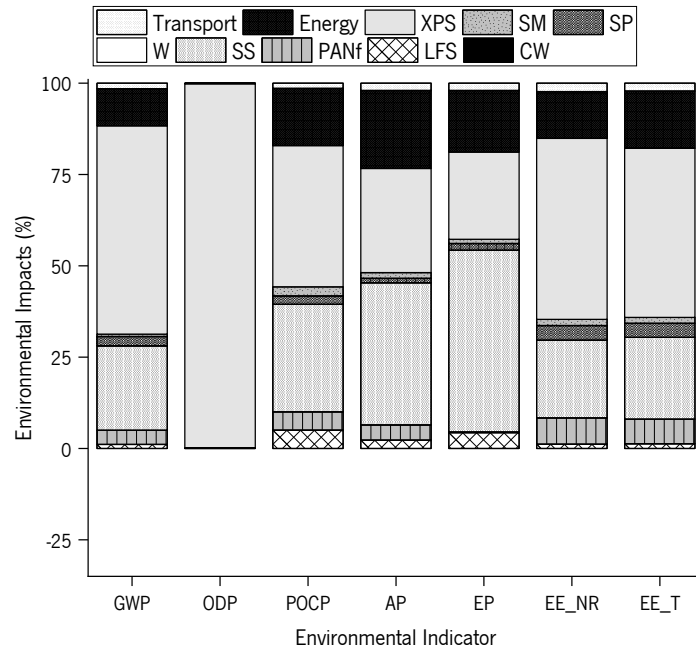
(a)
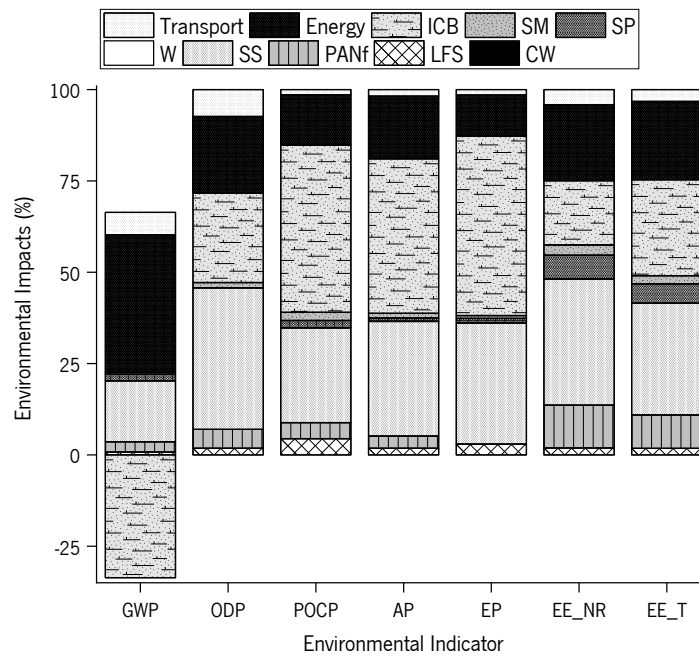
(b)

Figure 7-5. Contribution analysis for (a) AP$_{XPS}$, and (b) AP$_{ICB}$.

7.5.3. Comparative Analysis of Sustainability

This section shows the results for the two proposed half-sandwich (AP$_{XPS}$ and AP$_{ICB}$) versus the chosen conventional technologies (HWR, LWR, LSW). Table 7-7 presents the normalized impact categories. This lets a better understanding of which solutions have better environmental, functional, or economic

performance. Based on the normalized figures, it can be observed that the HWR had the worst environmental and functional performance, with exception of ODP. In terms of CO_2 emissions, the AP_{ICB} was the best among all solutions, while the AP_{XPS} was placed in the second to the last position. Additionally, the AP_{XPS} performed the worst in the ODP and the ADP impact categories, which was attributed to the use of XPS as insulating material as already described in section 7.5.2. However, in terms of eutrophication potential, the AP_{XPS} had the lowest environmental burden, ranking first, followed by the LWR, LSW, and AP_{ICB}.

As mentioned above, for the functional and economic parameters, a single value was assumed for each case, therefore, the results will be analyzed below in the sustainability assessment.

Table 7-7. Normalized values of the studied impact categories

Impact category		Building solution				
		AP_{XPS}	AP_{ICB}	HWR	LWR	LSW
Environmental	GWP	0,65	1,00	0,00	0,70	0,76
	ODP	0,00	1,00	0,98	1,00	1,00
	POCP	0,54	0,41	0,00	0,26	1,00
	AP	0,62	0,43	0,00	0,63	1,00
	EP	1,00	0,59	0,00	0,87	0,80
	ADP_FF	0,59	0,93	0,00	0,89	1,00
Functional	U	0,92	0,82	0,00	1,00	0,99
Economic	CC	1,00	0,57	0,69	0,01	0,00

The sustainability assessment resulting from the MARS-SC considers the analysis of three aspects, i.e., the sustainable profile, the environmental (ND_A), functional (ND_F), and economic (ND_E) performance, and the Sustainable Score (SC) which are presented in Table 7-8. In the sustainable profiles, the fill area in gray denotes the overall performance of each proposed half-sandwich panel (AP_{XPS} and AP_{ICB}) that outcomes from the values obtained in each impact category. The reference solutions, i.e., HWR, LWR, and LWS are represented by a solid, dash, and dot line, respectively. The closer the SC value is to one, the better the solution.

From the analyzed building technologies, the most sustainable alternative at the environmental level was the conceptual design for the lightweight sandwich wall (LWS), $ND_A = 0.88$, and the worst performance presented by the conventional hollow brick partition wall (HWR), $ND_A = 0.12$. The AP_{ICB} ($ND_A = 0.79$) and the AP_{XPS} ($ND_A = 0.54$) were placed as the second and fourth options, respectively. The results showed that the type of insulating material used in a partition wall significantly affects the

environmental burden caused. For instance, the use of vegetable fibers and wood by-products, such as sisal and cardboard, represents a positive contribution to environmental performance [19], [4]. On the other hand, several studies have revealed that the main environmental burdens of alkali-activated materials are associated with the use of alkali activators [3], [14], [36]. However, after evaluating the contribution of environmental impacts from the developed building solution systems (AP_{XPS} and AP_{ICB}), it was found that the XPS had the greatest environmental bulk in most impact categories, positioning the alkali activator as the second contributor. In contrast, when the ICB was used, a notable reduction in the environmental impacts was evidenced. Finally, although the LWS system achieved the best results in the ND_A, the GWP of AP_{ICB} building solution was negative (Table 7-6), which is a noteworthy outcome.

Regarding the functional performance, it had been identified the traditional lightweight solution (LWR), $ND_F = 1.00$, and the HWR, $ND_F = 0.00$, had the best and worst performance, respectively. Considering that the analyzed building solutions were developed as an interior partition element with and without thermal requirements, the thermal transmission coefficient alone was selected as an indicator. From Table 7-8, it can be observed that the ND_F values for the AP_{XPS} (0.92) and the AP_{ICB} (0.82) are closer to one, suggesting that both half-sandwich panels are also good alternatives from the functional point of view. The results also allow determining that the use of fibrous and foam materials as insulation behaves better than the corkboard insulation. This is in agreement with the thermal conductivity values of the different insulating materials presented by LNEC [37], where for instance the XPS has a lower U value when compared to ICB, resulting in lower U values for the partition wall system. The lower the thermal conductivity, the better the insulating performance.

As regards the economic level, the AP_{XPS} ($ND_E = 1.00$) and the LWS ($ND_E = 0.00$) was determined as the best and worst performances. The high price of the LWS solution is attributed to the use of medium-density fiberboard (MDF) as coating material and the steel used for the fixing structure. On the other hand, the major economic contributor of the proposed semi-sandwich panels is the insulation material, either XPS or ICB, which represents around 37% and 53% of the total cost, respectively. Currently, in the Portuguese market, the ICB is around 80% more expensive than the XPS. Regarding the rigid layer that is the AAc, the main economic contribution was associated with the activator, 27% for the AP_{XPS} and 18% for the AP_{ICB}, but even so, its economic impact is lower compared to the insulating materials.

In the global analysis estimated by SC, according to the dimensions of sustainability considered and the weights assigned, the most sustainable alternative for interior partition wall was the AP_{XPS} (SC=0.79) and the worst corresponds to HWR (SC=0.25). It is worth mentioning that the SC (0.73) obtained for the AP_{ICB} solution is slightly lower than AP_{XPS}, which also makes it a promising sustainable candidate compared to the reference solutions. From the results obtained, it can be concluded that, in addition to the environmental parameter, functional and economic factors are essential in the decision process when a new building solution is benchmarked. In this way, it has been demonstrated that the developed solutions, AP_{XPS} and AP_{ICB}, are the ones that best combine those factors. Thus, these alternatives are considered optimal options from the eco-efficiency point of view.

Table 7-8. Sustainable performance results

Building Solution	Sustainable Profile	Performances			Sustainable Score
		ND_A	ND_F	ND_E	
AP_{XPS}		0.54	0.92	1	0.79
AP_{ICB}		0.79	0.82	0.57	0.73

Table 7.8 (continued) Sustainable performance results

Building Solution	Sustainable Profile	Performances	Sustainable Score	Building Solution	Sustainable Profile
HWR		0.12	0.00	0.69	0.25
LWR		0.71	1.00	0.01	0.59
LWS		0.88	0.99	0.00	0.65

7.5.4. Sensitivity analysis

The sensitivity analysis (SA) allows the results to be more reliable since it assesses how the outcomes are influenced by the information input and the methodology used during the sustainability assessment [38]. Several authors [39], [40] have stated the significance of this analysis since it lets determine the

uncertainty and correlation between the data used as inputs and the acquired results. Moreover, this also supports the confidence level of the conclusions and comparisons made. The results of the sensitivity analysis using the aforementioned methodology are shown in Figure 7-6. It can be seen that the AP_{XPS} alternative had the best performance for the largest number of weight combinations and the AP_{ICB} is positioned as the second option which is consistent with the global results obtained by the sustainable score. Considering only the functional aspect, it can be noted that the LWR is the best solution. While the LSW is limited to being the best alternative only from an environmental perspective. Finally, the HWR did not appear in the Hofstetter triangle, confirming that it is the worst construction technology when environmental, functional, and economic dimensions are considered. The conclusions drawn from the sensitivity analysis agree with the results obtained in section 7.4.2.
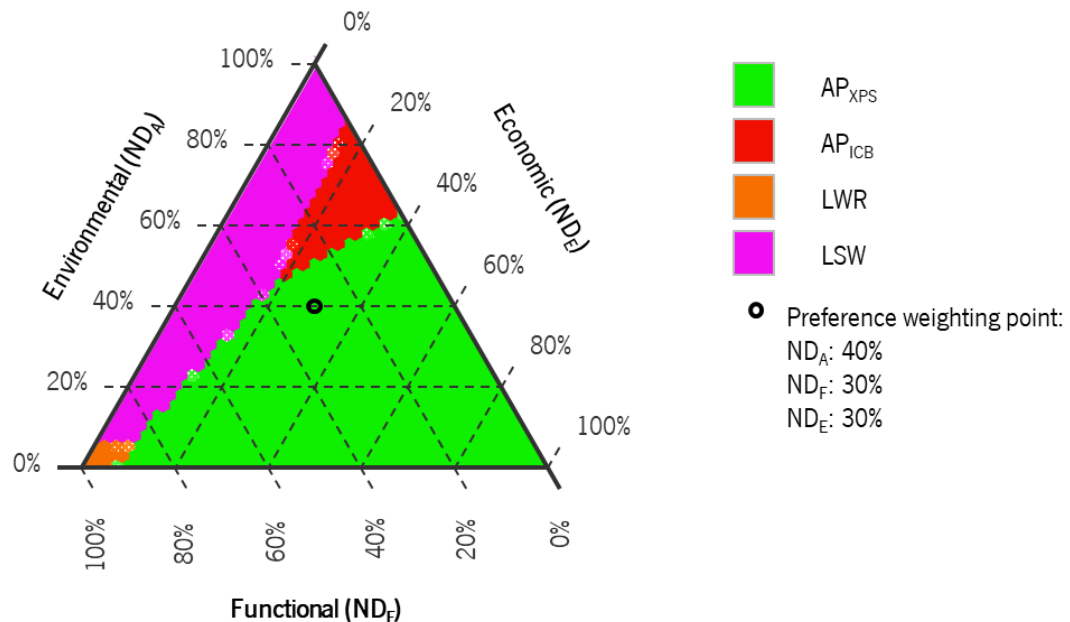
Figure 7-6. Sensitivity Analysis

7.6. CONCLUSIONS

This study dealt with the sustainability assessment of two half-sandwich panels based on alkali-activated ceramic wastes/slag cement, never been investigated before as far as the authors know. The results were compared with two conventional technologies for partitioning in interior applications used in the Portuguese construction market, the hollow brick partition wall (HCM) and the plasterboard partition wall (LWR). Besides, it was also contrasted with one conceptual building solution proposed

by Mateus et al. [19], a lightweight sandwich wall (LWS). All, the proposed building solutions, and the reference samples had an equivalent declared unit of 1 m². Therefore, the environmental, functional, and economic performances of the above mentioned alternatives were analyzed. Based on the obtained results, the following conclusions were made:

1. From an environmental point of view, most of the analyzed impact categories of the developed panels (AP_{XPS} and AP_{ICB}) were significantly influenced by the type of thermal insulation material used. As in the case of AP_{XPS}, for GWP and most impact categories, XPS (∼57%) contributed more than sodium silicate (∼23%), which normally when alkali-activated materials are studied separately, the activator is the main contributor. In contrast, the use of ICB registered a negative net CO_2 emission of around -37%. Thus, the largest portion of the environmental burden on the GWP was attributed to the energy used and the sodium silicate, representing around 38% and 17%, respectively. Therefore, it is shown the importance of evaluating a new building material as a system, rather than investigating each material isolated. This let to have a better overview of the system's environmental performance;

2. Of the five partition wall technologies analyzed, considering the environmental, functional, and economic performance, the two proposed half-sandwich panels (AP_{XPS} and AP_{ICB}) resulted in the most sustainable alternatives versus the two conventional technologies (HWR and LWR), and the conceptual design of lightweight sandwich walls (LWS) that were taken as a reference. Of which the AP_{XPS} obtained the best overall results and the HWR was the least favorable sustainable profile. Regarding the AP_{ICB}, the use of ICB positively impacted the environmental performance, however, it negatively influenced the economic aspect, and consequently, the final sustainable score was lower. Therefore, it was found that besides the environmental factor, functional and economic parameters are fundamental in the decision process when a new construction technology is benchmarked;

3. The sensitivity analysis supported the interpretation of sustainability analysis results. It confirmed that the AP_{XPS} and AP_{ICB} are the ones that combine the best environmental, functional, and economic performance, since in an overall view they made a lower impact on the categories analyzed. Sensitivity analysis also demonstrated that LWR and LWS perform better when only functional and environmental parameters were considered, respectively. It also concluded that from all perspectives the HWR is the worst option, therefore, it is not within the Hofstetter triangle.

Finally, this study leads to the conclusion the introduction of industrial wastes or by-products lowered the environmental load of the developed building solutions. However, the selection of each element and material with better physical and functional capacities, such as the insulating material, will be a determining factor to produce sustainable building materials with lower GWP. Furthermore, when the functional and economic factor is taken into account to define the most sustainable profile, the optimal solution will be determined as the one that better merges all these considerations.

Due to the lack of studies found, specifically on the use of alkali-activated ceramic/slag waste cement in the development of interior partition walls, further analysis on design optimization is encouraged, such as the thickness of each layer of the panel, either the rigid face or the insulating material. It might allow for improving the functional parameters (e.g., thermal conductivity) required according to the intended use to potentiate the sustainability of this new construction material.

ACKNOWLEDGEMENTS

REFERENCES

[1]   T. E. C. A. Cembureau, "Activity Report," Brussels, 2020. Accessed: May 16, 2022. [Online]. Available: https://cembureau.eu/media/m2ugw54y/cembureau-2020-activity-report.pdf.

[2]   F. N. Costa and D. V. Ribeiro, "Reduction in CO2 emissions during production of cement, with partial replacement of traditional raw materials by civil construction waste (CCW)," *J. Clean. Prod.*, vol. 276, Dec. 2020, doi: 10.1016/J.JCLEPRO.2020.123302.

[3]   I. Bianco, B. Ap Dafydd Tomos, and R. Vinai, "Analysis of the environmental impacts of alkali-activated concrete produced with waste glass-derived silicate activator – A LCA study," *J. Clean. Prod.*, vol. 316, p. 128383, Sep. 2021, doi: 10.1016/J.JCLEPRO.2021.128383.

[4]   C. Frazão, J. Barros, R. Toledo Filho, S. Ferreira, and D. Gonçalves, "Development of sandwich panels combining Sisal Fiber-Cement Composites and Fiber-Reinforced Lightweight Concrete," *Cem. Concr. Compos.*, vol. 86, pp. 206–223, Feb. 2018, doi: 10.1016/J.CEMCONCOMP.2017.11.008.

[5]   H. Ulugöl *et al.*, "Mechanical and microstructural characterization of geopolymers from assorted construction and demolition waste-based masonry and glass," *J. Clean. Prod.*, vol. 280, p. 124358, Jan. 2021, doi: 10.1016/J.JCLEPRO.2020.124358.

[6]   G. F. Huseien, A. R. M. Sam, K. W. Shah, M. A. Asaad, M. M. Tahir, and J. Mirza, "Properties of ceramic tile waste based alkali-activated mortars incorporating GBFS and fly ash," *Constr. Build. Mater.*, vol. 214, pp. 355–368, Jul. 2019, doi: 10.1016/J.CONBUILDMAT.2019.04.154.

[7]   M. Sarkar and K. Dana, "Partial replacement of metakaolin with red ceramic waste in geopolymer," *Ceram. Int.*, vol. 47, no. 3, pp. 3473–3483, Feb. 2021, doi: 10.1016/J.CERAMINT.2020.09.191.

[8]   K. Fang, J. Zhao, D. Wang, H. Wang, and Z. Dong, "Use of ladle furnace slag as supplementary cementitious material before and after modification by rapid air cooling: A comparative study of influence on the properties of blended cement paste," *Constr. Build. Mater.*, vol. 314, p. 125434, Jan. 2022, doi: 10.1016/J.CONBUILDMAT.2021.125434.

[9]   C. L. Hwang, M. Damtie Yehualaw, D. H. Vo, and T. P. Huynh, "Development of high-strength alkali-activated pastes containing high volumes of waste brick and ceramic powders," *Constr. Build. Mater.*, vol. 218, pp. 519–529, Sep. 2019, doi: 10.1016/j.conbuildmat.2019.05.143.

[10]   S. A. Zareei, F. Ameri, N. Bahrami, P. Shoaei, H. R. Musaeei, and F. Nurian, "Green high strength concrete containing recycled waste ceramic aggregates and waste carpet fibers: Mechanical, durability, and microstructural properties," *J. Build. Eng.*, vol. 26, p. 100914, Nov. 2019, doi: 10.1016/J.JOBE.2019.100914.

[11]   Z. Bayer Öztürk and İ. İ. Atabey, "Mechanical and microstructural characteristics of geopolymer mortars at high temperatures produced with ceramic sanitaryware waste," *Ceram. Int.*, vol. 48, no. 9, pp. 12932–12944, May 2022, doi: 10.1016/J.CERAMINT.2022.01.166.

[12]   P. Santos, J. R. Correia, L. Godinho, A. M. P. G. Dias, and A. Dias, "Life cycle analysis of cross-insulated timber panels," *Structures*, vol. 31, pp. 1311–1324, Jun. 2021, doi: 10.1016/J.ISTRUC.2020.12.008.

[13]   J. I. T. Garces, I. J. Dollente, A. B. Beltran, R. R. Tan, and M. A. B. Promentilla, "Life cycle assessment of self-healing geopolymer concrete," *Clean. Eng. Technol.*, vol. 4, p. 100147, Oct. 2021, doi: 10.1016/J.CLET.2021.100147.

[14]   D. A. Salas, A. D. Ramirez, N. Ulloa, H. Baykara, and A. J. Boero, "Life cycle assessment of geopolymer concrete," *Constr. Build. Mater.*, vol. 190, pp. 170–177, Nov. 2018, doi: 10.1016/J.CONBUILDMAT.2018.09.123.

[15]   Z. H. Joudah, G. F. Huseien, M. Samadi, and N. H. A. Shukor Lim, "Sustainability evaluation of alkali-activated mortars incorporating industrial wastes," *Mater. Today Proc.*, vol. 46, pp. 1971–1977, Jan. 2021, doi: 10.1016/J.MATPR.2021.02.454.

[16]   K. K. Ramagiri and A. Kar, "Environmental impact assessment of alkali-activated mortar with waste precursors and activators," *J. Build. Eng.*, vol. 44, p. 103391, Dec. 2021, doi: 10.1016/J.JOBE.2021.103391.

[17]   M. U. Hossain, D. Xuan, S. T. Ng, and B. Amor, "Designing sustainable partition wall blocks using secondary materials: A life cycle assessment approach," *J. Build. Eng.*, vol. 43, p. 103035, Nov. 2021, doi: 10.1016/J.JOBE.2021.103035.

[18]   S. Fernando *et al.*, "Environmental evaluation and economic analysis of fly ash-rice husk ash blended alkali-activated bricks," *Environ. Impact Assess. Rev.*, vol. 95, p. 106784, Jul. 2022, doi: 10.1016/J.EIAR.2022.106784.

[19]   R. Mateus, S. Neiva, L. Bragança, P. Mendonça, and M. Macieira, "Sustainability assessment of an innovative lightweight building technology for partition walls – Comparison with conventional technologies," *Build. Environ.*, vol. 67, pp. 147–159, Sep. 2013, doi: 10.1016/J.BUILDENV.2013.05.012.

[20]   N. Gaibor *et al.*, "Fiber Reinforced Alkali Activated Cements from Ceramic Waste and Ladle Furnace Slag cured at ambient temperature (under review since 04-23-2022)," *J. Mater. Civ. Eng.*, no. Manuscript number: MTENG-14776, 2022.

[21]   R. Mateus and L. Bragança, *Tecnologias Construtivas para a Sustentabilidade da Construção, [Building technologies for sustainable construction]. (In Portuguese)*, Ecopy. Porto, 2010.

[22]   "ISO, 2006. 14040:2006 - Environmental Management-Life Cycle Assessment-Principles and Framework. International Organisation for Standardisation, Geneva, Switzerland," 2006.

[23]   G. W. Ruiz, E. Moreno L. Valsasina, D. FitzGerald, A. Symeonidis, D. Turner, J. Müller, N. Minas, G. Bourgault, C. Vadenbo, D. Ioannidou, "Documentation of Changes Implemented in Ecoinvent Database V3. 7 & V3. 7.1," Zürich, Switzerland. Accessed: Jun. 02, 2022. [Online]. Available: https://ecoinvent.org/the-ecoinvent-database/data-releases/ecoinvent-3-7-1/.

[24]   N. Gaibor, D. Leitão, T. Miranda, N. Cristelo, E. N. B. Pereira, and V. M. C. F. Cunha, "Effect of polyacrylonitrile fiber on the properties of alkali-activated ceramic/slag-based mortar," *J. Build. Eng.*, vol. 44, p. 103367, Dec. 2021, doi: 10.1016/J.JOBE.2021.103367.

[25]   "EXPANDED INSULATION CORKBOARD (ICB) ENVIRONMENTAL PRODUCT DECLARATION," Accessed: Jun. 03, 2022. [Online]. Available: www.daphabitat.pt.

[26]   ISO 9869, *ISO 9869. Thermal insulation – building elements – in-situ measurement of thermal resistance and thermal transmittance. International Organization for Standardization (ISO)*. 1994.

[27]   Presidência do Conselho de Ministros, *Decreto-Lei n.º 101-D/2020 | DRE*. Portugal: DIARIO DA REPUBLICA - 1.ª SERIE, Nº 237 Supl, de 2020-12-07, Pág. 7-(21) - 7-(45), 2020, pp. 21–45.

[28]   I. N. de E. INE, "Portal do INE. Atualização de Valores com Base no IPC," *Statistics Portugal*, 2022. https://www.ine.pt/xportal/xmain?xpid=INE&xpgid=ipc&xlang=en (accessed Jun. 08, 2022).

[29]   L. Díaz-Balteiro and C. Romero, "In search of a natural systems sustainability index," *Ecol. Econ.*, vol. 49, no. 3, pp. 401–405, Jul. 2004, doi: 10.1016/J.ECOLECON.2004.02.005.

[30]   E. P. A. EPA and S. A. B. SBA, "Reducing Risk: setting priorities and strategies for environmental protection," pp. 13–4, 2000.

[31]   P. Hofstetter, *Perspectives in Life Cycle Impact Assessment: A Structured Approach to combine models of the technosphere, ecosphere and valuesphere*. London, England: Kluwer Academic Publishers, 1998.

[32]   Z. Cao, L. Shen, J. Zhao, L. Liu, S. Zhong, and Y. Yang, "Modeling the dynamic mechanism between cement CO2 emissions and clinker quality to realize low-carbon cement," *Resour. Conserv. Recycl.*, vol. 113, pp. 116–126, Oct. 2016, doi: 10.1016/J.RESCONREC.2016.06.011.

[33]   C. Ouellet-Plamondon and G. Habert, "Life cycle assessment (LCA) of alkali-activated cements and concretes," *Handb. Alkali-Activated Cem. Mortars Concr.*, pp. 663–686, Jan. 2015, doi: 10.1533/9781782422884.5.663.

[34]   A. S. Tártaro, T. M. Mata, A. A. Martins, and J. C. G. Esteves da Silva, "Carbon footprint of the insulation cork board," *J. Clean. Prod.*, vol. 143, pp. 925–932, Feb. 2017, doi: 10.1016/J.JCLEPRO.2016.12.028.

[35]   European Extruded Polystyrene Insulation Board Association., *EPD-EXI-20140155-IBE1-EN, 2014. Environmental Product Declaration of Extruded Polystyrene (XPS) Foam Insulation with Alternative Flame Retardant*. 2014.

[36]   R. Robayo-Salazar, J. Mejía-Arcila, R. Mejía de Gutiérrez, and E. Martínez, "Life cycle assessment (LCA) of an alkali-activated binary concrete based on natural volcanic pozzolan: A comparative analysis to OPC concrete," *Constr. Build. Mater.*, vol. 176, pp. 103–111, Jul. 2018, doi: 10.1016/J.CONBUILDMAT.2018.05.017.

[37]   Santos C and Matias L., "Coeficientes de Transmissão Térmica de Elementos da Envolvente dos Edifícios Coleção Edifícios – ITE 50," Lisbon, ISBN: 978-972-49-2065-8, 2006. Accessed: Sep. 20, 2021. [Online]. Available: http://home.fa.utl.pt/~lcaldas/LNEC_ITE_50.pdf.

[38]   Y. E. Valencia-Barba, J. M. Gómez-Soberón, M. C. Gómez-Soberón, and M. N. Rojas-Valencia, "Life cycle assessment of interior partition walls: Comparison between functionality requirements and best environmental performance," *J. Build. Eng.*, vol. 44, p. 102978, Dec. 2021, doi: 10.1016/J.JOBE.2021.102978.

[39]   D. C. Gámez-García, J. M. Gómez-Soberón, R. Corral-Higuera, H. Saldaña-Márquez, M. C. Gómez-Soberón, and S. P. Arredondo-Rea, "A Cradle to Handover Life Cycle Assessment of External Walls: Choice of Materials and Prognosis of Elements," *Sustain. 2018, Vol. 10, Page 2748*, vol. 10, no. 8, p. 2748, Aug. 2018, doi: 10.3390/SU10082748.

[40]   A. Ferrández-García, V. Ibáñez-Forés, and M. D. Bovea, "Eco-efficiency analysis of the life cycle of interior partition walls: a comparison of alternative solutions," *J. Clean. Prod.*, vol. 112, no. 1, pp. 649–665, Jan. 2016, doi: 10.1016/J.JCLEPRO.2015.07.136.

General conclusions and future works

8.1. CONCLUSIONS

The research presented in this thesis addresses the development of a cementitious material through the alkaline activation technology of industrial wastes, to be incorporated in creating new building solutions, such as non-structural partition panels. This work is a significant contribution to the circular economy as it has demonstrated the feasibility of using two abundant and less-common industrial wastes, namely ceramic waste (main precursor) and ladle furnace slag (complementary precursor), which the production rate is increasing, especially, in Europe. Furthermore, this mitigates the imminent environmental burden if these materials are disposed in landfills with no treatment. To fulfill the objectives, a comprehensive experimental program was conducted partially at the Laboratory of Civil Engineering of the University of Trás-os-Montes e Alto Douro in Vila Real, and mostly at the Department of Civil Engineering, School of Engineering, at the University of Minho in Guimarães, Portugal. The conclusions drawn are summarized below, grouped by research objectives as defined at the outset:

In chapter II, a literature review to achieve the first objective of this doctoral thesis was elaborated. This was "*to define and establish the relevance of the treatment of ceramic solid waste and the subsequent use as a precursor for alkali activation in non-structural materials in the construction sector*". This bibliography revision let to conclude that, today, it is a fact that the enormous industrial and economic development that society has experienced in recent centuries has brought about a series of environmental problems whose consequences do not go unnoticed by anyone. In this regard, the growing awareness from the social, academic, governmental, and industrial sectors of these problems has prompted the search for new technologies and behaviors that are respectful of the environment, promote development, and guarantee the welfare state but, in turn, safeguard the available natural resources.

Indeed, one of the main environmental problems facing today's society is global warming caused by the emission of greenhouse gases into the atmosphere. In this regard, the cement and concrete

industry is one of the main responsible for the CO_2 emission of anthropogenic origin, representing ~8% of the global CO_2 emissions to the atmosphere and around 36% of the worldwide energy consumption. For this reason, alkali-activated cement (AAc) and concretes have been introduced as a new sustainable construction material to replace the traditional OPC-based cement mortars and concrete. In addition to the fact that the production of alkaline cement allows the reuse of waste, its manufacture represents considerable energy savings and a significant reduction in CO_2 emissions compared to traditional Portland cement. Evidently, wastes that none or minor treatment are required to be used as precursors are preferred, as is the case of ceramic wastes (CW). In this way, it was found that about 30% of the total production from the ceramic industry goes to waste, while ceramic materials coming from construction and demolition waste represent around 45%. Thus, the safe use of the CW by recycling them through alkali activation, can transform large-scale waste streams into sustainable materials and at the same time relieve the ceramic industry waste disposal problem, suggesting a win-win situation from both the sustainable and economic points of view.

Chapters III, IV, and V were developed to accomplish the second objective, "*to know the fundamental properties of the ceramic residue and the starting materials to determine the optimum mixtures from the mechanical and physical point of view, complemented by a mineralogical and microstructural characterization*". For the results achieved, several mixtures had to be developed and evaluated considering the mechanical, physical, mineralogical, and microstructure properties. So that, on the one hand, knowledge was created about the behavior of this type of waste when integrated into a mixture and chemically activated. And on the other hand, the optimal or most suitable solution was determined for the specific purpose of its application, i.e., non-structural partition panels. The key findings were as follows:

- **Chapter III** was the first phase of the experimental work, where the alkali activation of ceramic waste (CW) from construction and demolition wastes mixed with fly ash (FA) or ladle furnace slag (LFS) in presence of sodium silicate (SS) or sodium hydroxide (SH) as alkaline solutions were analyzed as a preliminary study. Of the four different groups of mixtures with five different compositions each, it was determined that the blend constituted of 75% CR + 25% LFS and activated with SS was the best in terms of mechanical performance, since it reached the highest compressive strength values, up to around 60 MPa at 90 days of curing. Therefore, it was established as the optimum blend composition to be used in later stages of the research. It was

also found that differences in mechanical strength were attributed to the chemical composition of the starting materials, thus, the combination of precursors CR+FA or CR+LFS regardless of the alkaline solution (SH or SS) were categorized as calcium-poor or calcium-rich aluminosilicates, respectively. Hence, evidence that higher calcium content positively affects the strength of the mixture.

- **In chapter IV**, the origin and type of the main precursor used in this part of the work were different, i.e., wastes from a ceramic brick manufacturing company were used instead. Thus, the fundamental properties of this precursor were conducted first and as expected, different values for the chemical composition were obtained, but even so, this ceramic waste was rich in both, silicon dioxide and aluminum oxide, the same as the precursor studied in chapter III. Therefore, the selected mixture composition in the previous chapter was adjusted and a superplasticizer was added (SP) to the blend composition (72% CR + 28% LFS / SS-based + SP) in an attempt to get acceptable workability of the paste to facilitate the incorporation and its subsequent dispersion of the polyacrylonitrile (PAN) fibers.

  It was observed that the PAN fibers addition (0%, 0.5%, and 1% in volume) under thermal curing (70°C and 60% HR ± 5%) did not significantly influence the physical properties (open porosity and capillarity). In contrast, mechanical properties were positively affected by fiber incorporation, registering an enhancement of about 20% on compressive and tensile under flexural strength and nearly 12% in elasticity modulus compared to plain AAc at 90 curing days, hence justifying the addition of the fibers. Moreover, the main advantage of the fiber reinforcement was identified at the post-cracking stage of the flexural responses for 1% of fiber content. Finally, the mineralogical and microstructural characterization determined that the main product of the alkali-activated reaction was the C-A-S-H gel-type and SEM micrographs revealed a good interfacial bond between PAN fibers with the AAc.

- **Chapter V** focused on improving the results obtained in the previous chapter, specifically, the mechanical performance and a more sustainable way to produce activated alkaline cement were considered. In this way, first, the composition of the earlier mixture was refined again, and water was also added (75% CR + 25% LFS / SS-based + SP + water), but the same PAN fiber content (i.e., 0%; 0.5%, and 1% in volume) was maintained. Thus, an improvement in the workability of

the cement was observed and therefore a more homogeneous dispersion of the fibers in the matrix which was verified with the enhancement of the flexural strength results. Secondly, curing conditions (20°C and 60% HR ± 5%) control the water available during the matrix hardening, hence, it had a significant effect on the development of mechanical properties of cement. As expected, lower compressive strengths ranging from 25 to 29 MPa were registered at 90 days for the studied series, but still considered satisfactory results. Concerning the physical properties (water absorption by immersion and capillarity), similar results to those of the previous chapter were obtained, that is, they were not substantially affected by the incorporation of fibers. The C-A-S-H gel was also recognized as the main reaction product of the developed AAc. It is worth mentioning that, curing without temperature has a positive environmental and economic impact since it let to reduce energy consumption, cost, and CO_2 emissions.

Finally, considering the most suitable physical, mechanical, and mineralogical behavior, the ambient cured alkali-activated cement containing 1% of PAN fiber was selected to be used in the next phase, which is the manufacture of the non-structural panels.

Chapter VI is dedicated to complying with the third objective, *"to study the feasibility of the optimum defined mixture to be used in the construction of non-structural panel elements, performing conformance and functional tests related to mechanical and thermal behavior"*. Therefore, within the scope of this objective and the time available to carry out this work, the two studied solutions for sandwich panels, composed of a slender layer formed by an alkali-activated cement (AAc) reinforced with fibers, based on ceramic waste and ladle slag, and a thicker insulation layer of either extruded polystyrene foam (panel named, AP_{XPS}) or expanded cork agglomerate (panel named, AP_{ICB}) were under an extensive experimental campaign which let to conclude that:

From the mechanical behavior point of view, in general, results showed clear differences between the two proposed solutions. The interfacial tensile strength was higher for the AP_{XPS}, however, better bond strength was observed between layers of the AP_{ICB} since the failure took place out of the interface area, revealing a weak inner structure of the ICB. Regarding the shear bond strength, lower values for the AP_{ICB} were achieved, however, the irregular surface of the ICB board positively influenced the adhesion with the AAc layer, inhibiting the interfacial slip between both panel layers. In contrast, although the direct shear results of the AP_{XPS} were nearly two times greater, regardless of the direction of the load applied to the grooves (parallel or perpendicular) a total debonding between the XPS and AAC layer

was observed. Concerning the flexural strength, after the first peak load, which most probably was associated to the starting of the delamination of the AAC layer and the XPS board, the AP_{XPS} continued increasing the flexural load attaining a higher load-bearing capacity and energy absorption capacity comparatively to the AP_{ICB}. In the latter, a sharp softening branch was observed.

From a thermal performance perspective, the thermal resistance value ($R'_{(ntotal)}$) obtained for the AP_{XPS} was slightly higher (~12%) compared to AP_{ICB}. This was mostly attributed to the lower thermal conductivity of the XPS. In general, the results achieved of the two proposed insulated panels demonstrated an enhancement regarding the thermal properties as the thermal resistance showed at least a twofold increase with respect to the common hollow ceramic brick wall and the lightweight concrete blocks. And when compared to a conventional solution of ceramic solid brick, the $R'_{(ntotal)}$ values of around sevenfold higher were registered. Another important finding was the theoretical value (0.12 W/m°C) of the thermal conductivity (λ) for the panel (without an insulating layer) of activated alkaline cement based on waste and ceramic slag only, which was significantly lower than the specified λ of traditional construction materials. This may suggest that the thermal conductivity of the developed ceramic waste/slag-based cement was improved by the alkali-activation technology.

Chapter VII allowed the understanding of the potential of the introduction of the studied industrial wastes into the proposed panels. Thus, fulfilling the last objective of this doctoral work, "to a*ssess the sustainability of the proposed non-structural panels based on industrial wastes compared with other traditional solutions offered by the construction sector*". In light of the obtained results, it was possible to conclude that the incorporation of industrial wastes lessens the environmental burden of new building material, however, the overall environmental impacts will be significantly influenced by the selection of each element of the system. It was noticed from the two proposed panels (AP_{XPS} and AP_{ICB}) that the type of thermal insulation material substantially affected Global Warming Potential (GWP) and most impact categories considered. For instance, the use of extruded polystyrene foam (XPS), represented the highest contribution to the GWP (~57%). In contrast, when the expanded cork agglomerate board was used, a negative contribution (-37%) to the CO_2 emissions was found, which is mainly due to the cork being a renewable raw material. Besides, it has significant embodied carbon since cork absorbs carbon during its growth and the net energy consumption and GHG emissions through the ICB's life cycle are very low in comparison to its embodied carbon. In both cases, the

alkali activator (sodium silicate) was ranked in second place. Usually, when the alkali-activated materials are studied separately, the highest environmental burden is related to the activator.

Furthermore, from the Sustainability Assessment (LCA) it was possible to comprise that the best solution is the one that better merges the environmental, functional, and economic factors. So, findings showed that the two half-sandwich panels proposed were the most sustainable alternatives when compared to the two conventional technologies, namely, the heavyweight conventional partition wall (hollow brick wall), and the lightweight gypsum panels wall (plasterboard wall), also against the conceptual design of lightweight sandwich walls taken as references. This interpretation was supported by the sensitivity analysis.

Finally, the strength classes for the developed alkaline-activated cement (AAc) according to the EN 206-1 standard have been defined as a reference. Therefore, the AAc under thermal curing (70°C and 60% HR ± 5%) would correspond to the C40/50 strength class and when curing at ambient temperature (20°C and 60% HR ± 5%) would be a C20/25 strength class. Hence, it can be stated that the developed alkali-activated cement has a great potential being a promising alternative to conventional Portland cement-based materials to be used in several applications, some out of the scope of this work such as structural applications, thus contributing to a circular economy and sustainability in the AEC sector. Therefore, the presented non-structural panels are just an alternative.

8.2. FUTURE RESEARCH DIRECTIONS

This thesis has mainly been concerned with the development of an alkali-activated ceramic waste/slag cement (AAc) and its feasibility to be used in the construction of non-structural panels for partition walls. The research presented in this thesis has significantly advanced the understanding in this field, but much further research is still needed for the safe and reliable application of the AAc and the developed panels in the practical field of Architecture, Engineering, and Construction (AEC) sector.

- **The durability of the alkali-activated cement** should be investigated since research is scarce on this topic. It might include tests such as chloride penetration, sulfate resistance, the aggregate/alkali reaction, freeze-thaw resistance, and carbonation;

231

- **Further analysis on design optimization** is encouraged, such as the thickness of each layer of the panel, either the rigid face or the insulating material. It might allow for improving the functional and mechanical properties according to the intended use;

- **Complementary mechanical and functional tests for panels are recommended.** To complement the tests carried out in the present work, there are others that, due to time limitations, it was not possible to perform, to mention some: impact tests, fire resistant behavior, sound reduction index, sound absorption, hygrometric behavior, among others. It will allow a complete characterization of the panels;

- **Real scale panel manufacturing** is required in order to evaluate, through experimental studies, the assembly structure to be used for on-site installation.

Annexes

ARTICLES

I.   **Gaibor, Norma**, Leitão, D., Miranda, T., Cristelo, N., Pereira, E. N. B., & Cunha, V. M. C. F. (2021). Effect of polyacrylonitrile fiber on the properties of alkali-activated ceramic/slag-based mortar. Journal of Building Engineering, 44, 103367. https://doi.org/10.1016/J.JOBE.2021.103367

II.   **Gaibor, Norma**, Leitão, D., Miranda, T., Cunha, V., & Cristelo, N. (2021). Effect of curing conditions on compressive strength behavior on alkali-activated ceramic wastes. Polo Del Conocimiento, 6(3), 977–990. http://repositorium.sdum.uminho.pt/handle/1822/70790

III.   **Gaibor, N**, Coelho, J., Leitão, D., Miranda, T., Tavares, P., & Cristelo, N. (2020). Alkali activation of recycled ceramic aggregates from construction and demolition wastes. Materiales de Construcción, 70(339), 222. https://doi.org/10.3989/mc.2020.13619

IV.   **N. Gaibor**, D. Leitão, T. Miranda, and N. Cristelo, "Development of alkali-activated ceramic residue and fly ash blends," in Wastes: Solutions, Treatments and Opportunities III, CRC Press, 2019, pp. 591–599. https://doi.org/10.1201/9780429289798-94

PARTICIPATION IN CONFERENCES

I.   **Norma Gaibor**; Dinis Leitão; Pedro Tavares; Nuno Cristelo; Eduardo N.B. Pereira; Vítor M.C.F. Cunha, "Effect of curing conditions on the mechanical behavior of fiber reinforced alkali activated ceramic/slag-based cements", IMFAHE´s VIII International Conference, 30th May, Boston - Massachusetts, Oral Communication.

II.   **Gaibor, Norma**, Leitão, D., Miranda, T., Cristelo, N., Pereira, E. N. B., & Cunha, V. M. C. F., "Generation, Management and treatment of industrial ceramic wastes", VIII International

Congress of Industrial Processes, Hydrocarbons, and the Environment, 20 – 22 October 2021, ESPOCH Ecuador, Oral Communication.

III. **Gaibor Norma**, Leitão, D., Miranda, T., Cunha, V., & Cristelo, N, "Effect of curing conditions on compressive strength behavior on alkali-activated ceramic wastes", VII International Congress: Application, Transport and Fluid storage in industrial process, hydrocarbons, and environment, 21 – 23 October 2020, ESPOCH Ecuador, Oral Communication.

IV. **N. Gaibor**, D. Leitão, T. Miranda, and N. Cristelo, "Development of alkali-activated ceramic residue and fly ash blends", 5th International Conference WASTES: Solutions, Treatments, and Opportunities, 4 – 6 September 2019, Caparica, Portugal, Oral Communication.